An Ecosystem Design Approach for
Marine Aquaculture Site Selection and Operation

NOAA Marine Aquaculture Initiative Program, Final Report

Award Number: NA08OAR4170859

Co-Principal Investigators:

Dr. Dale A. Kiefer
Dr. Jack Rensel
Mr. Frank J. O'Brien
System Science Applications

Dr. David W. Fredriksson
United States Naval Academy

Dr. James Irish, University of New Hampshire
Woods Hole Oceanographic Institution (Emeritus)

Institutional Representative:
Mr. Frank J. O'Brien
System Science Applications
3 Trovita
Irvine, CA 92620-1952

May 31, 2011

Executive Summary

With the growing worldwide demand for seafood, and the depletion of many fish stocks in the natural environment, aquaculture has become a crucial source of protein and now accounts for nearly half of the worldwide supply of fish consumed by humans. Concerns about the water column and benthic impact of fish farming requires a thorough analysis of locations for aquaculture operations that cannot be performed the old fashioned way…. by guessing and hoping for the best.

With support of NOAA's Aquaculture Program, System Science Applications and marine scientists from Woods Hole Oceanographic Institute and the US Naval Academy have expanded and tested the capabilities of AquaModel to evaluate environmental effects of singular and multiple fish farm sites. AquaModel is an environmental software package that simulates the operations of marine fish farms and fate of organic and inorganic waste production in sediments and receiving waters. The software is designed to be user friendly so that it can be operated by aquaculture stakeholders after some initial training and regional tuning by AquaModel specialists. Thus, virtual farms can be designed, configured, placed and operated by stakeholders to simulate and evaluate environmental sustainability and concurrent economic success. The system is flexible and can assimilate a broad range of input data from general seasonal information to spatially and temporally detailed data such as hourly observations of current velocity, direction, dissolved oxygen, and nutrient concentration.

Project Objectives

The objectives of our work were to:

1. Develop an interface for coupling AquaModel software to 3 dimensional coastal circulation models.
2. Develop a far-field version of AquaModel that will simulate the water column effects of multiple commercial scale farms over large regions.
3. Test the enhanced model in two coastal regions which have been well studied but differ greatly in terms of physical and biochemical conditions.
4. Conduct sensitivity analyses of key parameters.

The first 3 of these objectives have been accomplished during building and running the Gulf of Maine and the Southern California Bight simulations. The 4th objective was accomplished during tuning of AquaModel for each of these two simulations.

The two regions selected to evaluate the model performance and simulation predictions included the southern coast of the Southern California Bight near San Diego and the New Hampshire coast. The California coastal region was selected because it has been well studied and it included a site where Hubbs SeaWorld Research Institution had proposed to develop an experimental, commercial-sized farm for striped bass which we previously modeled for near field effects. The New Hampshire coastal ocean was selected because it included the University of New Hampshire's Open Ocean Aquaculture site which has been intensely monitoring for several years during fish farm studies. Our development and simulation runs with AquaModel included both near-field studies of the ecological impact of a single farm on water quality and benthic conditions and far-field studies on the impact of multiple farms upon water quality and the planktonic community (including nitrogen, phytoplankton and zooplankton dynamics).

Southern California Bight Far-Field Simulation

A far-field AquaModel simulation of the Southern California Bight (SCB) was run for the month of May, 2007. Eight fish farms were simulated part-way through a culture cycle with a biomass of ~21,000 metric tons of striped bass. The fish farms were positioned north to south along ~80 km of the coast, mostly in very deep water. The simulation was driven by output from a 3-dimensional coastal circulation model provided by the NASA's Jet Propulsion Laboratory and imported into AquaModel. Hydrographic data on physical and biochemical parameters measured by the California Cooperative Fisheries Investigation were imported as independent variables to the calculations.

Patterns in the distribution of nitrogen, phytoplankton, and zooplankton within and beyond the nutrient enriched plumes produced by the farms were mapped and compared to the current velocity and direction vectors. These maps are presented as a weekly time series that can be found in Section 3 of this report, but AquaModel users may view them in any time increment selected, from minutes to days or more during model replay mode.

In this region and time of the year, mesoscale (< 10 km diameter) eddies cause rapid change in the shape of the plume of fish farm enriched dissolved inorganic nitrogen, phytoplankton, and

zooplankton. The nutrient plumes were limited to a small area around each farm, no more than a few kilometers away. Within the plumes concentrations of dissolved inorganic nitrogen reached transient values of near 1 µM in close proximity to the farms when currents were slow, but most commonly concentrations at those locations rarely exceeded 0.4 µM, which was about 4 times ambient concentrations. The spatial distribution of dissolved inorganic nitrogen was limited by both turbulent mixing of the plume with ambient waters but also because of assimilation by the planktonic community.

The spatial extent of the phytoplankton-enriched plumes were much greater than the spatial extent of the nutrient plumes, and thus the phytoplankton-enriched plumes appeared to "break free" from the nutrient enriched plumes produced by the farm. These features are easily explained by the fact that the response time of phytoplankton assimilation of DIN was about 8 days, while response time of zooplankton grazing upon phytoplankton was 20-30 days. The concentration of phytoplankton within the waste plumes rarely exceeded 0.7 µM nitrogen which was slightly greater than a factor of 2 above the ambient concentration.

Finally, the magnitude of the response of phytoplankton to nutrient enrichment was greater than the response of zooplankton to phytoplankton enrichment. Specifically, the highest concentrations of zooplankton in the plumes were 0.6 µM nitrogen, which was only 0.2 µM nitrogen higher than ambient concentrations. As stated above, the highest concentration of phytoplankton in the plume was 0.7 µM nitrogen which was 0.4 µM higher than ambient concentrations. Such a difference in response was caused by the slower response time of zooplankton growth that provides additional time for dispersion to reduce the concentration of phytoplankton within the plume and there-by reduces the yield of zooplankton. Although measurable, neither the increased concentration of phytoplankton nor the increased concentration of zooplankton would be considered a bloom in this region.

Gulf of Maine Near-Field and Far-Field Simulations

The Gulf of Maine net-pen simulations featured detailed hydrographic data for a complete annual cycle to drive AquaModel simulations. We purposely created very large fish farms in both the near and far-field simulations in order to examine a "worst case" scenario. At this site, near-field simulations were run for farms with either 12 or 24 cages to assess both benthic and water column effects. In April of the initial year, the virtual farm was stocked with 200 gram

Atlantic salmon at a density of 0.6 kg/m3. Detailed data files of local conditions over short time scales (minutes to weeks) were read into the simulation as boundary and ambient conditions, as the software tracked the fish growth and waste production and spatial fate. The model was run for 14 months when the fish were harvested at average fish weight that was slightly greater than 5 kg. The total biomass at harvest for the 12 and 24 cage farms was 7,290 and 13,932 metric tons, respectively, which far exceeds production from the largest of all salmon farms anywhere.

In contrast to the Southern California Bight, annual variations of environmental variables were large in the Gulf of Maine simulation. For example, water temperatures ranged between 3° C in winter to 20° C in summer; concentrations of dissolved inorganic nitrogen in surface waters ranged between 2 μM in summer and 17 μM in winter, or from nutrient poor to nutrient replete. This seasonal variability was expressed as intrusions of ambient water masses into the far-field modeling domain forced by varying boundary and ambient concentrations of key parameters, including dissolved inorganic nitrogen concentrations and phytoplankton and zooplankton stocks. By running the model with, and without fish in the pens, it was clear that the variability in the planktonic system caused by these intrusions greatly exceeded the variability caused by nutrient-enriched plumes from the fish farms. Only when ambient nutrient concentrations were lowest did nitrogen plumes from the fish farms produce a significant change in the nutrient and phytoplankton fields.

Because we purposely created very large fish farms for this study, our near-field simulation of benthic impact clearly indicated significant perturbation to sediments and benthic community beneath the cages before the time of fish harvest. Conditions became degraded under the cages fairly rapidly with total organic carbon exceeding one percent dry weight, a concentration that is modestly high for sandy sediments that prevail beneath and near the vicinity of the fish farm. Adjacent to the cages, the enriched sediment zone formed an elliptical shaped area, extending to the northwest and southeast; this orientation matched measured long-term orientation of bottom current vectors arrayed in a polar diagram. Because of the very large fish production, benthic degradation that we calculated would likely be unacceptable to regulatory agencies and the public. However, we wished to evaluate operational conditions required to produce a large, measurable footprint. The simulation demonstrates that open ocean sites are not unlimited in their waste assimilation capacity, despite relatively greater depth and distance offshore. We

caution that had we reduced the simulated production by a factor of ~3 for the Gulf of Maine site we would have greatly reduce the impact to a level comparable to existing large salmon farms in the states of Maine and Washington. In those cases, fish farms must meet the very stringent limitations on the extent of sediment impact.

Finally, with regard to objective 4, we evaluated the sensitivity of AquaModel calculations to variation and uncertainty in the values for environmental parameters and the coefficients of equations during mathematical tuning of the plankton and benthic routines. In the case of the plankton routine, we tuned the system of equations to provide a "best fit" of calculated values to measured values obtained during detailed monitoring of physical and biochemical parameters over an annual cycle. In the case of the Southern California Bight, we drew upon quarterly oceanographic monitoring conducted by the California Cooperative Oceanic Fisheries Investigations. In the case of the Gulf of Maine study, we drew upon the extraordinary detailed monitoring at the University of New Hampshire's experimental fish farm, which is described in Section 5. During tuning of the regional, far-field model, we noted that the most critical physiochemical variables that determined the fate of dissolved wastes were horizontal eddy diffusivity, mixed layer depth, water turbidity, and the concentrations of primary and secondary macronutrients. The most critical biological variables are those that describe zooplankton dynamics. These are the two coefficients in the system of equations that determine grazing rates and the two coefficients that determine excretion rates.

For tuning of the benthic routine used in the Gulf of Maine, comprehensive field data were limited from the site because prior fish culture biomass was small. Instead, we drew upon the Atlantic salmon farm studies of Findlay and Watling (1991, nearby coastal Maine) and Chamberlin and Stucchi (2007, in British Columbia). During tuning of our benthic routine, we observed that most critical physical parameters were the areal rate of waste production by the farm, current speeds throughout the water column and particularly near the bottom, the depth of the water column, and the oxygen concentration, water temperature and porosity of the sediments. The most critical biochemical parameters are the values for bottom current velocity, thresholds velocity of waste deposition, erosion, and resuspension, the maximum specific assimilation rates of particulate organic carbon for aerobes and anaerobes, the half saturation constant for oxygenic respiration, and the half saturation constant for oxygen inhibition of anaerobic respiration.

Table of Contents

Acknowledgements

This work should be cited as:

Kiefer, D.A., J.E. Rensel, F.J. O'Brien, D.W. Fredriksson and J. Irish. 2011. An Ecosystem Design for Marine Aquaculture Site Selection and Operation. NOAA Marine Aquaculture Initiative Program, Final Report. Award Number: NA08OAR4170859. System Science Applications, Irvine CA. in association with United States Naval Academy and Woods Hole Oceanographic Institution. 181 p

1. Project Description

Economics of scale and environmentally sustainable are two concepts that are challenging the development of marine aquaculture in the United States. Within the present social climate, the industry must proceed with caution basing decisions on sound scientific and engineering knowledge. Trial and error techniques are not acceptable practices. With the use of high level, robust planning and analysis tools, aquaculture farms will be more likely to succeed as successful business entities. Such tools are necessary to understand the complex physical, chemical and biological interactions so that the systems can be optimally designed with an optimal configuration. A primary purpose of this project is to remedy the lack of useful and accurate aquaculture simulation and assessment tools by adapting a developing GIS-based model known as AquaModel for regional use with multiple fish farm sites.

Proper site selection and system configuration may be optimized to achieve maximum biomass and fish health while minimizing environmental impact. Modeling is the most efficient method to achieve this goal and without the development and application of fish farm models, planning and carrying capacity estimates for new installations in United States coastal waters will be difficult, if not impossible.

Specifically, we had several major objectives:

1. To develop AquaModel's capacity to assess regional concern of farm placement and environmental impact by developing an interface between AquaModel and commonly used 3 dimensional coastal circulation models. Further development of integrated GIS-modeling techniques will enhance the ability of a fish farm applicant to evaluate site location, configuration and size and the ability of government to conduct rational management such as limiting production based on carrying capacity estimates, not just arbitrary societal-view prejudice.

2. To demonstrate the utility of the enhanced model by running multiple simulations under differing environmental conditions and farm operations for two farms in regions where the oceanographic conditions are well known but differ greatly. These are the experimental University of New Hampshire's Atlantic fish farm site and at locations in the Southern California Bight near San Diego for marine finfish including the Hubbs-

SeaWorld Research Institute (HSWRI) proposed site.

3. To conduct sensitivity analyses of multiple simulations of the two regions to determine the environmental and operational parameters most important in producing reasonably accurate output that will lead to ecologically safe and economically profitable operations.

4. To provide outreach involving a new website with an interactive GIS in which visitors can run selected simulations of fish farms. It will also include development and presentation of material for several graduate and undergraduate level lectures regarding scientific analysis of the costs and benefits of marine fish farms. Presentations and lectures were given about the model in national or international meetings.

2. Description of AquaModel

2.1. Background

To the best of our knowledge, AquaModel is the only software that provides a complete, dynamic model of farm operation and environmental impact. It is also the only software that fully integrates environmental information with model computations within a GIS. More information can be found at www.AquaModel.org and simplified demonstrations of model use can be found at http://netviewer.usc.edu/projects.htm (only use Internet Explorer and closely follow browser options). The GIS program EASy is described at http://www.runeasy.com/.

The GIS software EASy provides a 4-dimensional framework (latitude, longitude, depth, and time) to run simulation models and analyze field measurements as graphical, numerical and statistical outputs. EASy, whose components are summarized in Figure 1, runs in Windows. It is a geographical information system designed for the storage, dissemination integration, analysis and dynamic display, of spatially referenced series of diverse oceanographic data. It provides the tools to import, display, and analyzes environmental information obtained from satellite-ocean thermal and color sensors and field surveys of currents, nutrients, oxygen, chlorophyll and other related parameters.

EASy graphically renders dynamically in time, within their proper geo-spatial context, both field and remotely sensed data and model outputs as diverse types of plots, including vector, contour, false color images and includes a built-in data contouring feature. Vertical structure of data, critical in oceanographic applications, is depicted as vertical contours for transects or depth profiles at selected point locations. Time series for measurements and relationships such as vertical profiles within the database at individual stations can also be visualized interactively as XY-plots. Presently there are over 50 different X-Y plots available for different parameters viewed as vertical profiles or horizontal cross sections that are dynamically updated in real time simulations. The software also provides access to data, integrated visualization products, and analytical tools over the Internet via Netviewer, a client-server, plug-in for EASy (Tsontos and Kiefer, 2002 and 2003).
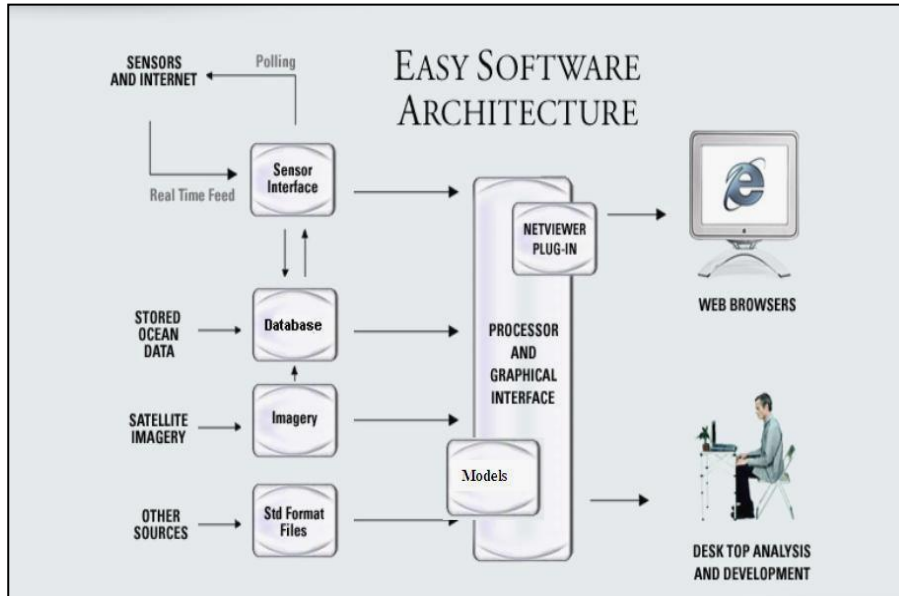
Figure 1: EASy software architecture and data integration and communication capabilities.

AquaModel is a plug-in model to EASy and simulates the dynamics of fish farms that can be "placed" within a selected water body and operated under the conditions found at that location. Most importantly, AquaModel fully integrates environmental conditions into the calculations of the growth and physiology of the penned fish.

The model is designed to simulate both the growth and metabolism of farmed fish species and the environmental impact of waste produced by the farm. It is to be used by developers and environmental agencies to assess both the optimal placement of farms and appropriate size of the farm for environmentally safe and sustainable operations. Several variables including the water temperature, the dissolved oxygen concentration, current speed, average wet weight of the fish, their density within each pen and the daily food ration define the initial state of conditions in the fish farm. Each pen is tracked separately and different species can be stocked in separate pens and each pen allows different initial size of fish. Outputs from the simulation include three dimensional maps of the two types of waste plumes (dissolved and particulate) created by egestion, excretion, and respiration by the farmed fish. Outputs also include the growth rate and standing stock of the fish, and the concentrations of nitrogenous nutrients, oxygen, and particulate waste (feces) within the farm. Many other parameters and plots of vertical profiles or transects can be viewed simultaneously, and all data can be written to spreadsheet or database for statistical and other types of post-model processing.
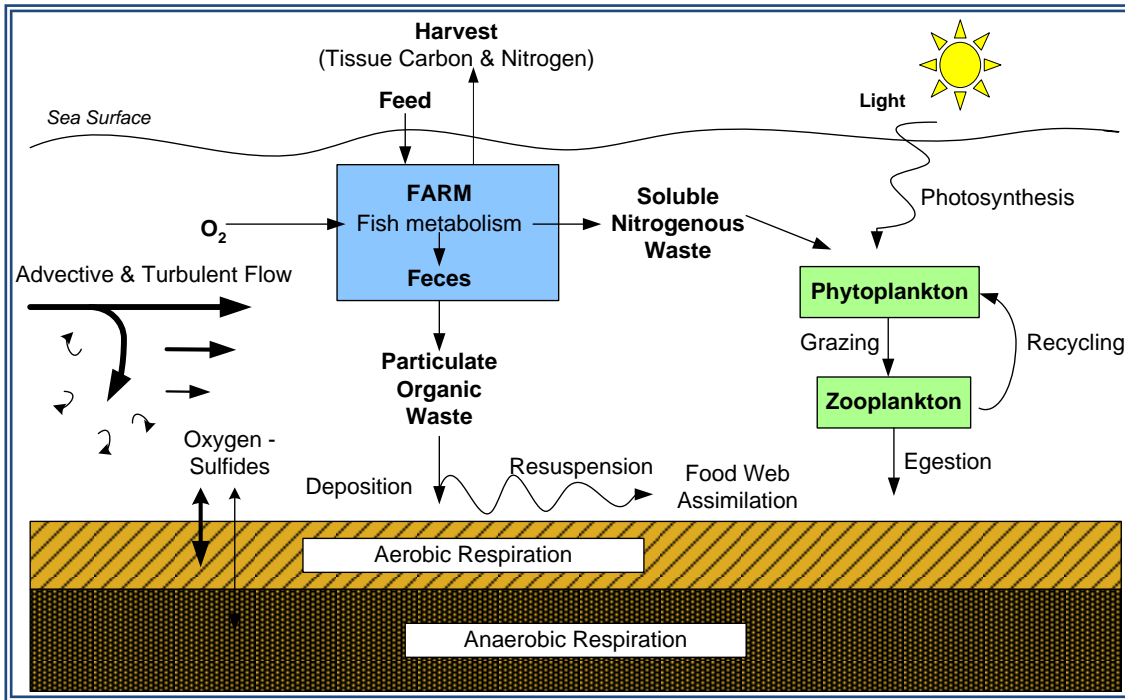
Figure 2: Key processes simulated in AquaModel include the growth and metabolism of farmed fish, the flow of water through the pens and transport of dissolved and particulate wastes produced by the fish, and the ecological transformations of these wastes.

The model is best described as consisting of 4 linked computational routines: a 2 or 3 dimensional description of water circulation, a description of the growth and metabolic activity of the cultured fish within the farm, a description of the planktonic community's response to nutrient loading, and a description of benthic effects (Figure 2). Carbon, nitrogen and oxygen fluxes are traced and rate functions vary with operational and environmental conditions. Operational conditions are the size and position of the pens, the quantity and composition or rations, and the density and size of the fish. Environmental factors that determine metabolic rates are current speed, the temperature of the water and the concentration of oxygen in the water. As water passes through the farm, a "waste water plume" and a "waste particle plume" are created downstream. The characteristics of this plume will depend upon the metabolic activities within the farm as well as the advective and turbulent flows that shape the plume.

AquaModel is also designed to be user friendly so that it can be quickly put in the hands aquaculture stakeholders with basic understanding of commercial software. Thus, virtual farms are first designed by the stakeholder and simulations are then run using several graphical interfaces. For example Figure 3 is such an interface in which the user enters information on the

location, size, and operation of a virtual (or real) fish farm as well as key environmental information. In this figure the "Pens" tab has been selected in which the user selects the number of pens in the farm, the species of fish in each pen, the geographical position of the pens, the size and shape of the pens, the average weight of fish at the start of grow out, and the stocking density of these fish. In addition from this interface the user can also chose to run a simulation, run and capture the results in a file, or replay a "results file". Moreover, one can select whether to run the simulation with a 2-dimensional or 3-dimensional flow field.
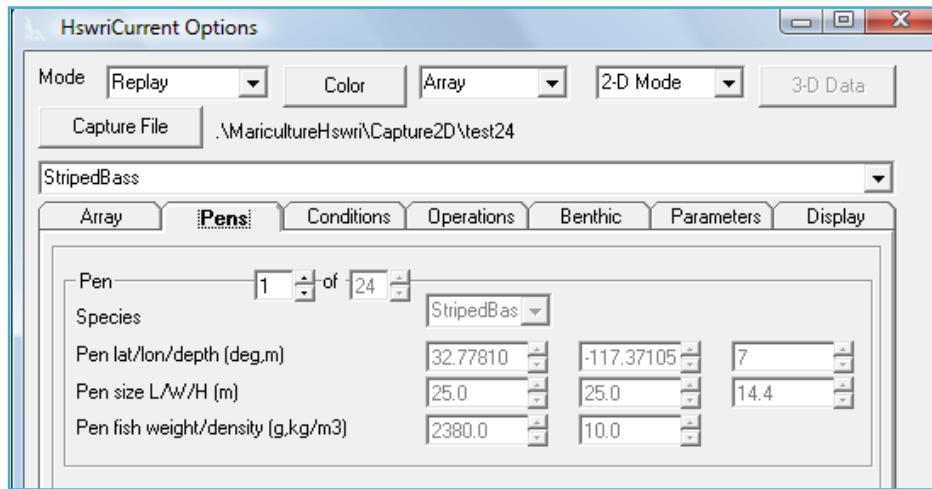
Figure 3: The user interface for entering information on the location, size, and operation of a virtual (or real) fish farm as well as key environmental conditions.

2.2. Circulation Routine

AquaModel's circulation routine flushes cages with ambient waters and transports wastes from them. The computations during each step of the simulation occur within each element of a 3-dimensional grid of rectangular cells that populate an array of such cells. The size, orientation, and geospatial location of the array as well as the number and dimension of the cells that populate the array are entered by the users. The array of cells begins at the sea surface and extends to the sea floor. The geometry and flow at the sediment/water interface is described in more detail in the Benthic Routine Section and the farm layout is described in the site description section. The time steps for the simulation vary between 1 and 5 minutes depending upon the speed of the currents.

The system of equations describing circulation is a simple finite element description of advection and dispersion. Each element of the array is treated as a box model in which materials flow across the 6 interfaces of each element, top, bottom and the four sides. Each element is treated

as instantly mixed throughout. These movements are tracked using a simple, finite difference calculation. Conservative tracers such as water and elements are conserved within the computational array.

Water and dissolved and suspended materials also move across the boundary of the array; however, here the values for the concentrations of dissolved and particulate materials at the boundaries are determined by the boundary conditions of the computational array. During the course of our NMAI project we added the capability to vary the values of current velocities and the concentration of tracers at the boundary to vary at a time step specified by the user. If the calculations of such a model are to be trusted, the array must be sufficiently large such that the exchange across the boundary does not significantly perturb the results of calculations. At the sediment-water interface uneaten feed and feces from the farm are transported, deposited into the sediments, resuspended from the sediments, or consumed by benthic organisms. These processes will be described in the next section.

The flow field in AquaModel can be either 2- or 3-dimensional. In 3-dimensional simulations the movement of water between adjacent cells has no constraints other than the requirement of conservation of mass. Convergent and divergent motion can be represented within the array as well as local eddies. In addition the water depth can vary within the array. Since 3-dimensional flow on small spatial and temporal scales is rarely measured in the field, our 3-dimensional simulations draw upon 3-D coastal circulation models. The spatial scale of these models is generally no smaller than 1 km and thus small scale turbulence is not included in the output. However, AquaModel provides the user the option to add specified levels of horizontal and vertical eddy diffusivity. While rates of horizontal dispersion are constant throughout the computational array, the rates of vertical dispersion can be specified for two layers, the upper mixed layer and the underlying stratified waters. The depth intervals of the mixed layer and the stratified layers vary with season as a sinusoidal oscillation.

In 2-dimensional simulations advection only occurs horizontally; neither divergence nor convergence flow occurs within the array. Small scale horizontal and vertical turbulent motions are treats as described in the previous paragraph. Much of the data on circulation collected at mariculture sites come from field measurements with acoustic Doppler current profilers, drogues, or current meters. In other cases information may come from simple tidal models.

Such information is well suited to 2-dimensional simulations.

As discussed in our introduction, we have run both near field and far field simulations for fish farms off the coast of New Hampshire and southern California. We obtained the flow field for the New Hampshire simulations by importing a field data on current velocities from the Isle of Shoals experimental farm and output from a 3-dimensional ADCIRC tidal simulation model. The two records were then merged and used to drive 3-dimensional flow.

We obtained the flow field for the San Diego simulations by importing output from the NASA Jet Propulsion Laboratory's ROMS Model. This model, which is a 3-dimensional, wind and tidally driven simulation, can be viewed at the SCOOS (Southern California Ocean Observing System). We obtain NetCDF files of the flow field directly from Dr. Yi Chow, who is director of the ROMS team at JPL. AquaModel provides a user interface for importing both 2- and 3-dimensional output from current meters and circulation models, and automatically interpolates in time and space such output in order to "fit" the computational grid selected by the user.

2.3. Farm Operations and Fish Metabolism Routines

The fish farm is characterized by physical layout and size of its cages and by its stocking, feeding, and harvesting regime. The physical layout of the farms requires one to enter:

- The number of cages.
- The location of the cages as described by their geographic co-ordinates (latitude, longitude, depth).
- The size of the cages including the length, width, and height. These setting may have to be adjusted to best fit the size of the cells within the computational array.
- The fractional difference between the current speed within the cages and ambient current speed.

Farms operations require one to enter for each cage:

- The species of farmed fish. Although the system of equations describing the growth and metabolism is invariant with species, the coefficients found within these equations will likely vary with species.
- Mean weight of fish in grams wet weight at initial stocking or at selected time intervals.

- Density of fish in mass of fish per cubic meter at initial stocking or at selected time intervals.
- Feed rate in grams dry weight of feed per day. This rate can be entered manually or calculated automatically by AquaModel as an optimal feed rate.
- Estimate percentile of uneaten feed loss from the cages.

Prior to this project we developed the fish metabolism routine that is based upon extensive review of the literature describing the growth and metabolism of commercial species (e.g. see Brett's work on sockeye salmon in references). This information has been supplemented by our own unpublished laboratory experiments and has been incorporated into a series of equations that track the transformations of oxygen, carbon, and nitrogen. (See Rensel, Kiefer, and O'Brien 2006 and Rensel et al., 2007 for more background.) The routine includes a description of oxygen-limited metabolism- an important feature since fish are raised at high densities, and in some cases farms are found in ambient waters of moderate or low dissolved oxygen concentration. In our NMAI simulations the cages of the New Hampshire Farm contained Atlantic salmon, *Salmo salar*, while cages of the Southern California Farm hold striped bass, *Morone saxatilis*.

As indicated in Figure 4, the routine includes the processes of ingestion, egestion, assimilation, respiration, excretion, and growth. Carbon, nitrogen, and oxygen fluxes are all computed, and of course the rates of these fluxes vary with operational and environmental conditions. The operational independent variables are listed above while the environmental variables that determine metabolism are:

- Water temperature.
- Ambient oxygen concentration which is one of the determinants of the concentration of oxygen with a cage.
- Ambient current velocity, which is another determinant of oxygen concentration within the cage as well as a determinant of the respiration rate required of the fish to swim at a speed in order maintain their position within the cage.
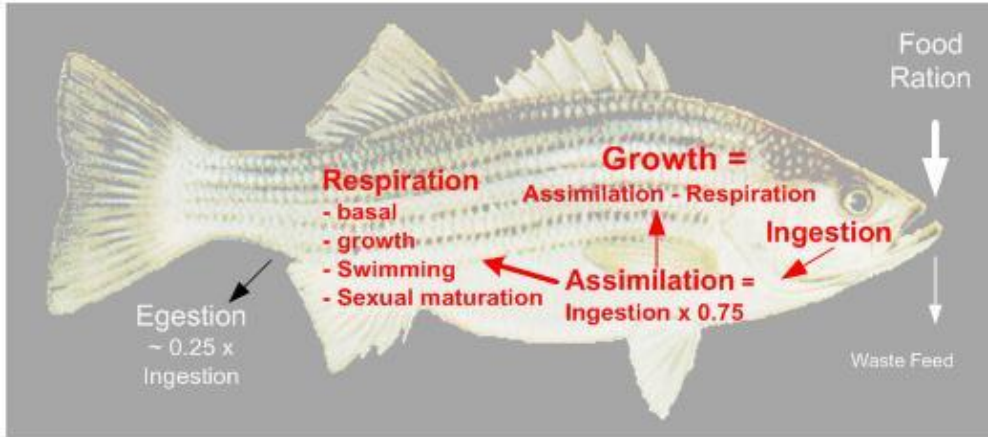
Figure 4: Metabolic processes described by our metabolic routine for fish metabolism. (*Background drawing by Duane Raver, USFWS*).

The striped bass routine consists of a series of functions describing the fluxes of carbon, nitrogen, and oxygen as determined by the basic features of metabolism, ingestion, egestion, assimilation, respiration, and growth. Specifically, each element is tracked according to these 5 basic features, which are related to each other by conservation of mass:

1. ingestion rate = egestion rate + assimilation rate
2. rate of growth = assimilation rate - rate of respiration
3. respiration rate = resting rate of respiration (i.e. basal) + respiration rate of activity (i.e. swimming) + respiration rate of anabolic activity (i.e. growth)
4. rate of feces production = egestion rate
5. rate of loss of uneaten feed = feed rate – ingestion rate

The functions for the 5 basic metabolic processes can be summarized as follows. Ingestion rate is determined by both the rate of supply of food and rate at which the fish can assimilate ingested food (Process 1). If the rate of supply of food exceeds the sum of the rate of egestion and the rate of assimilation, then a fraction of the food will be uneaten and contribute to the particulate waste produced by the cage (Process 5). Egestion is assumed to be a fixed fraction of ingestion; the value of this fraction is determined largely by the nutrient composition of the feed. The rate of egestion is in fact the rate of feces production (Process 4). The assimilation rate of the fish will be a function of the size (age) of the fish, the temperature of the water, and the concentration of oxygen within the cage. The assimilated nutrients are then either consumed by respiration or contribute to the growth of the fish (Process 2). Note that we assume that there are no reproductive demands within the cage. The rates of respiration, which include both the

consumption of oxygen and excretion of nitrogen, are determined by three processes, basal metabolism, swimming metabolism, and anabolic metabolism demanded by growth (Process 3). Basal metabolism is a function of water temperature and the size of the fish, swimming metabolism is a function of the fish size and its swimming speed, and anabolic metabolism is proportional to growth rate. The growth rate of the fish is simply calculated by subtracting the rate of respiration from the rate of assimilation.

Information on *Salmo salar* and *Morone saxatilis* metabolism that we used to determine the values for coefficients found in the system of equations for the two species came from a number of sources including publications of growth and metabolism in the laboratory and field (see our references), reports provided by our collaborators, and FishBase, which distributes data over the Internet on morphometrics, respiration rates, growth rate, and in some cases gill surface area. Data from these sources were used to tune the equations of the metabolism by searching for coefficient values that provided the best fit to the data. Because of its commercial value, *Salmo salar* has been thoroughly studied, and data for tuning is comprehensive. *Morone saxatilis* is less studied and our review of the literature included information for wild stocks (e.g., Hung et al. 1993, Chesney et al. 1993, Duston et al. 2004) as well as stocks by our collaborators at the Hubbs Sea World Research Institute. Examples of the goodness of fit between routine predictions and measurements for both species follow *(*Rensel, et. al., 2006).

 Figure 5 compares our routine predictions (dashed lines) of the growth of sockeye salmon, *Oncorhynchus Nerka*, with laboratory measurements (continuous lines) at different temperatures and feeding rates (Brett, 1964). The accuracy of predictions is also good. The growth rates are in units of the fractional change in body weight per day, and the feed rates of 0.06, 0.03 and 0.015 are in units of fractional body weights of food per day. Note that the routine accurately predicts the decreases in the temperature of optimal growth with decreases in feed temperature. The predicted growth rates are calculated from the functions describing all the physiological aspects shown in Figure 4. We wish to acknowledge here the importance of the measurements and concepts of Brett and co-workers in designing our routine (Brett, Shelbourne, and Shoope, 1969; Brett and Zala, 1975; Brett, 1976).
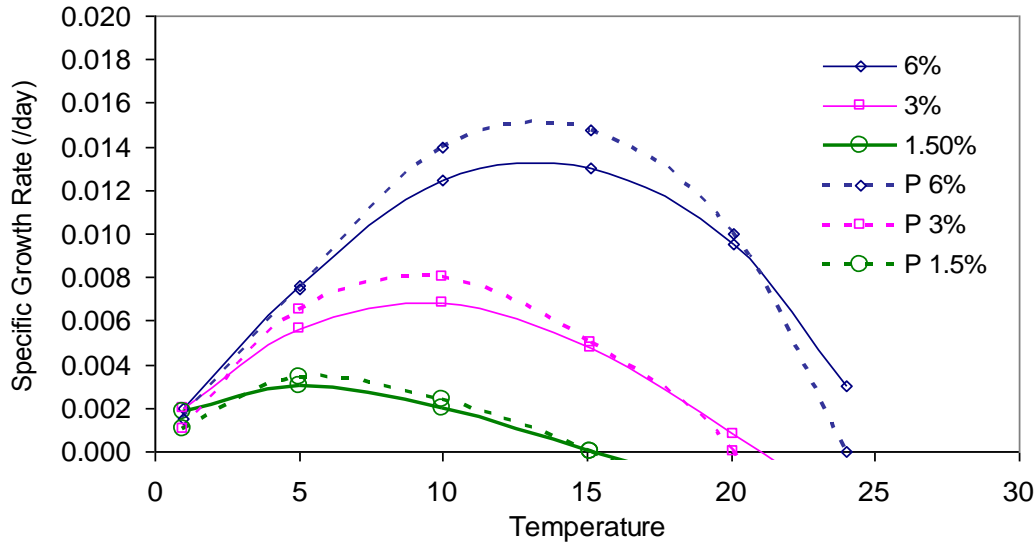
Figure 5: Predicted (dashed line) and measured (continuous line) specific growth rates for sockeye salmon grown at different temperatures and feed rates. The specific growth rates are the daily fractional change in fish weight and the feed rates in the upper right corner are the daily fraction of the fish weight provided by dry feed. The fish weights are about 200 g (Brett, 1964).
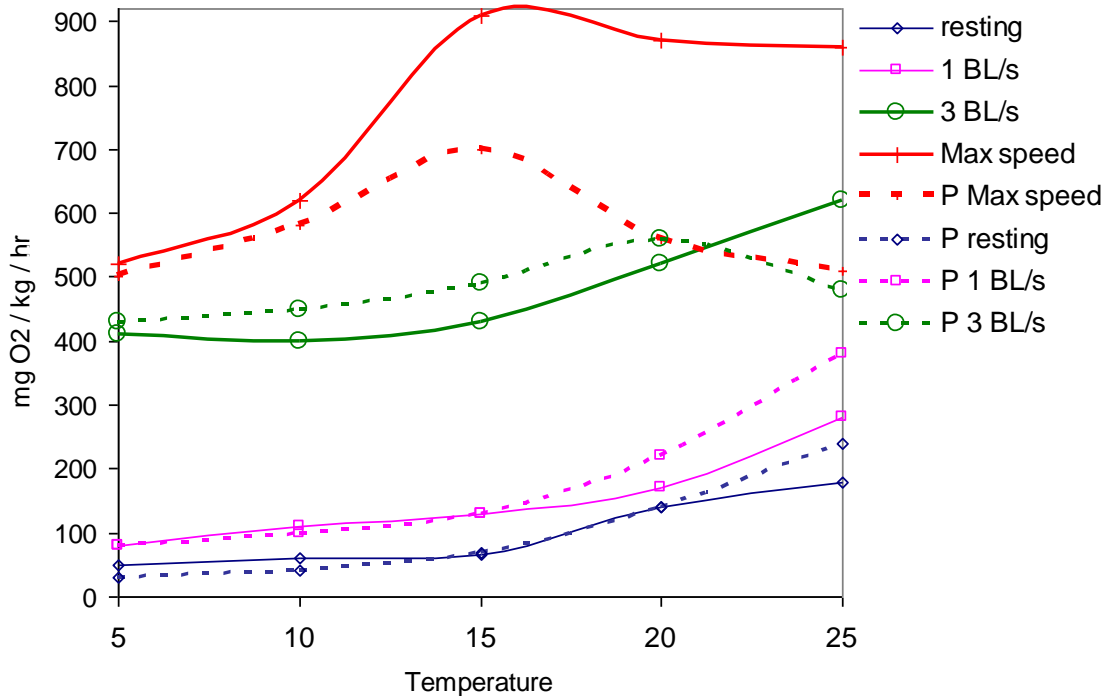
Figure 6: Predicted (dashed lines) and measured (continuous lines) respiration rates for sockeye salmon grown at different temperatures and swimming speeds. The respiration rates are in units of mg O2/(kg fish wet weight* hour) and swimming speed is in units of body lengths per second. Fish weights are about 200 g (Brett, 1964).

Figure 6 shows predicted (dashed lines) and measured (solid lines) respiration rates for young

sockeye salmon swimming at different speeds (legend) and at different temperatures (abscissa).

The swimming speeds found in the legend are in units of body lengths per second. Although our model describes steady state conditions as opposed to the short time interval during which the measurements was made, the fit is still good except at maximal swimming speeds.
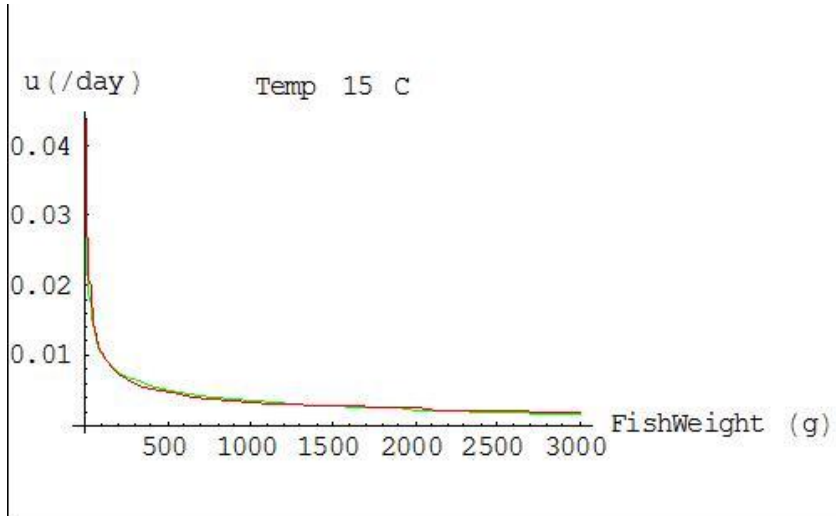
Figure 7: The specific growth rate of striped bass of differing size (age). The red line is calculated from the von Bertalanffy growth curve found in FishBase and the (almost exactly superimposed) green curve is the predicted growth rate under optimal culture conditions from the AquaModel fish metabolism routine.

Figure 7 is a third example of the performance of the fish metabolism routine, in which the calculated specific growth rate of *M. saxatilis* plotted against the weight of the fish over time. Two curves are plotted; one is results of calculations with our AquaModel routine and the other is derived from the von Bertalanffy growth curve (von Bertalanffy, 1960). The two curves fall nearly perfectly on top of each other. The fish metabolism routine was calculated for fish that are well fed, at rest, and cultured in water that is aerated and at a temperature of 15 °C.

2.4. Plankton Routine

The plankton routine describes the cycling by plankton of nitrogen and oxygen within each element of the array, both within the farm and the surrounding waters. This model is similar to the PZN models that have been published by Kiefer and Atkinson (1984) and Wroblewski, Sarmiento, and Flierl (1988). The "master" cycle describes the transforms of nitrogen between three compartments, inorganic nitrogen, organic nitrogen in phytoplankton, and organic nitrogen in zooplankton. The three biological transforms are:

- Photosynthetic assimilation of inorganic nitrogen by phytoplankton which is a function of

temperature, light level, DIN (dissolved inorganic nitrogen consisting of ammonia, nitrite and nitrate) concentration.

- Grazing by zooplankton on phytoplankton which is a function of temperature and concentrations of zooplankton, and phytoplankton.

- Excretion of DIN by zooplankton, which is a function of temperature and the concentration of zooplankton.

All three components are transported by advective and turbulent flow as described above. The model displays predator-prey oscillations, which dampen over time and reach a steady state. The default simulations for DIN, phytoplankton, and zooplankton stabilize at roughly 1 mg-at N m^{-3}, for all 3 components respectively. In order to calculate the concentrations and rates of loss by respiration and production by photosynthesis, we have assumed a constant flux ratio of oxygen to nitrogen of 6 moles O_2 gm-at N, consistent with the Redfield ratio. The inputs to this model consist of the time series of exchange coefficients produced by the hydrodynamic model, surface irradiance, and water temperature as well as concentrations of dissolved oxygen, dissolved inorganic nitrogen, cellular nitrogen in phytoplankton and zooplankton. Outputs of this model consist of a time series of the concentrations of dissolved inorganic nitrogen and oxygen, phytoplankton (traced as chlorophyll), and zooplankton. This routine provides estimates of the response of the planktonic community to the discharge of nitrogenous nutrients from fish farms. Specifically, it focuses on the question of whether such discharges can initiate phytoplankton blooms.

Figure 8 is a schematic of the plankton routine. During the simulation, this subroutine runs within each cell of our 3-dimensional computational grid. As shown, the subroutine calculates within each cell transformations of two tracers, nitrogen and oxygen, by the planktonic community. In fact the concentrations of oxygen and nitrogen within each cell vary with time because of both the local transformations with each cell and the vertical and horizontal transport of these elements among cells.

Although oxygen is shown as two components, atmospheric oxygen and dissolved oxygen in seawater, we assume that the concentration of atmospheric oxygen remains at a constant value of 0.209 atmospheres (i.e., the normal sea level concentration of oxygen as about 21% of air), and thus only the concentration of dissolved oxygen varies with time. For computational cells at the

sea surface, local variations are caused by the rate of exchange across the air-water interface (indicated by the blue horizontal line) and rates of photosynthesis by phytoplankton and respiration by zooplankton. Below the sea surface, local changes are caused only by the rates of photosynthesis and respiration. The routine consists of five components: atmospheric oxygen, dissolved oxygen, phytoplanktonic nitrogen, zooplanktonic nitrogen, and dissolved inorganic nitrogen. The concentrations of inorganic nitrogen and oxygen will vary with environmental conditions as well as rates of fish metabolism within the fish pens and transport from the pens. The routine includes descriptions of the influence of temporal and spatial variations in temperature and light on rates of photosynthesis and grazing. The description of light intensity includes calculations of the concentration of chlorophyll within the water column and its influence on the diffuse attenuation of downwelling irradiance. The routine also includes a tuning algorithm to obtain values for the coefficients for zooplankton grazing and excretion that provide a best fit to field measurements of concentrations of phytoplankton, zooplankton, and nutrients.
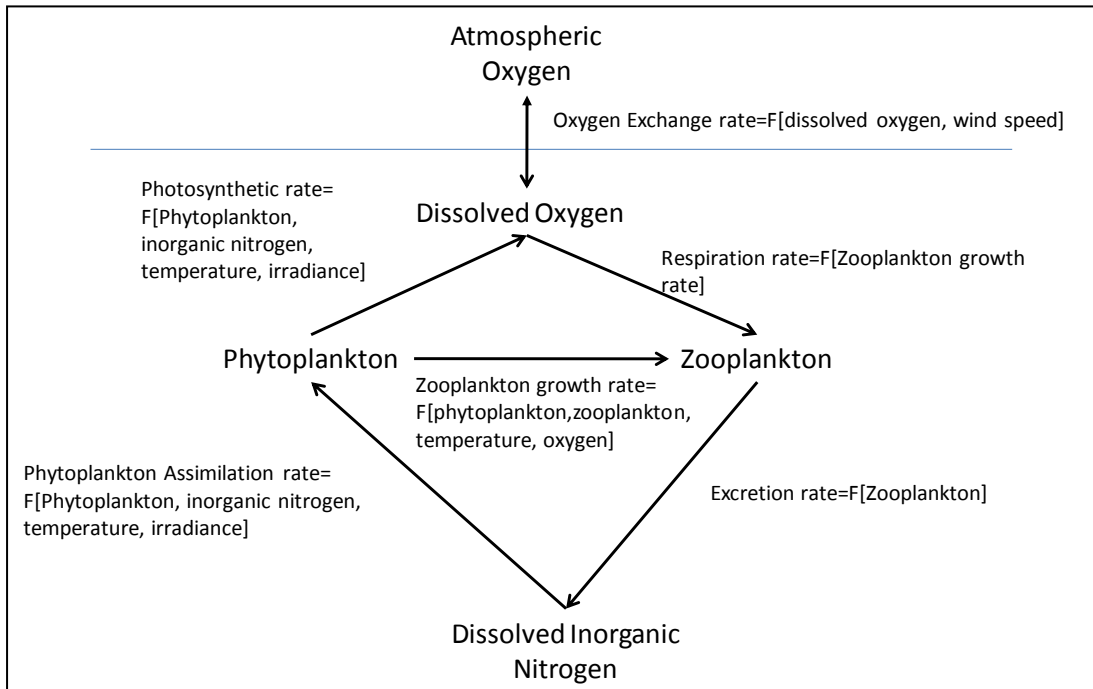

Figure 8: Processes and components of the AquaModel plankton routine. Processes include oxygen exchange across the air-sea surface (but of course not in the computation cells below the surface), the cycling of nitrogen by phytoplankton, zooplankton, and dissolved inorganic nitrogen, and the biological production and consumption of oxygen associated with the cycling of nitrogen.

Figure 9 shows an example of the dynamics of the plankton routine when it is tuned to the conditions in the Southern California Bight. This simulation shows the response of the phytoplankton and zooplankton community to a sudden increase in dissolved inorganic nitrogen in a closed system in which there is neither transport of material in nor out of the system. The conditions within the system are those of the summer upper mixed layer several kilometers off the San Diego coast: because of warm water and high irradiance in a shallow mixed layer the growth rate of phytoplankton is only limited by nutrient concentration.

During the first 20 days of the simulation the planktonic community is in a nutrient-limited, steady state in which the concentrations of dissolved inorganic nitrogen, phytoplankton nitrogen, and zooplankton nitrogen are 0.2, 0.3, and 0.4 mg-at N/m^3, respectively. On day 20 the concentration of dissolved inorganic nitrogen is suddenly increased from 0.2 to 4.4 mg-at N/m^3. This increase in the limiting nutrient stimulates a phytoplankton bloom that assimilates the excess nutrient within a week. This bloom then quickly grazed by the zooplankton, and a new steady state is established by the end of the simulation in which the concentrations of nutrient, phytoplankton, and zooplankton are 0.2, 2, and 3.5 mg-at nitrogen/m^3, respectively.

This simulation is provides a sense of the type of plankton response one might expect within the nutrient enriched plume downstream of a very large commercial fish farm, provided that there is no dispersion of the plume as it is transported from the site. In fact, given the time scales of the plankton response, the mixing of the plume with ambient waters will greatly reduce concentrations within the plume well below the values shown in this figure.
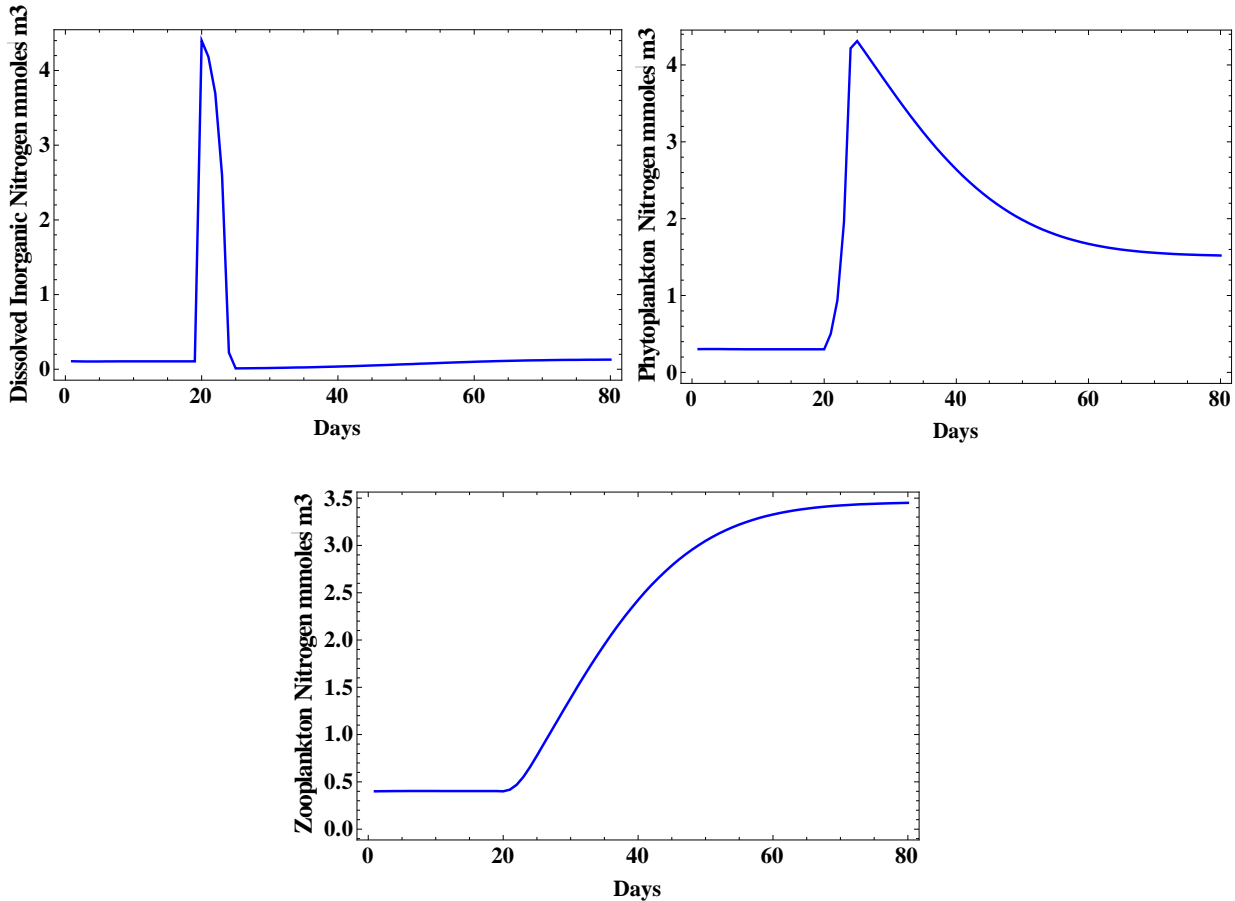
Figure 9: A simple simulation of the plankton routine for a closed system in which there is no transport of material into or out of the system. The environmental conditions are constant during the 80 day simulation except that on day 20 the concentration of dissolved inorganic nitrogen is suddenly increased from 0.2 to 4.4 mg-at N/m^3. This increase in the limiting nutrient stimulates a phytoplankton bloom and subsequently a zooplankton bloom.

Figure 10 is an example of the dynamics of the plankton routine when it is subjected to a simple tuning to the conditions at the Gulf of Maine site. It shows a one year simulation for a closed system in daily changes in the concentration of dissolved inorganic nitrogen is an input to the calculation. Here the phytoplankton and zooplankton communities respond to the large seasonal changes in the water temperature, nutrient concentration, mixed layer depth, and sea surface irradiance. A comparison of these calculated time series with field measurements at the Gulf of Maine farm found in this report indicates that the routine provides a reasonably good description of the spring and fall bloom of phytoplankton and zooplankton. The timing of the bloom and the variations in phytoplankton crop are good; however variations in zooplankton biomass are much too large. This is the consequence of assuming a closed, cycling system with only 3 components.
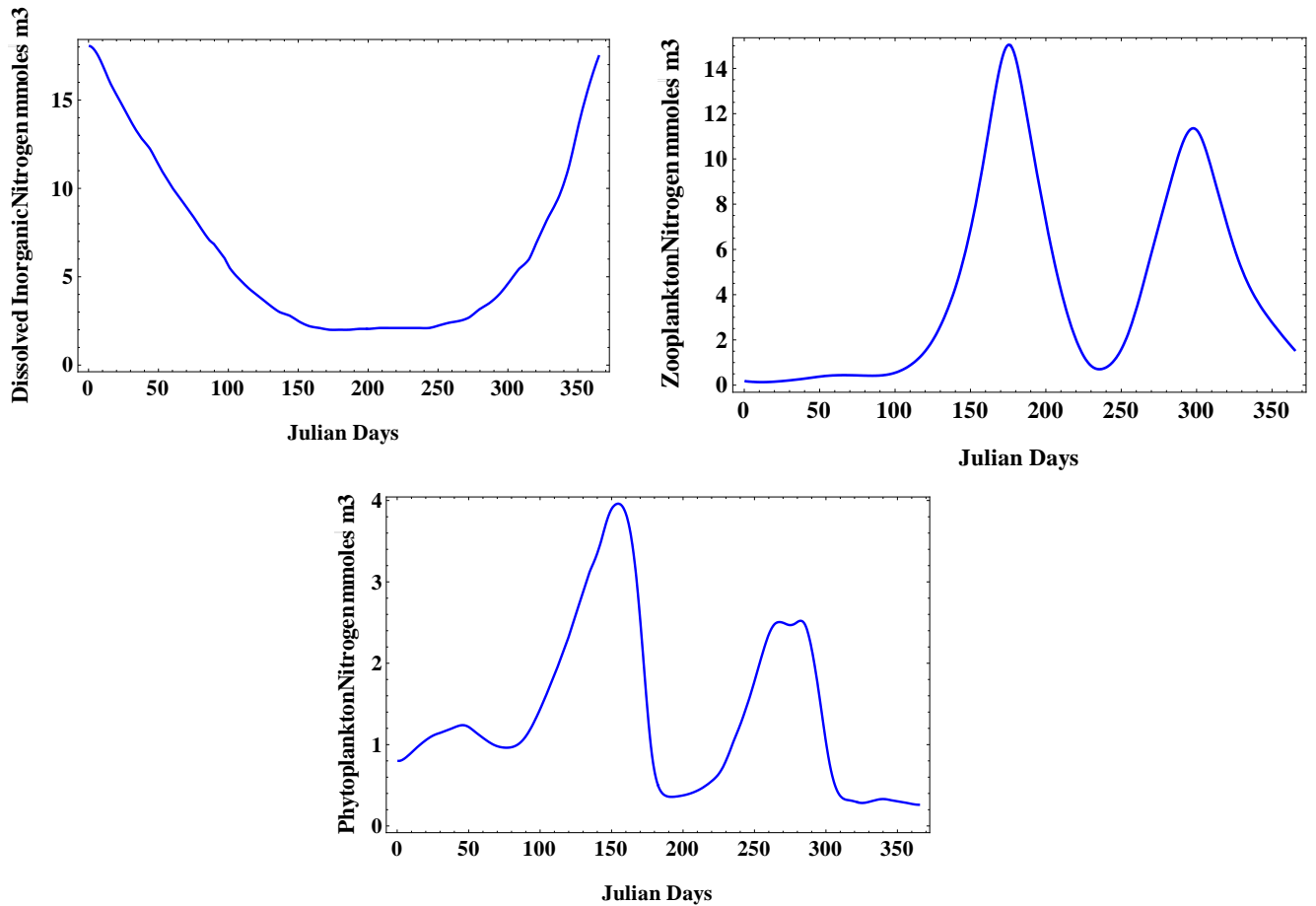
Figure 10. A one year simulation by the plankton routine for a closed system in which there is no transport of material into or out of the computational cell. A comparison of these calculated time series with field measurements at the Gulf of Maine farm found in sections 4.7- 4.8 indicates that the routine provides a reasonably good description of the spring and fall bloom of phytoplankton and zooplankton.

The tuning algorithm that is referenced above is executed by solving the system of differential equations found in the plankton routine for values of coefficients found in these equations. The solutions are obtain by assuming that there exists quasi-steady state conditions for the key dependent variables of the plankton routine, i.e., the concentrations of nutrients, phytoplankton, and zooplankton. Under such conditions one can solve for the value of unknown coefficients that provide a "best-fit" between calculated values the independent variable and values for these variables measured in the field. Tuning for the Gulf of Maine simulation matched predicted and measured values during the summer period when the concentrations of the three dependent variables were low and both the spring and fall periods of the phytoplankton bloom. Tuning for

the Southern California Bight simulation matched predicted and measured values during the summer period when the concentration of nutrients are low and zooplankton high and the winter period when the concentration of nutrients are high and zooplankton low.

The development and application of the tuning algorithm provided us with information on the sensitivity of calculated values for the dependent variables to uncertainties in the values for independent environmental variables such as water temperature, current flow, and nutrient concentration as well as uncertainties in the value of coefficients. In the case of the plankton routine it appears that predictions are most sensitive to the values of such environmental variables as vertical and horizontal eddy diffusivity, mixed layer depth, water turbidity, and primary and secondary macronutrient concentrations. Coefficients most critical to accurate predictions are those that describe zooplankton dynamics. These are the two scalar coefficients that determine specific rates of grazing and excretion and the two exponential coefficients that describe the variation in the specific rates of grazing and excretion with the size of the zooplankton biomass. Finally, the sinking rate of the phytoplankton, which we have set to zero in our simulations, is most important. Unfortunately, the values for most of these parameters are difficult to measure and predict.

2.5. Benthic Routine

The benthic loading component of our model is based upon several literature citations and functions found in the existing, previously-verified DEPOMOD model (Cromey et al. 2002 a &b; Cromey, Provost, and Black, 2003; Cromey and Black, 2005) that in turn was based on the G-model of carbon degradation (Westrich and Bernier 1984; see also Panchang, Cheng, and Newell, 1997; Brooks and Mahnken, 2003). DEPOMOD is presently the international standard for assessing the impact of loading of organic carbon in sediments underlying fish farms and in some countries calculations with the code are a requirement for obtaining fish farm permits. Since DEPOMOD only addresses the transport of particulate waste from the pens to the sediments, we have written a more comprehensive environmental description of fish farms that includes waste production within the pens, transport from the pens to the sediments, and the biochemical response of the benthic community to waste deposition.

As uneaten feed and feces produced by fish in each cage sink through the water column, they are transported downstream of the cage. Since uneaten feed pellets are larger and denser than feces,

the routine tracks both uneaten feed and feces. Not only will these different classes of particles sink at different rates and be transported at different distances from the farm, but also when they reach the bottom boundary layer their shear thresholds for deposition and resuspension will also differ, leading to further separation. Eventually, both uneaten feed and feces will either be consumed by the benthos or consolidated into the sediments and no longer subject to resuspension. Thus, AquaModel has three categories of particulate waste within the sediments, uneaten feed, feces, and consolidated waste.

2.6. Physical Description of Deposition

As illustrated in the Figure 10, we have simplified the formulation of physical processes. This was required because simulations running on a PC became too time-consuming or mathematically unstable with a more detailed formulation. For each time step the waste particles produced in the farm are "collected" as "capsules" that sink through the water column at a rate determined from measurements in the laboratory. These capsules are shown as brown dots in the figure. As these capsules sink, the ambient currents transport them through the 3-dimensional array of cells. This is somewhat analogous to water moving through an unsecured garden hose that is in continual motion but in this case is driven by variations in current velocity and direction. The waste particles are however not subject to turbulent dispersion as is the case for the dissolved wastes. As the capsules near the bottom the waste particles are "released" and evenly distributed into the cells of the suspension layer as indicted in Figure 10. This array of cells consists of a single layer that lies immediately above the sediment surface. The length and width of these computational cells are the same dimensions as the cells within the overlying water column, but their depth is user selectable. In the case of the demonstration farm, we have chosen a depth of 1 meter. Once released into the suspension layer the particles are now treated as suspended particles and subject to both advection and turbulent dispersion.
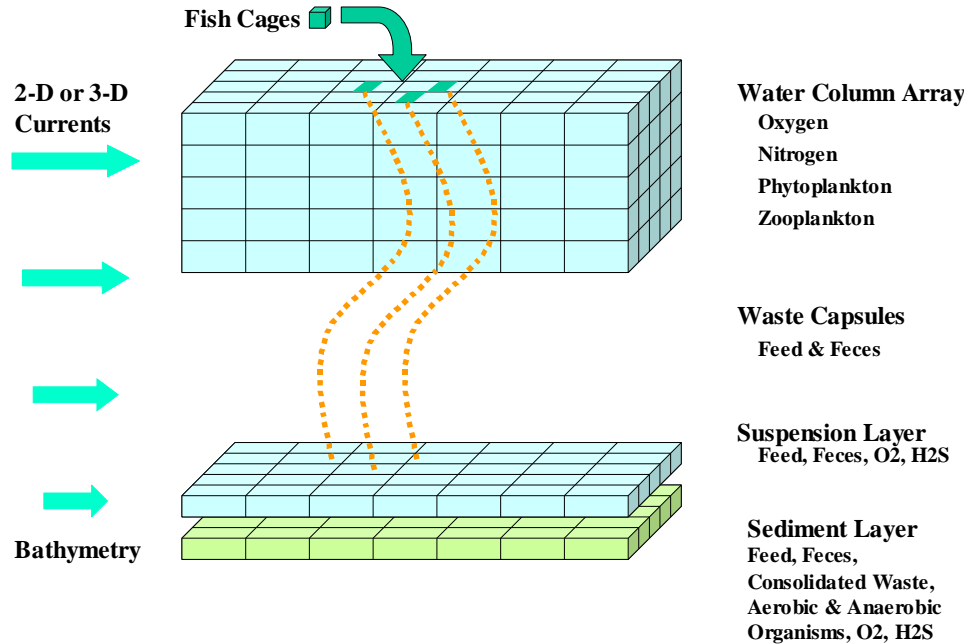
Figure 10: The physical layout of the transport and deposition of particles in the benthic routine. Fish wastes consisting of uneaten feed and feces are transported by advection to the suspended layer that is immediately above the sediment layer. Depending upon the shear at the sediment surface waste particles within the suspended layer will either remain suspended and transported within the suspended layer or deposited in the sediments. The value of shear at the interface will also determine whether waste particles in the sediment layer will remain there or be resuspended into the suspended layer.

Once particles reach the "suspension layer", the routine executes the formulations of DEPOMOD (Cromey et al. 2002a, 2002b) to calculate whether these particles stay in suspension and transported further from the pen or deposited in the sediments. According to these formulations, waste particles in the suspension layer are deposited into the sediment layer when shear between the sediment and the bottom water falls below a threshold value (See also Fox, 1988). The rate of deposition increases with the concentration of particles in the layer and with decreases in shear. On the other hand when shear at the interface exceeds a threshold value, waste particles in the sediment layer will be resuspended into the suspension layer and thus subject to further transport and dispersion from the site. The thresholds for deposition and resuspension differ with the size, density, and stickiness of the particles and thus will differ between feed and feces. When shear at the bottom falls between the threshold for deposition and the threshold for resuspension, the particles in the suspension layer will be remain in suspension and thus transported further from the pen.

Finally, wastes deposited in the sediment will compact into organic particles that are no longer subject to resuspension. Cromey and his co-workers have derived a function for this process in which compaction begins at a given rate after a 4 day delay. We have on the other hand chosen a simple first order rate function in which a fixed fraction of the mass of feed and feces in the sediments consolidates each day.

2.7. Biochemical Processes in the Benthic Community

The 3 types of waste found in the sediments, uneaten feed, feces, and consolidated feed and feces are to varying degrees energy and nutrient sources for the benthic community, which consist of both macroscopic and microscopic organisms. Although the compounds found in feed and feces will consist of refractive and labile fractions, we have assumed in our simulations that all compounds are labile. We feel that this is a worst case assumption. Thus, at a given time, the concentration of waste in the vicinity of a farm will depend upon the previous physical processes of deposition and resuspension as well as the previous biochemical processes of growth and remineralization by the benthos. As shown in Figure 10, we treat the sediment layer as a single layer; this is despite the fact that vertical profiles within sediments indicate sharp, predictable biological and chemical gradients. In our simulations we have chosen a depth interval of 2 cm for each cell of our sediment array. This depth was chosen because it is the standard depth for sediment monitoring (core collection) in and around fish cages in many North American jurisdictions. The length and width of these cells are the same as those within the water column and the suspension layer. Our functions provide predictions of average biological and chemical conditions within the layer.

Describing the complexity of biochemical processes within the sediments has challenged marine scientists, and the models that have been developed (including ours) are relatively crude and lack comprehensive testing. Despite these limitations, field data describing benthic responses to variations in organic loading of the sediments show clear understandable patterns, and that when tuned to local conditions models such as the pioneering G-Model of Westrich and Bernier (1984), can provide good quantitative estimates of the response.

Figure 11 shows the components and processes that are described by our benthic routine. These components consist of dissolved compounds, oxygen, sulfate, hydrogen sulfide, carbon dioxide, which flow between the suspension and sediment layers by diffusion. These components also

include particulate organic carbon (POC) produced in overlying waters from farm waste or the planktonic community. Finally, they include two communities within the benthos, the community of aerobic species that respire only oxygen and the community of anaerobic species that respire sulfate. Although these communities consist of both macroscopic and microscopic species, it is our view that the biochemical transformations shown in Figure 11 are largely mediated by microbes.

These dissolved compounds will be transported across the sediment-water interface depending upon both their diffusivity and the size of the concentration gradient at the interface. The same can be said for their transport within the sediment. The local concentration gradient will depend upon local rates of metabolism by the benthos as well as diffusivity. Furthermore, diffusivity itself will depend upon the porosity of the sediment, temperature, and the chemical properties of the compound.

The aerobes respire dissolves organic compounds released from the particulate organic material and oxygen in order to grow and meet other metabolic demands. The main by-products of their metabolism are carbon dioxide and water. If either the concentration of oxygen or POC decreases below saturating concentrations, rates of growth and respiration will decrease. Furthermore, at the lower extremes of oxygen or POC availability, aerobe growth will stop and respiration will be reduced to a basal level.   The anaerobes, which here consist only of the sulfate reducing micro-organisms, respire POC and sulfate in order to grow and meet other metabolic needs. The main by-products of their metabolism are carbon dioxide and hydrogen sulfide (or other reduced sulfur compounds). If either the concentration of sulfate or POC decreases below saturating concentrations, rates of growth and respiration will decrease. Additionally, at the lower extremes of oxygen or POC growth will stop and respiration will be reduced to a basal level. If produced at a sufficient rate the hydrogen sulfide produced by anaerobes will inhibit the growth of the aerobes. On the other hand, oxygen inhibits the growth of the anaerobes.
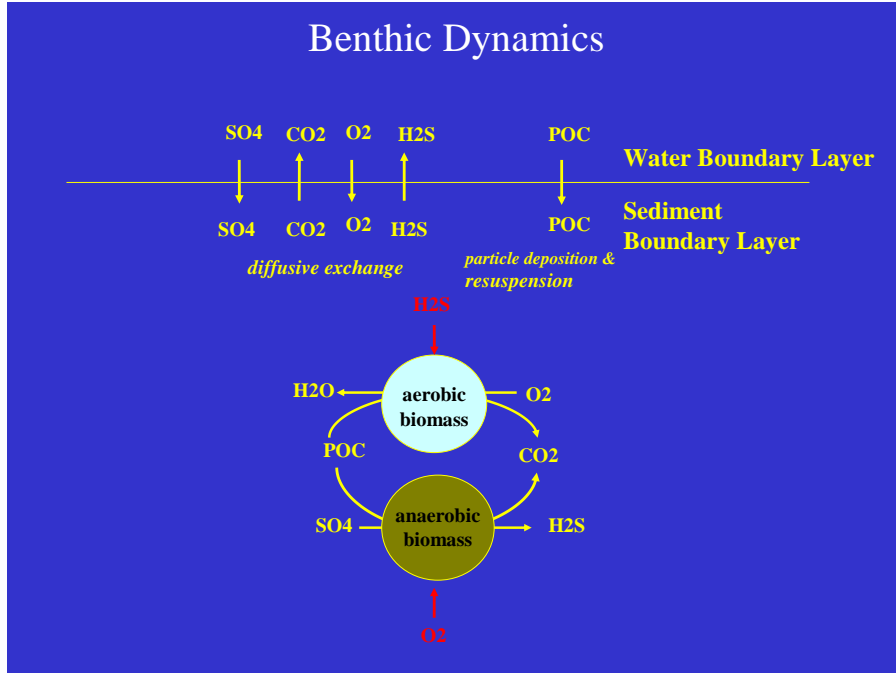
Figure 11: The biochemical components and transformations of the benthic routine. The transformations are mediated by two communities consisting of aerobic and anaerobic species. These two communities compete for organic carbon supplied by particulate organic carbon (POC) produced in the farms and plankton communities in the overlying water column. The rates of assimilation by these two communities will depend upon the supply of POC, the biomass of the two communities, and the concentration of respiratory substrates (here limited to O_2 & SO_4) and metabolic inhibitors (O_2 and H_2S) of the two communities.

It is clear from Figure 11 that the size and growth rate of the aerobes can be limited by the supply of oxygen from the overlying water column. In our routine the rate of supply of oxygen to the sediments is determined by the diffusion of oxygen from the suspension layer into the sediment layer, and the rate of diffusion will be determined by the difference in the concentration of oxygen in the suspension layer and the sediment layer, the thickness of the diffusion boundary layer at the interface:

$$JO2 = \frac{O2DiffCoef[temperature] * (O2\ suspended - O2sediment)}{Z[velocity]}$$

Here JO_2 is the flux of oxygen into the sediment layer, O_2DiffCoef is the diffusion coefficient of oxygen, which varies with temperature, O_2suspended is the concentration of oxygen in the suspended layer, O_2 sediment is the concentration of oxygen in the sediment layer a, and Z is the thickness of the diffusion boundary layer, which is less than a millimeter in most open waters, and as indicated varies with the velocity of flow in the suspended layer. If the current speed in

the suspension layer increases the thickness of the boundary layer will decrease and the rate of diffusion will increase. The concentration of oxygen in the sediments is in steady state such that the rate of oxygen consumption by the aerobes, which varies with the concentration of oxygen and the concentration of particulate organic carbon within the layer, is equal to the rate of oxygen supplied by diffusion.
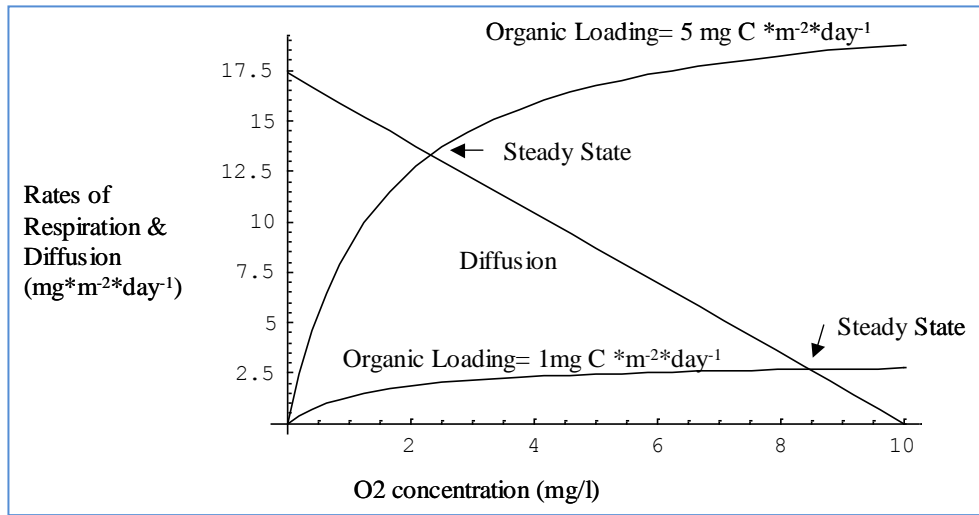

Figure 12: An example of the calculation of the relationship between the organic loading of sediments and the concentration of interstitial oxygen in the sediment layer. The abscissa is the O2 concentration in the sediment layer and the ordinate show the rate of diffuse of oxygen into the layer as well as the rate of aerobic respiration in the layer. The straight line is the steady rate of diffusion into the layer when the concentration of O2 in the overlying water is 10 mg/l. The 2 hyperbolic curves are the rates of aerobic respiration in the sediment for rates of loading of 1 and 5 mg carbon/(m2*day). The steady state conditions for the two rates are indicted by the arrow.

One should note that at each of the two steady states the growth rate of the aerobic community is zero and the community's respiration rate is basal. At the higher loading rate the aerobic community is much larger, but the steady state growth rate of the community is zero because of oxygen limitation. This limitation to aerobic growth allows the anaerobic community to grow by assimilating the flux of POC that is unassimilated by the aerobes. At the lower loading rate the aerobic community is much smaller, but the steady state growth rate of the community is zero because of the limited supply of POC. The growth of anaerobes remains check because of the high concentrations of oxygen.

A similar diagram and similar arguments can be presented for regulation by POC deposition and sulfate diffusion for the anaerobes. However, because of the high concentrations of sulfate in seawater, the rates of diffusion of sulfate into the sediments layer are sufficiently high to rarely

constrain the growth rate and biomass of the anaerobic community in the upper sediments. It is clear from this diagram that increases in organic loading decreases the concentration of oxygen in the sediments, thereby releasing anaerobic organisms from their oxygen limitation of growth. As a consequence, the biomass of anaerobes will increase and possibly competing for POC with the aerobes and producing hydrogen sulfide. The latter may inhibit the metabolism and growth of the aerobes. Consequentially, if the aerobic community declines, oxygen concentrations will increase inhibiting growth of the anaerobes. Such interactions will tend to drive the system toward a well defined steady state determined by the rate of organic loading, as well as the temperature, concentration of oxygen, and current velocity in the suspended layer above the bottom.

The differential equations that are found in the routine can be solved for steady state conditions in which the state variables of the routine are constant with time or solved during each time step of a simulation. The results of simulations for our New England and southern California studies will be shown in the sections that follow. Here we present an example of the behavior of the routine for steady state conditions. We then compare these results with field observations.

In Figure 13 we plot calculated concentrations of oxygen, hydrogen sulfide, and the biomass of aerobic and anaerobic species as a function of the rates of deposition of particulate organic carbon under conditions typical of those found under the Atlantic salmon farms of New England and British Columbia. In Figure 13A we see that the concentration of aerobic biomass in the upper sediment layer increases with deposition up to a rate of about 0.3 g carbon/(m^2*d); above this threshold it remains constant. In Figure 13B we see that the concentration of anaerobic biomass is 0 until deposition reaches a rate of about 0.3 g carbon/(m^2*d); above this threshold it increases linearly (not obvious on this log-linear plot) with deposition. In Figure 13C we see that the concentration of oxygen in the upper sediment layer is decreases with increases in deposition until it reaches a value of 2.38 mg O_2/m^3 at which deposition has increased to of about 0.3 g carbon/(m^2*d); above this threshold it remains constant. In Figure 13D we see that the concentration of POC in the sediments remains relatively constant at a value of about 270 g carbon/m3 over the range of deposition rates. This organic carbon is almost exclusively the refractive component with little nutritive value. The labile fraction particulate carbon is assimilated by the benthos. In Figure 13E we see that the concentration of hydrogen sulfide in the upper sediment layer is 0 until deposition increases to 0.3 g carbon/(m^2*d); above this

threshold it increases linearly with deposition (not obvious on this log-linear plot). In Figure 13 ^{o}F we see that the flux of O_2 g /(m^2*d) diffusing into the sediments increases with deposition until deposition reaches 0.45 g/(m^2*d); above this threshold it remains constant at a value of 50 g O2/(m^2*d).

Unfortunately, although there are abundant measurements of the concentration of organic carbon under fish farms, there have been very few direct measurements of the daily deposition of waste carbon. There are even fewer such measurements that have been supplemented by measurements of current velocity, the biomass of the communities of aerobic and anaerobic organisms, and concentrations and fluxes of oxygen, hydrogen sulfide, and carbon dioxide. The studies of Findlay and Watling (1997) and Chamberlin and Stucchi (2007) are not only comprehensive but also praiseworthy, and in fact the work of Findlay, Watling and co-workers has helped guide development of the benthic routine. In 1991 Findlay and Watling undertook a comprehensive study during summer grow-out of the benthic community beneath an Atlantic salmon farm off Swans Island, Maine (Findlay, Watling, and Meyer, 1995; Findlay and Watling, 1997). This study is important because it clear demonstrated that there is a critical threshold rate of waste deposition that determines the biochemical response of the benthic community. If rates of deposition are below this threshold the rate of growth and respiration of the community is sufficient to remineralize most if not all of the particulate organic material reaching the sediments. In short, below this threshold a steady state appears to be established in which the rates of organic carbon deposition are matched by the rates of release of respired carbon dioxide; neither organic waste nor biomass of the benthos will increase significantly. Above this threshold, this balance is lost and the rates of carbon dioxide release are much lower than the rates of organic carbon deposition. This imbalance appeared to reflect an increase in the biomass of the benthos and possibly an accumulation of waste carbon.
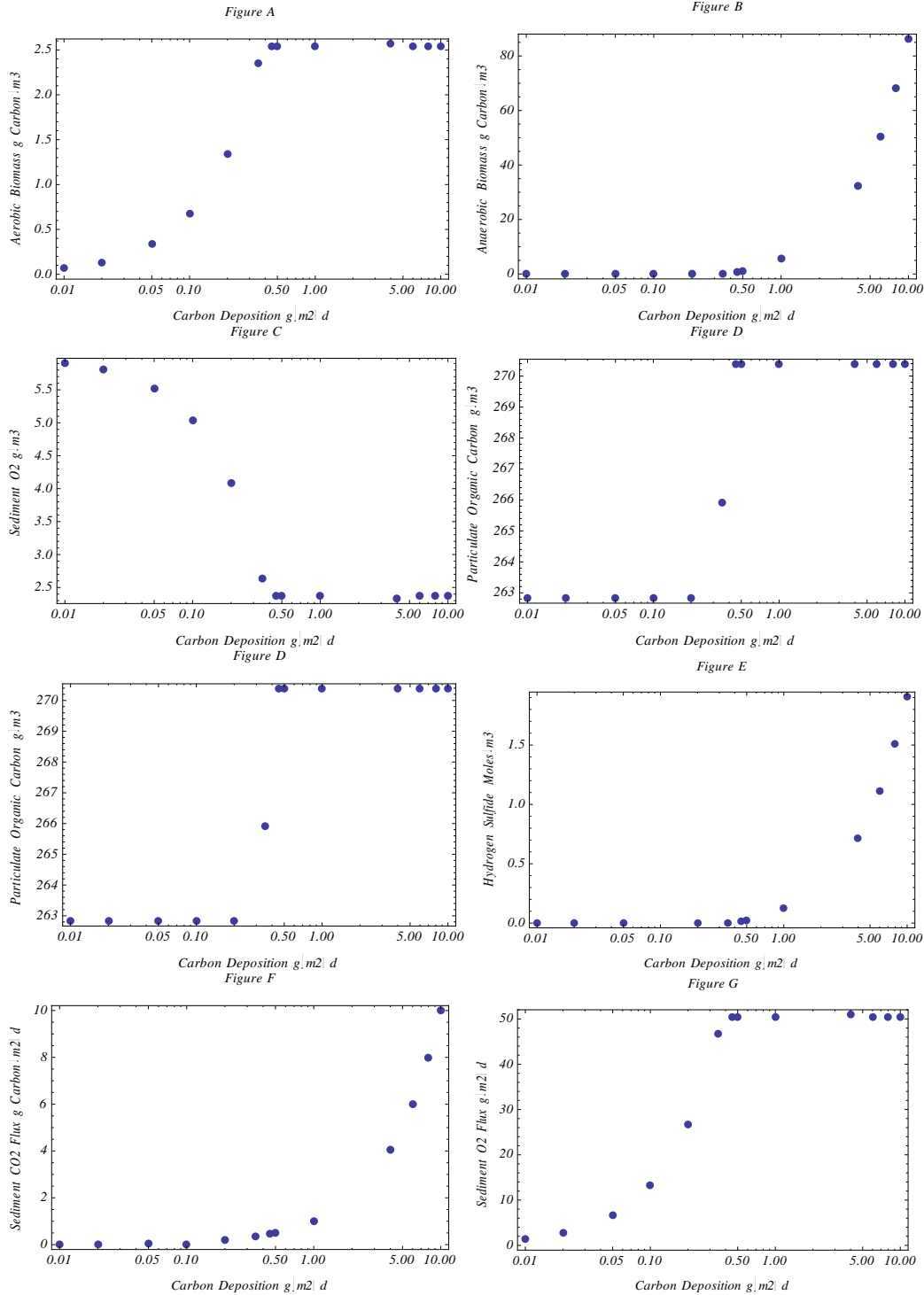
Figure 13: Steady state solutions of the benthic routine. The response of the benthic community to changes in particulate carbon deposition is plotted under conditions common to the sediments in Atlantic salmon farms in Maine and British Columbia. Figures A through G show in the upper sediment layer for the concentration of aerobic biomass, anaerobic biomass, O_2, particulate organic carbon (POC), and H_2S, respectively. Figures F and G show calculations of the flux of CO_2 out of the sediments and O_2 into the sediments over the range of deposition.
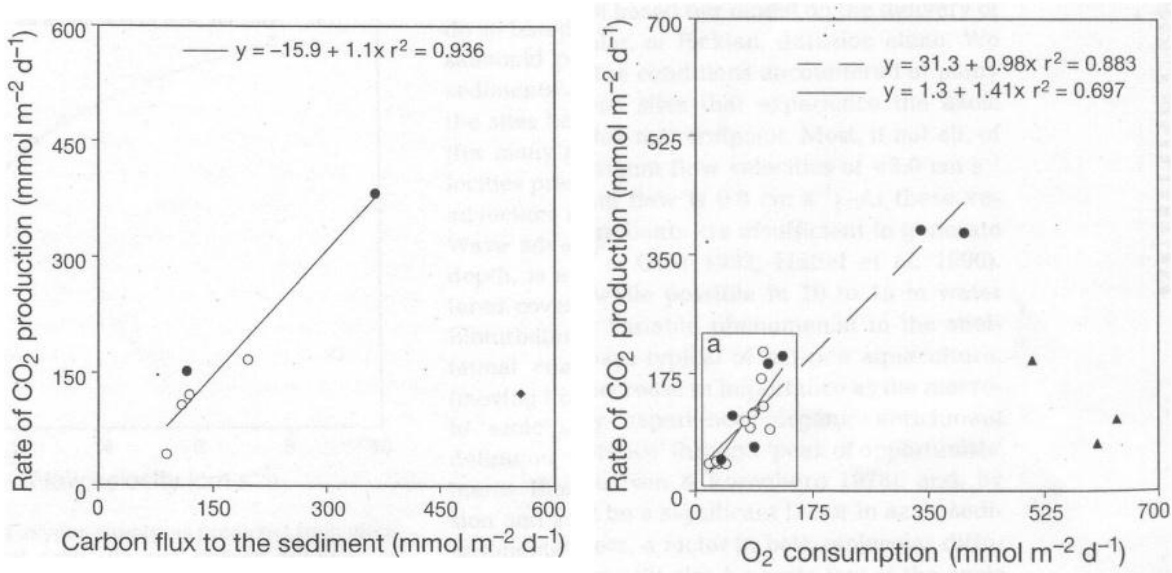
Figure 14: Field measurements of organic deposition, CO2 flux from sediments, and O2 flux into sediments collected during the growing season at an Atlantic salmon farm off Swans Island, Maine. The left graph shows the flux of particulate organic carbon to the sediments beneath the farm and the rate of CO2 release from sediment cores incubated in the laboratory. The right graph shows the respiratory stoichiometry of CO2 to O2 of sediment cores sampled during the growing season (Findlay and Watling, 1997).

Figure 14 summarizes their field measurements of organic deposition, CO_2 flux from sediments, and O_2 flux into sediments. The left graph shows the flux of particulate organic carbon to the sediments beneath the farm and the rate of CO_2 release from sediment cores incubated in the laboratory. At loading rates of less than 400 mmoles/m^2*day carbon deposition is roughly equal to respiration. The single point above this threshold indicates a net accumulation of organic carbon beneath the farm. The right graph shows the respiratory stoichiometry of CO_2 to O_2 of sediment cores sampled during the growing season. The expected ratio of 1.4 fell rapidly as rates of deposition exceeded the deposition threshold of than 400 mmoles carbon/m^2*day. This imbalance coincided with the sudden appearance and rapid growth of *Beggiatoa*, a Proteobacteria, that not only respires sulfide and oxygen but also fixes CO_2. Although itself a chemolithoautotroph, this species is key indicator of the development of a dominant anaerobic benthos. Its presence as a dense mat at the sediment surface explains both the drop in CO_2 release. The disappearance of respiratory stoichiometry for CO_2/O_2 may be explained by the onset of both anaerobic and chemioautrophic metabolisms.

Although the scales abscissa of Figure 13 is logarithmic and that of Figure 14 is linear, a careful comparison of the two figures indicates that general features of our benthic routine fits well with these field data. An examination of Figures 13F and 13G show calculated rates of CO2 release and O_2 assimilation as functions of organic deposition. In Figure 13F one sees that the benthic routine predicts that the respiratory release of CO_2 by aerobes at low rates of deposition combined with respiratory release of CO_2 by anaerobes at high rates of deposition will balance rates of carbon deposition over a broad range of deposition rates. We propose as do the authors that the presence of a threshold deposition at 400 mmoles carbon/m^2*day is set by the appearance and growth of *Beggiatoa* when the rates of production of hydrogen sulfide by anaerobes is sufficient to support colonization by this species. With the addition of a 3rd benthic component consisting of sulfide oxidizing autotrophs to our routine, such a threshold will emerge.

In Figure 13G one sees that O2 assimilation matches rates of carbon deposition up to a deposition threshold of 0.5 g carbon/m^2*day or 42 mmoles carbon/m^2*day; above this threshold the rate of O2 assimilation is fixed and no longer matches the increased rates of deposition. This is about 10-fold lower than the threshold measured in the study. Although large, this difference may be easily by a the differences between calculated and field variables such as the oxygen concentration of water at the sediment interface, the bottom current speed, the porosity of the sediments, and the biomass of epibenthic aerobic species.   We also note that the benthic routine was not tuned to the Swan Island study and adjustments in the values for several coefficients would certainly much improve quantitative predictions.

More recently Chamberlin and Stucchi (2007) have assembled time series field data on sediment conditions including concentrations of organic carbon and sulfide concentration, currents, and waste production at an Atlantic salmon farm in British Columbia. Simulations with DEPOMOD provided them with a corresponding time series of deposition rates beneath the farm which they then compared to their field measurements. Figure 15, which is one of their most interesting results, shows the relationship between sulfide concentration and organic carbon deposition. Their log-linear plot can be directly compared to the benthic routine's predictions shown in Figure 13E. The fit is good despite the fact that there was no tuning of the routine.
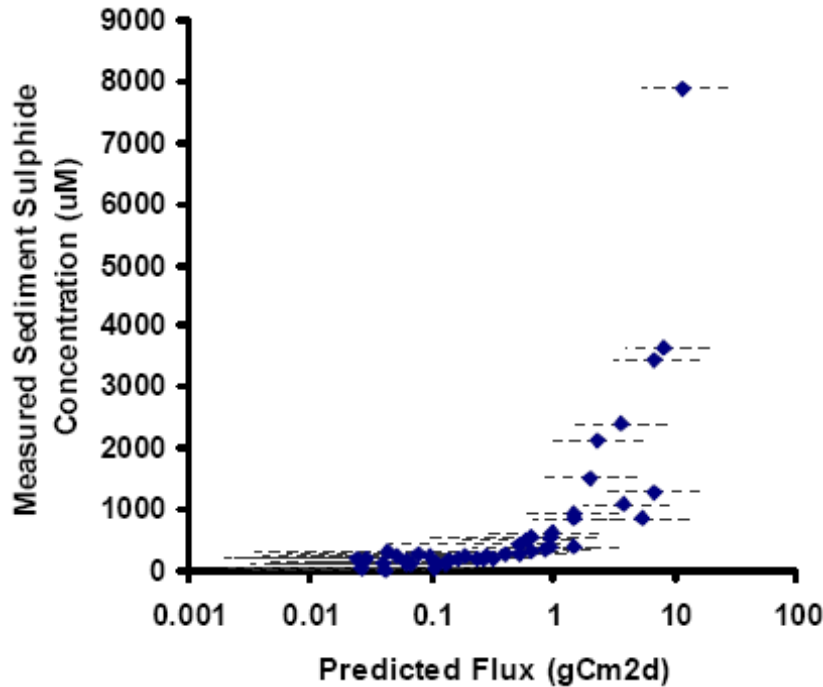
Figure 15: Field measurements of sulfide concentration in sediments and organic loading of sediments calculated with DEPOMOD under salmon farms in British Columbia (Chamberlin and Stucchi, 2007). The increase in sulfide concentration with deposition is an indication of increases of total metabolism of anaerobes in the surficial sediment layer. Comparisons of such field data with predictions by our benthic routine shown in Figure 13 indicate good agreement.

Because we have not yet obtained a comprehensive and diverse dataset on the benthic impact of fish farms, we have not been able to test the accuracy of our benthic routine much beyond the comparisons shown in Figures 13- 15. However, during the development of the benthic routine and its initial runs, we have been able to identify those environmental and mathematical parameters whose variation most influences the benthos. The most important physical parameters are the areal rate of waste production by the farm (in units of g waste/m^2*day),   current speeds throughout the water column and particularly the bottom layer, the depth of the water column, the oxygen concentration and temperature in the bottom layer, and the porosity of the sediments. The most important biochemical parameters are the values for threshold for deposition, erosion, and resuspension, the maximum specific assimilation rates of particulate organic carbon for aerobes and anaerobes, the half saturation constant for oxygenic respiration, and the half saturation constant for oxygen inhibition of anaerobic respiration.

This relatively long list of key parameters indicates that there is no fixed "short list" of critical variables that can be applied to fish farms of differing sizes and locations. According to our

routine, the dynamics of the benthic community is highly nonlinear because of thresholds and fundamental nonlinearities in the response of benthic species to the concentration of diverse electron donors and acceptors as well as their response to metabolic inhibitors. Because of this complexity we propose that accurate predictions of impact will require computations with models such as our benthic routine that have been tuned and validated.

2.8. Section References

Bertalanffy, L. von (1960). Principles and theory of growth, pp 137-259. In Fundamental aspects of normal and malignant growth. W. W. Wowinski, ed. Elsevier's, Amsterdam.

Brett, J.R. (1964). The respiratory metabolism and swimming performance of young sockeye salmon. J. Fish. Res. Bd. Can. 21:1183-1226.

Brett, J.R. (1976). Scope for metabolism and growth of sockeye salmon, Oncorhynchus nerka, and some related energetics. J. Fish. Res. Bd. Can. 33: 307-313.

Brett, J.R., Shelbourne, J.E. and C.T. Shoope. (1969). Growth rate and body composition of fingerling sockeye salmon, Oncorhynchus nerka, in relation to temperature and ration size. J. Fish. Res. Bd. Can.26:2363-2394

Brett. J.R. and C.A. Zala. (1975). Daily patterns of nitrogen excretion and oxygen consumption of sockeye salmon (Oncorhynchus nerka) under controlled conditions. J. Fish. Res. Board Can. 32:2479-2486.

Brooks, K. and C.V.W. Mahnken. (2003). Interactions of Atlantic salmon in the Pacific Northwest environment II: Organic Wastes. Fisheries Research. 62:255-293.

Chamberlain, J. & Stucchi, D. (2007) Simulating the effects of parameter uncertainty on waste model predictions of marine finfish aquaculture. Aquaculture 272, 296-311

Cromey, C.J. and K.D. Black. (2005). Modelling the impacts of finfish aquaculture. Chapter 7 in: The Handbook of Environmental Chemistry. Environmental Effects of Marine Finfish Aquaculture. Volume 5: Water Pollution. Springer, Berlin Heidelberg New York.

Cromey, C.J., T.D. Nickell, and K.D. Black. (2002a). DEPOMOD - Modelling the deposition and biological effects of waste solids from marine cage farms. Aquaculture 214: 211-239.

Cromey, C. J., T.D. Nickell, K.D. Black, P.G. Provost, and C.R. Griffiths. (2002b). Validation of a fish farm waste resuspension model by use of a particulate tracer discharged from a point source in a coastal environment. Estuaries 25: 916-929.

Cromey, C. P. Provost, K. Black. (2003). Development of monitoring guidelines and modelling tools for environmental effects from Mediterranean aquaculture. Newsletter 2. Scottish Association for Marine Science Dunstaffnage Marine Laboratory, Oban, Argyll, PA34 4AD, Scotland, UK

Findlay, R.H, L. Watling, and L. Mayer. (1995). Environmental Impact of Salmon Net-Pen Culture on Marine Benthic Communities in Maine: A Case Study. Estuaries Vol. 18, No. IA, p. 145-179.

Findlay, R.H, and L. Watling. (1997). Prediction of benthic impact for salmon net-pens based on the balance of benthic oxygen supply and demand Marine Ecology Progress Series 155:147-157.

3. Far Field Modeling of Open Ocean Aquaculture in the Southern California Bight

3.1. Background

Previously and upon request by the Hubbs SeaWorld Research Institute (HSWRI), we prepared and operated a model of a proposed open ocean site to be located about 5 miles (8 km) due west of Mission Beach in San Diego. The reader should refer to a technical report (Kiefer et al. 2008) for site specific details of a near field assessment of mostly benthic effects of a net pen site designed to rear striped bass (*Morone saxatilis*). The project had been envisioned as a demonstration farm, to assess the technical and environmental feasibility of offshore fish farming in the Southern California Bight. The plan was to initially monitor benthic or other effects of a small fish farm consisting of 8 individual 25 meter diameter cages to rear about 1,000 metric tons of striped bass. Eventually the farm was to be increased to 24 cages in order to reach an annual production of 3,000 metric tons. Striped bass are relatively widely distributed on the U.S. west coast and Mexico, ranging from northern Baja, California, Mexico to the Columbia River. The species has good fish cultural characteristics, market acceptability, and most importantly, seed stock was available in the Southwest U.S. Our prior study found that there would be little or no measurable benthic effect of the fish farm as proposed in terms of sediment total organic carbon or related effects. The application to install this farm was retracted sometime after submission because it was apparent that no decisions on how to manage offshore fish farms in the EEZ would be forthcoming from Washington D.C. in the near future.

This chapter focuses on the water column effects of eight relatively large fish farms spread over the open ocean waters of the southern portion of the Southern California Bight (SCB). <u>There is no proposal for these farms by any person or organization but we provide this assessment as a first step in understanding the opportunities and limitations of fish culture in this area</u>. The environmental conditions in this region vary greatly from that of the University of New Hampshire's offshore site.

Figure 16 represents the locations of the eight theoretical farms that are centered in the southern half of the SCB; the northern most fish farm is located roughly 50 km east of the south end of Santa Catalina Island and the southern-most farm is 10 km north of the proposed HSWRI project. Depths for most of the virtual farms are about 700 m, which would involve massive,

single point mooring arrays although the furthest south farm (Site H) is at 92 m depth and at the same depth and location of the previously proposed HSWRI site. Vectors in this figure are only indicative of a short time period of circulatory flow.

The purpose of this phase of our study was to evaluate pen aquaculture effects on phytoplankton communities and gain insight into the fate of waste nitrogen produced by the fish. Waste nitrogen can at some locations be useful for supporting aquatic and fisheries food webs but can also be harmful as a source of eutrophication at other locations that are usually characterized by shallow, nearshore, and poorly flushed waters. Undesirable, noxious or even toxic blooms may be embellished by waste discharges but on the other hand the open ocean has a tremendous capacity for organic and inorganic waste assimilation into the food web, and recent studies indicate that open ocean productivity has actually been declining for many decades (Boyce et al. 2010), although this analysis has been disputed in other, subsequent analysis. Moreover, open ocean nitrogen cycles appear to be disconnected from coastal ocean nitrogen dynamics because most riverine nitrogen that reaches coastal waters is denitrified before mixing with the open ocean (Galloway et al. 2004).

In our study we wished to evaluate the possible encroachment of net pen aquaculture wastes toward shallow and more sensitive nearshore waters that are already highly influenced by anthropogenic effects from runoff and other sources (e.g., Corcoran et al. 2010, inner Santa Monica Bay).

In order make this evaluation we coupled output form an existing Regional Ocean Model System (ROMS) provided by the Jet Propulsion Laboratory (JPL) in Pasadena, California with our plankton routine (described in section 2), and then run a simulation to map the distribution and fate of wastes from the farms. This was a preliminary exercise and not meant to be as exhaustive as the New Hampshire evaluation in this report. The simulation was only for one month using regionally specific on water quality from quarterly California Cooperative Oceanic Fisheries Investigations (CALCOFI) data reports and JPL's circulation out for May, 2007. Examination of the CALCOFI reports indicates that unlike the Gulf of Maine, seasonal variations in coastal conditions in the SCB are minor.
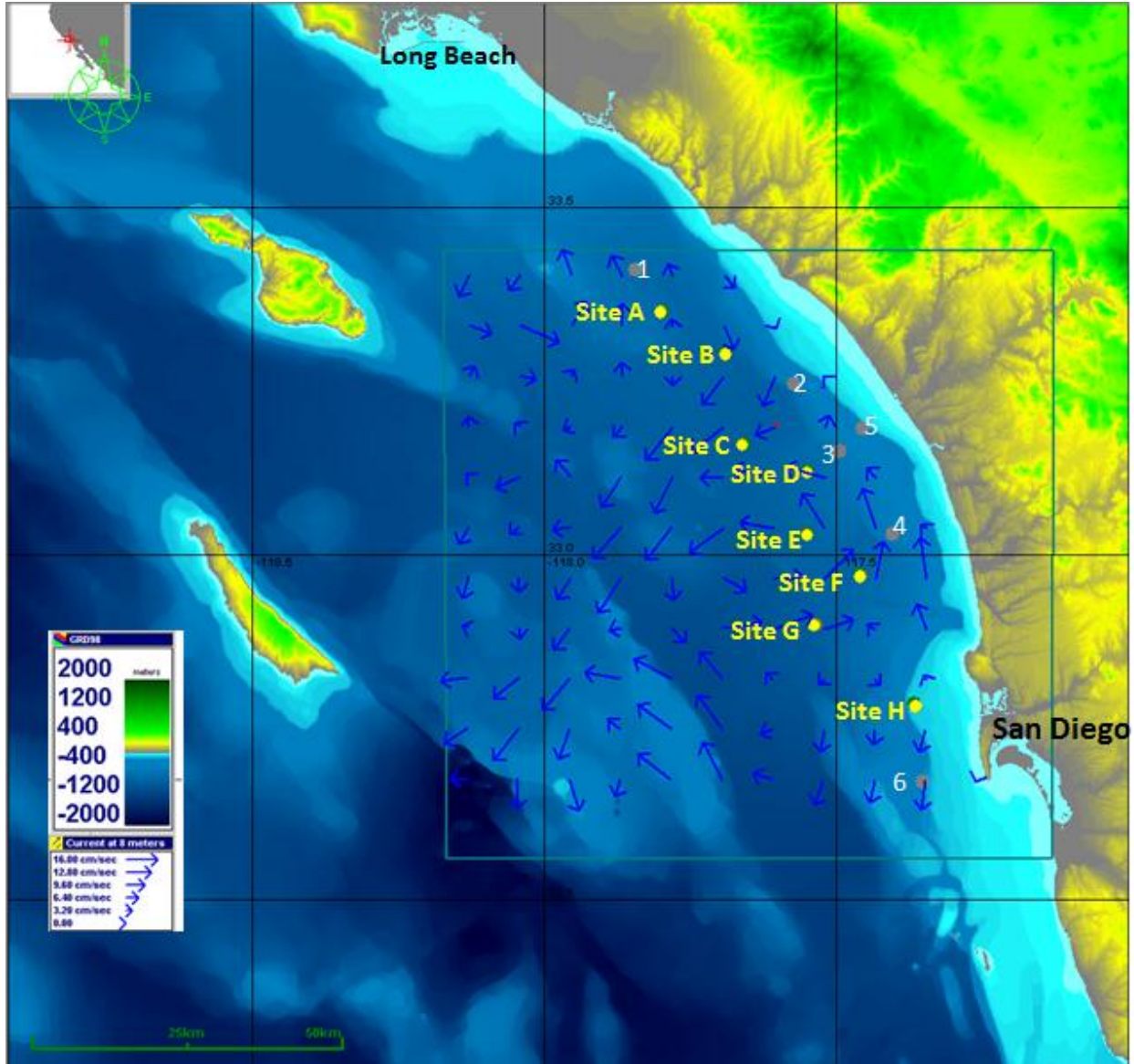
Figure 16: Southern California Bight with eight theoretical net pen sites (yellow dots, A to H) and six data capture cell locations (brown dots, 1 to 6) in a modeling domain of 98 x 98 km shown within the light blue square outline.

3.2. Background Hydrographic Conditions in the Southern California Bight

There is a plethora of data regarding hydrographic conditions in the Southern California Bight which is a component of the California Coastal Current system that begins near British Columbia and flows south past California. We make no attempt to relate all that information here, but rather focus on key factors involved in operating AquaModel within the Bight.

The CALCOFI program and numerous journal articles reporting aspects of the biological

oceanography of the of the Southern California Bight (SCB) report that offshore waters have moderately low primary productivity in the range of 150 g^{-1}C m^{-2}yr^{-1} (Smith and Eppley 1982) and modest, episodic upwelling that brings nitrogen to the surface mixed layer. The surface waters are normally depleted of dissolved inorganic nitrogen (DIN) relative to the physiological requirements of phytoplankton. Currents within both inshore and offshore waters are replete with moderate scale eddies with the majority less than 10 km in scale (Mann and Lazier 2006). The majority of these eddies spin in a counterclockwise (cyclonic) direction- some are transient and others are semi-transient. Upwelling of nutrients from the relatively shallow "deep layer" is associated with these eddies but concentrations of near-surface DIN is typically within or below the range of phytoplankton ½ saturation constants for phytoplankton uptake or growth. Low concentrations of DIN tend to mask the flux of nitrogen from the deep layer that is rapidly assimilated by plankton and contributes to the moderate rate of primary production of the region.

Such low concentrations contrast to both the New Hampshire open ocean site where nutrient concentrations in the mixed layer and euphotic zone are often in excess of phytoplankton growth requirements, and to most main basins of the Salish Sea (Puget Sound and Strait of Juan de Fuca) where we previously modeled salmon farm production (Rensel et al. 2007). In addition, water temperatures are much less variable in the SCB, where they range between 13 and 20 ^{o}C, than in either the Salish Sea, where they range between 6 and 16 ^{o}C and the Gulf of Maine, where they range between 3 and 21 ^{o}C. In waters north of San Diego at depths where pens could be anchored surface currents generally northward as part of the Davidson Counter Current which at times surfaces off San Diego (Hickey et al. 2002). This current occurs inshore of the San Diego Trench, which is delineated in Figure 16 by the deep blue colored area oriented NNW to SSE. However, this flow from the south was not found in 3.5 month current meter record during winter from at the HSWRI site shown as Site H in Figure 16. On the contrary this record indicated a strong north to south flow at both the surface and near bottom. This north to south flow is probably due to the narrowing of the deepwater trench off of San Diego and entrainment of water flowing south in the California Coastal Current. We thus conclude that the direction of flow within this region is variable with probable seasonal variation.

In order to assess a worst case scenario, we purposely place all but one of the eight virtual fish farms in the San Diego Countercurrent area in order to study the effects of these farms in an area replete with eddy circulation and that lacked the strong north to south flows identified by at

HSWRI's proposed fish farm location. If we chose to place the farms offshore of San Diego and southward, we would expect little measurable effect of nutrient discharge due to strong advection of water masses to the south.

3.3. Circulation Model

The ROMS configuration we used consisted of a single domain covering the southern California coastal ocean from Santa Barbara to San Diego at a resolution of 1 km. Boundary conditions for this domain are provided from a separate ROMS domain - run as part of the Monterey Bay forecast system - that covers the U.S. West Coast at a resolution of 15 km. In-situ and satellite measurements that are available in near real-time are assimilated into ROMS using a multi-scale, 3-dimensional, variational (MS-3DVAR) data assimilation scheme. The data assimilation window is six hours. The ROMS now-cast is issued every six hours at 03, 09, 15, and 21 GMT hours, and a 72-hour hour forecast is made daily on the JPL website.

The JPL ROMS uses a sigma-type vertical coordinate in which coordinate surfaces follow the bottom topography. The vertical resolution of the model is mapped onto 40 unevenly-spaced sigma-T surfaces used with the majority of these clustered near the surface to better resolve processes in the mixed layer and seasonal thermocline. For visualization purposes, model data are interpolated to constant depth surfaces using a cubic-spline interpolation method.

3.4. Input Model Conditions

Table 1 is a summary of some of the key input variables used in this simulation. Although there have been numerous studies and routine monitoring of various portions of the Southern California Bight, in the southern region there are few routine data that cover large areas and time spans other than the CALCOFI database. Due to the fact that only one month's circulation data were available at this time and the fact that seasonal variations of environmental forcing factors such as water temperature and dissolved inorganic nitrogen are much less than in other temperate areas of U.S. waters, we opted to run this preliminary assessment with the data as shown in part below.

Table 1: Summary of the Southern California Bight AquaModel settings and some key parameters.

Characteristic or Parameter	Modeled Value
Dimensions of a single farm footprint	1000m x 300m x 15m (L x W x D)
Depth of water at net pens A through G	~700 m
Depth of water at net pen H	92 m
Entire far field modeling domain	82 x 82 cells, each cell 1,200 m square = 1.4 km^2
Fish stocking size	200 gram
Duration of simulation	One month
Initial fish loading of all simulations	0.6 kg m^{-3}
Total initial loading per individual farm	0.6 kg m^{-3} x 4.5 km^3 each = 2,700 MT
Total initial loading for all eight farms	8 farms x 0.6 kg m^{-3} x 4.5 km^3 each = 21,600 MT
Feed C & N composition (Fraction)	Carbon 0.44, Nitrogen 0.07
Biomass per farm & per 8 farms initial	2,694 MT; 21,552 MT
Biomass per farm & per 8 farms 30days later	3,343 MT; 26,744 MT
Feed loss rate	3%
Horizontal diffusion rate Kh	0.1 m^2 s^{-1}
Vertical diffusion rate Kv	0

In order to model multiple farms over a very large area we configured our computational array so that each farm consisting of uniformly multiple pens that are uniformly distributed within a single computational cell.

Table 2 is a copy of a "boundary condition" file for the SCB AquaModel simulation. Unlike the Open Ocean site in New Hampshire, which was modeled with hourly to daily data, we used quarterly data from the four seasons and relied on the interpolation calculations within AquaModel to calculate linear transitions between inputs.

Table 2: Table of seasonal input values for SCB AquaModel used in this case. DIN = dissolved inorganic nitrogen. Units are micromoles μM = μg atoms L^{-1}.

Date	Water Temp ^{o}C (0 m)	Water Temp ^{o}C (15m)	Water Temp ^{o}C (88m)	Oxygen mg/L (0 m)	Oxygen mg/L (15 m)	Oxygen mg/L (88 m)	Irradiance E m^{-2} d^{-1}	DIN μM (0m)	DIN μM (15m)
1/30/2007	15.9	15.9	11.7	8.4	8.4	4.5	62.3	0.11	0.11
4/4/2007	15.5	14.0	10.3	8.4	8.4	4.5	83.1	0.11	0.11
7/17/2007	20.0	16.0	10.0	8.4	8.4	4.5	90.0	0.11	0.11
10/20/2007	20.5	17.8	11.4	8.4	8.4	4.5	76.2	0.11	0.11

Date	DIN μM (88m)	Phyto-plankton μM N (0 m)	Phyto-plankton μM N (15 m)	Phyto-plankton μM N (88 m)	Zoo-plankton μM N (0 m)	Zoo-plankton μM N (15 m)	Zoo-plankton μM N (88 m)	Mixed Layer Depth (m)
1/30/2007	15.0	0.30	0.30	0.03	0.40	0.40	0.05	15
4/4/2007	15.0	0.30	0.30	0.03	0.40	0.40	0.05	15
7/17/2007	15.0	0.30	0.30	0.03	0.40	0.40	0.05	15
10/20/2007	15.0	0.30	0.30	0.03	0.40	0.40	0.05	15

Figures 17 through 30 are AquaModel screen prints illustrating the distributions and dynamics of dissolved inorganic nitrogen (DIN), phytoplankton, and zooplankton in the Southern California Bight as determined by the production of dissolved nitrogenous waste by the eight fish farms. The simulation runs during May, 2007, and screen prints at weekly intervals are presented. During this time of year mesoscale (~10km) eddy circulation is often more prevalent in the SCB than at other times of the year. Figure 17 is a snapshot of the distribution of dissolved inorganic nitrogen (DIN) after the first week of the simulation. We notice from the vector field in the base-map that there are large eddies offshore to the west and smaller eddies to the east. We also note from the raster image of the surface concentration of DIN that the farms have released sufficient DIN to produce small and dilute plumes of elevated DIN downstream of the farms. The red dot superimposed upon capture cell 3 provides vertical profiles of DIN, phytoplankton nitrogen, and zooplankton nitrogen within the upper 30 m of the water column. These profiles are shown in the plots to the right. The concentrations of all three components of the planktonic system are constant with depth and equal to initial ambient values of 0.1, 0.3, and 0.4 µM, for DIN, phytoplankton, and zooplankton, respectively.

A word of explanation is needed for interpreting these vertical profiles. When setting up initial conditions for our SCB simulation, we failed to provide values for vertical eddy diffusivity within the mixed layer and the underlying stratified waters, and computations were made with values set to 0. Since vertical diffusivity in stratified waters is very small given the duration of our simulation, this oversight will not affect our results. On the other hand vertical eddy diffusivity in the surface mixed layer is at least 100 times higher than the underlying waters, and the surface mixed layer, which is 15 meters deep in our simulations, is rapidly mixed. Thus, the concentrations of DIN, phytoplankton, and zooplankton will be constant with upper mixed layer and equal to the average value for variable that are displayed at depths of 2, 6, and 12 meters.

A week later (Figure 18) flow has reversed to the north and that the offshore eddies have disappeared while the inshore eddies continue. The farm plumes of enriched DIN are now larger. The light green contour represents the 0.4 µM concentration of nitrogen and the darker green contour represents 0.6 µM. In addition vertical profiles sampled at capture cell 3, indicate a significant increase in the concentration of phytoplankton and zooplankton. We will soon see

that these increases were caused by DIN produced by the farm at site D.

By the end of two weeks (Figure 19), the situation remains essentially similar to the previous week. However, after three weeks (Figure 20) there is a broadening of the nitrogen plumes, and we see that capture cell 3 (the red dot) is now downstream of the DIN plume from farm site D.
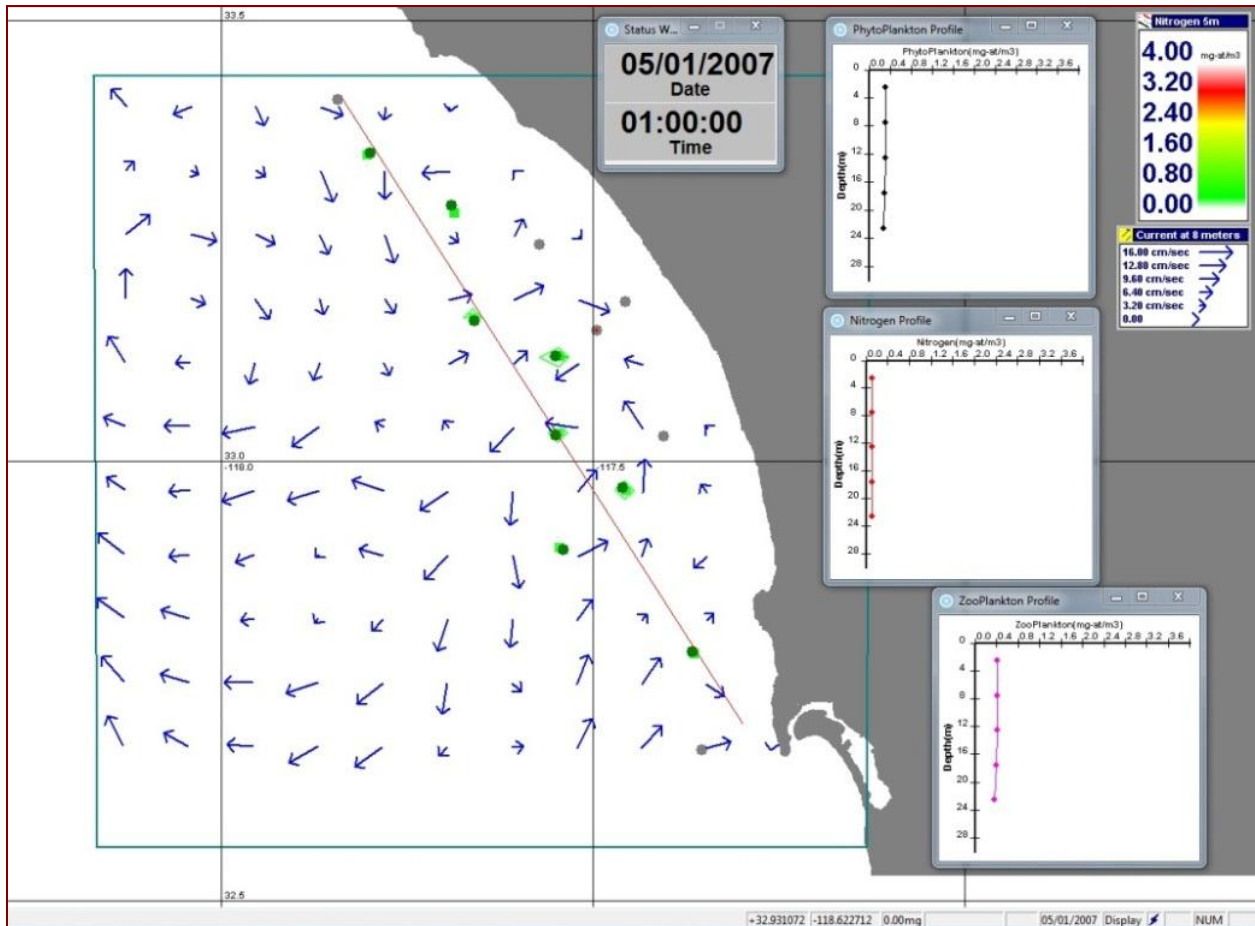

Figure 17: The start of the Southern California Bight simulation. The base-map shows vectors of the flow field (scale in the upper right hand corner), and a false color image of the concentration of dissolved inorganic nitrogen in surface waters (scale in upper right hand corner). The red dot at capture cell 3 provides vertical profiles of the upper 30 meters of the water column of the concentrations of dissolved inorganic nitrogen (DIN), phytoplankton nitrogen, and zooplankton nitrogen. The profile values for the 3 components of the planktonic system are those of the initial values for ambient waters.
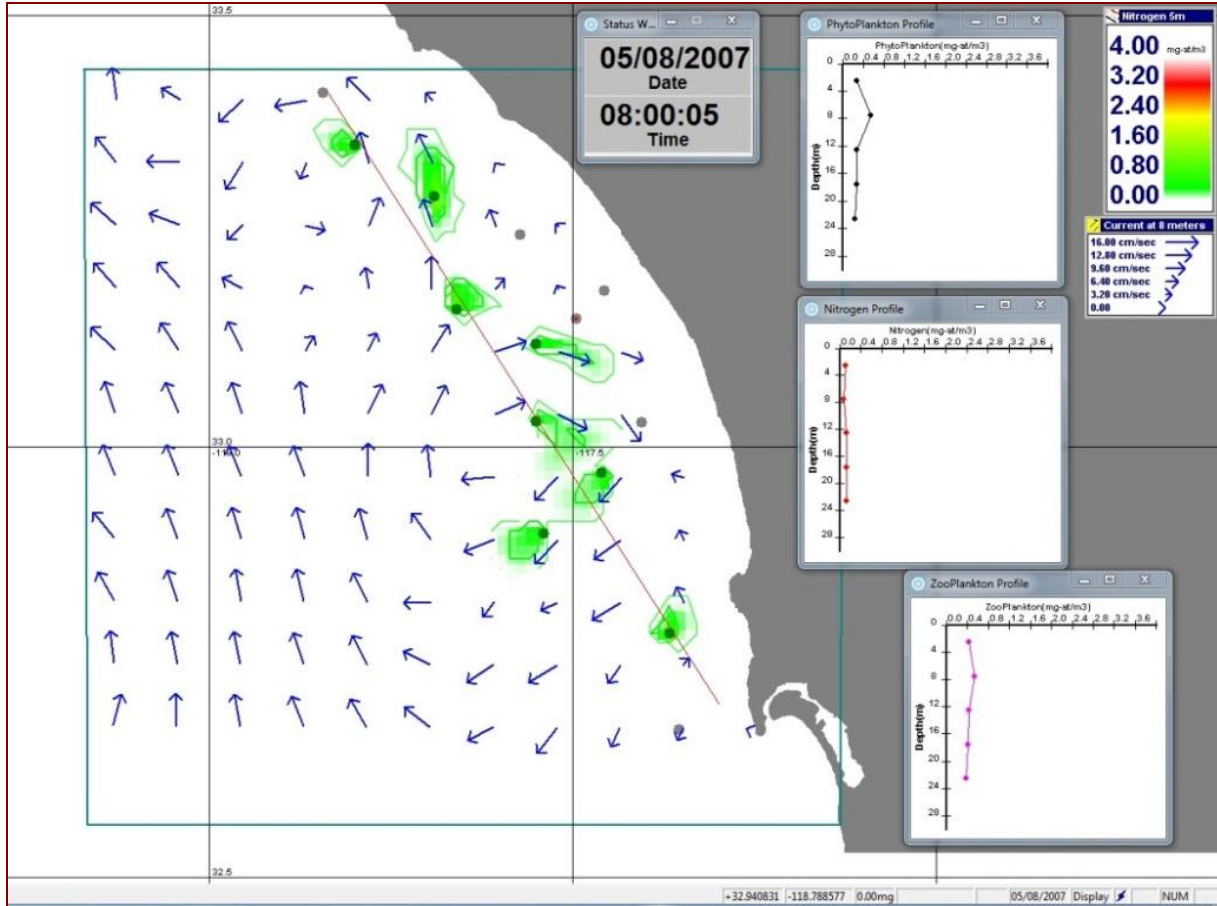
Figure 18: DIN in surface water after 1 week of simulation. The light green and dark green contours represent concentrations of DIN of 0.4 μM and 0.6 μM, respectively. The vertical profiles at capture cell 3 display the depth distribution DIN, phytoplankton nitrogen, and zooplankton nitrogen.
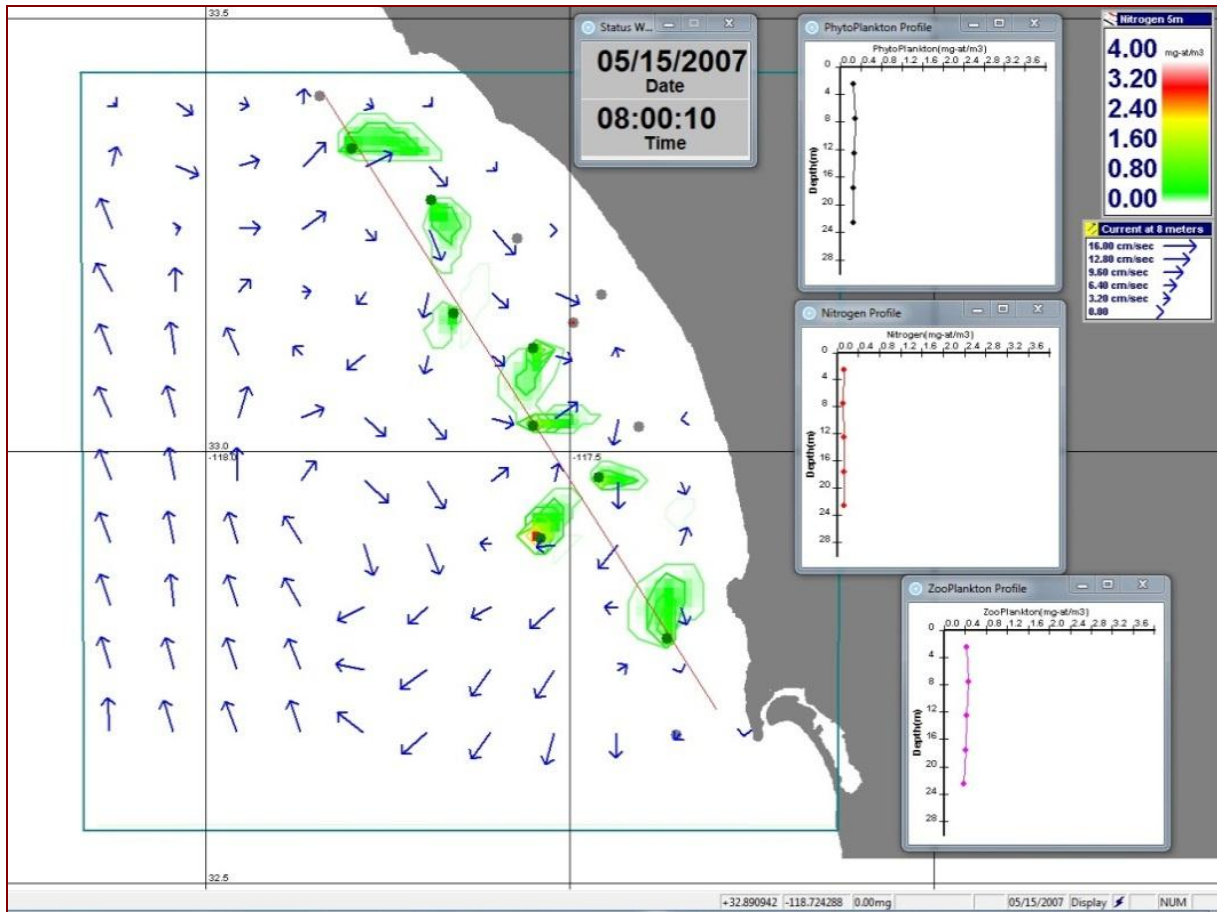
Figure 19: The concentration of DIN at 5m depth after 2 weeks and vertical profiles at capture cell 3 of phytoplankton abundance, nitrogen concentration and zooplankton abundance showing ambient conditions.
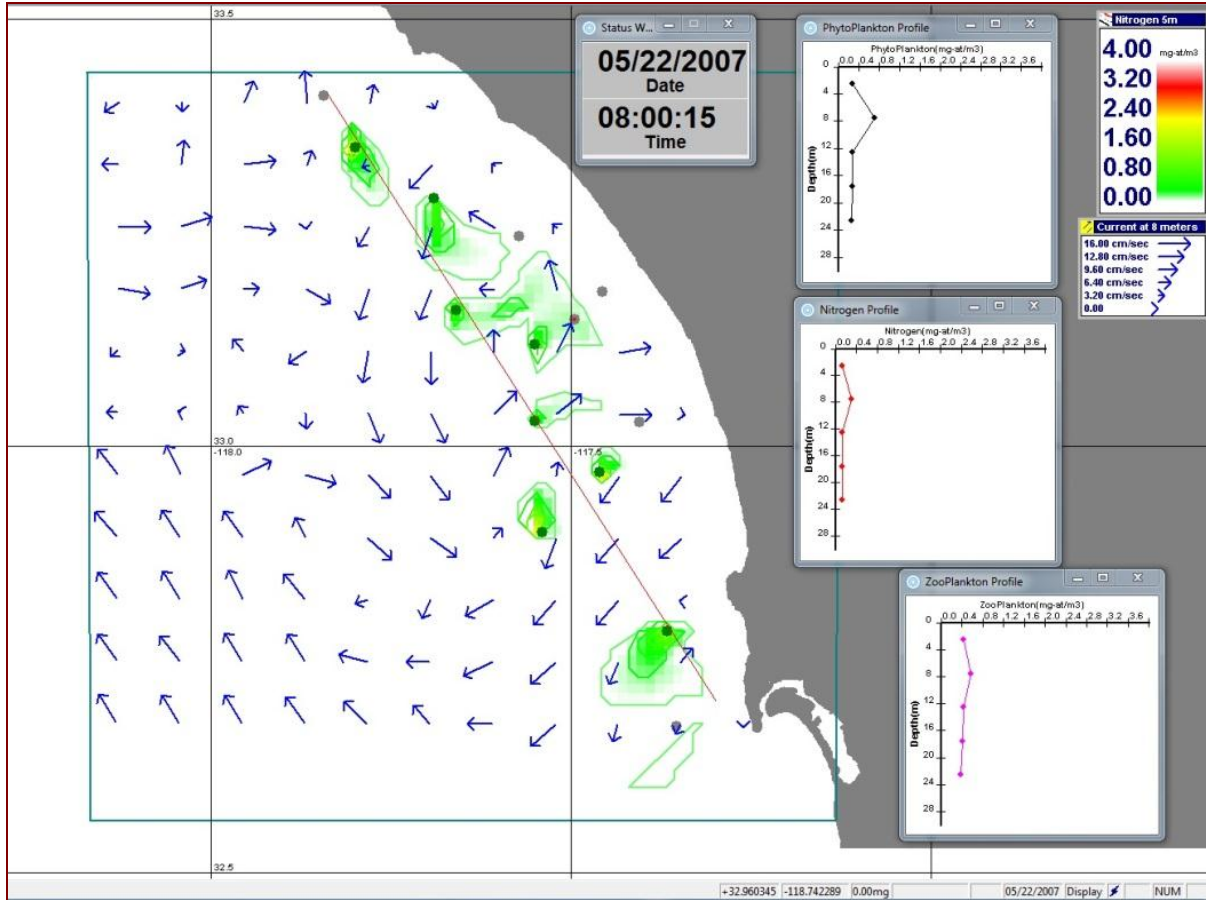
Figure 20: DIN in surface waters after 3 weeks. The vertical profiles at capture cell 3 reveals a large increase in the concentration of phytoplankton in surface waters caused by the waste plume from the nearest farm (at site D).

Figure 21, which is a snapshot at the end of the month, shows that the current vectors near most of the farms are shorter, indicating slower water movement. This explains the shrinkage of the nutrient plumes since the previous week. We also see that a very large eddy has set-up throughout most of the modeling domain. Such motion will of course help retain dissolved wastes from the farm within the bight. The vertical profile at capture cell 3 shows that at 8 m. the concentration of phytoplankton nitrogen has increased to about 0.7 μM.

In summary, the mapping of dissolved inorganic nitrogen indicates that the nutrient enriched plumes from the farms are both dilute and limited in their spatial extent. Concentrations of DIN reach transient values of over 1 μM in close proximity to the farms when currents are slow, but most commonly concentrations rarely exceed 0.4 μM, which is about 4 times ambient concentrations. We will see below that constrains on the spatial distribution of DIN result
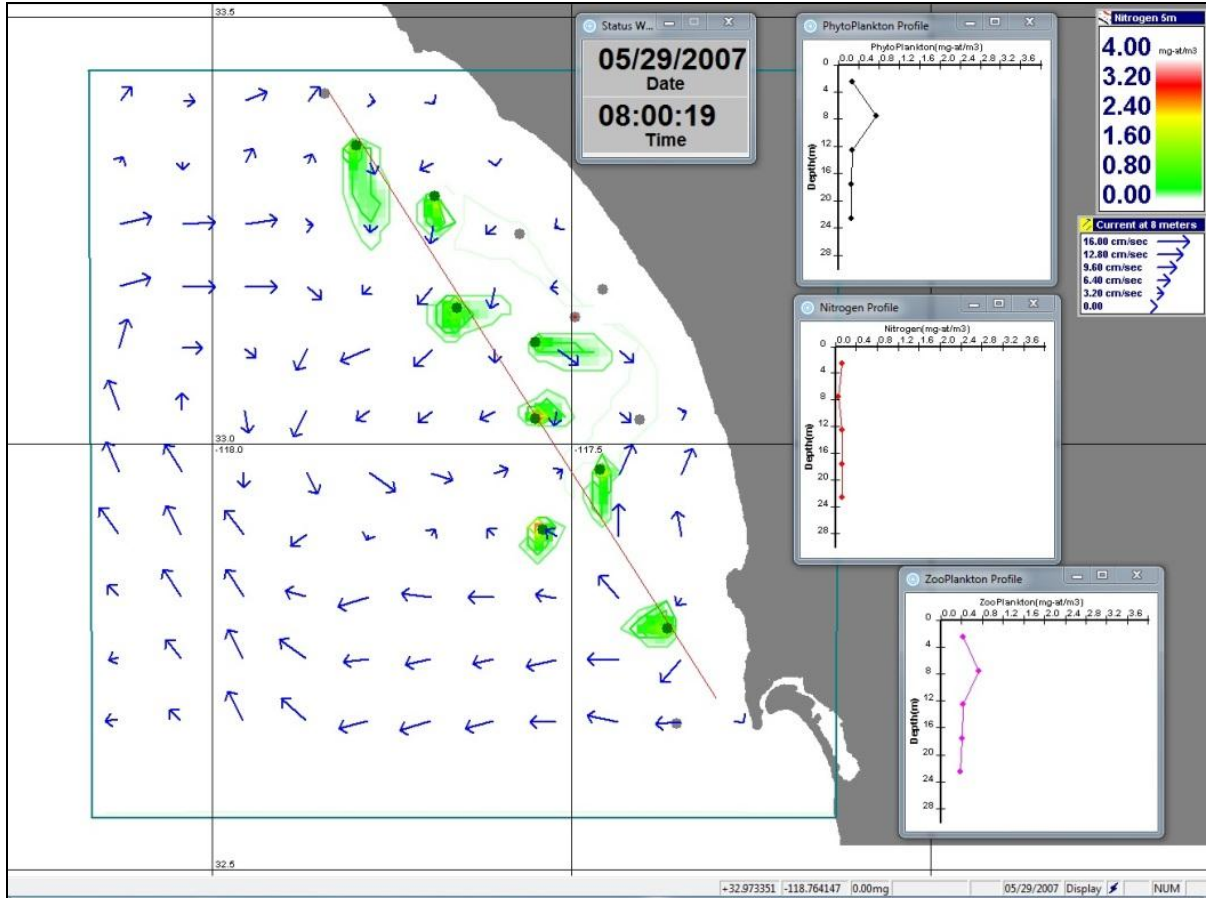
Figure 21: The concentration of DIN in surface waters after 4 weeks. Despite the recent shift in currents from the previous week, the vertical profiles at capture cell 3 reveal an increased concentration of phytoplankton that is caused by the waste plume form the near-by farms at site D and possibly at site C.

not only because of turbulent mixing of the plume with ambient waters but also because of assimilation by the planktonic community.

The next series of figures show screen prints for the same time series for the distribution of phytoplankton concentration, which is reported here in terms of either the concentration of chlorophyll *a* in units of μg of pigment L^{-1} or the concentration of phytoplankton nitrogen in units of μM nitrogen. Here we make the simplifying assumption of a 1:1 ratio of chlorophyll a to phytoplankton nitrogen.

Figure 22 shows initial conditions when the ambient concentration of chlorophyll is 0.3 μg L^{-1}. For reference, a bloom of phytoplankton in coastal waters of the SCB is considered to occur when concentrations of chlorophyll increase to about 3 to 4 μg L^{-1}, which is roughly an order of magnitude above the annual average concentration. In other regions, such as the Pacific

Northwest, a bloom might be classified as occurring at > 5 to as much as 20 µg L^{-1}.

Figure 23 shows the distribution of chlorophyll after one week. The light green contour encloses waters where the concentration of chlorophyll is at least 0.4 µg L (0.1 µg L greater than ambient concentration) and the darker green contour encloses waters where the concentration of chlorophyll is at least 0.6 µg L. The patch of chlorophyll at farm site A was most likely caused by a local, small scale eddy that temporarily trapped the waste plume in the vicinity of the farm. We also note that capture cell 3 is now downstream of the plume from farm site D. This is confirmed by the sudden increase in phytoplankton concentration at a depth of 8 m.

After 2 weeks (Figure 24) both the spatial distribution of the plumes has increased as has the concentration of phytoplankton within the plumes. The eddy that trapped the plume at site A appears to have collapsed, and the plume has shifted to the south. The farms at sites C, E, F, and G are now associated with the higher concentrations of chlorophyll of about 0.8 µg L. Captured cell 3 is no longer downstream of the plume from farm site D. Evidently, the local phytoplankton enriched plume has been swept away.

Figure 25 shows that after 3 weeks the growth in the spatial distribution of phytoplankton has slowed as has the increase in phytoplankton concentration. The plume of phytoplankton enriched water has moved to the southeast of the plume found the week earlier. Inspection of the current vectors indicates that this movement is driven by the currents. The highest concentrations of chlorophyll are similar to the highest values of the previous week. This indicates that a quasi-steady state in the dynamics of the phytoplankton has been established by the third week. This steady state condition for the phytoplankton represents a balance between the growth of the phytoplankton within the plume and losses caused by turbulent mixing of plume water with ambient waters and losses caused by the grazing of zooplankton. We also note that capture cell 3 is once again downstream of farm site D and as indicated by the vertical profile for phytoplankton. After 4 weeks (Figure 26), the size of the plumes and the concentration of phytoplankton within the plumes have stabilized. On the other hand, currents have altered its shape and driven many of the plumes to the southeast.

Several features of these simulations are noteworthy. First, the images and profiles of phytoplankton distribution clearly show that the spatial extent these plumes are much greater than the spatial extent of the nutrient plumes. This is easily explained by the fact that the

response time of phytoplankton assimilation of DIN is about 8 days while response time of zooplankton grazing upon phytoplankton is 20-30 days. These time scales are clearly shown in Figure 9 of Section 2 of this report. Second, the concentration of phytoplankton within the waste plumes is never greater than a factor of 3 larger than ambient concentrations. Third, both the currents and the positions of the farms determine the shape of the overlapping phytoplankton plumes.   Fourth, the patterns shown in this simulation for May are likely to be quite different from those at other times of the year. For example current meter measurements at Site H during winter months clearly indicate a strong and continuous north to south flow (Kiefer et al. 2008).
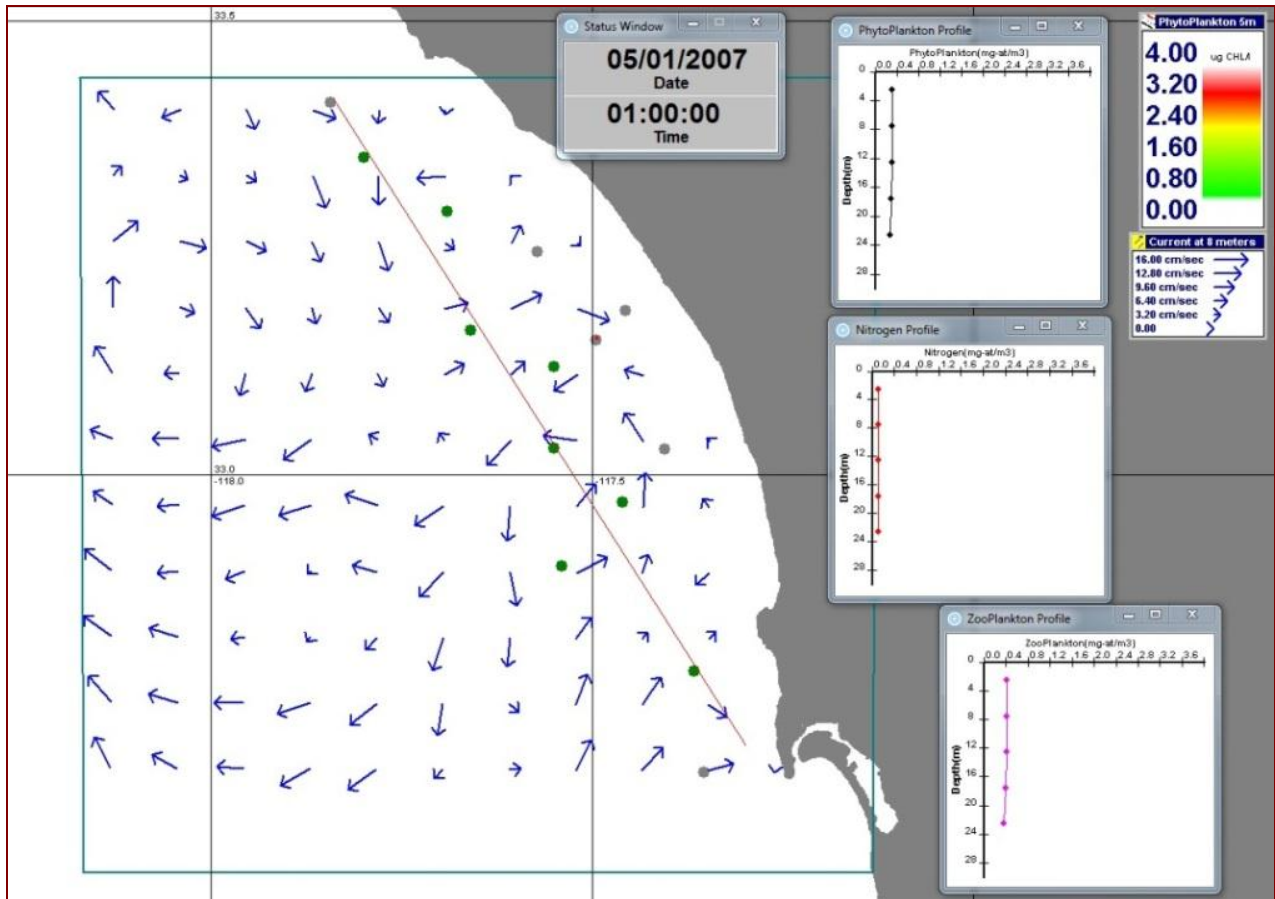
Figure 22: Ambient conditions at the start of the simulation on May 1, 2007. As indicated in the base-map the concentrations of phytoplankton are 0.3 μg chlorophyll L^{-1} throughout the computational array. The vertical profiles at capture cell 3 (indicated by the red dot on the base map) show initial ambient concentrations of 0.11, 0.3, and 0.4 for DIN, phytoplankton nitrogen, and zooplankton nitrogen in the upper 30 meters of the water column.
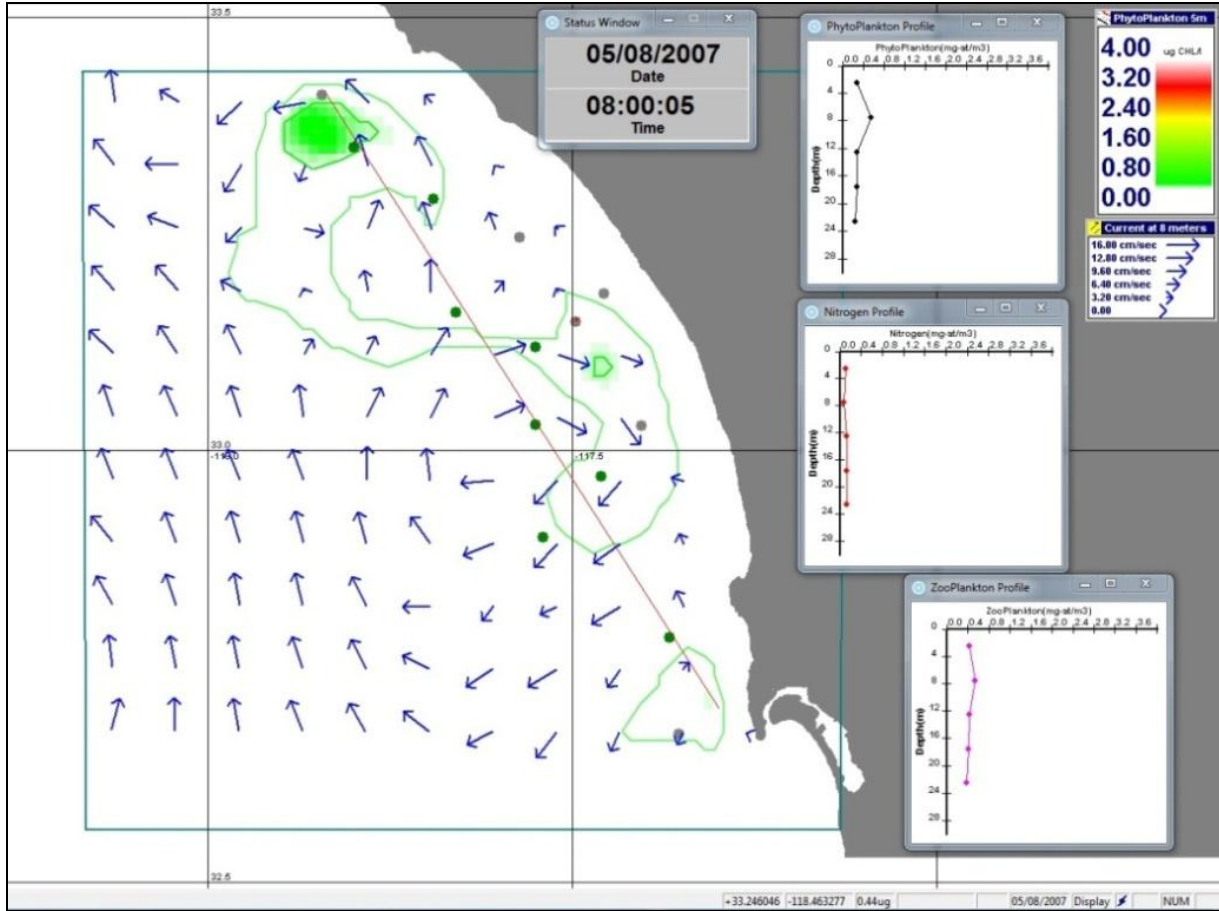
Figure 23: After 1 week of the simulation, plumes of enriched phytoplankton (generally less than 0.5 µg chlorophyll L^{-1}) are in the vicinity of most of the farms. The light green contour has a value of 0.4 µg chlorophyll L^{-1}. The enriched plume at site A appears to result from a small eddy at the site that has "trapped" the enriched water.
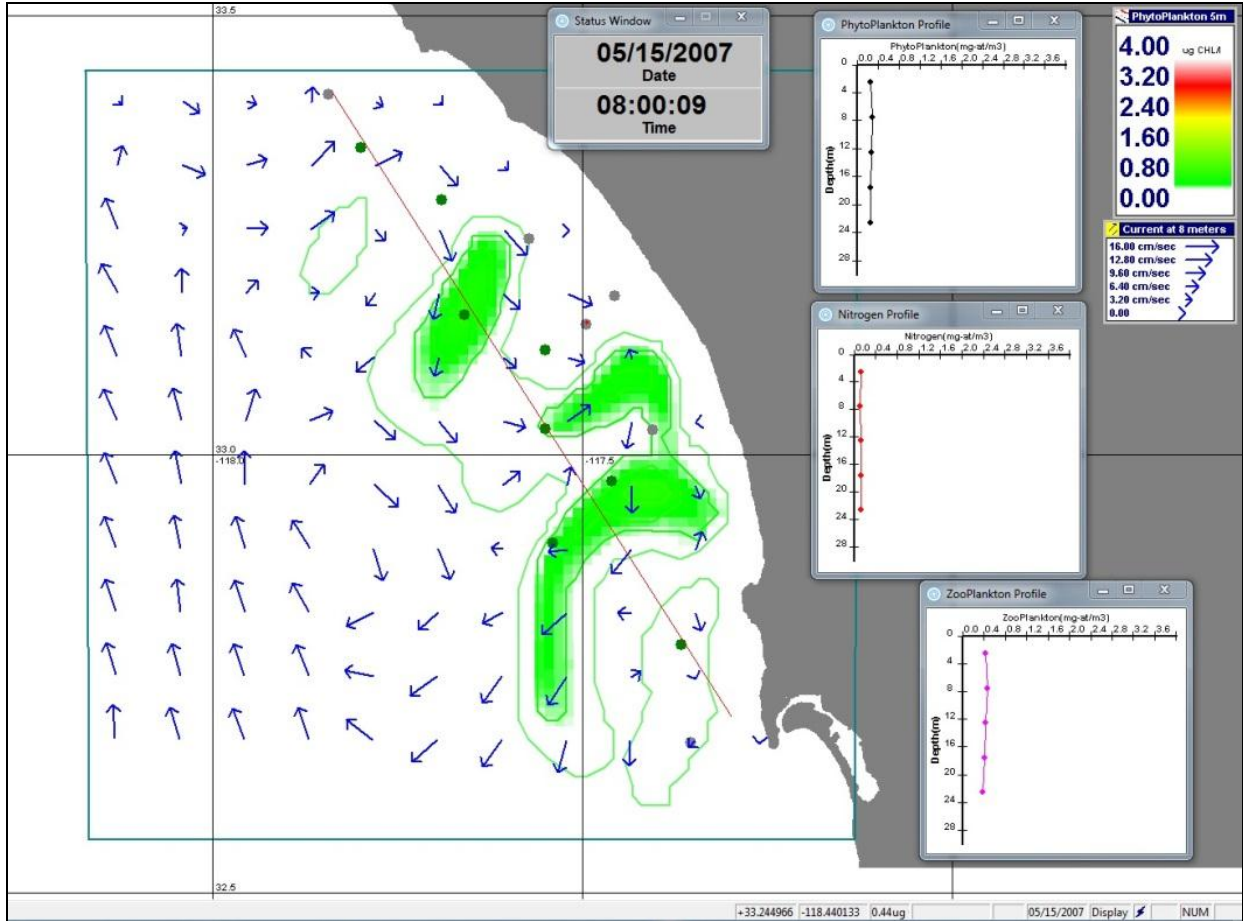
**Figure 24: After 2 weeks the plumes of enriched phytoplankton have expanded and concentrations have increased to about 0.75 µg L^{-1} in the core of the plume. The eddy at site A has disappeared and strong currents to the south during the second week have moved the plume immediately south of the site. The vertical profiles at capture cell 3 indicate that the phytoplankton plume has shifted -most likely also to the south.**
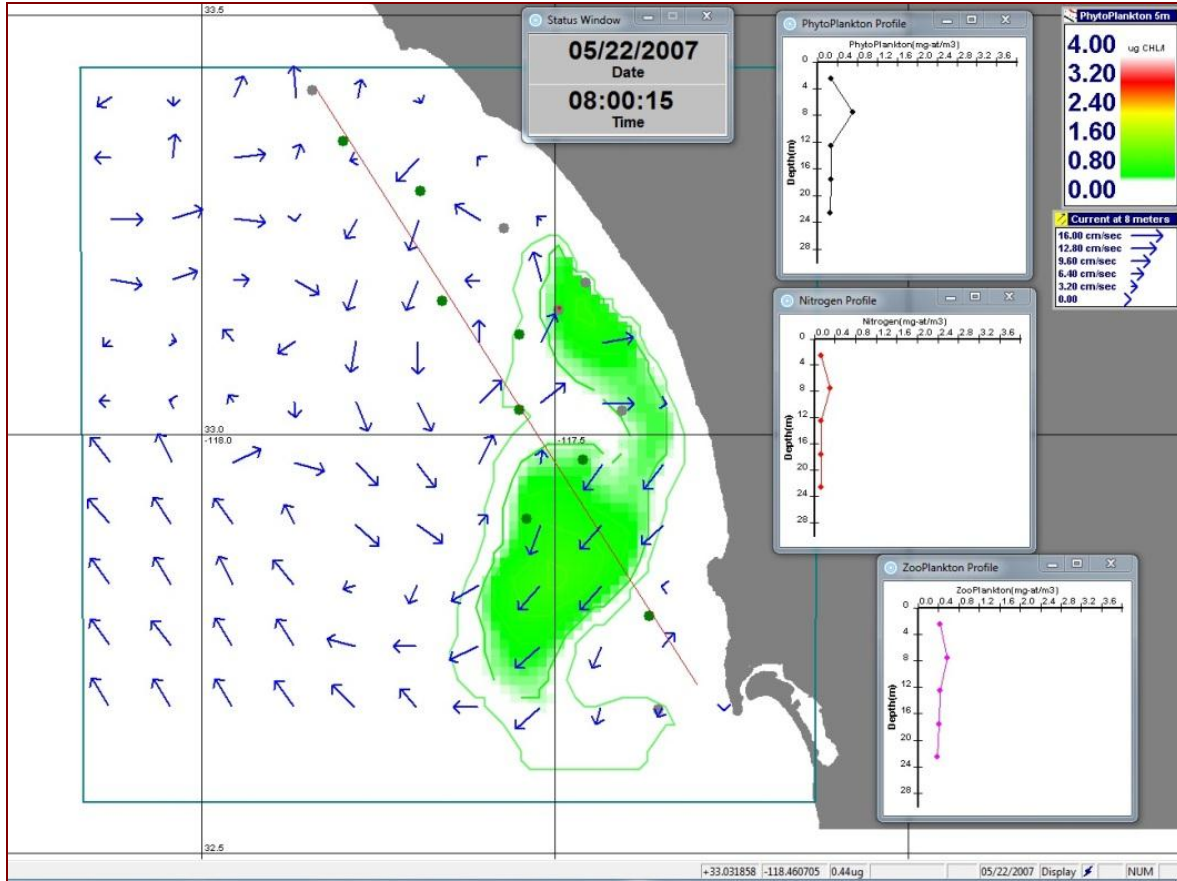
Figure 25: After 3 weeks the plumes of enriched phytoplankton have moved southeast and have experienced a moderate increase in size. The concentration of phytoplankton found in the core of the plume has changed little from the previous week. Capture cell 3 is now surrounded by the plume, and the vertical profiles within the cell indicate high concentrations of both phytoplankton and zooplankton in surface waters.
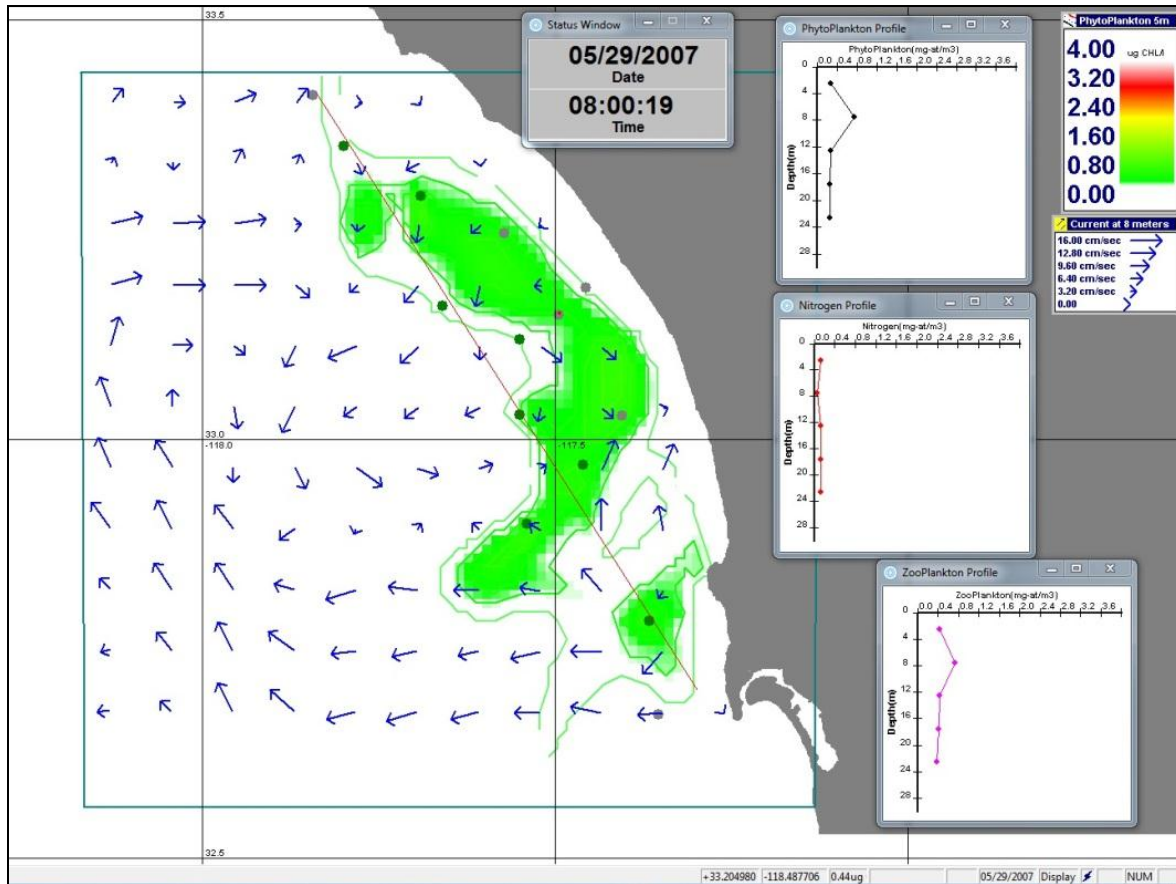
Figure 26: After 4 weeks the plumes of enriched phytoplankton have moved north and the spatial extent has increased a little. The highest concentrations of phytoplankton are equal to those of the previous week but the spatial extent of core water is greater than that of the previous week. This increase is mostly likely caused by relaxation of the strong southerly currents of the previous week. The vertical profiles at capture cell 3 show small increases in the concentration of phytoplankton and zooplankton relative to the previous week.

The final series of screen prints of the SCB simulation map the distribution of zooplankton nitrogen in units of µM. After the first week of the simulation (Figure 27) the concentration of zooplankton near the farms is slightly higher than the ambient concentration of 0.4 µM. In figure after two weeks (Figure 28) four zooplankton enriched plumes appear. From north to south: the first plume is associated with site A, the second is associated with site C, the third, which is much larger than the others, is associated with overlapping contributions from sites E, F, and G, and the fourth is associated with site H. In Figure 29 we see that after third weeks both the size and the concentration of zooplankton in the overlapping plumes have continued to increase but at a decreasing rate. We also note that the southerly flow found in the center of the array has pushed the zooplankton plume to the south while flow to the northeast in the southwest corner of the array has pushed the southern portion of the plume to the northwest. In Figure 30 we see that

after four weeks the zooplankton enriched plumes have stabilized in terms of the size and concentration of zooplankton. However, the shapes of these plumes have changed because of shifts in the flow field. At this time the concentration of zooplankton nitrogen in the core of the plumes is no higher than 0.6 µM, which is only 0.2 µM above ambient.

We can draw several conclusions from the zooplankton time series. First, by comparing the phytoplankton time series (Figures 22-26) with the zooplankton time series (Figures 27-30), we see that zooplankton enriched plumes generally track phytoplankton enriched plumes. This is to be expected since increases in the concentration of the zooplankton are driven by increases in the concentration of phytoplankton and they are subject to the same water current patterns with some exception due to vertical migration behavior. Second, the phytoplankton enriched plumes appear earlier than the zooplankton enriched plumes. This is also to be expected since the growth rate zooplankton is a function of phytoplankton concentration rather than nutrient concentration. Furthermore, as shown in Figure 9 of Section 2, in the Southern California Bight the response time of phytoplankton to nutrient enrichment is about 8 days while the response time of zooplankton to phytoplankton enrichment is 20-30 days. Third, the magnitude of the response of phytoplankton to nutrient enrichment is greater than the response of zooplankton to phytoplankton enrichment. Specifically, the highest concentrations of phytoplankton in the plumes was about 1 µM nitrogen, which is 0.7 µM higher than ambient concentrations. On the other hand, the highest concentrations of zooplankton nitrogen in the plumes was 0.6 µM, which is only 0.2 µM higher than ambient concentrations. This difference in response is caused by the fact that the slower response time of the zooplankton provides additional time for dispersion to reduce the concentration of phytoplankton within the plume and there-by reduce the yield of zooplankton. Fourth, as discussed earlier, the patterns shown in the May simulation will likely to be quite different at other times of the year.
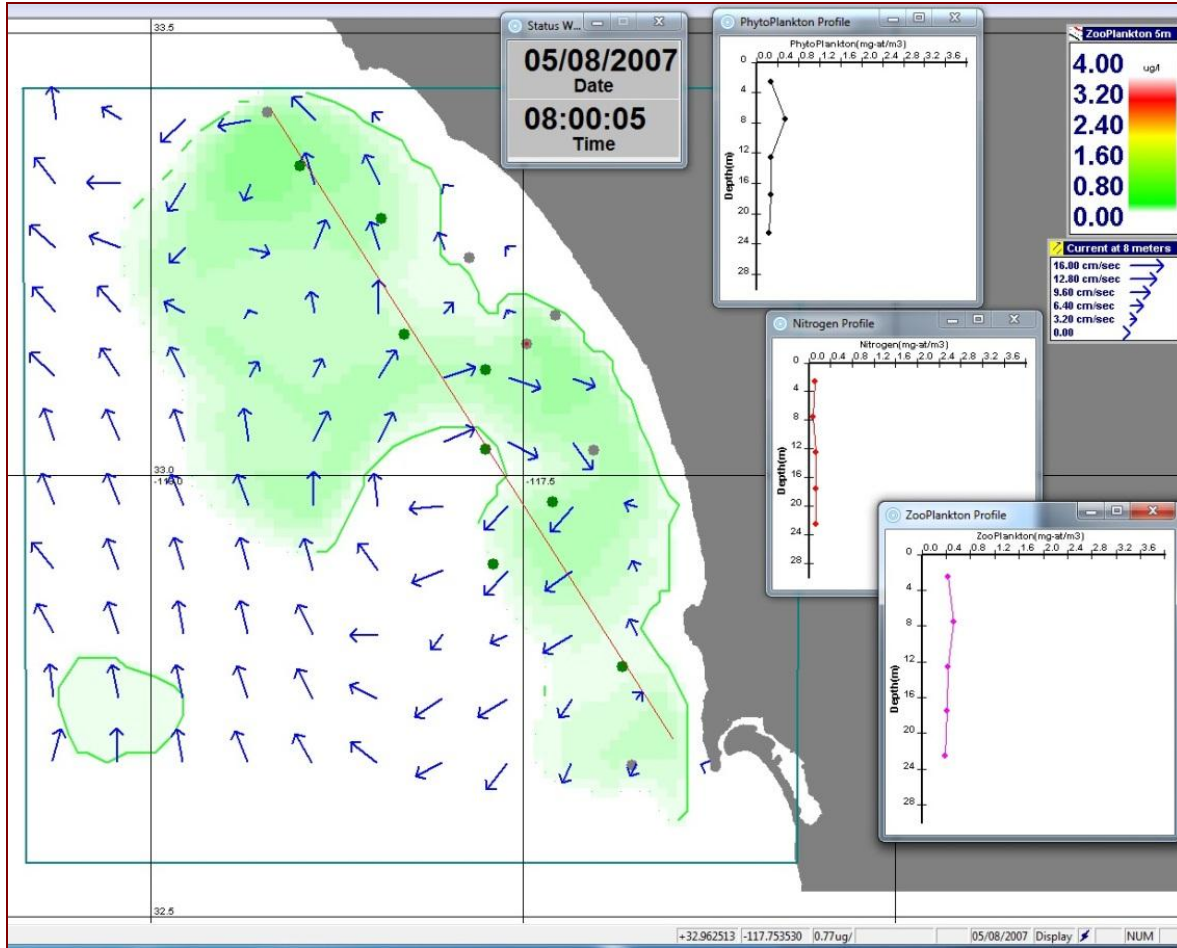
Figure 27: The concentration of zooplankton nitrogen in surface waters after 1 week of the simulation. The value of the contour line for zooplankton is 0.4 µM, which is the equal to the ambient concentration. Thus, the green shading represents a small increase in zooplankton concentration above ambient.
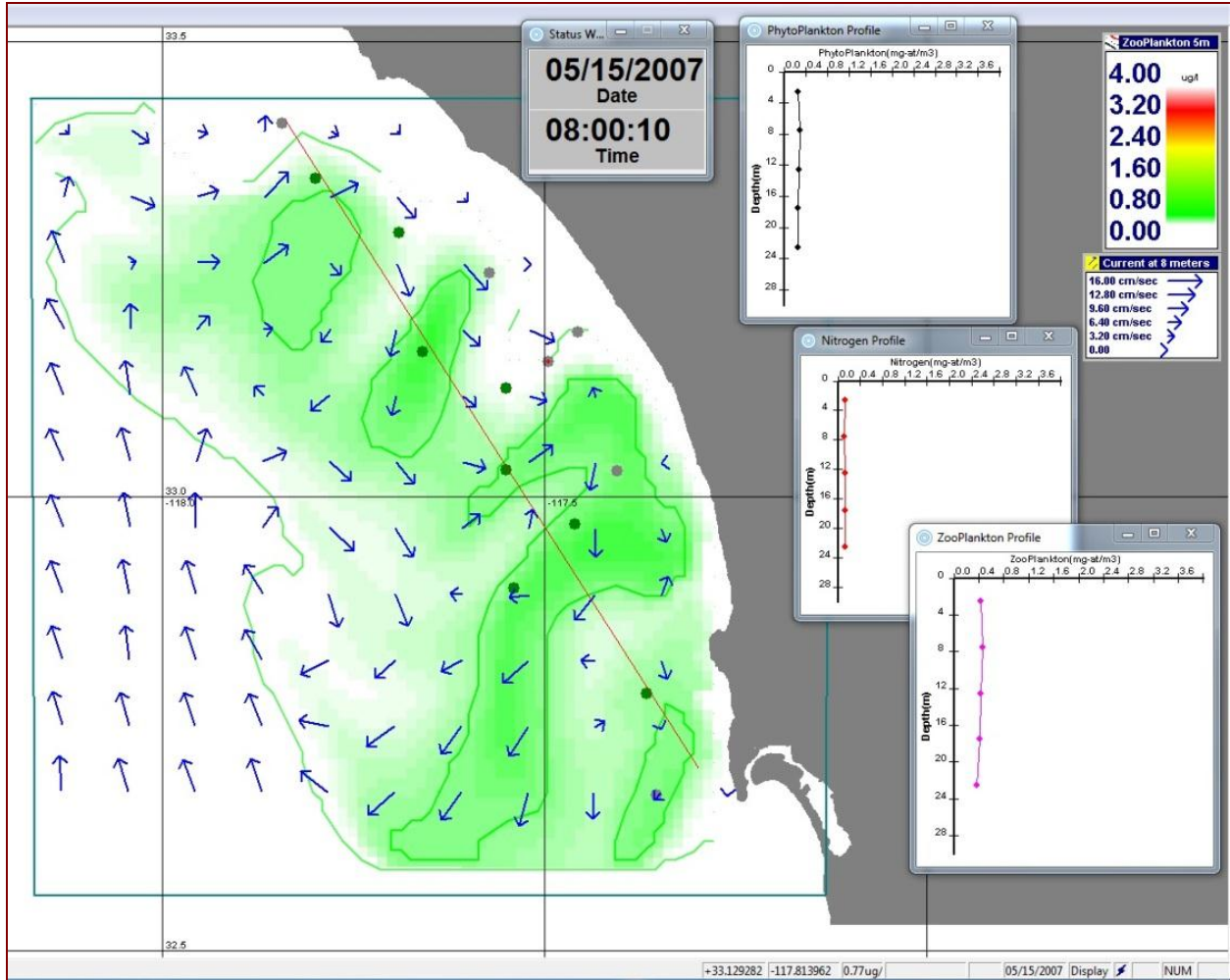
Figure 28: The concentration of zooplankton nitrogen after 2 weeks of the simulation. Concentrations are slightly higher than the prior week, and the size of the zooplankton enriched plume has increased. The spatial pattern of the zooplankton resembles somewhat the spatial pattern for phytoplankton for the 2nd week.
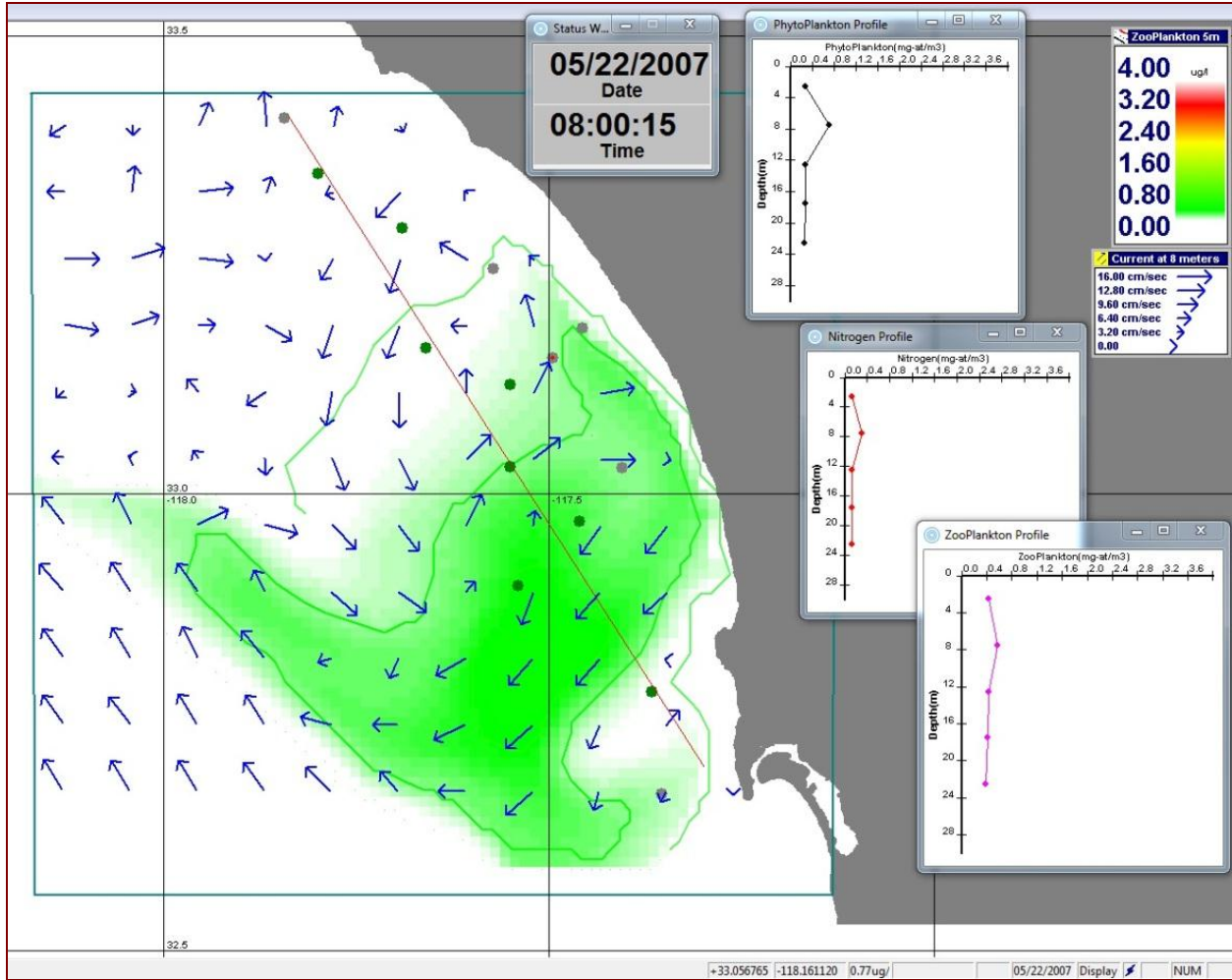
Figure 29: The distribution of zooplankton concentrations after 3 weeks of the simulation. Both the size and the concentration of zooplankton in the plumes have increased slightly from the previous week. The southerly flow found in the center of the array has moved the zooplankton plume to the south while flow to the northeast in the southwest corner of the array has moved the southern portion of the plume to the northwest.
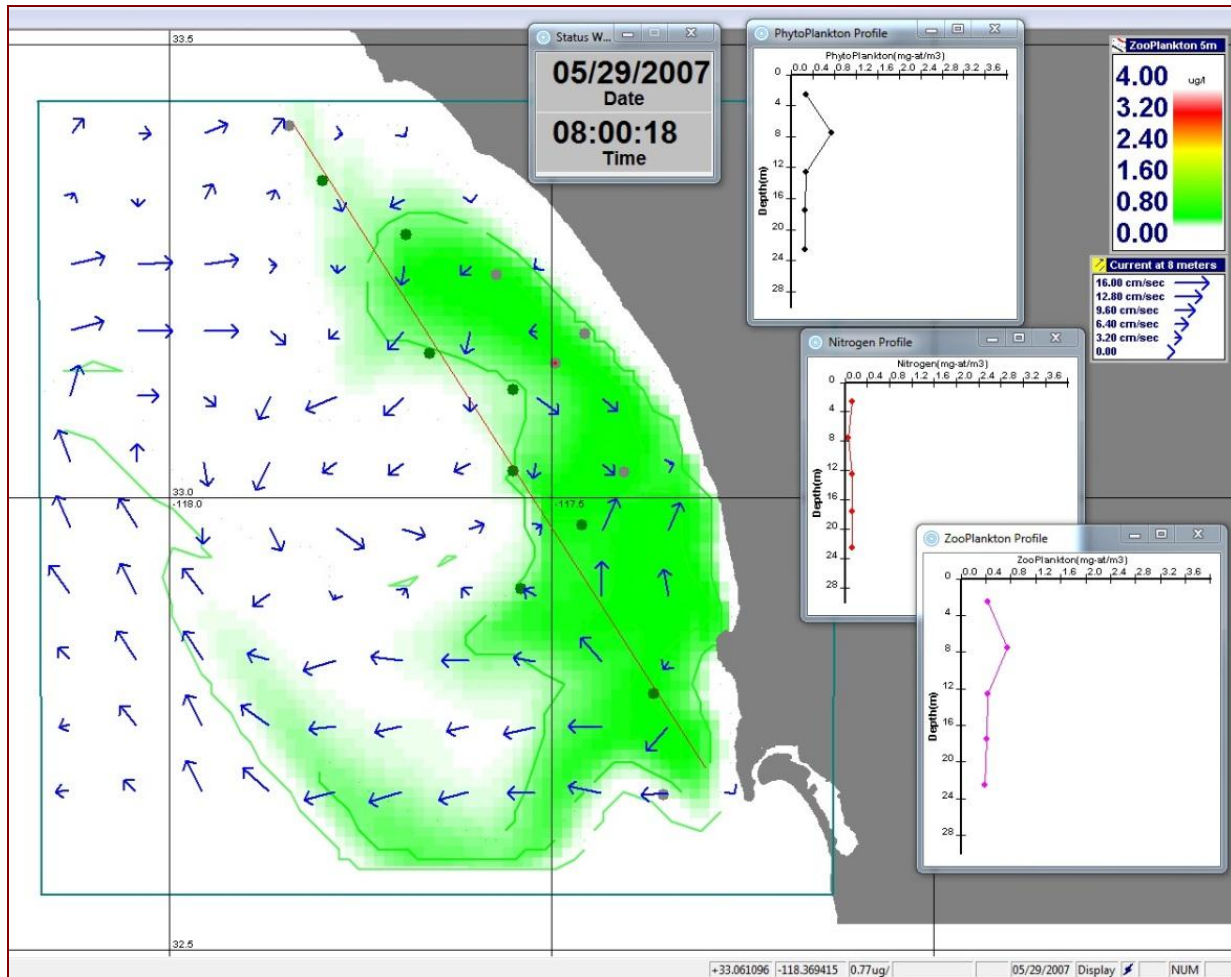
Figure 30: The distribution of zooplankton concentrations after 4 weeks of the simulation. The zooplankton enriched plumes has stabilized in terms of the size and concentration of zooplankton. However, the shape of the plumes has changed as determined by the recent history of the field of current velocity. The concentration of zooplankton nitrogen in the core of the plumes is no higher than 0.6 µM, which is only 0.2 µM above ambient.

Finally, we point out that DIN is not a pollutant in aquatic ecosystems unless discharged into sensitive areas (e.g., near shore, shallow, poorly flushed) because plankton in open ocean waters has the capacity to sequester it for growth. Only a few types of plankton are "harmful", and not all of these have physiological ecology where increased DIN leads to increased toxin. In marine waters near California domoic acid producing species of *Psuedo-nitzschia* occur and are a recurring concern. Many teleost fish including striped bass produce (dissolved) ammonium nitrogen and small amounts of urea wastes but *Pseudo-nitzschia australis,* a common toxigenic form in California, grows better with nitrate and ammonium but produces significantly more toxin with urea (Armstrong-Howard et al., 2007).

3.5. Quantitative Model Predictions

AquaModel has the ability to report all parameters from all vertical and horizontal cells of the sampling grid in the modeling domain. Here we utilize that feature from the above described simulation to quantitatively describe various results, beginning with the current velocity results, an important parameter for any fish culture operation.

Current velocity was predicted for surface and bottom layers at all fish farm sites and capture cells. Hourly data comparing surface and bottom current velocities at Site D are shown in Figure 31 (top panel) and at HSWRI Site H (bottom panel). Site D is a centralized location in the subject area and provides a good contrast to HSWRI Site H, the southernmost farm site and the one located closest to San Diego and in the shallowest depths.
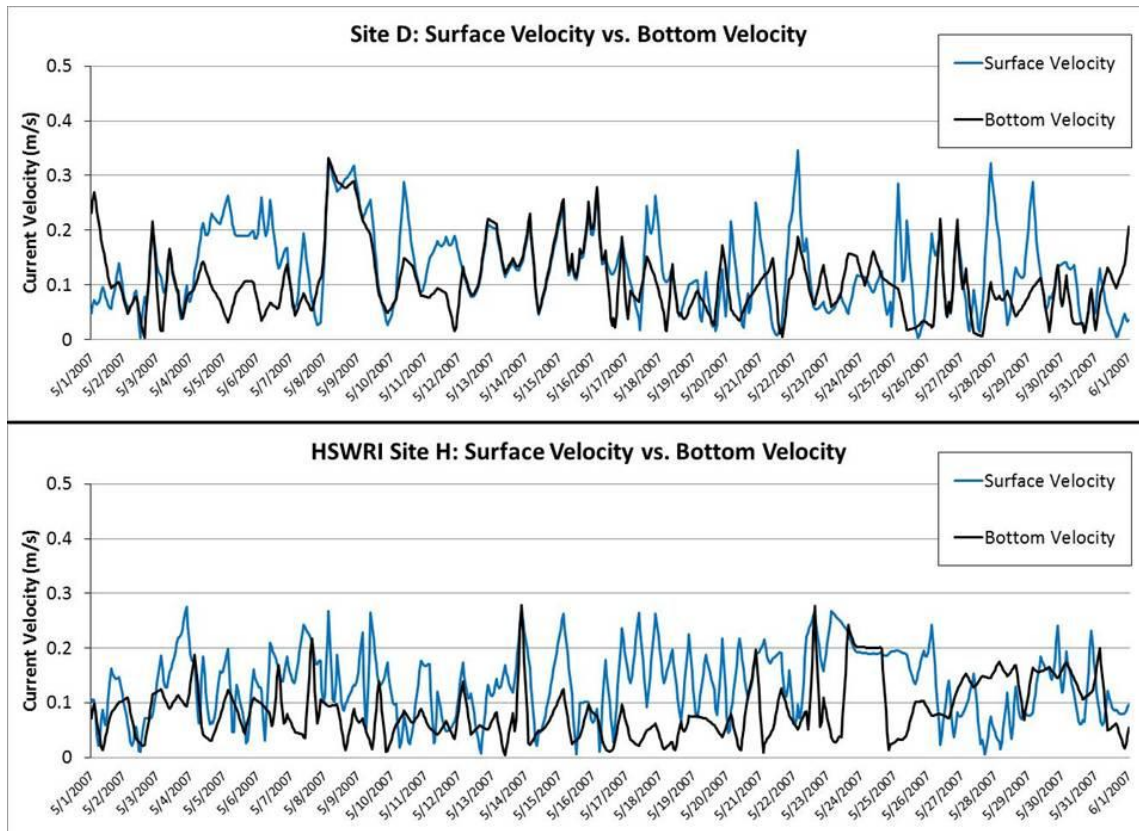

Figure 31: Hourly surface velocity and bottom velocity at Farm Site D and HSWRI Site H.

At both sites, overall average current velocities estimated by the JPL ROMS model were greater at the surface than at the bottom: at Site D, average surface velocity was 0.13±0.7 m/s and average bottom velocity was 0.11±0.06 m/s; at HSWRI Site H, average surface velocity was

0.13±0.06 m/s and average bottom velocity was 0.09±0.05 m/s. (Variation reported here, as well as in the rest of the text and figures, is ±1 standard deviation). Predicted surface velocities at Site D vs. HSWRI Site H were similar (Figure 32). Tabular summary current data for Site D and HSWRI Site H are found in Table 3.
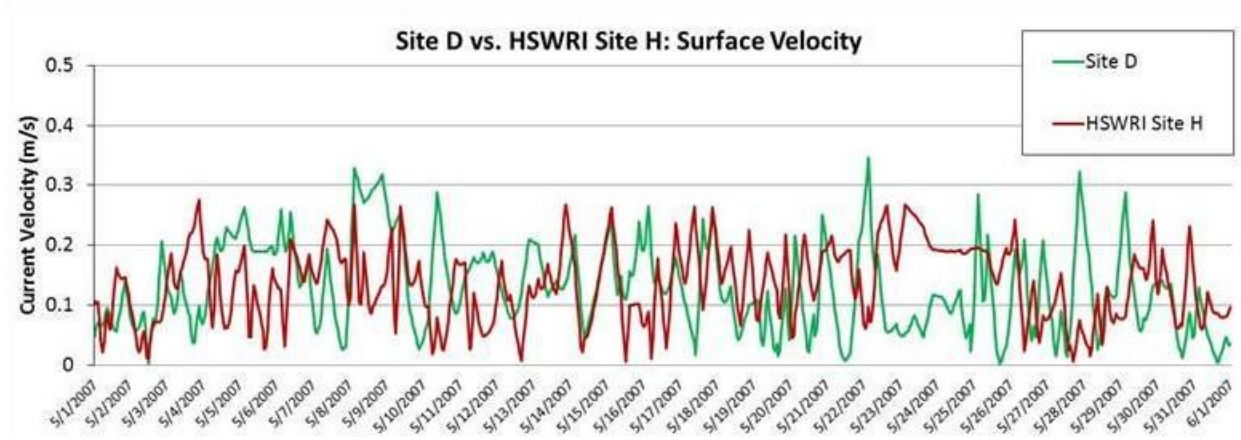

Figure 32: A comparison of hourly surface velocity at Farm Site D and HSWRI Site H.

Table 3: Summary data for currents and current headings at Farm Site D and HSWRI Site H.

SITE D	Surface Velocity (m/s)	Pen Velocity (m/s)	Bottom Velocity (m/s)	Surface Heading (deg)	Pen Heading (deg)	Bottom Heading (deg)
Mean	0.13	0.12	0.11	2.48	2.55	3.35
SD	0.07	0.07	0.06	1.16	1.17	0.95
Min	0.00	0.00	0.00	0.90	0.90	0.90
Max	0.35	0.33	0.33	4.50	4.50	4.50
Skew	0.50	0.66	1.10	0.36	0.25	-0.87
HSWRI SITE H	Surface Velocity (m/s)	Pen Velocity (m/s)	Bottom Velocity (m/s)	Surface Heading (deg)	Pen Heading (deg)	Bottom Heading (deg)
Mean	0.13	0.12	0.09	2.59	2.64	3.50
SD	0.06	0.05	0.05	0.97	0.98	0.63
Min	0.01	0.01	0.00	0.90	0.90	0.90
Max	0.28	0.25	0.28	4.50	4.49	4.50
Skew	0.05	0.05	0.87	0.37	0.28	-1.80

Average predicted surface and bottom velocities for all eight farm sites are shown in Figure 33. Site location progresses from North to South as the figure reads left to right; Site A is furthest north while HSWRI Site H is furthest south. Similar to the current data from Site D and HSWRI Site H presented above, surface velocity is higher than bottom velocity at each farm site. Notably, both surface and bottom velocities are generally higher at the more centrally-located sites (Sites C-G) than at the outskirt sites (A, B and H).
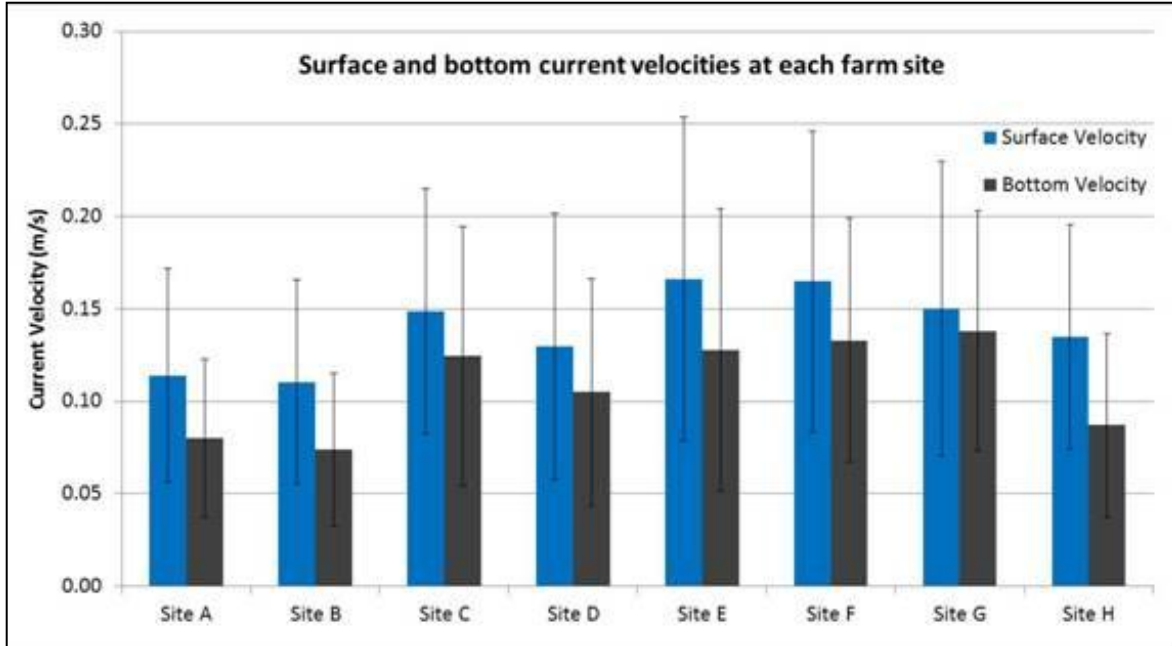
Figure 33: Mean surface and bottom current velocities at each farm site.

As Farm Site D and HSWRI Site H provide some useful comparisons based on location, so too do capture cells 3 and 5. Cell 3 is closer to the central fish farms and is in deeper water (~450m depth) than cell 3, which is more shallow and closer to shore (~200m depth). Figure 34 compares current velocity between capture cell 3 (offshore) and capture cell 5 (nearshore), as well as between cell 5 and HSWRI Site H. As expected, bottom current velocities (Figure 34, dashed lines) are consistently lower than cell/surface velocities (Figure 34, solid lines) at both cells as well as at Site H. In addition, the nearshore capture cell 5 (in black, both top and bottom Figure 34) has much lower cell and bottom velocities than either capture cell 3 or Site H. Because capture cell 5 is located on the shallower portion of the coastal shelf, it is somewhat isolated from the strong currents that affect cell 3; further analysis later in this section shows that this isolation also helps control local nutrient and other water quality factors. In Figure 34, note that capture cells 3 and 5 show cell velocity and bottom velocity, while HSWRI Site H shows surface velocity and bottom velocity. Cell/surface velocity represented by solid lines; bottom velocity is represented by dashed lines.
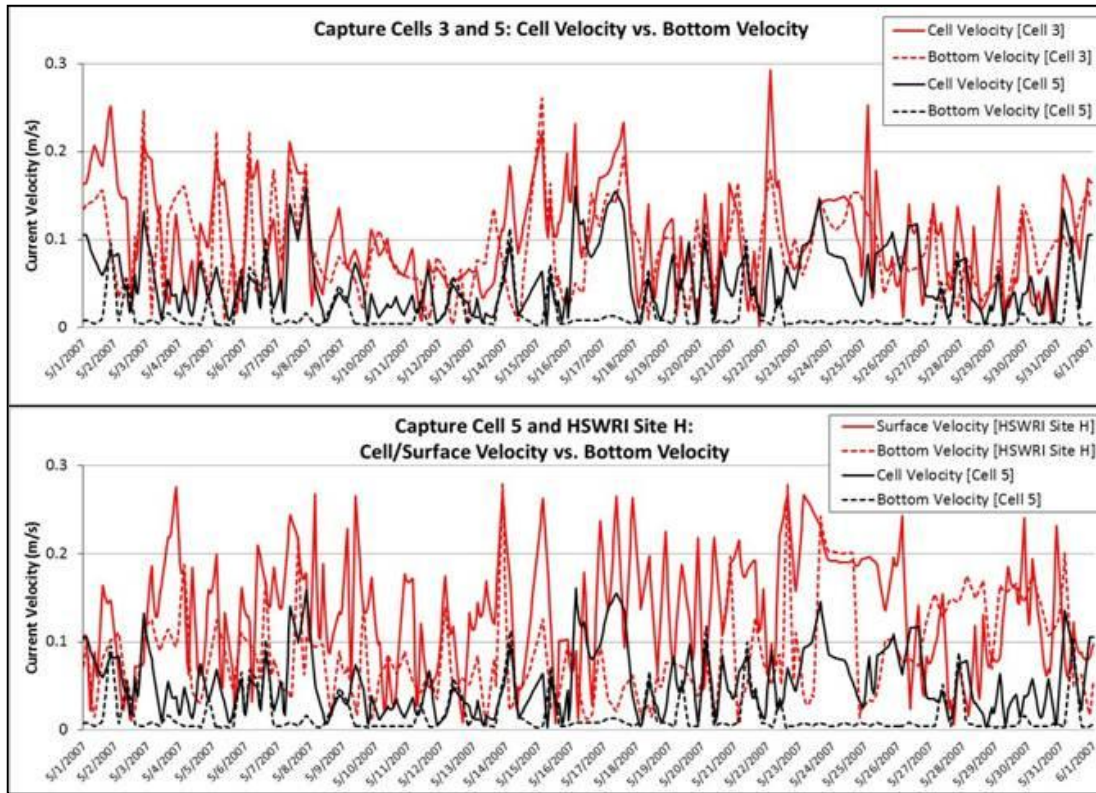
Figure 34: Comparisons of hourly velocities between capture cells 3 and 5, and between capture cell 5 and HSWRI Site H.

While considering our predicted current results, we can look at predicted water quality outputs and gain additional insight into the potential effects of this virtual fish farm array. Dissolved inorganic nitrogen and dissolved oxygen were predicted for each farm site and capture cell. Site D and HWSRI Site H provide one comparison of DIN and DO data (Figure 35). DIN and DO at both sites are variable but are fairly similar overall. DIN at Site D averaged 1.50±0.79 µmol/l while HSWRI Site H had a slightly lower average DO of 1.36±0.59 µmol/l; average DO levels at both sites were close to identical (8.06±0.20 mg/l at Site D and 8.09±0.15 mg/l at Site H).
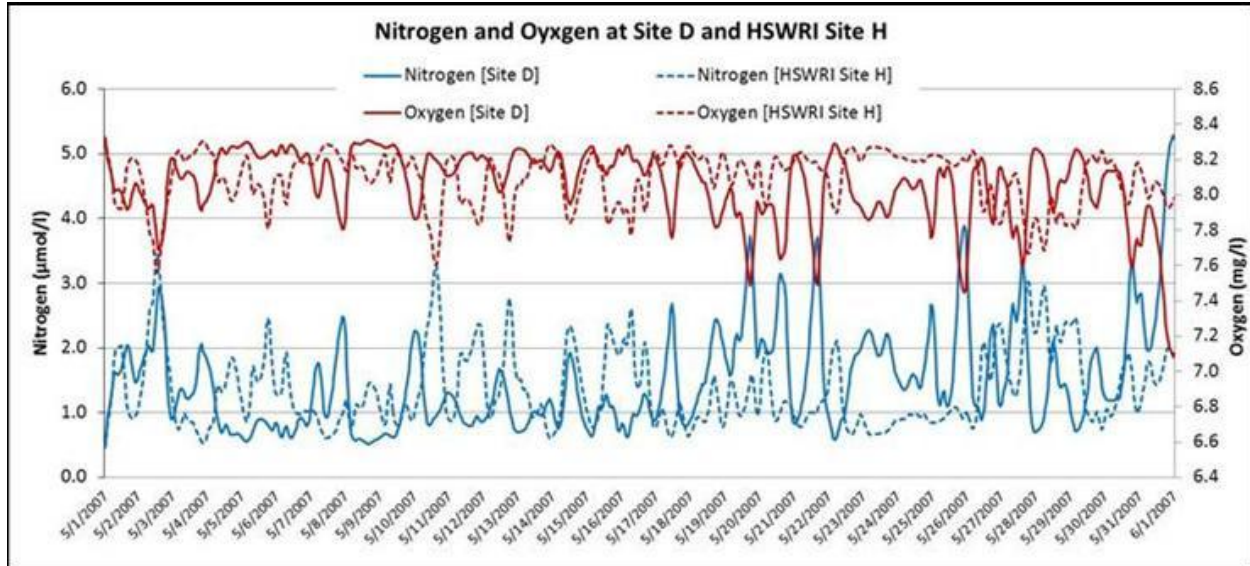
Figure 35: Hourly nitrogen and oxygen records from Farm Site D and HSWRI Site H. Site D data are represented by solid lines and HSWRI Site H data are represented by dashed lines. Nitrogen scale is on the left in µmol/l; oxygen scale is on the right in mg/l.

Dissolved inorganic nitrogen and oxygen, as well as phytoplankton, were also tracked at our six capture cells. Figure 36 displays DIN, phytoplankton and DO hourly predicted values at capture cell 3 (solid lines) and capture cell 5 (dashed lines). It is evident that all three measured qualities are much more consistent at the nearshore capture cell 5. DIN, phytoplankton and DO each experienced more variation at cell 3 than at cell 5. In addition, DIN and phytoplankton were both greater on average at offshore cell 3, with a particular emphasis on phytoplankton. Oxygen, on the other hand, was slightly lower at offshore cell 3.

Much of the low variation observed at nearshore cell 5 can be explained by the currents presented earlier (refer back to Figure 34). Lower surface and bottom currents at the nearshore cell mean that less material from the central fish farms is reaching cell 5. This correlates well with the water quality data in Figure 36: nitrogen, most likely originating at the central fish farms, is much more prevalent at cell 3 than at cell 5. Phytoplankton levels are also higher at cell 3 (Figure 37). To some degree, phytoplankton levels are directly correlated with nitrogen levels: several peaks observed in the phytoplankton data in Figure 36 occur as nitrogen increases. Furthermore, oxygen levels tend to decrease as phytoplankton and DIN levels increase – and oxygen is depleted at the fish farm sites due to the heavy concentration of respiring fish – which explains the occasional decreases in oxygen observed at cell 3 compared to the nearshore cell 5.
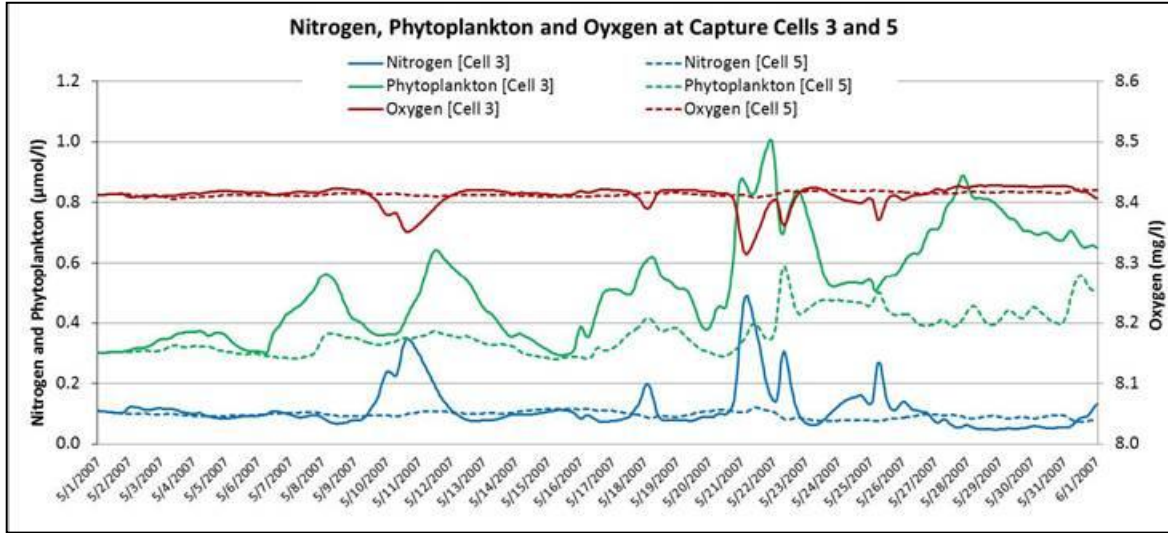
Figure 36: Hourly nitrogen, phytoplankton and oxygen records from capture cells 3 and 5. Cell 3 data are represented by solid lines and cell 5 data are represented by dashed lines.
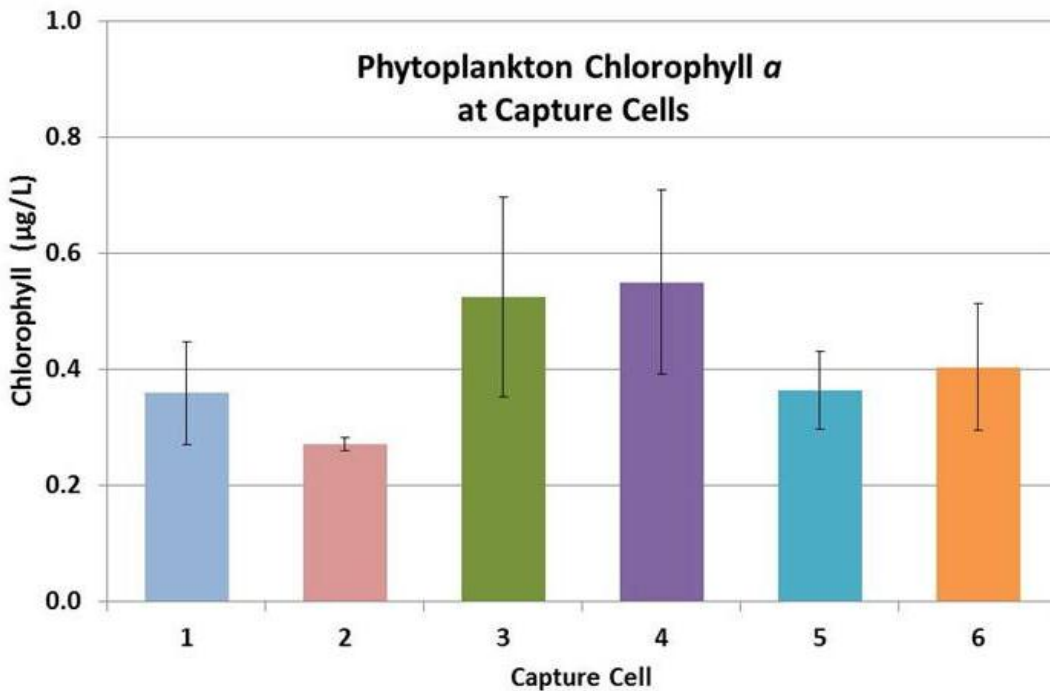

Figure 37: Phytoplankton as chlorophyll *a* at capture cell locations.

It is evident that some variation in dissolved inorganic nitrogen and dissolved oxygen between capture cells is likely due to area fish farms and current patterns. However, when comparing water quality data from capture cells to data taken at the farm sites themselves, it becomes clear that the capture cell locations are relatively unaffected compared to the area in immediate

proximity to the fish farms. Figure 38 shows that the fish farms have a much larger effect on the immediate area than on the capture cells, which are typically 5-10 km away from the farm sites. By comparing DIN levels predicted at the eight farm sites to DIN levels of the six capture cells, we see that DIN is much higher at the farm sites than at the capture cells. This difference is due to a) the relatively rapid dispersion of DIN as materials are carried away from the fish farm sites due to complex regional currents, and b) the fact that much of the fish farm material sinks into deeper water before making it to the capture cell areas 5-10 kilometers distant.
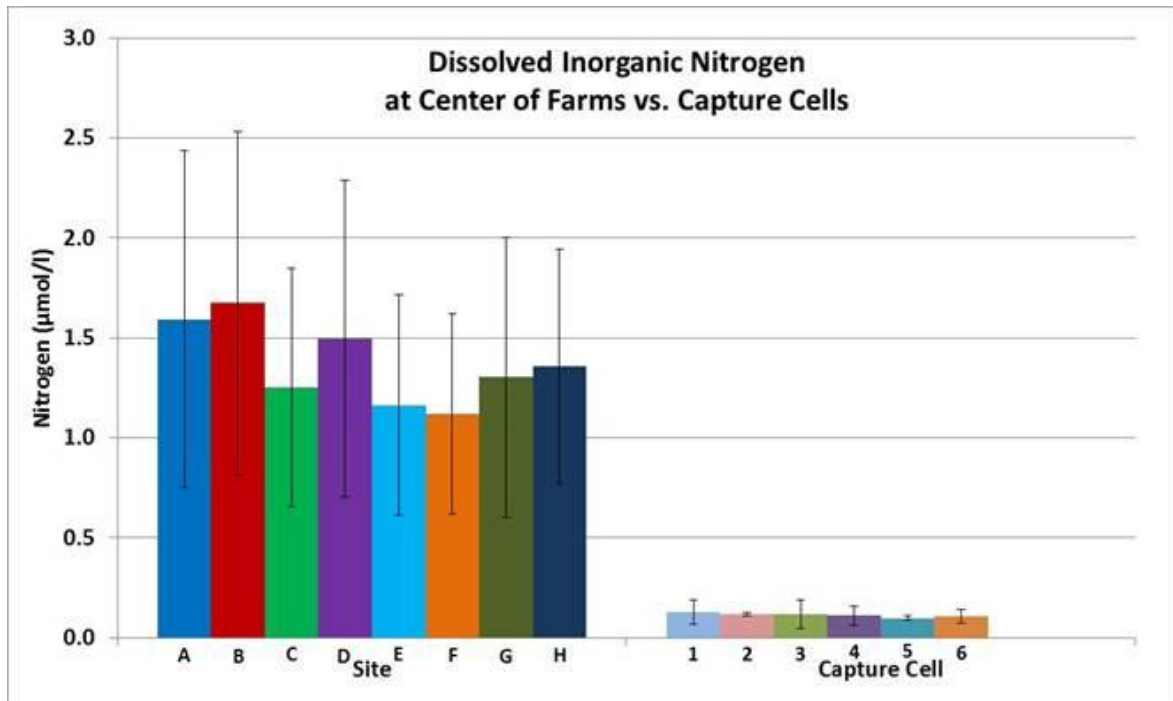

Figure 38: Mean dissolved inorganic nitrogen recorded at each farm site (left) and capture cell (right).

When examining dissolved oxygen levels, the opposite is true: DO levels at capture cells are higher than DO at the farms (Figure 39). Again, this is directly tied to activity at the fish farms: high numbers of farmed fish use a significant amount of oxygen via respiration. While this results in lowered DO values at each farm site, numerous field studies have shown that DO values return to background by just a few tens of meters downstream and at the capture cell locations (5-10 km away) DO values are certainly higher. DO values at each capture cell are all very similar, with extremely low standard errors, suggesting that there is no significant effect of fish farms on capture cell dissolved oxygen levels due to circulation and strong mixing of farm and non-farm water and phytoplankton production of oxygen.
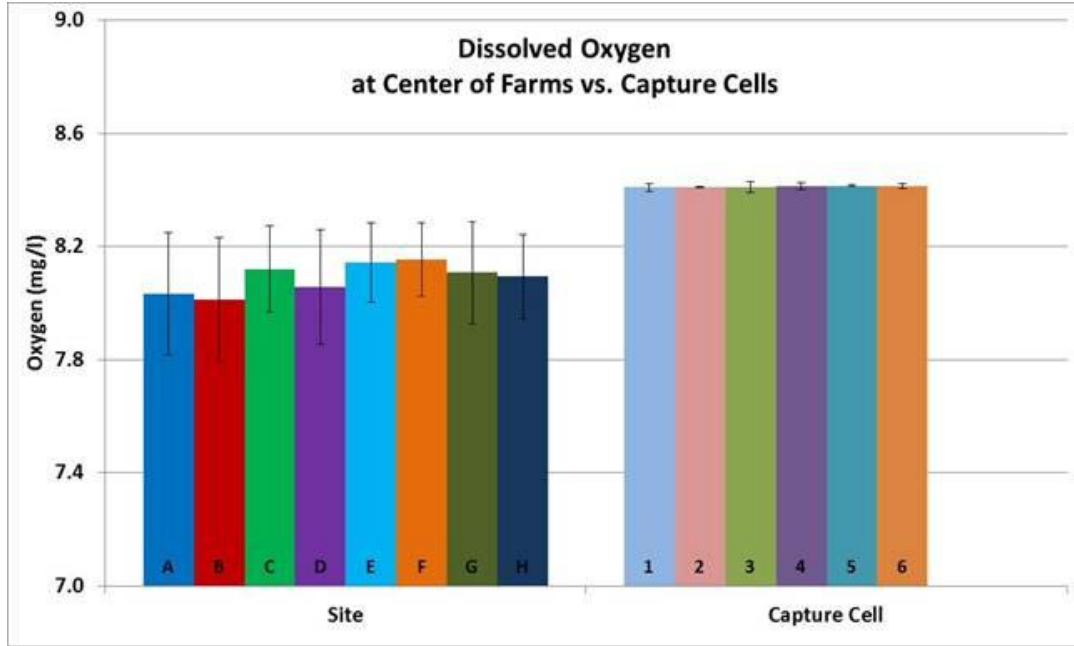
Figure 39: Mean dissolved oxygen recorded at each farm site (left) and capture cell (right).

3.6. Section References

Armstrong-Howard, M.D. et al. (2007). Nitrogenous preference of toxigenic *Pseudo-nitzschia australis* (Bacillariophyceae) from field and laboratory experiments. Harmful Algae. 6: 206-217.

Boyce, D.G., M.R. Lewis and B.Worm. (2010). Global phytoplankton decline over the last century. Nature 466, 591-596.

Corcoran A.A., K. M. Reifel, B.H. Jones, R.F. Shipe. (2010). Spatial and temporal development of physical, chemical, and biological characteristics of stormwater plumes in Santa Monica Bay, California (USA) Journal of Sea Research 63:129–142.

Galloway, J.N., et al. (2004). Nitrogen cycles, past, present and future. Biogeochemistry 70: 153–226.

Kiefer D.A., J.E. Rensel and F.J. O'Brien. (2008). AquaModel simulation of Water Column and Sediment Effects of Fish Mariculture at the Proposed Hubbs-SeaWorld Research Institute Offshore Aquaculture Demonstration Project. Prepared for Hubbs SeaWorld Research Institute, San Diego, CA by Systems Science Applications, Inc. and Rensel Associates Aquatic Sciences. 68 pp. Available on request from HSWRI or SSA.

Mann, K.H., Lazier, J.R.N. (2006). Dynamics of Marine Ecosystems: Biological-Physical Interactions in the Oceans. Third Edition. Blackwell Publishing. Pp. 166–167, 194-204.

Rensel, J.E., D.A. Kiefer, J.R.M. Forster, D.L. Woodruff and N.R. Evans. (2007). Offshore finfish mariculture in the Strait of Juan de Fuca. Bull. Fish. Res. Agen. No. 19, 113-129,

http://www.fra.affrc.go.jp/bulletin/bull/bull19/13.pdf.

Smith, P. E., and R. W. Eppley. (1982). Primary production and the anchovy population in the Southern California Bight: comparison of time series. Limnol. Oceanogr. 27, ppl-17.

4. Ambient Conditions at the Gulf of Maine Open Ocean Aquaculture Study Site

4.1. Background

The cool and productive waters of the southwestern portion of the Gulf of Maine have shown open ocean aquaculture potential. The University of New Hampshire (UNH) operated an open ocean aquaculture (OOA) site in the region from late 1999 until 2010. The site is in approximately 55 meters of water depth and located 2.6 km south of the Isles of Shoals in the state waters of New Hampshire (USA) as shown on Figure 40. As most recently described in Grizzle et al. (In preparation), it has been the focus of numerous aquaculture systems and fish deployment studies. For research purposes, the fish cages used were relatively small with containment volumes ranging from 600 to 3,000 m^3 with the largest fish stocking abundance occurring from April 2006 to February 2009. During that particular study, 48,000 Atlantic cod (*Gadus morhua*) at 30 g were grown to 2,200 g with 60% survival. Even though the amount of biomass used as part of this study was small compared to commercial levels, the economic potential was evident. Success, however, will require substantial more fish and the quantification of the environmental effects.
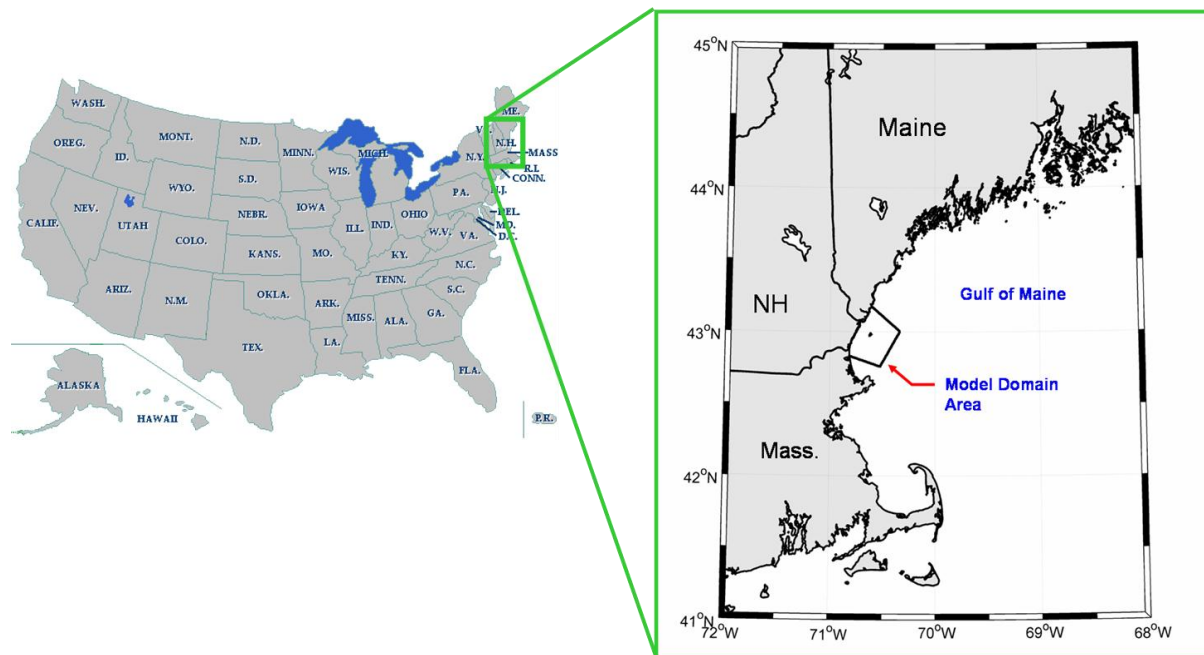

Figure 40: The area of interest is in the Gulf of Maine, off the coast of New Hampshire.

As part of a comprehensive aquaculture study project, Grizzle et al., (In preparation) also describes the robust monitoring program conducted for each of the six deployment years. For

this study, data sets from this and other complimentary monitoring programs were used to represent the yearly ambient conditions at the site. An extensive number of data sets were acquired from the region. The composite ambient data sets were then used as input to AquaModel to calculate the bioenergetics in a fish farm, the production of solid and dissolved wastes, the transport and fate of the wastes and characteristics of the benthos (e.g., aerobic and anaerobic biomass, total organic carbon and sulfide loading). Note that Atlantic salmon (*Salmo salar*) were the test species in our simulations because the bioenergetics are already described within AquaModel and these fish are suited to environmental conditions in the region for producing reasonable results. Simulations also produce perturbations of water column nitrogen and dissolved oxygen, and interaction between phyto- and zooplankton communities. Once the extensive set of ambient conditions were established as input to AquaModel, the program was then used to investigate the dynamic response of the surrounding environment to possible commercial level operations.

4.2. Data Collection Site Overview

Growth performance influences both the economic viability and environmental impact of a marine aquaculture facility. By understanding the local ambient conditions within an analytical tool system, growth performance may be enhanced and calculations made through use of the cultured species bioenergetics and the estimated response. Also from the application of bioenergetics modeling of the fish, waste production can be quantified and fate determined through physical and biological submodels simulating distribution and assimilation in the environment. Grow-out cycles often span 1-2 years and in areas like the Gulf of Maine, ambient seasonal and inter-annual condition variability can be substantial, and therefore long-term observations are needed to represent the conditions. In an effort to characterize the variability at the UNH aquaculture site, observations of several key environmental parameters were made from 2001 into 2008. Data sets were obtained primarily from a near-field oceanographic buoy (Irish and Fredriksson, 2003 and Irish, et al, 2004) at the OOA site. Complementary data sets were also collected from a far-field oceanographic buoy, operated by the UNH Center for Coastal Ocean Observation and Analysis (COOA), and near- and far-field water sampling stations as shown on Figure 41.
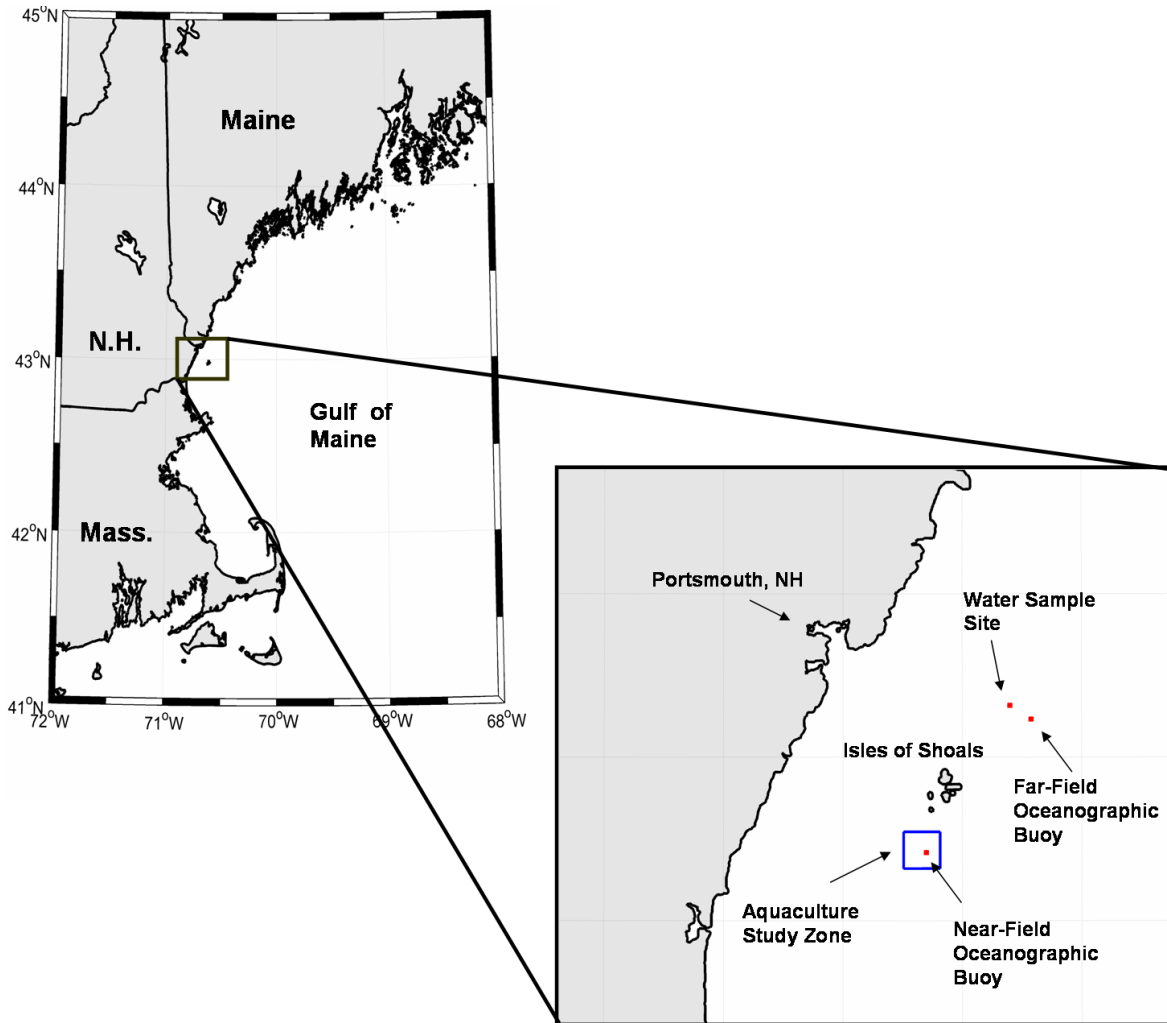
Figure 41: Data sets to describe the ambient conditions were obtained from multiple locations in the region.

From the near-field oceanographic buoy platform, temperature and salinity were measured at the surface (about 0.75 m depth), at about 22 to 25 m mid-water depth, and near the bottom approximately 53 m in 55 meters of water depth. An upward looking Acoustic Doppler Current Profiler (ADCP) located near the bottom provided current profile data from 11 to 47 m depth. Instruments on the mooring also sampled oxygen, chlorophyll-*a* and turbidity time series at 22 and 53 m depth. The near-field oceanographic buoy was located at 42º 56.5' N x 70º 37.8' W and was installed for nearly 6 years. During this time, the system was typically deployed and recovered 3-4 times per year. An example data record (Figure 42) shows the multi-year time series plot of the temperature and salinity records at the depths of 1-, 22- and 53-m for 21 deployments.
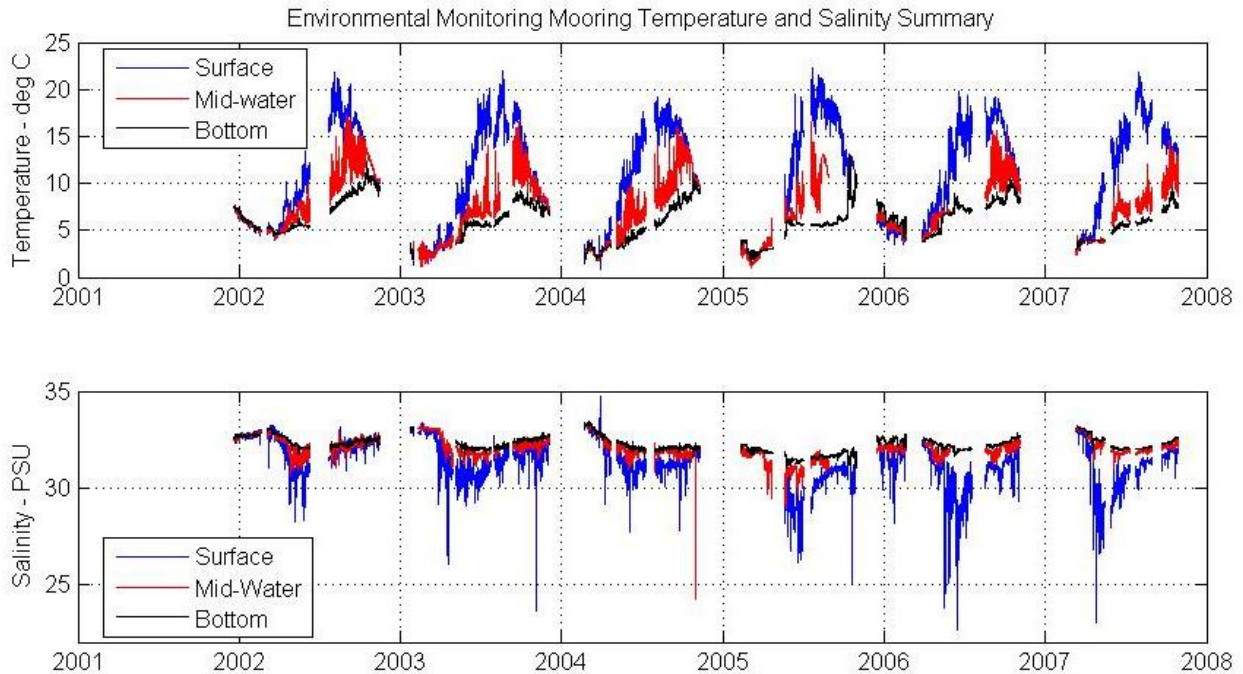
Figure 42: Temperature and salinity data results for each deployment during the six-year period.

In addition to data sets from the near-field oceanographic buoy, information was also gathered from a far-field water sampling site (also shown on Figure 41) at 43º 1.9' N x 70º 33.6' W in about 60 m of water. This site is about 10 km NNE of the UNH aquaculture study zone. Data sets from a far-field oceanographic buoy platform (Irish, et al., 2010) were also used to represent the regional ambient conditions. The location of this system was at 43º 1.4'N x 70º 32.53'W, about 1.7 km from the far-field water sampling station in about 69 m of water (see Figure 41).

A primary goal of this work was to establish representative data sets for ambient conditions for the region and velocities for the site. Values from specific regional data collection locations had to be similar in spatial and temporal scales and units. An initial review examined where data sets overlapped in time with those from the OOA site. It was found that the general trends and values agreed. Therefore, it was assumed reasonable to use these values of the conditions in the Western Gulf of Maine as being representative of ambient conditions at the OOA site and for regional simulations. This assessment can be further justified since a general flow of water moves south from the Maine and New Hampshire Coasts towards Cape Cod Bay of Massachusetts. For the AquaModel simulations, the nitrogen and biological data sets were collected from the far-field water sampling station. The temperature and oxygen data are from

measurements from the near-field oceanographic buoy, with modification of the surface oxygen from three years of collecting-bottle data taken at the aquaculture site. Four years of surface oxygen data from the far-field oceanographic buoy were utilized. Wind data were collected from the Isles of Shoals between the near- and far-field sites. Irradiance (PAR) was collected from a variety of data sets in the Gulf of Maine region. Current direction and velocity were collected from the near-field mooring. A summary of the data sets used in this analysis is provided in Table 4.

Table 4: Data set source summary

Aqua Model Input Parameters	Primary Source	Sample Dates	Secondary Source
Temperature	Near-field buoy	12/2001-11/2007	Near- and Far-field sample
Thermocline depth	Near-field profiles	6/2001-10/2007	Far-field profiles
Dissolved oxygen	Near-field buoy and samples	12/2005-11/2007	Far-field buoy
Dissolved inorganic nitrogen	Far-field samples	4/2004-9/2009	n.a.
Particulate organic Nitrogen	Far-field samples	4/2004-9/2009	n.a.
Phytoplankton	Far-Field samples	4/1004-9/2009	n.a.
Nitrogen from phytoplankton	Far-field samples	4/2004-9/2009	n.a.
Zooplankton	Far-field samples	4/2004-9/2009	n.a.
Nitrogen from zooplankton	Far-field samples	2002-2007	n.a.
Irradiance	GLOBEC Far-field buoy	1997-1999	Flux Buoy & Near-field buoy
ADCP Current – flow, tides and weather forced	Near-field buoy	2003-2006	n.a.
Wind Speeds	NDBC IOSN3	4/2009-9/2010	Far-field buoy

4.3. Environmental Data Processing

To obtain a composite representation of the ambient conditions during short time intervals over several years, the data sets from all the instrument deployments, water samples and profiles at both the near- and far-field sites were plotted in a year scale, beginning with April 1). Time

series data sets from the near-field oceanographic buoy were acquired at the nominal depths of 1, 22 and 53 meters (sampled at 15-minute intervals). Discrete samples from the water sampling stations were also plotted for the 0-2, 10-25, and 25-bottom depths. The samples were typically taken monthly from 2004 to 2009. Profile information was qualitatively included as a check for consistency and to determine thermocline depth. All of the data sets were used to produce composite raw-data plots at nominal surface (~1 meter), mid-water column (~22 m) and deep (~53 m) vertical locations. From the composite raw-data plots, each year data set was subjectively smoothed and interpolated to obtain weekly values. During the subjective smoothing process, it was found that uneven coverage existed with more summer than winter information, but an average was selected for "obvious" times with little variation from year to year, then interpolated between using a best visual fit. The "raw" data show that there is large inter-annual variability in the data, especially during the spring runoff (see Figure 42). In addition, it was found from the data sets that high frequency variations existed. The variability was averaged to obtain weekly values. It is likely that the high frequency oscillations were created by the tidal currents advecting offshore gradients past the sensors and by internal solitary waves advecting the water vertically.

4.4. Temperature

A multi-year temperature data set was acquired from the near-field oceanographic buoy at the OOA site. Included in the raw data set were discrete samples taken from the both the near- and far-field sampling stations. Each of the data sets were then checked with conductivity (i.e. salinity), temperature and depth (CTD) instruments. The results are shown on Figure 43 where a clear seasonal pattern was exhibited showing stratification during the warmer months and a well-mixed water column during the colder months. The start of April 1 is about the time that stratification is observed in the water column. Note that the Gulf of Maine simulations performed as part of this study were started in April as the waters would begin to warm at that time after the winter and salmon smolts are often available in the spring. The data set is assumed typical of environmental conditions in the coastal Gulf of Maine. The edited weekly temperature data were added to the weekly ambient data file for AquaModel input.
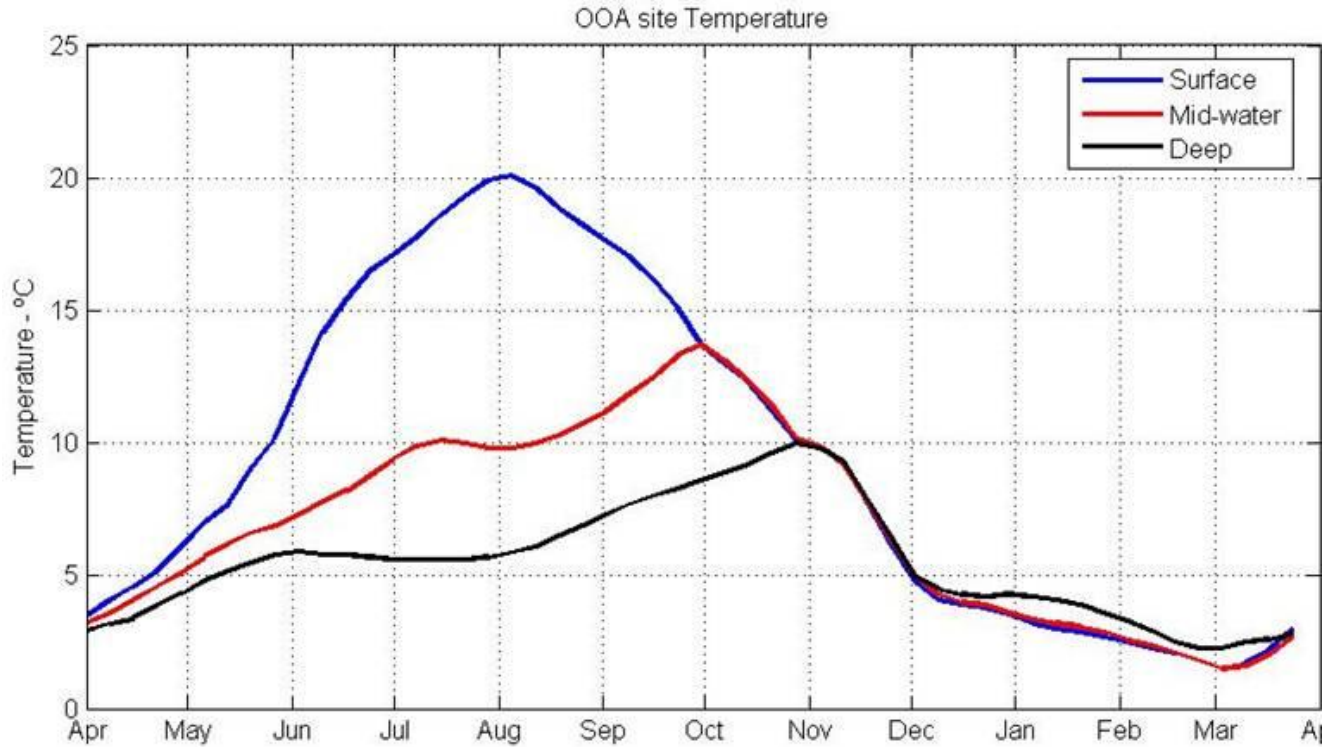
Figure 43: The composite yearly temperature cycle where surface– from 2 to 21ºC, mid-water ~22 m – 2 to 14ºC and bottom at ~53 m– 2 to 10º C.

Temperature and its variability is one of the most important parameters to understand in the operation of a fish farm. It affects the growth of the fish within the farm and the assimilation rate of waste products by the food web organisms that benefit from the wastes, directly and indirectly through enhanced primary or secondary production. This in turn affects the flux of dissolved oxygen in the region. In general, the water during the winter is nearly well-mixed from the top to the bottom. Often temperature profiles show winter temperature changes of less than 0.01ºC from top to bottom. In the spring (late March) the surface waters start to warm until early August when they reach a temperature of approximately 21ºC before they start to cool. Mid-water temperatures also start to increase in late March and early April, but not as much as the surface waters approaching approximately 14ºC in early fall. The temperature values of the mid-water can vary greatly in periods of time when the thermocline depth is near 22 m (rather than a more typical 15 m) and the sensors first see warmer surface waters, then deeper, cooler waters. Bottom waters also start to warm in late March, but warm the least amount, reaching only about 10ºC maximum. As the surface waters cool in the fall, they are seen to mix deeper and deeper

and merge first with the mid-water temperatures as the storm mixing progresses deeper. In November, the water column is well mixed and temperatures continue to decrease reaching minimum values around 2ºC in February. At this and similar low temperatures, salmon stop growing and the food consumption rate drops significantly. In the spring, the cycle begins again as the water starts to warm and vertical stratification builds.

4.5. Thermocline/Halocline/Pycnocline Depth

Modelers often use a two-layer configuration to represent vertical diffusion/dispersion and to take into account the warmer surface layers and cooler deep layers, where the surface layer is uniform in properties and well mixed due to the winds. The CTD profiles from the OOA site were examined for the depth of the thermocline (i.e., the high gradient region between the warmer surface water, and cooler deeper water), and this depth plotted versus time (Figure 44). The figure shows that the onset of stratification starts in early April when it becomes strong enough to prevent mixing by the weaker storms. In general, the thermocline, halocline and pycnocline occur at approximately the same depth. Therefore, the thermocline depth was used as the stratification-indicating parameter for mixed layer depth. This data set is also used as input to AquaModel, creating two vertical strata within the water column. In each depth strata, a different vertical and horizontal mixing regime was applied during a simulation. The edited weekly thermocline depth data were added to the weekly ambient data file for input to AquaModel.
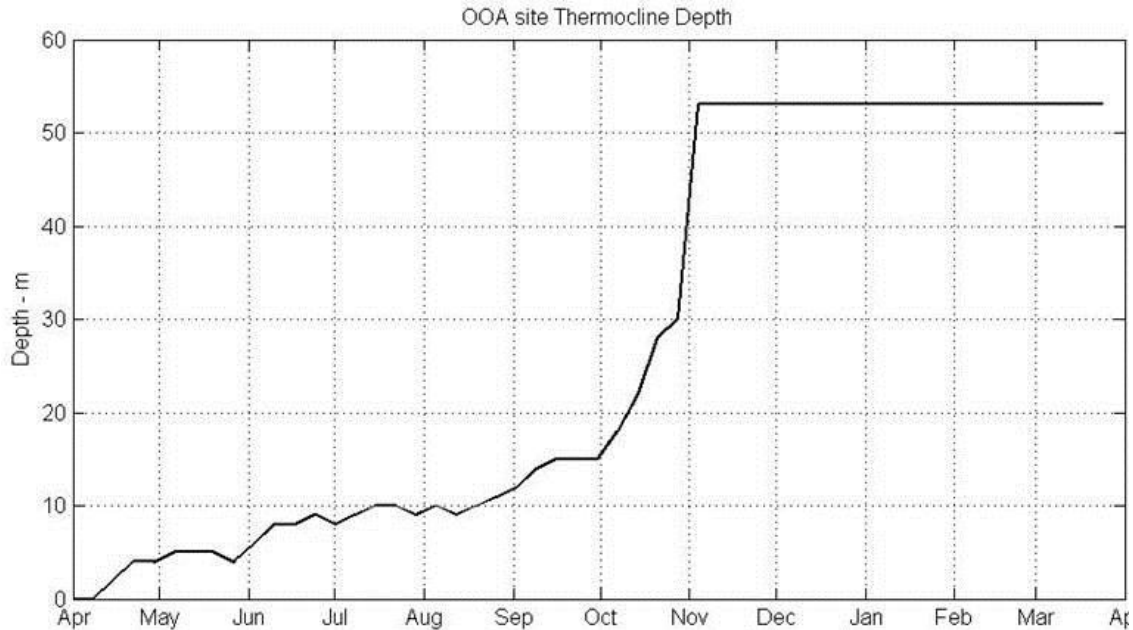
Figure 44: Smoothed averaged depth of the thermocline representing the depth of the upper mixed layer.

4.6. Dissolved Oxygen

Unlike the temperature data sets, the dissolved oxygen data were more difficult to evaluate. Dissolved oxygen sensor data sets were analyzed from those obtained from the near-field oceanographic buoy from 2005 to 2007, calibrated with Winkler titrations of bottle water samples. The bottle data were used to remove the drift in the moored time series observations (Irish, et al., 2008). The water samples were taken monthly from 2004 to 2009 from April through October. The bottle data were taken near the surface (0 to 2 m depth), mid-water (22 m depth), and near the bottom (about 53 m). Then the data from each depth was plotted along with the time-series data, and again a smooth, visual curve was fit to the time series.

The near-field buoy did not have an oxygen sensor near the surface, but the far-field buoy did. The data from this mooring was used with the near-field Winkler bottle data to create the surface oxygen time series. Note that the bottle data were taken at a single point in time, and so may show the tidal variability that was averaged out of the time series data. Therefore, the "heavy" smoothing of the bottle data is justified due to the large tidal variations. The final data set used as input to the AquaModel is shown on Figure 45 starting at April 1. The edited weekly dissolved oxygen data were added to the GOM Weekly Ambient Excel file for input to AquaModel.
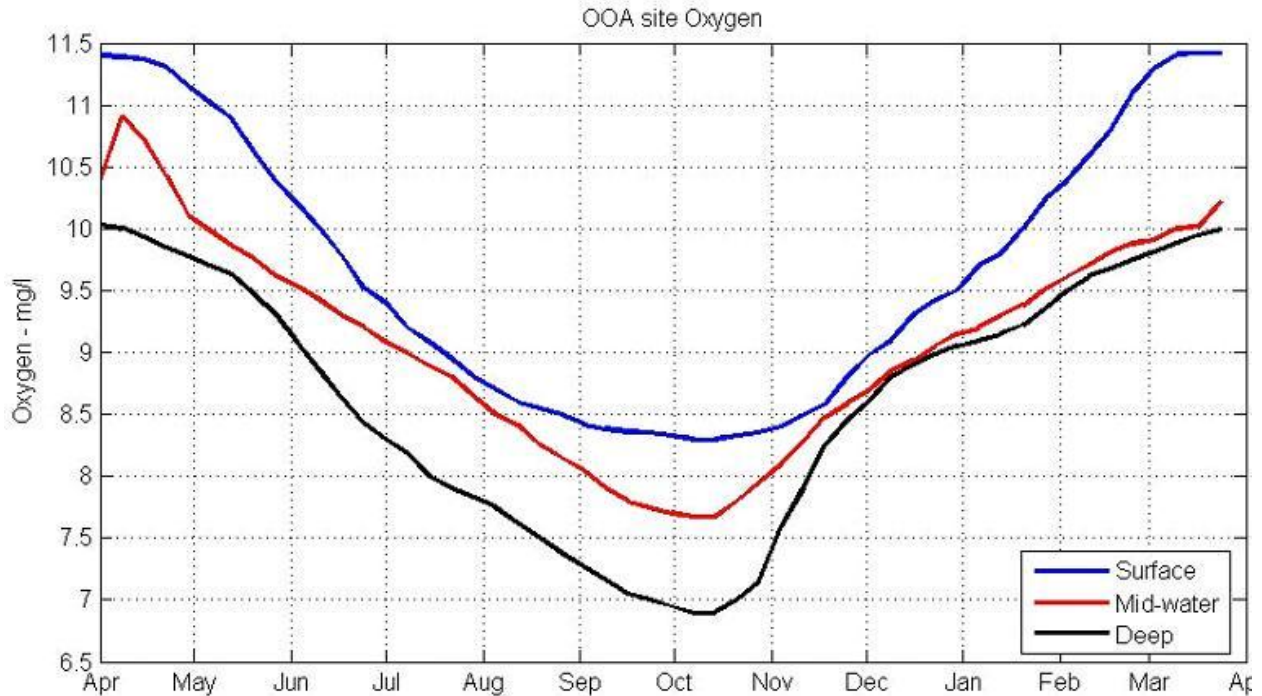
Figure 45: Smoothed ambient dissolved oxygen data.

The surface oxygen data shows values ranging from approximately 8.4 to 11.5 mg/L, with slightly lower concentrations in the fall when overturning mixes the higher oxygen concentrations in the surface water with lower concentrations in deeper waters. Normally, the surface water oxygen concentrations are about 105 to 110% of saturation, except during this fall mixing time. The mid-water and bottom oxygen concentrations obtained from the near-field oceanographic buoy were validated with profile data sets and Winkler bottle samples. The information shows that the water column is well mixed in the winter (December through April). Oxygen levels in waters below the thermocline start decreasing with the onset of vertical stratification and continue until the fall storms overturn the water in late October or early November.

The mid-water dissolved oxygen data set shows signs of spring and fall phytoplankton activity with increased oxygen concentrations, at the beginning of the data set in April. During the mid-summer, the mid-water (22 m) oxygen starts to decrease with time until the fall bloom and the occurrence of overturning and mixing. It should be noted that the dissolved oxygen values at the site do not become critical for aquaculture applications since the Maine coastal current from the northeast is transporting new water into the site (mainly during spring and summer). In general,

the site seems to have adequate dissolved oxygen levels throughout the year and water depth, especially in comparison to west coast U.S. sites that are impacted by oceanic upwelling of cool, low dissolved oxygen water during summer and fall.

4.7. Particulate Organic Nitrogen

Particulate Organic Nitrogen (PON) data sets were collected north of the aquaculture site in the far-field by the COOA personnel during monthly cruises from 2004 through 2009. The data sets were organized into bins representing the surface (0-2 m), mid-water (10-25 m) and deep (25 m to bottom) water column locations. Only a few samples were recovered during May in the deep water (values of ~ 1.6 µMol/m³), so these data are not plotted. The available results were plotted, and a subjectively fitted through the observations at the two depths. This line was digitized and the PON concentrations in µMol/l plotted in Figure 46.
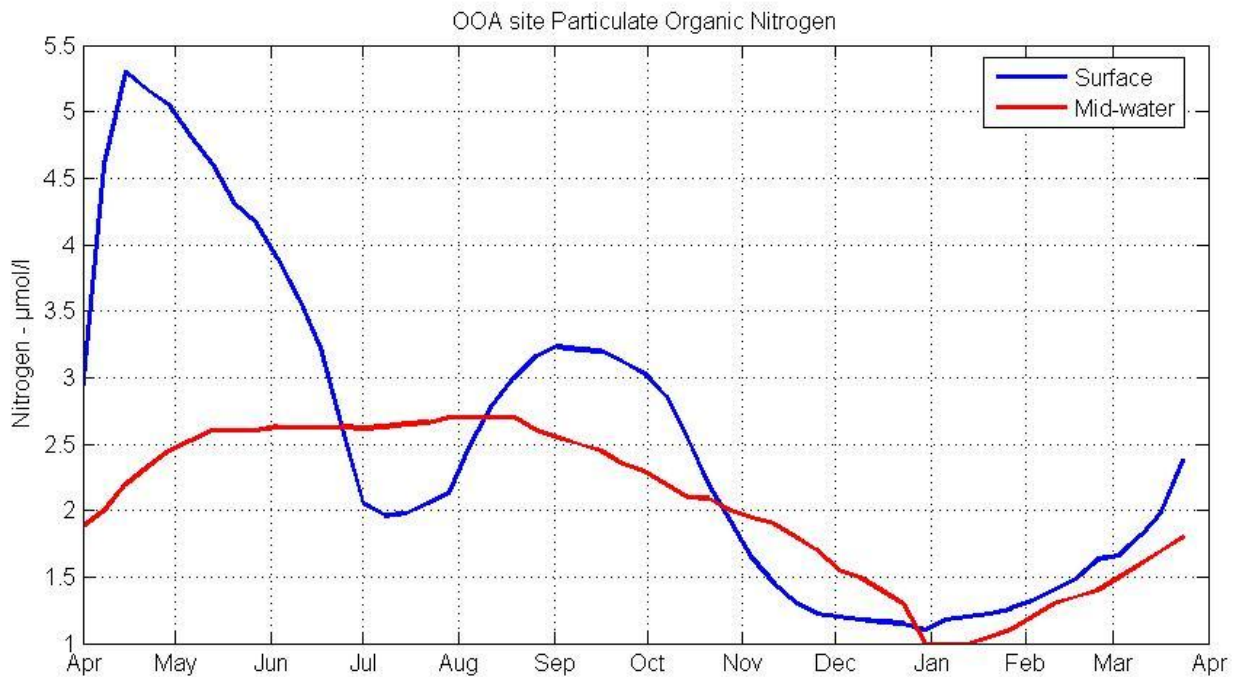

Figure 46: Particulate Organic Nitrogen in the top two layers.

4.8. Dissolved Inorganic Nitrogen

Dissolved inorganic nitrogen (DIN) is the ambient nitrogen input into AquaModel and is the sum of the nitrate (Figure 47), nitrite (Figure 48) and ammonium (Figure 49). As with the Particulate Organic Nitrogen (PON), the DIN data were collected north of the aquaculture site by the same

COOA personnel at the University of New Hampshire during monthly cruises from 2004 through 2009.   These data were organized into bins representing the surface (0-2 m), mid-water (2-25 m) and deep (25 m to bottom) water column locations. The results were then plotted and a subjective line drawn through the observations at the three depths. This line was digitized and the dissolved inorganic nitrogen concentrations in µMol/l plotted in Figure 50. Note that µMol/l is the same as mMol/m³ also expressed as µg atom/l or µM) and in any case is the AquaModel input requirement for nitrogen. The edited weekly DIN data set was added to the GOM Weekly Ambient Excel file for input to AquaModel.
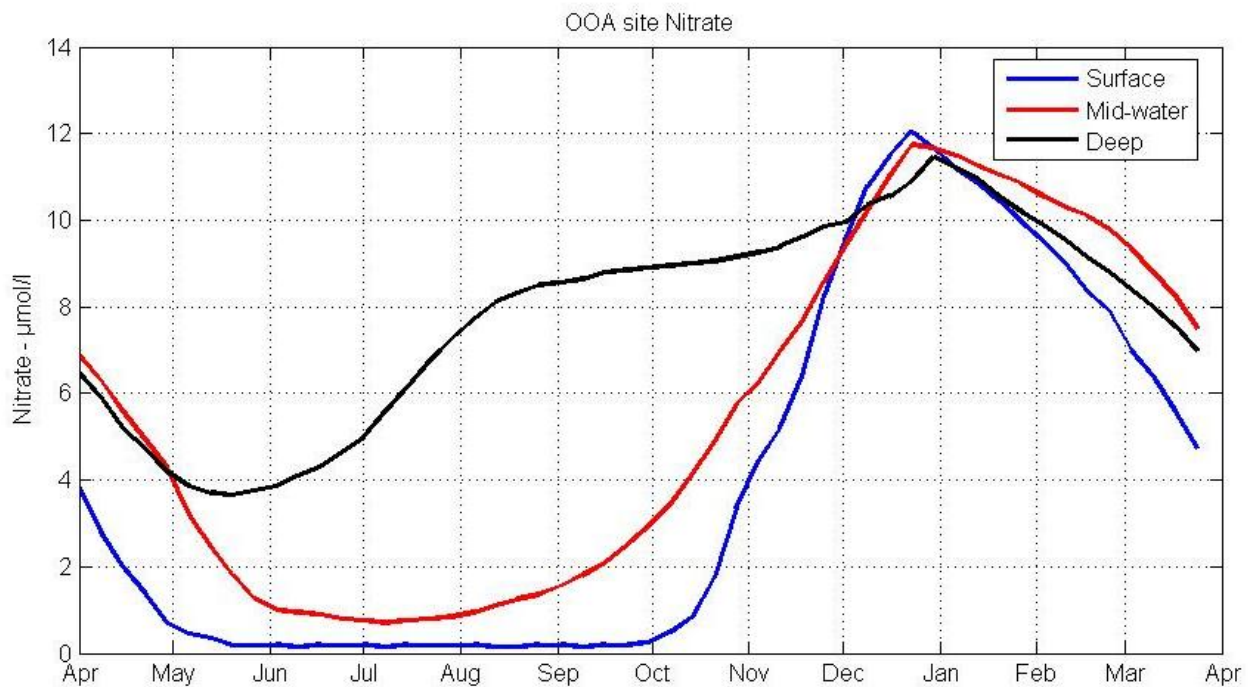

**Figure 47: Smoothed ambient nitrate.**
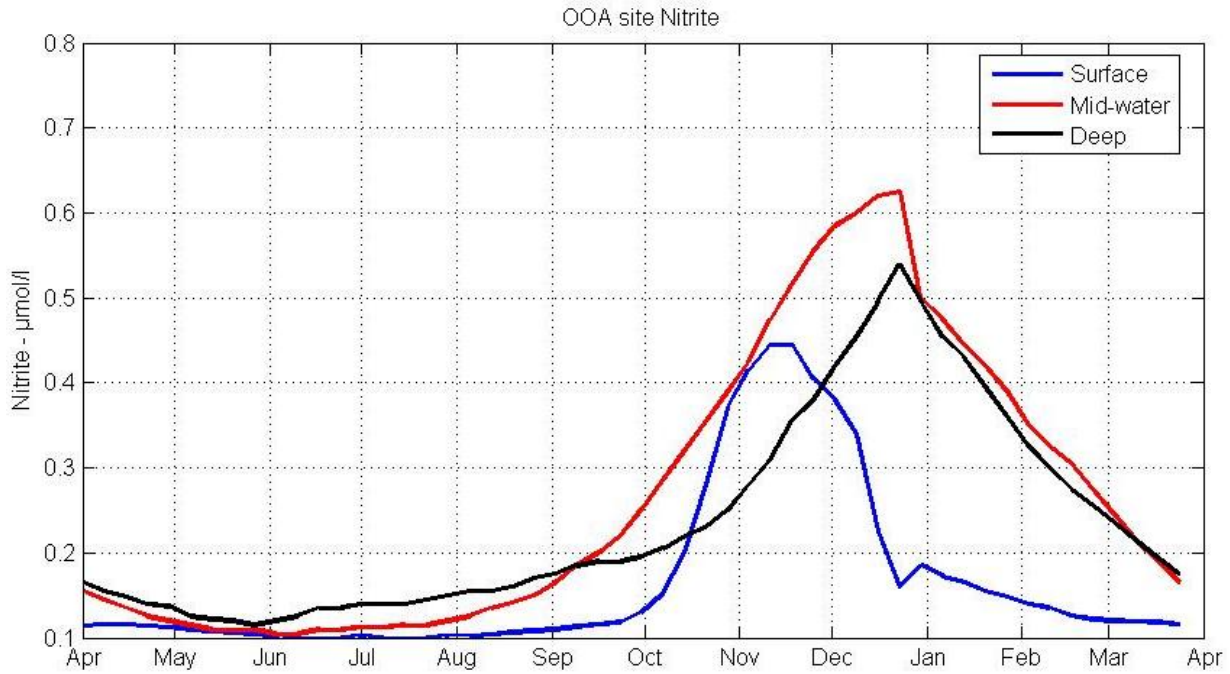
**Figure 48: Smoothed ambient nitrite.**
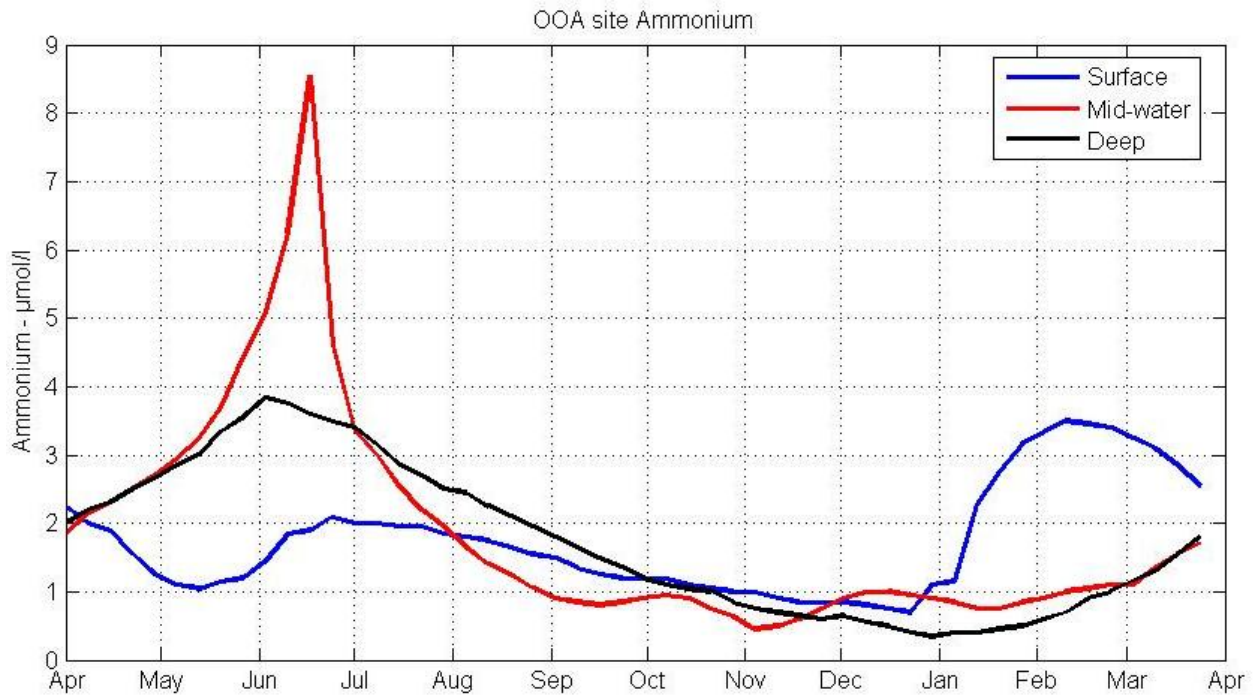
**Figure 49: Smoothed ambient ammonium.**
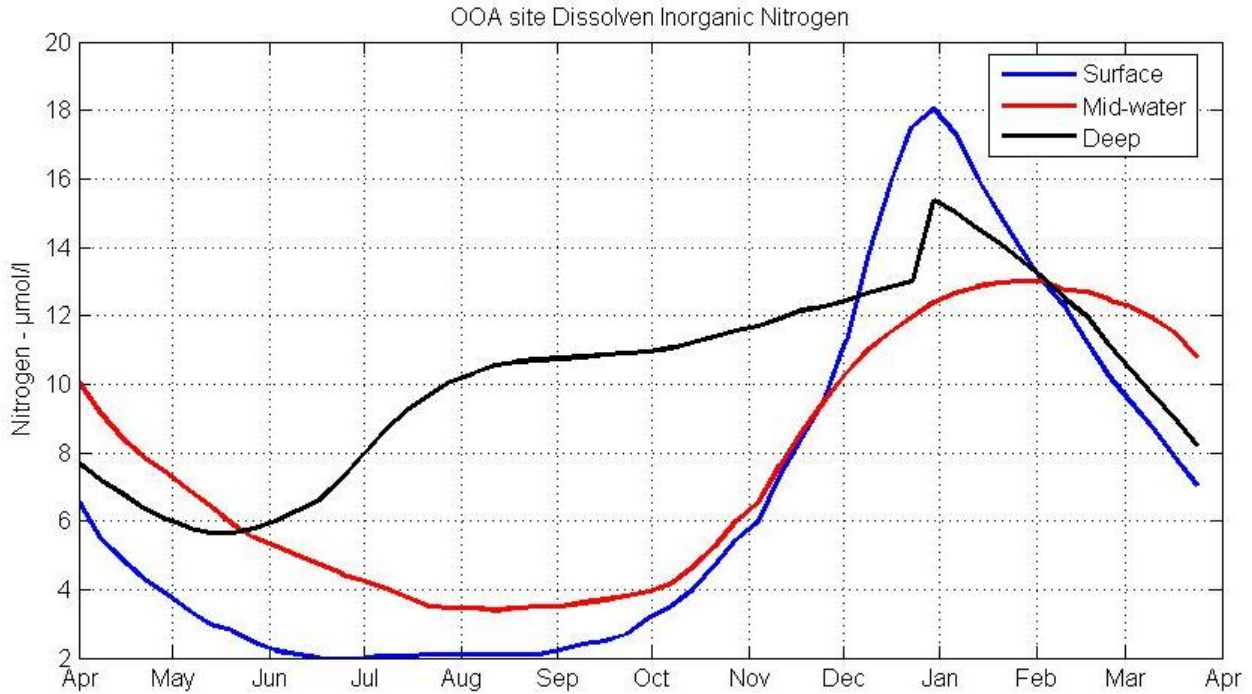
Figure 50: Smoothed ambient dissolved inorganic nitrogen.

4.9. Phytoplankton Nitrogen

The estimates of phytoplankton concentrations at the OOA site were made by fluorometric techniques detecting chlorophyll-a. This data set was collected at the far-field site by the COOA personnel at the University of New Hampshire during monthly cruises from 2004 through 2009. It was collected from a profiling fluorometer on a CTD and the data selected at the standard bin depths representing the surface (0-2 m), mid-water (2-25 m) and deep (25 m to bottom) water column locations. The results were then plotted in the same year-day format and a subjective line drawn through the observations at the three depths. This line was digitized and the seasonal phytoplankton concentrations in mg/m³ determined from standard fluorometer calibrations and plotted (Figure 51).
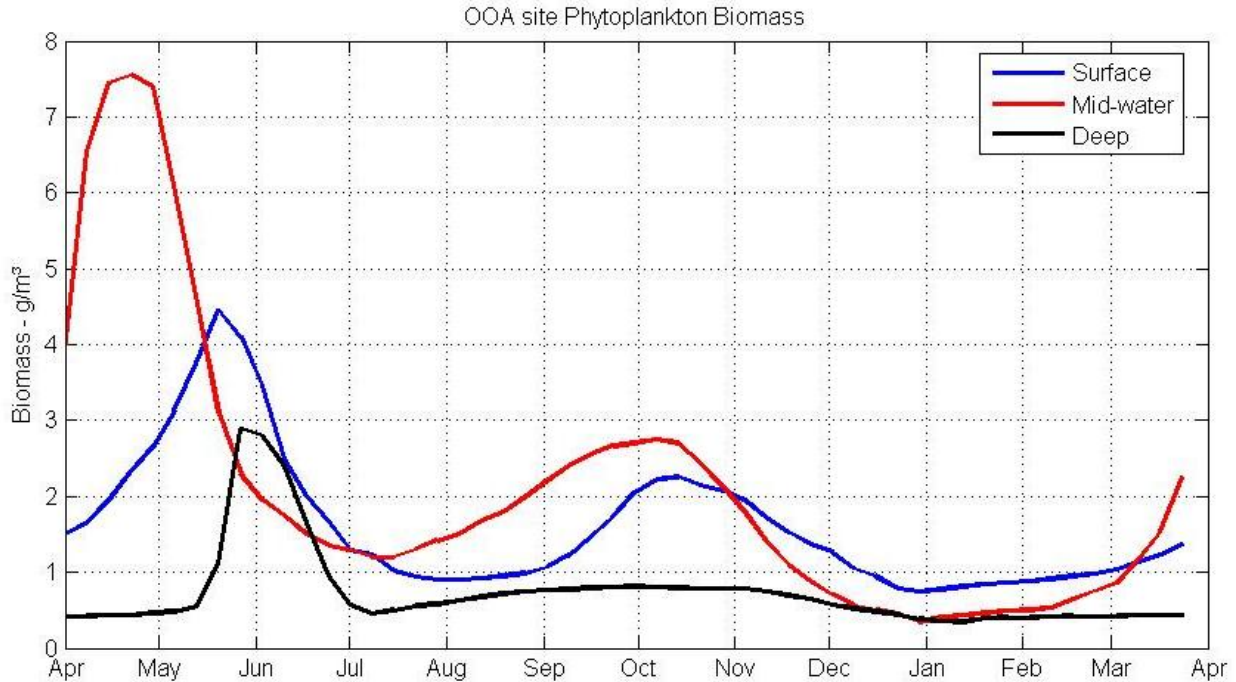
Figure 51: The phytoplankton biomass.

The spring plankton bloom starts about April and rapidly peaks and decreases as the nitrate is exhausted. Then again in the fall there is a smaller plankton bloom when the nitrate increases due to fall overturning, bringing up higher nitrogen waters. The conversion factor to convert mg mass/m³ of phytoplankton to moles of nitrogen/m³ concentration is about 1. The normalized phytoplankton nitrogen set was then entered into the GOM Ambient Excel file for input into AquaModel.

4.10. Zooplankton

The estimates of zooplankton concentration were probably the least accurate data set created. The information was obtained by the COOA survey team from vertical ring-net tows taken from near the bottom to the surface at the far-field site. Therefore, the results are the integrated zooplankton dry mass per square meter of sea surface (Figure 52). To obtain information on the stratification of the zooplankton and the depth they were concentrated, data from oblique tows of the Multiple Opening/Closing Net and Environmental Sensing System (MOCNESS) were used. The MOCNESS was towed obliquely through the water column and nets were opened and closed to collect the organisms in the surface waters (0 to 20 m), midwater (30 to 40 m) and the bottom water (40 m to the bottom) at the far field site. The bottom at the far-field site was about 60 m

deep. These samples from each net were counted for the number of organism (about 120 different ones identified) in each depth range. *Calanus Finmarchinus* stages I to V were selected as indicators of where the zooplankton was located in depth. All the stages were used to get a general idea of the numbers in the three depths ranges over time. The results were about 67% in the 0 to 20 m depth, 25% in the 20 to 40 m depth and 8% in the 40 m to bottom depth. The total mass of zooplankton from the ring net tows was then multiplied by the fraction in each depth bin and divided by the height of the depth bin to get an estimate of the g dry weight/m³ in each of the depth bins.
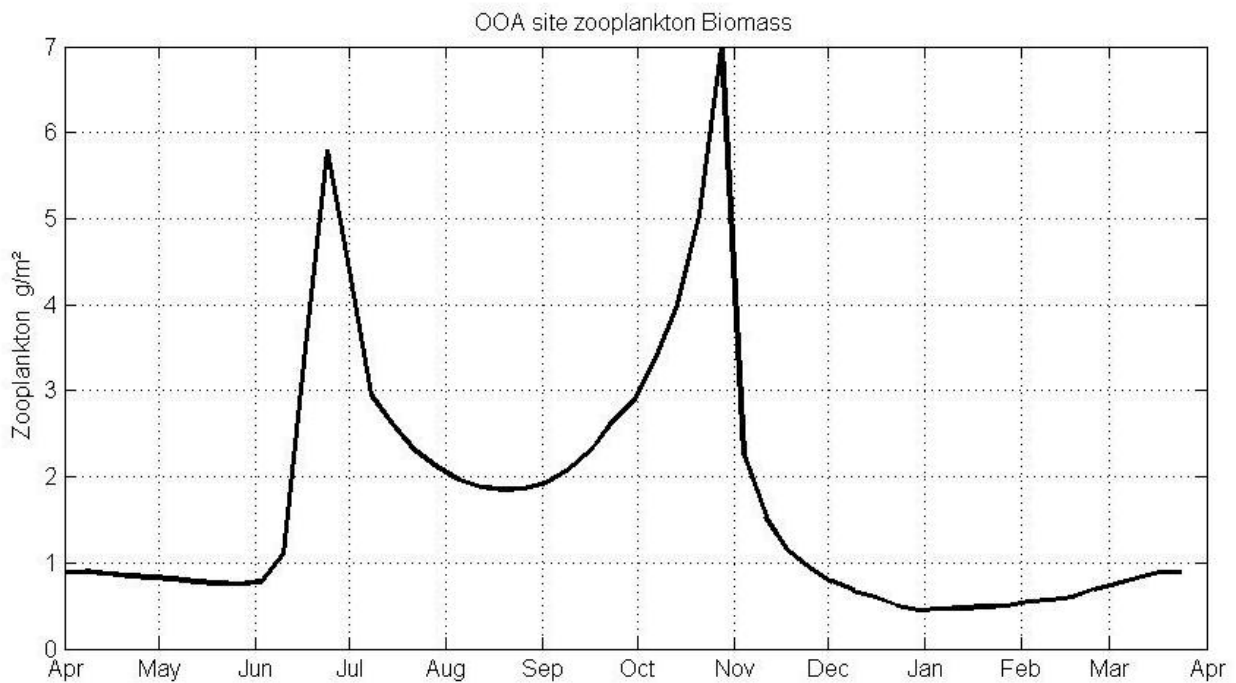

Figure 52: The weekly values of zooplankton dry mass in g/m² of surface area are integrated from near the bottom to the surface by a ring-net tow.

The zooplankton population increases naturally follows that of the phytoplankton. At the end of the phytoplankton bloom in the spring and fall, the zooplankton population peak, then falls back again as the density of phytoplankton decrease. There is probably some grazing higher trophic level predators that furthers this decline also.

4.11. Zooplankton Nitrogen

Zooplankton biomass was then converted to µmoles of Nitrogen/m³ by multiplying by 6.944 mMols/m³ per g/m³, or uMol/l per g/m³. The resulting nitrogen concentrations for the three

layers are shown in Figure 53. As with nitrogen and fluorometric chlorophyll observations, the zooplankton dry weight was plotted, a subjective line fit to the observations and the data digitized. The edited weekly zooplankton nitrogen data were added to the GOM Weekly Ambient Excel file for input to AquaModel.
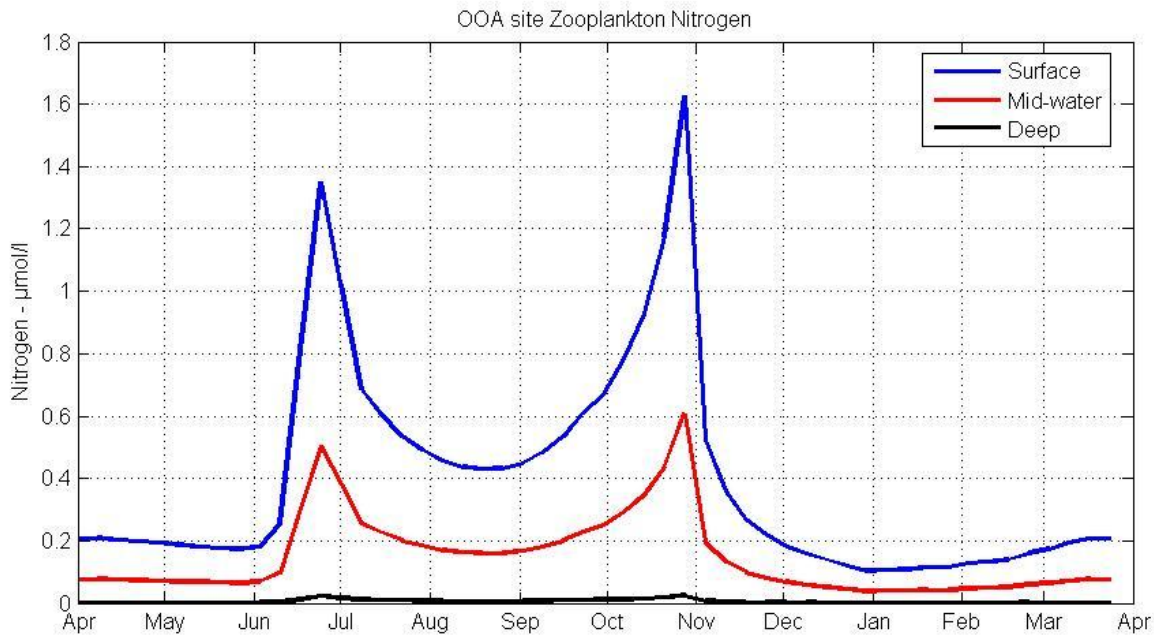

Figure 53: The stratified estimate of zooplankton nitrogen at the OOA site.

4.12. Irradiance

Irradiance information is used in AquaModel to drive primary productivity algorithms and is often referred to as PAR (Photosynthetically Active Radiation). PAR is the incoming solar radiation in the 400-700 nm wavelength band. The PAR records taken at the aquaculture site were not continuous, and the PAR sensor was not mounted on the near field oceanographic buoy for much of the time. Therefore, the PAR record was made up from GLOBEC data in the eastern Gulf of Maine (Irish, et al., 2005), a few records from the near-field site oceanographic buoy, and the COOA Flux Buoy deployed by aquaculture and COOA personnel in 2009 at the aquaculture site. This last buoy had a short wave radiation sensor instead of PAR which has a wider bandwidth than PAR, extending from about 200 to 1,500 nm wavelength, but largely composed of light from the 400 to 700 nm visible band. These records were used to create an 18-month hourly record, which still contained gaps but were filled by repeating sections of the record at the same time of year, and in one case reflecting one section of record to fill a gap. The

18-month hourly record is shown in Figure 54.
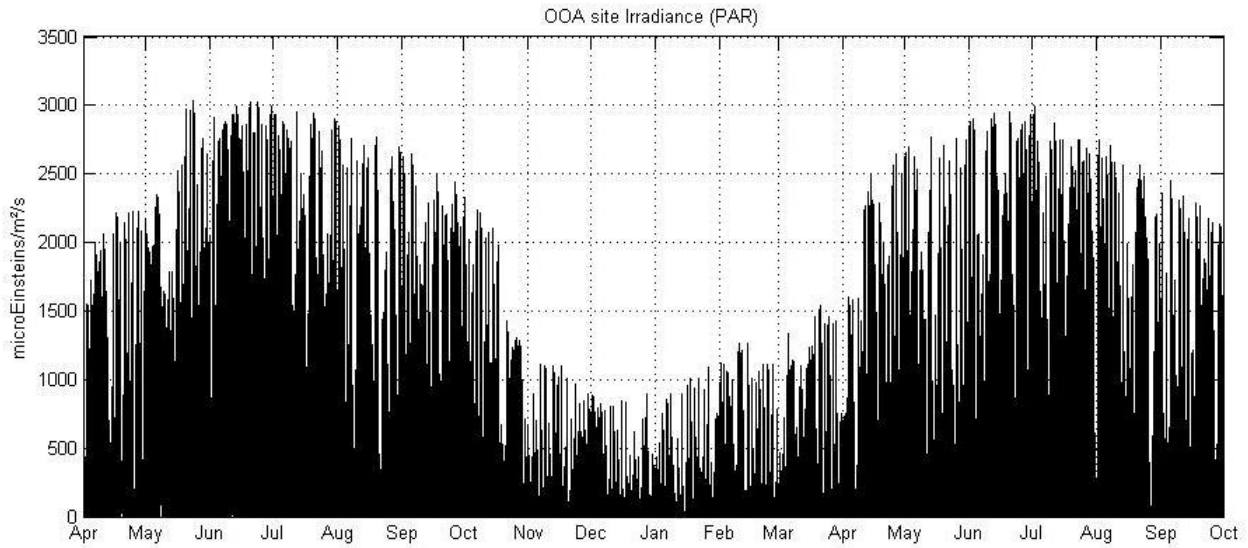
Figure 54: The hourly irradiance as measured by PAR as created from several records in the Gulf of Maine.

These hourly data sets were then further processed to average radiation per day in Einsteins/m²/day for input to AquaModel. An Einstein is Avogadro's number of Photons, and a standard measure of PAR. These daily values (Figure 55) were then added to the GOM daily ambient data file for input into AquaModel.
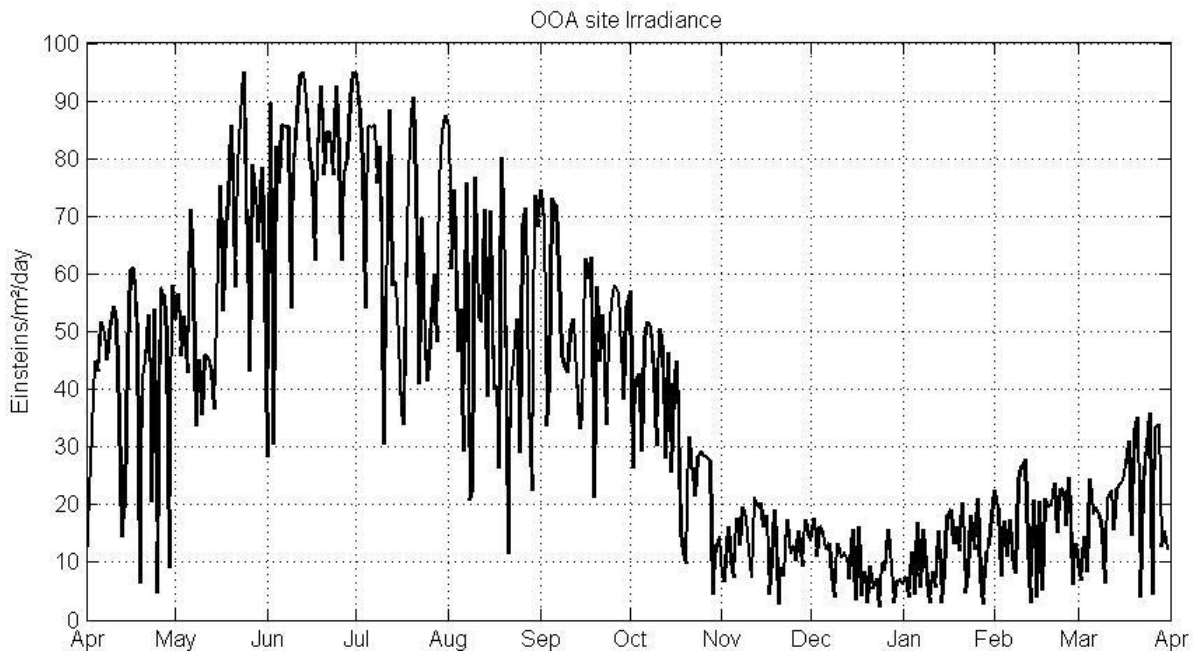
Figure 55: The daily averaged PAR record for input to AquaModel.

4.13. Observed ADCP Currents

During 2001 through 2008, the near-field oceanographic buoy at the UNH OOA site had an upward looking 300 kHz RD Instruments Workhorse ADCP (Acoustic Doppler Current Profiler) recording 15 minute averages of three components of velocity in 2 m depth bins. About 9 months of data were recovered each year, but no one year had a continuous current record for 12 months. Also, the mooring was serviced around December each year, so there is no data during the middle of December. To obtain a representative 18-month long record, a time series was constructed by selecting records from seven deployments in 2003, 2004, 2005, and 2006, and joining the pieces together (truncating them to join together in time) to make a continuous record. No data were used twice. Thus, data from different years could be found in adjacent sections. To fill gaps (however, few), including the one in December, a record was moved forward or backward a day or two in time. This provided a record of observed currents at the OOA site, but made up from records of various years. Hence, a tidal analysis could not be done, but the statistics of the currents would be representative of the environment at the OOA site.

The upper most depth where good currents were observed was 11 m depth, so this depth was selected as representative of the upper layer. Shallower observations were often contaminated by surface side-lobe reflections so were not used. The deepest, most usable record was at the 47 m depth, so it was used to represent the deep-water velocity. The 25 m depth was selected as characteristic of the mid-water layer at about the depth of the moored temperature, salinity and oxygen data sets. These east-going and north-going components were converted to current speed (cm/s) and direction (º True) for input to AquaModel. The current speed data at the three depths are plotted in Figure 56. The speed and direction data from the three depths were added to the hourly ambient data file used as input to AquaModel (for the near-field simulations).
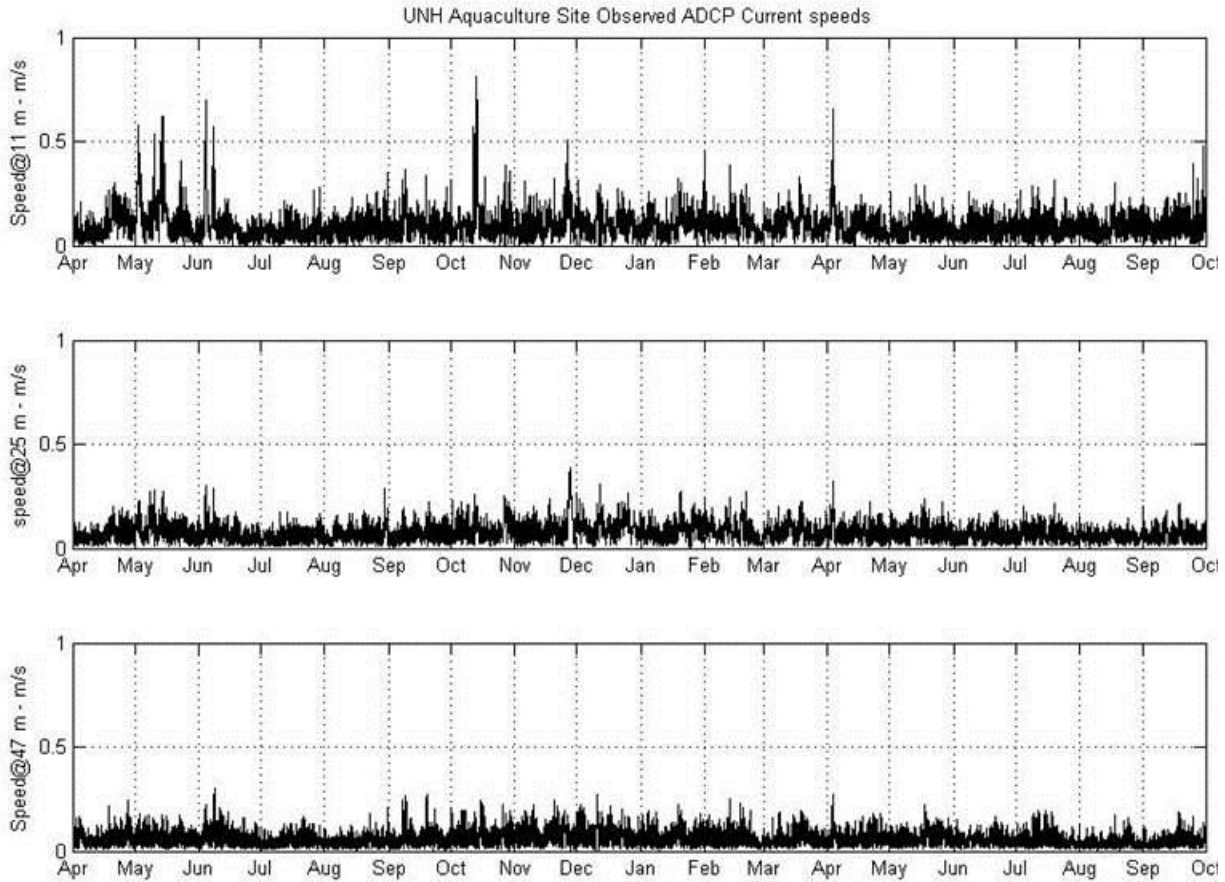
Figure 56: The observed ADCP current speeds from 1 April through 31 September at the three depths.

4.14. Low Frequency Wind Driven and Geostrophic Currents

The ADCP currents from the three depths were then low-passed (filtered) to remove tidal and higher frequency variations, and leave only the general geostrophic coastal current and the longer term weather forced flow variations. Generally, these fluctuations are greater in the upper layer and lowest in the bottom layer as seen in the current speeds in Figure 56. Note that the higher frequency energy is largely due to the tides and shorter wind events with periods less than 1 day. Thus a stratified representation of the three depths would represent this variation in depth of the low frequency, wind driven currents.

The currents were low-pass filtered with the PL66TN filter that was derived from the PL33 developed by C. Flagg and R. Beardsley (see Limeburner, 1985). This filter has a half-power cutoff at 38 hours, and folds the series over at both ends when doing the convolution so as not to lose the usual filter length at each end. These low-pass filtered data (Figure 57) were then added

to the hourly ambient data file, which is superimposed with the tidal velocity data set in the AquaModel Program. As the high frequency components of the currents are missing, the data can be plotted as the east-going (red) and north-going (blue) components in Figure 57. Again the decrease in geostrophic and low frequency weather forced currents is evident in the record. The low-frequency currents are assumed to be relatively uniform in the extended region of the Western Gulf of Maine or at least be representative of the currents in the region.

Another way of interpreting the current velocity data is a histogram of the amount of time that the current occurs at each speed. This presentation (Figure 58) again shows the lower velocities in the deeper waters as is often encountered and the shape of the curves described by the bar chart is skewed significantly to the higher speeds with median values at lower speeds. These data are particularly useful as it shows that the site has only moderately active current velocities in the surface waters and at depth with magnitudes that typically do not exceed resuspension thresholds for waste feed, but do so for waste fecal matter, as described in a following chapter.
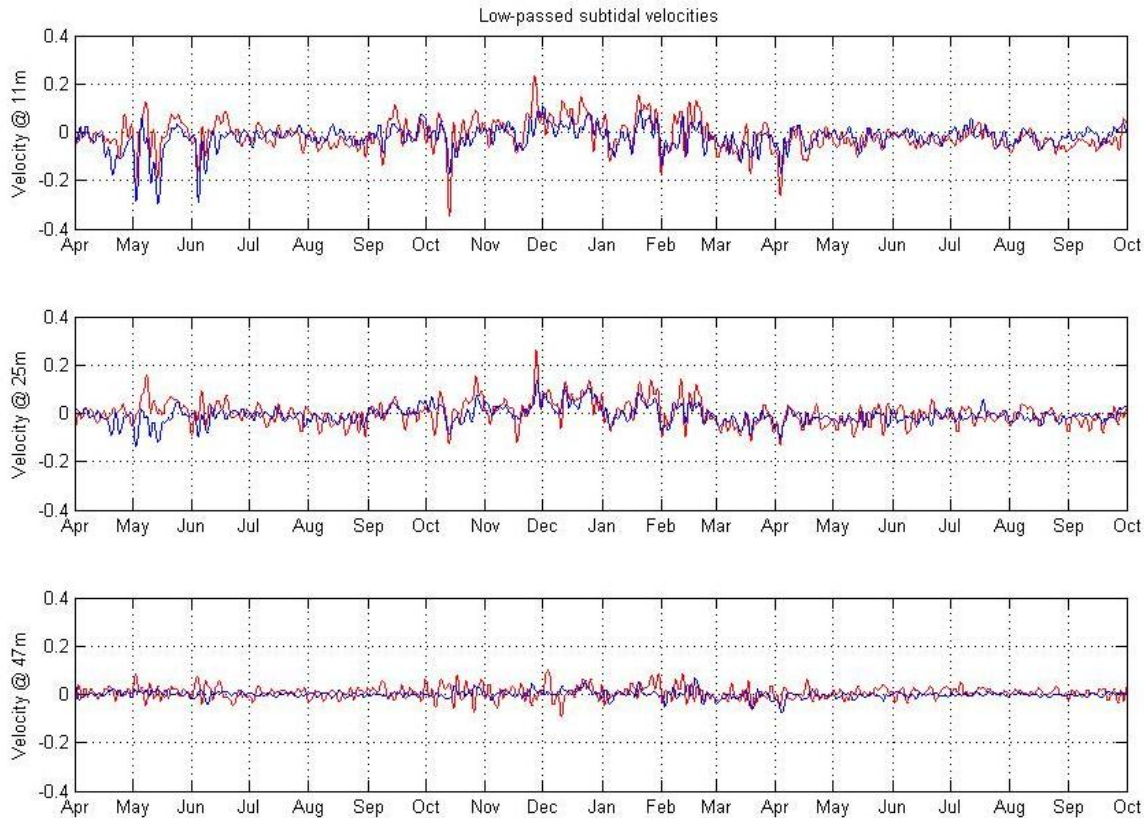
Figure 57: The low-passed, sub-tidal currents at the three depths. The 11 m is in the upper panel, the 25 m data is in the middle panel, and the 47 m is in the bottom panel. The decrease with depth of the weather forced signals can be clearly seen.
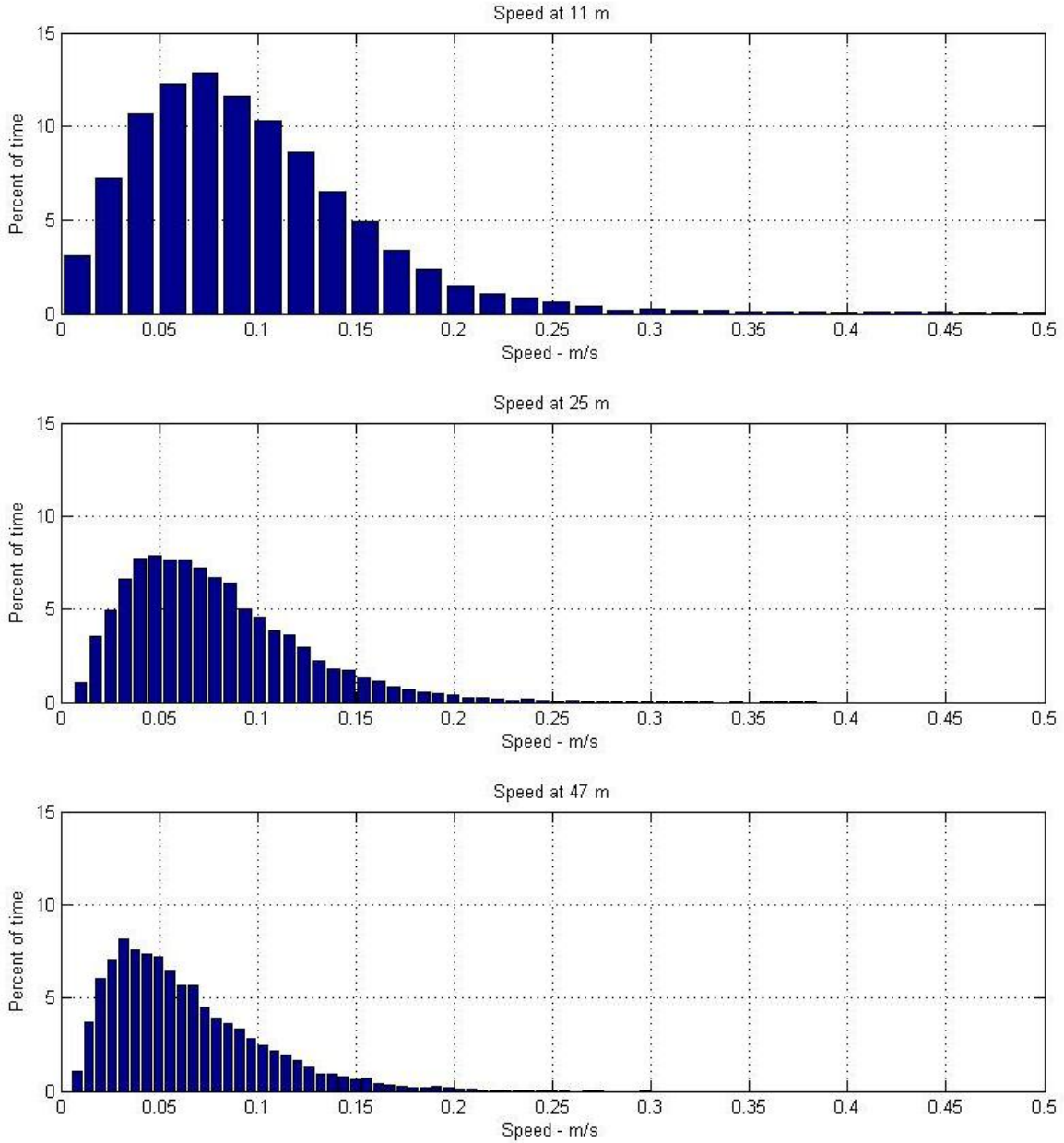
Figure 58: Percent of time that the current is at each velocity.

4.15. Tides

Tidal velocities were also examined with the ADCP data set. Review of the tidal profile information indicated minimal difference throughout the water column and therefore depth-averaged velocities were calculated. This assessment was made by examining both the tidal constituents obtained from the depth-averaged currents and the average constituent values from each depth time series.

Tidal constituents were then obtained from the longest continuous time series from the 6 years of instrument deployments using the techniques described in Pawlowicz et al. (2002). The results are provided in Table 5 in elliptical representation. The parameters in the table include the tidal constituent name and frequency (1/hr), the major axis velocity and calculated 95% error value (cm/s), the minor axis component and its calculated error value (cm/s), and the inclination (counter clockwise from the east axis, so normal orientation clockwise from the north axis is 90º-inc). The 95% confidence limits estimates are from Irish and Brown (1986) who borrowed the approach from Munk and Cartwright (1996). The rotation of the current vector is indicated by the sign of the minor component – negative indicating clockwise rotation, and positive counterclockwise rotation. From these constants, an hourly prediction was made starting 1 April 2009 for 18 months. The east and north-going currents were converted to speed and direction and tabulated in a GOM hourly input to AquaModel.

Table 5: UNH-OOA site major and minor axis tidal constituent velocities

Tide	Freq hr^{-1}	Major cm/s	Minor cm/s	Inclination deg	phase deg	Signal Noise Ratio
O1	0.038731	0.43±0.32	0.14 ±0.31	150.5±53.3	143.0±49.5	1.9
K1	0.041781	0.71±0.34	0.35±0.27	124.9±39.4	114.6±43.3	4.4
PHI1	0.042001	0.41±0.29	-0.01±0.29	134.8±43.9	192.5±48.3	2
N2	0.078999	1.28±0.19	0.52±0.24	153.1±11. 9	1.6±9.2	44
NU2	0.079202	0.33±0.18	0.14±0.18	164.0±42.7	37.8±40.9	3.2
M2	0.080511	5.08±0.23	2.04±0.19	148.0±3.0	32.1±3.1	510.0
L2	0.082024	0.39±0.16	0.17±0.19	146.6±34.1	62.0±29.7	5.9
S2	0.083333	0.63±0.20	0.12±0.24	162.2±20. 9	81.7±18.8	9.8
SO3	0.122064	0.18±0.15	-0.05±0.16	150.7±84.8	54.2±73.7	1.4
MN4	0.159511	0.15±0.12	-0.04±0.13	160.8±70.1	199.4±67.0	1.5
M4	0.161023	0.23±0.14	-0.01±0.13	1.2±38.2	75.3±36.9	2.8
M6	0.241534	0.15±0.11	0.04±0.10	33.8±49.6	332.9±56.1	2.1

Note that during the processing procedure that ratio (in percent form) of the total predicted variance to the original variance was 28%. With each of the tidal components, hind- and forecasts can then be made with the appropriate nodal factors and equilibrium arguments. An example of the velocity vector results are shown on Figure 59. In the Figure the North-South velocity component is plotted vs. the East-West velocity component with a dot plotted for the tip of the velocity vector for each time step generating a form of a tidal ellipse. Note that the major

axis of the ellipse is largely in the East-West direction and the tide sweeps out an ellipse, rather than a back and forth movement as under a wave or in a channel. Therefore, there is velocity to spread any waste products from the aquaculture site over a wider area, but not to advect the material off site. This is done by the low-frequency component of the flow shown in Figure 57 and is why these low-frequency components are added to the ADCIRC tidal predictions for application in the regional modeling effort discussed later in the report.
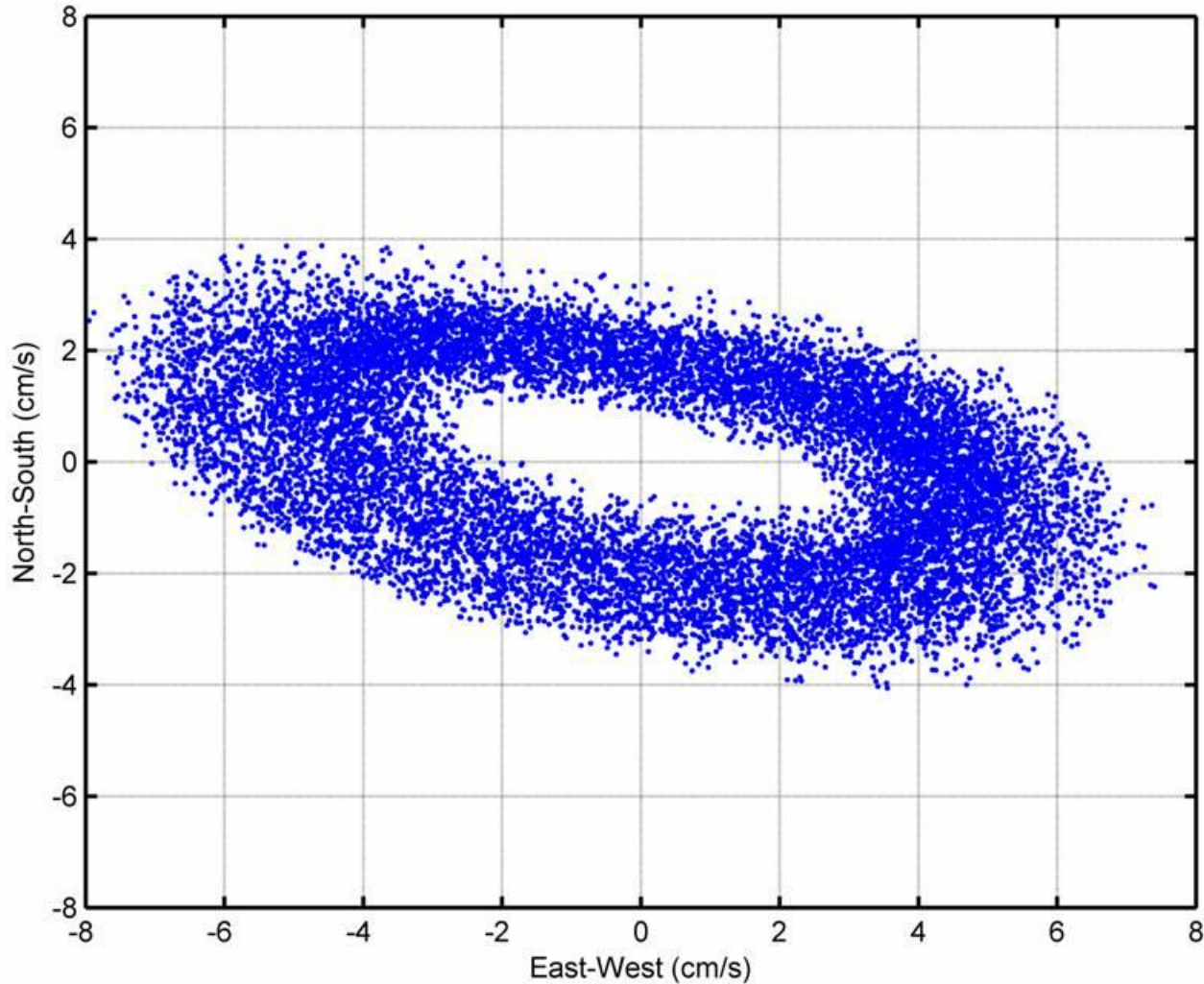

Figure 59: A form of a tidal ellipse generated with North-South and East-West velocity vector components.

4.16. Winds

The National Data Buoy Center (NDBC) maintains a network of weather stations around the country as part of the National weather service. The Isles of Shoals has a C-MAN station (IOSN3) located on the White Island lighthouse about 1.7 km North of the OOA study site.

NDBC archives data from this station and data from 2009 and 2010 were retrieved from the NDBC web site. The data from 1 April 2009 through 31 September 2010 were selected, and the wind speed, wind direction, atmospheric temperature and atmospheric pressure data were retrieved. The wind speed data (Figure 60) were edited and missing or questionable data interpolated across to create a continuous hourly record. The edited hourly wind speed data were added to the hourly ambient data file for input to AquaModel.
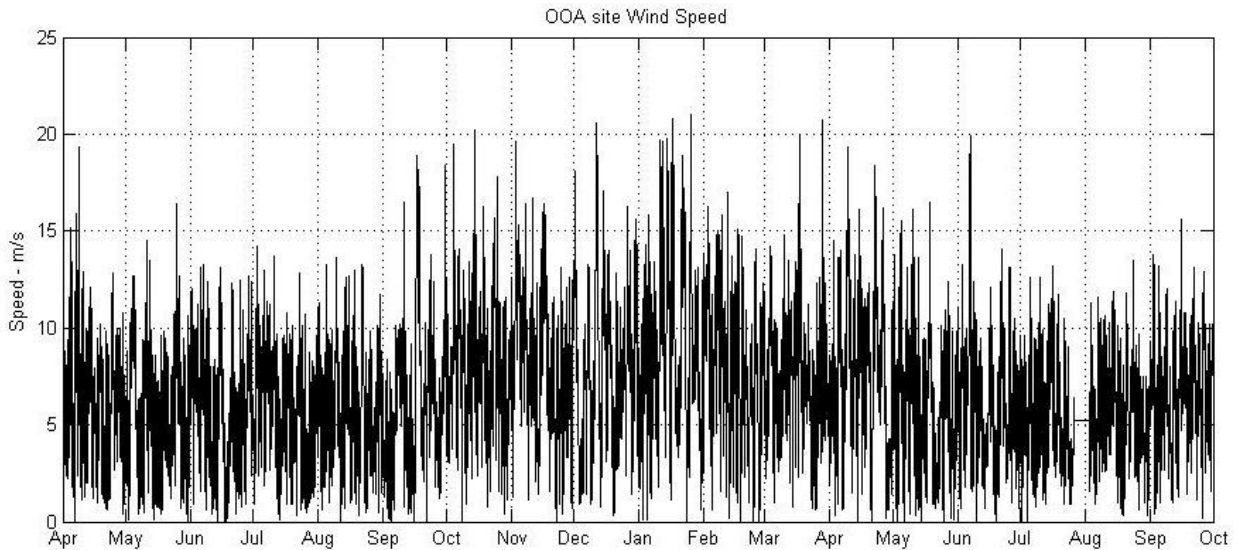

Figure 60: The hourly wind speed in m/s from the Isles of Shoals NDBC C-MAN station for 1 April 2009 through 31 September 2010. The gaps are due to missing data, which were filled with linear interpolations.

4.17. Bottom Sediments

In addition to the water column data sets, work was conducted to determine bottom sediment type for the AquaModel simulations since hydrodynamic induced bottom stress can affect the movement of wastes in the region and affect the ultimate benthic impact. In general, the New Hampshire shelf is composed of outcropping bedrock, as well as modern and relict sediments ranging from gravel to mud. In the region surrounding the aquaculture study site (Figure 61), a number of intermediate to large bedrock outcrops occur which are 10 to 200 meters across with elevations mostly <5 m (Ward et al., 2001).
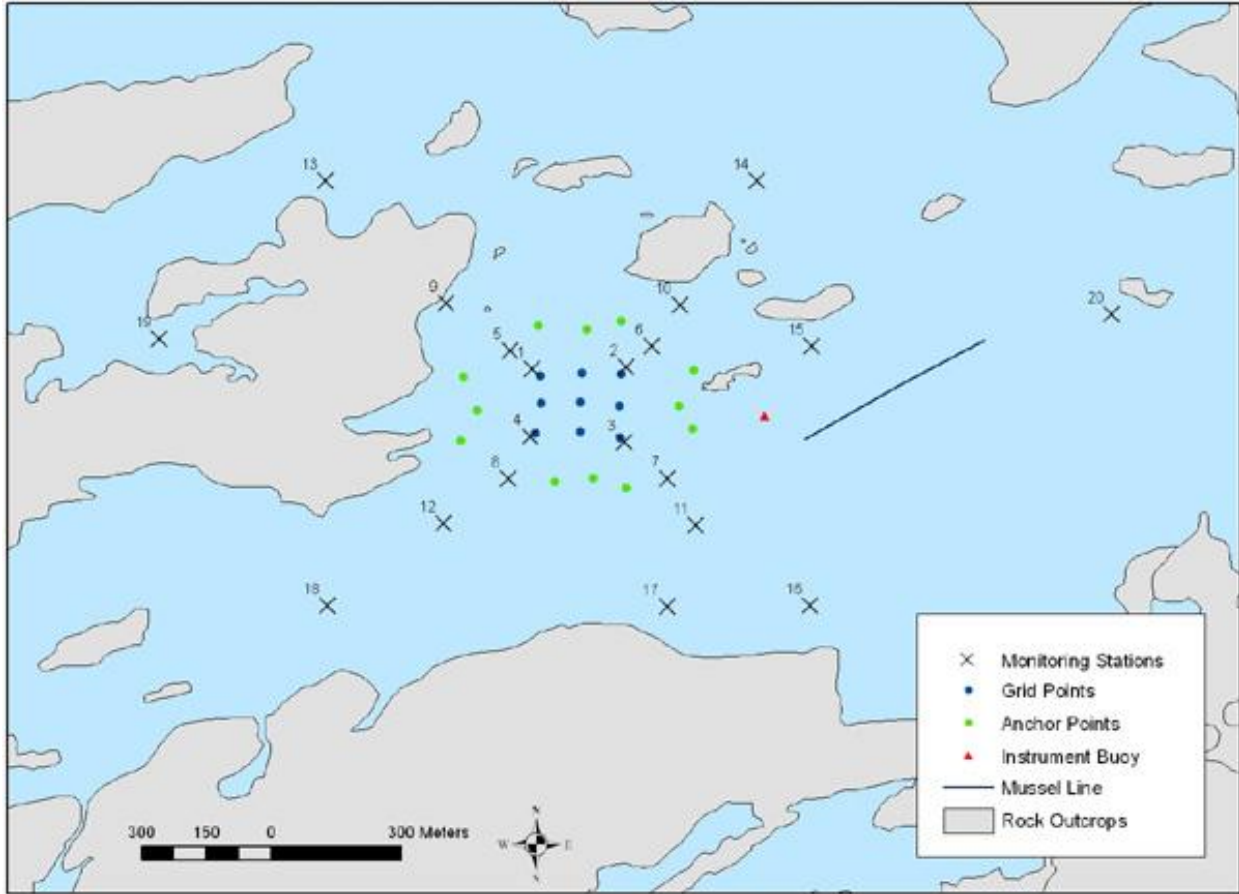
Figure 61: Rock outcroppings (grey shaded regions) around the aquaculture study site. The moored grid and anchor positions are shown, as well as the monitoring stations for 2005 and 2006 (Ward et al., 2006).The bottom sediments at the Gulf of Maine aquaculture site are mainly muddy sand. Table 3 provides the analysis using the criteria described in Folk (1954) and (1980).

As shown on Figure 61, Stations 1 through 8 are nearest to the fish cages. These stations typically do not contain gravel (except station 7), have an average of 79% sand (particles less than 2 mm and greater than 63 µm in size) and contain 21% mud (less than 63 µm). The mud can be further divided into 13% of the total as Silt (63 µm to 4 µm) and 8% as clay (less than 4 µm). This small component of clay is large enough make these sediments cohesive (that is the clay component will stick together by electrostatic and surface tension) and "glue" the bottom sediments together so they are harder to suspend and transport. It is likely that the site bottom sediments will be less subject to erosion than the addition of new aquaculture operation wastes (feces and excess feed). Therefore, it is expected that only severe storm events may suspend and transport the older sediments except for waste salmon feces, that tend to lay on the surface of the bottom and are resuspended at relatively slow current velocities of near 3.5 cm/s as discussed

later. These unconsolidated "wastes" from an extensive aquaculture operation may be suspended and transported more easily unless they remain undisturbed for some indeterminately long period of time when they become consolidated. Therefore, it can be assumed that the suspension and transport of the pre-existing bottom does not need to be done separately from the aquaculture operation deposits. A detailed description of the bottom sediments at the site, taken from Ward et al (2005), is provided in Table 6.

Table 6: Bottom sediment classification around the aquaculture site (Ward et al., 2005).

Station	Classification After Folk 1980	% Gravel	% Sand	% Mud	% Silt	% Clay	Mean Size phi	Mean Size mm	Sorting Phi	Skewness
1	mS	0	76	24	15	9	3.9	0.069	1.71	0.640
2	mS	0	81	19	13	9	3.7	0.080	1.35	0.562
3	slightly mS	1	85	14	6	9	3.5	0.091	1.45	0.493
4	slightly mS	0	83	17	11	6	3.5	0.086	1.29	0.539
5	mS	0	79	21	13	8	3.7	0.077	1.50	0.641
6	mS	0	73	27	18	9	4.1	0.060	1.97	0.729
7	slightly gmS	4	78	18	11	7	3.6	0.084	1.55	0.450
8	mS	0	75	25	15	10	3.9	0.068	1.69	0.635
9	No Recovery	---	---	---	---	---	---	---	---	---
10	gmS	11	74	14	---	---	3.2	0.110	2.36	-0.110
11	mS	0	72	28	17	11	4.2	0.055	2.00	0.711
12	mS	0	79	21	13	8	3.7	0.076	1.50	0.569
13	slightly gmS	2	82	16	9	7	3.3	0.099	1.54	0.374
14	mS	10	83	17	10	7	3.4	0.096	1.57	0.488
15	slightly gmS	1	76	23	14	9	3.7	0.076	1.81	0.622
16	mS	0	73	27	15	12	4.8	0.035	2.72	0.852
17	mS	0	76	24	15	10	3.8	0.071	1.63	0.642
18	mS	0	74	26	17	9	3.9	0.068	1.67	0.618
19	slightly gmS	1	83	16	9	7	3.2	0.107	1.74	0.269
20	mS	0	76	24	14	10	3.5	0.087	2.15	0.441

The bottom sediments are also composed of a low percentage of organic material, usually identified as <2.5% LOI (loss on ignition), and ~1.7% at the 8 sites nearest the fish cages (Table 7). Comparison of the results of the bottom sediment surveys from 1997 to 2005 show no seasonal or year-to-year variations in sediment grain size (Ward et al. 2005). Comparison of the LOI values from the spring and fall benthic survey for 2006 indicated no change in the particulate organic content of the bottom sediments during the summer period. This is true for samples taken at the stations within the predicted impact areas for fish wastes (excess food and feces), as well as those in the far field. In fact, there has been no consistent change in the organic content of the bottom sediments at the UNH OOA site since the beginning of the monitoring

period in 1997 (Ward et al., 2006).

Table 7: OOA bottom sediment percent of Loss on Ignition (Ward et al., 2005)

Station	June 5 (Sta 5-20) July 5 (Sta 1-4)	November 1
	%LOI	%LOI
1	2.5	Not Sampled
2	1.7	1.6
3	1.9	1.5
4	1.8	Not Sampled
5	1.3	1.4
6	2.0	1.6
7	1.6	1.6
8	1.8	1.9
9	No Recovery	1.4
10	1.6	1.8
11	2.4	2.3
12	1.5	2.0
13	1.6	1.9
14	1.6	1.6
15	2.1	1.7
16	2.2	1.9
17	1.6	2.0
18	1.5	2.0
19	1.5	3.0
29	1.8	1.6

4.18. Summary

It is clear from the plots that the Gulf of Maine aquaculture study site has large seasonal variability of most parameters. This implies that AquaModel must be run for an extended period of time (e.g 12-18 months) with weekly, daily or hourly varying parameters of ambient water properties. In addition, if localized simulations are to be performed, observed ADCP measured currents should be used. For regional AquaModel simulations, it is necessary to use circulation model input to account for spatial differences. In general, the higher latitude sites with greater variability put severe conditions on the engineering and environmental design of an optimum aquaculture operation, illustrating the need to demonstrate that AquaModel be capable of providing the required output to guide in aquaculture operation design.

4.19. Section References

Folk, R.L., (1954). The distinction between grain size and mineral composition in sedimentary-rock nomenclature. *Journal of Geology* 62, pp. 344–359.

Folk, R.L. (1980). Petrology of Sedimentary Rocks. Hemphill Publishing Company, 182 pp.

Grizzle, R., Ward, L., Irish, J., Fredriksson, D.W., Langan, R., Heinig, C., Greene, J., Abeels, H., Peter, C., and A. Eberhardt. (In preparation). Long-term seafloor monitoring at an open ocean aquaculture site in the western Gulf of Maine, USA: development of an adaptive protocol.

Irish, J.D., L.G. Ward and S.J. Boduch. (2008). Correcting and Validating Moored Oxygen Time-Series Observations in the Gulf of Maine. Proceedings of the Oceans 2008 MTS/IEEE Conference. Quebec City, Canada.

Irish, J.D., and S.J. Boduch, S.J. (2006). Aquaculture feed buoy control – Part 2: Telemetry, data handling and shore-based control. Proceedings of the Oceans 2006, MTS/IEEE Conference. Boston MA. 6 p.

Irish, J.D. and W.S. Brown, (1986). An Archiving and Analysis System for Geophysical Data, Marine Data Systems International Symposium, MDS86, pp. 64-69.

Irish, J. D. and D.W. Fredriksson, "Telemetering Environmental Monitoring Buoy and Mooring," *Proc. Oceans'03*, 2589-2595, San Diego, Sept. 03, 2003.

Irish, J.D., D.W. Fredriksson and Boduch, S. (2004). Environmental monitoring buoy and mooring with telemetry. Sea Tech. May 2004. pp 14-19.

Irish, J.D., S. Kerry, P. Fucile, R.C. Beardsley, J. Lord, and K.H. Brink. (2005). "U.S. GLOBEC Long Term Moored Program: Part 1 – Mooring Configuration," *WHOI Tech. Rept., WHOI-2005-11*, December 2005.

Irish, J.D., L.G. Ward and S.J. Boduch. (2008) "Correcting and Validating Moored Oxygen Time-Series Observations in the Gulf of Maine," *Proc. Oceans08*, Quebec City, Canada, Sept.

Irish, J.D., D. Vandemark, S. Shellito, and J. Salisbury. (2010). CO_2 Gas Exchange and Ocean Acidification Studies in the Coastal Gulf of Maine, Proceedings of the Oceans 2010, MTS/IEEE Conference, Seattle Washington, Sept.

Limeburner, R. (Editor), (1985). "Code-2: Moored Array and Large-Scale Data Report," WHOI Tech. Rept., 85-35, Woods Hole Oceanographic Institution, 234 pp.

Munk, W.H. and D.E. Cartwright. (1966). Tidal Spectroscopy and Prediction, Phil. Trans. Roc. Soc. London. Vol 259. No. 1105. pp. 533-581.

Pawlowicz, R, Beardsley, B and S. Lentz. (2002). "Classical tidal harmonic analysis including error estimates in MATLAB using T_TIDE", Computers and Geosciences 28, 929-937.

Ward, Larry G., Raymond E. Grizzle, and Frank L. Bub. (2001). OOA Environmental Monitoring Program, CINEMar/Open Ocean Aquaculture Annual Progress Report for the period 1/01/01 through 12/31/01. Report available at: http://ooa.unh.edu/publications/progress_reports/2001/2001_monitoring.html

Ward, Larry G., Raymond E. Grizzle, and James D. Irish. (2005). UNH OOA Environmental Monitoring Program, CINEMar/Open Ocean Aquaculture Annual Progress Report for the period 1/01/05 through 12/31/05. Report available at: http://ooa.unh.edu/publications/progress_reports/2005/2005_monitoring.html

Ward, Larry G., Raymond E. Grizzle, and James D. Irish. (2006). UNH OOA Environmental Monitoring Program, CINEMar/Open Ocean Aquaculture Annual Progress Report for the period 1/01/06 through 12/31/06. Report available at: http://ooa.unh.edu/publications/progress_reports/2006/2006_monitoring.html.

5. Gulf of Maine AquaModel Near-Field Simulations and Results

5.1. Operational Condition Input

5.1.1. Model Domain and Farm Array Configuration

Once the general ambient environmental conditions for the Gulf of Maine OOA site were established, AquaModel was setup to run at the site simulating "commercial" fish farm conditions. The AquaModel program was configured into a 91 x 51 x 4 (LxWxD) block cell domain. Each of the block cells was set with the dimensions of 50 x 50 meters square with a depth of 10 meters creating a computational domain with a size of 4.55 km x 2.55 km (see Figure 62). Within the domain, two representative case studies of a submerged "fish farm" system was configured. In both cases, each of the fish cages was modeled to be square with the dimensions of 50m x 50m x 15m meters with an internal volume equal to 37,500 m^3. The center of the cage was positioned at a depth of 15 meters with the top of the cage at a depth of 7.5 meters. While most gravity cages presently deployed in energetic conditions are circular, AquaModel computes concentration conditions within boxed shaped elements. The rectangular cage used in the model has the same internal volume as a 56 m diameter gravity cage (176 m circumference) with a depth of 15 meters. In the model, the cages were situated in a submerged state so they would be closer to the bottom to better investigate benthic impact.

In the first case simulation, the farm contained 12 cages in a 2x6 configuration (Figure 62 top). The program was then set to simulate the growth of Atlantic salmon stocked at 200 grams. The cages were initially sized with a stocking density of 0.6 kg/m^3 and 112,500 fish. If the fish grow to a harvest size of 5 kg (estimated value), then the total farm capacity would be approximately 6,750 metric tons with a stocking density of 15 kg/m^3, typical of many farm applications. Note that the AquaModel calculates growth of the fish throughout the simulation and in this case had a harvest target value of 5 kg). The model was then set to run for 15 months starting with fish stocking in April. Results can be analyzed by examining in-cage concentrations of parameters, or values obtained from strategically placed transect lines, profile points and capture cells. After a simulation is performed, it may be replayed and new capture data obtained rapidly from other locations. The capture cells are indicated by the grey circles on Figure 62. The northern and southern capture cells were labeled #1 and #3, respectively, with the middle cell as #2.
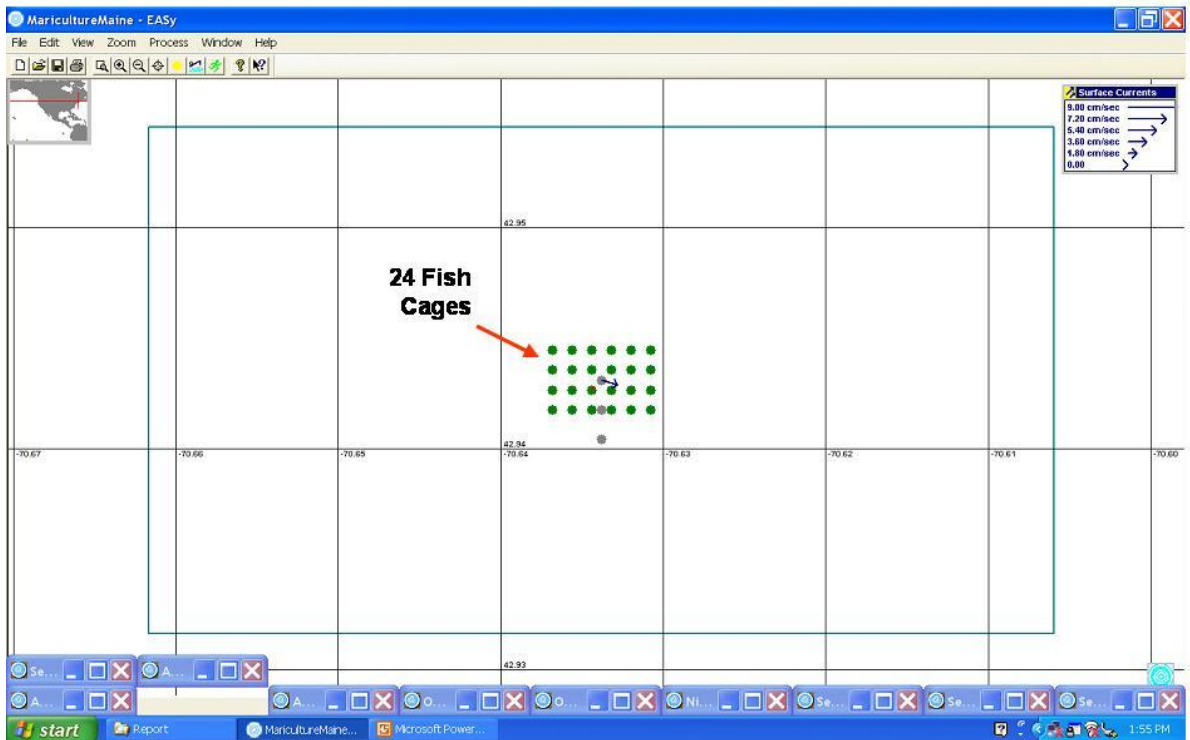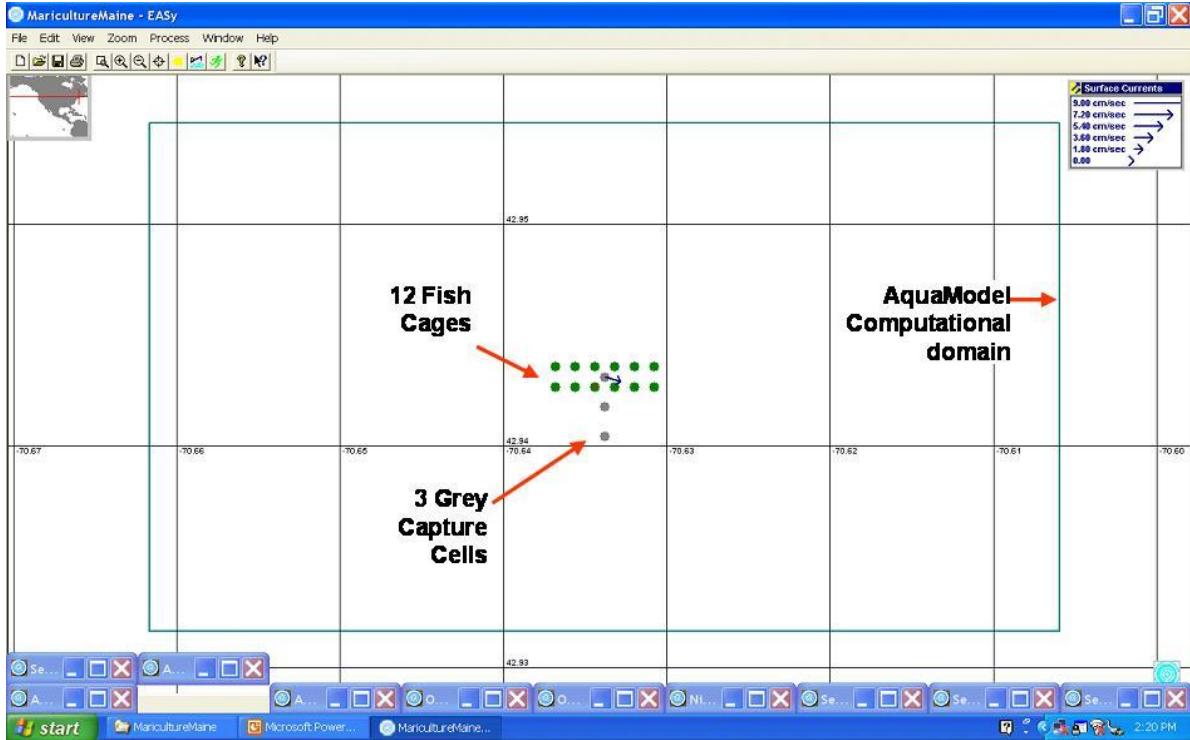
Figure 62: The first AquaModel computational domain included 12 cages in a 2x6 configuration, while the second doubled the amount of biomass using 24 cages. Note that the grey circles are "capture cells" used for data processing and that the boundaries of the computational domain indicated by the light blue rectangle. The capture cells are labeled #1 to #3 in a north-south configuration.

A second case simulation was also conducted using the same environmental and hydrodynamic conditions but with twice the amount of biomass in 24 cages. A schematic of this AquaModel configuration is shown on Figure 62 (bottom). The capture cell locations for 24-cage farm simulations were identical as those used for the 12-cage farm configurations.

5.2. Ambient Water Column Condition Input

5.2.1. Overview

AquaModel allows the user to set the ambient conditions, i.e., the inflowing water quality parameters. For the long-term simulations performed at the OOA site, however, many of the individual or seasonal values used in simpler simulations were replaced by input data files with parameters that changed as a function of time (e.g. weekly, daily, or hourly) as previously described. Some of the information is reviewed in the section *Known Parameters and Settings*, but the focus is on the various "Unknown Parameters" that are not in fact totally unknown, but rather are those with known ranges but determination of a single point estimate is complex or less possible. Typically, the unknown parameters are varied within likely ranges and model performance assessed. The two primary unknown parameters are not necessarily functionally linked, allowing them to be varied independently as discussed herein for local and regional values in the New Hampshire and Northeast U.S. coastal shelf areas.

5.2.2. Known Parameters and Settings

Enable oxygen model: The oxygen model component of the software represents the energetics of the biomass being simulated. The growth of the biomass is dependent on the species, flux of dissolved oxygen, water temperature and current speed. It was enabled for the simulations described in this project.

Enable plankton model: The plankton model component represents the dynamic interaction between the phytoplankton and zooplankton communities as a function of nitrogenous waste from the farm, DIN and dissolved oxygen in the water column. It was also enabled.

Surface and Bottom Temperature Winter/Summer: The individual surface and bottom temperatures for the winter and summer seasons were not used, instead an input data file for representing weekly averaged temperature at the surface, a depth of 22 m and at the bottom from

the OOA site was used by the program. See the previous for a description and time series details.

Nominal Wind Speed: Wind speed information was obtained from the National Data Buoy Center (NDBC) C-MAN station (IOSN3) located 1.7 Km north of the NH OOA site. These data sets are used to modify sea state and resultant flux of oxygen and carbon dioxide across the sea to air interface (Broeker and Peng, 1993). The data set was configured into representative hourly values from a continuous 18-month period (non-repeating) and loaded for constant input to AquaModel. Missing data points were linearly interpolated.

Mixed Layer Depth Winter/Summer: Multiple years of CTD profiles were assimilated into the same year-day format as previously described. Therefore, instead of using individual values for the summer and winter seasons, the depth of the stratified layer (based on the thermocline depth) was provided weekly for the entire year as an input data file as previously described.

Tidal Flow/Max Current Velocity: The ADCP measurements were obtained over multiple years and were combined into one representative 18-month current series at the three standard depths. Tidal constituents were obtained and used to create a 78-week time-series of hourly values (described in the previous section).

Oxygen: A full explanation of the dissolved oxygen values used as input to AquaModel, similar to the temperature input is given in the previous section.

Nitrogen: A full explanation of the nitrogen values (dissolved inorganic nitrogen – DIN) used as input to AquaModel, also is given in the previous section.

Phytoplankton: The phytoplankton was determined from profile observations of Chlorophyll-a fluorescence at the three standard depths and converted to phytoplankton biomass and is also described in the previous section.

Zooplankton: The total zooplankton biomass per unit surface area was measured by ring-net tows. A multiple net sampler (MOCNESS) was then used to capture zooplankton in depth bins, and this information used to divide the total zooplankton biomass into depth bins as described in the previous section

Plankton ambient nitrogen: The plankton concentrations discussed above were then converted into phytoplankton nitrogen (see the previous section).

5.2.3. Unknown Parameters

Diffusion Coefficients: The use of appropriate diffusion coefficients is needed to represent horizontal and vertical mixing. This can be a difficult process because a wide range of values exist for various conditions. The first step to determine the appropriate values to use was to perform a literature search.   The work performed by Gustafsson et al. (1998), provided a useful overview of other representative values typical of estuarine and coastal waters as a qualitative attempt to gauge the "reasonableness" of specific values. For instance, Gustafsson et al. (1998) cites that Okubo (1971) estimated values for horizontal diffusion in the coastal oceans to be between 0.6 and 8 m^2s^{-1}. Mixing in estuarine environments was observed by Fischer et al. (1979) to be within the range of 50 to 200 m^2s^{-1}. In the Gustafsson et al. (1998) study, where the dispersion of water in a Gulf of Maine strait (near Casco Bay) was investigated, values ranging from 20 to 40 m^2s^{-1} were estimated. While near established coastal aquaculture sites, Cromey et al. (2002a, 2002b, and 2003) measured values between 0.1 and 0.4 m^2s^{-1}. It is acknowledged that a site-specific dispersion/diffusion study should be performed for the UNH OOA site, since it is likely that it will vary considerably over time. Based on the previously stated justifications, the ideal approach would therefore be to use a range of values that would cover the representative conditions, as discussed by Benitez-Nelson et al. (2000). However, for the simulations presented in this report, only one set of values is used as a starting point for future studies. For instance a value 0.1 m^2s^{-1} is applied for the horizontal dispersion coefficient, and 10^{-3} m^2s^{-1} was used for the vertical dispersion coefficient above the stratified layer and a value of 10^{-4} m^2s^{-1} was used for below the stratified layer (e.g. thermocline). It is typical that the vertical values are estimated at 1-2 orders of magnitude less than the horizontal diffusion coefficient (see for example Eppley et al., 1978 and Benitez-Nelson et al., 2000). A summary of the ambient condition input parameters are provided in Table 8.

Table 8: Ambient condition input to the AquaModel

	Conditions	
1	Enable oxygen model	yes
2	Enable plankton model	yes
3	Surface temp win/sum (degC)	Data file
4	Bottom temp win/sum (degC)	Data file
5	Ave daily irradiance win/sum (mol/m^2/day)	Data file
6	Mixed layer depth win/sum (m)	Data file
7	Nominal wind speed (m/s)	Data file
8	Diffusion Kh/Kv mixed/Kv strat (m2/s)	0.1, 10^{-3}, 10^{-4}
9	Tidal flow	Data file
10	Max current velocity (cm/s)	Data file
11	Oxygen min/max/ambient (g/m3)	4.0, 12.0, data file
12	Nitrogen (mM/m3)	1.0, 11.0, data file
13	Phytoplankton min/max/ambient (mM/m3)	0.0, 3.20, data file
14	Zooplankton min/max/ambient (mM/m3)	0.0, 3.20, data file
15	Plankton ambient MLD, temp, irradiance	9.8, 19.3, 66.0
16	Plankton ambient nitrogen, PhN, ZoN (mM/m3)	2.1, 0.9, 0.83
17	Plankton plume MLD, temp, irradiance	5.3, 9.5, 54.0
18	Plankton plume nitrogen	2.8, 3.4, 1.73

5.2.4. Fish Farm Operation Input

This section describes the operational input parameters used in the AquaModel program.

Manual feed rate (fraction fish weight/day):   The manual feed rate may be selected to be set at any appropriate rate. For example if the value is set to 0.03, then the fish are fed 3% of their body weight per day.   Typically, however, we let the software calculate optimal feed rate as described below.

Feed rate: When the "feed rate" is set at manual, the value above is used in the simulation according to, FeedRate = [ManualFeedRate * FishWeight]. When is it is set at "optimal," the feed rate is calculated as, FeedRate = OptimalFeedRate * (1 + OptimalFeedWasted)].

Wasted Feed > optional (Fraction): For the simulations reported here, the optimal feed rate was condition was used with an additional feed loss rate of 3%. This value can be considered as a median estimate of actual feed loss experienced presently by major fish farming operations using feedback technology (e.g. cameras). It is acknowledged, however, that some operators report better (less conservative) rates.

Initial pen oxygen (g/m^3): The initial pen oxygen is a part of the weekly ambient data file.

Initial pen nitrogen (mM/m^3): As described for the initial pen oxygen, the initial pen nitrogen value was obtained from the weekly ambient data file as described in Chapter 3.

Fecal/Feed settling rate (cm/s):   The feed and fecal matter settling rates used for the AquaModel simulation were 10.0 and 3.2 cm/s, respectively and were obtained from Cromey et al. (2002a).

Fish growth rate min/max (1/day): The minimum and maximum fish growth rate parameters are used in the post-processing utility of the AquaModel and were set at 0.001 and 0.020/day, respectively.

A summary of these input parameters is provided in Table 9.

Table 9: Operational setting input to the AquaModel

	Settings	
1	Manual feed rate (fraction fish weight/day)	NA
2	Feed rate (No=manual, Yes=optimal)	yes
3	Wasted feed > optimal (fraction)	0.03
4	Initial pen oxygen (g/m^3)	Data file
5	Initial pen nitrogen	Data file
6	Fecal/Feed settling rate (cm/s)	3.2, 9.5
7	Fish growth rate min/max (1/day)	0.001, 0.02

5.3. Input to the Benthic Model

5.3.1. Overview

The ambient benthic condition settings used to simulate the benthic dynamics were obtained from multiple sources. Many of the parameters identified in this section are initial concentrations or rates that will vary with fish farm effects, many quite rapidly. Another goal is to provide an approximate value that is reasonably close to what would be expected. Other parameters such as waste feed and fecal matter settling rates can have a major and continual effect on model results and therefore must be calibrated as close as possible to known rates.

5.3.2. Known Parameters

Aerobic Biomass: The ambient aerobic biomass levels were measured as part of an extensive field study described in Grizzle et al. (In preparation). In this study, benthic samples indicate that the mean biomass levels were about 60 g/m^2 retained in a 0.5 mm sieve from the top 20 mm

of sediment.

Anaerobic Biomass: It is likely that anaerobic organisms do exist, but are found below the highly oxygenated surficial sediment layer. This assumption is made because grab (i.e. benthic) samples and observations indicate that there is an abundance of aerobic organisms at the site during the small scale fish farm trials that previously were conducted (see above). For modeling purposes, however, an initial value (albeit low) was set so that if during a simulation low dissolved oxygen conditions develop, anaerobic activity will respond in appropriately fast time scales.

Sediment Oxygen: Once again, because of the abundance of aerobes, it is assumed that the top 20 mm of sediment has the same initial oxygen level as the water above it. As described previously, dissolved oxygen measurements were obtained at approximately 1-2 meters above the ocean bottom and were found to be 7 mg/l (7 g/m^3). At the site, the sediments are approximately 80% sand and 20% mud/silt/clay (e.g., fairly course) therefore, a value 5 mg/l was used since the organisms are consuming oxygen. The initial value is not that critical since the sediment oxygen was calculated as part of the simulation.

Sediment Carbon Dioxide: The initial sediment CO_2 value was taken at a level approximately equal to that within the water column. The value was obtained by the UNH Center for Coastal Ocean Observation and Analysis (COOA) as described in (Salisbury et al., 2009) assuming that CO_2 was the predominant carbon component. Water column values were estimated at 2,100 μMole/kg of seawater. If the density of seawater is 1025 kg/m^3 and the molecular weight of CO_2 is 44 g/Mole, then the water column concentration was calculated to be 94.71 g/m^3. Since AquaModel requires a value for the top 2 cm of sediment, then the initial condition for the simulations was set at 1.89 g/m^2.

Sediment Sulfide: The work of Wildish et al. (2001) describes normal (non-hypoxic) concentrations of H_2S to be less than 0.3 moles/m^3 in their study of salmon fish farm sediments in the Bay of Fundy (Canada). Since no evidence exists that the surficial sediments at the NH site is hypoxic or even oxic transitory, this value was used as an initial level.

Sediment Total Organic Carbon: One of the techniques to estimate the total organic carbon levels in marine sediments is the Loss on Ignition (LOI) method. All of the sites sampled by Grizzle et al. (In preparation) indicate mean values of LOI less than 2%. However, many consider that the

LOI method a poor estimate of TOC. According to Magni et al. (2009), TOC results were greater than LOI by 2 or 3 times. At a several sites in Puget Sound, with sediments consisting 20% silt and clay, measurements have shown TOC levels are about 0.8% (J. Rensel, unpublished NPDES monitoring data). If values are overestimated, anaerobic conditions can occur prematurely. So if the LOI values from Grizzle et al. (In preparation) are "on the order" of 2%, the sediments at the N.H. site are approximately 20% silt and clay and the LOI values are overestimated by a factor between 2 and 3, a slightly conservative value of 0.75% could be used (to prevent premature anaerobic conditions from occurring).

Suspended Oxygen: Considered the same as Sediment Oxygen above.

Suspended POC: Initial values for ambient suspended POC were obtained from Ward et al. (2006) as part of the extensive monitoring study described in Grizzle et al. (In preparation). As part of the monitoring project, discrete total suspended sediment (TSS) were obtained at the surface, 22 meter depth and at the bottom at the same site as the near field oceanographic buoy. The samples were taken during the months of May through October in 2006. The TSS samples were subjected to the loss on ignition (LOI) procedure so that a total carbon value was estimated. The initial value of 0.47 g C / m^3 used as input to the AquaModel was a temporal and vertical average.

Water POC: The water particulate organic carbon was considered negligible.

Fecal/Feed ambient POC deposition (gC/m^2/d): Typically in temperate water, less than 1 gram of carbon per m^2 per day will result in surficial sediments remaining aerobic (based on the work of Wildish and others). In addition, the area also has a seasonally productive water column with substantial variability between winter and summer. Therefore it was assumed that the annual average background POC deposition rate was 0.1 gC/m^2/d, though it is likely that the value would be higher in the summer.

Fecal/Feed deposition threshold (cm/s): Values of 3.0, 4.5 cm/s as described by Cromey et al. (2002a) are used as input to the model.

Fecal/Feed erosion threshold (cm/s): Values of 6.0, 9.5 cm/s are used as input to the model. The fecal erosion threshold was an estimate. The feed estimate was taken from Cromey et al. (2002a).

Fecal/Feed erosion rate constant (g C/m^2/d): Values from Cromey et al. (2002a) cite 60.4 gC/m^2/day, though others from Cromey et al. (2002b) like Sanford et al. (1991) and Harris et al. (1993) have used values substantially higher, like 121 and 259 gC/m^2/day, respectively. Cromey et al. (2002b) explain that the lower value will produce more frequent re-suspension events.

5.3.3. Unknown Parameters

Fecal/Feed TOC consolidation rate (1/d): These values describe how much of the depositional waste fish feces and waste feed becomes consolidated into the sediments when near bottom currents drop below the deposition rate of waste feed or fish fecal matter. In general, in erosional sea bottom environments, there is much less or no consolidation, but in depositional environments, it can be a major factor. Most net pens sites are, however, in "transitional sites" that experience both extremes at different times. Consolidation is a function of the weight of deposited sediments and to some unknown degree, the "stickiness" of the materials deposited. Because this is an unknown factor, it can be varied from 1 to 100% as part of a sensitivity analysis. In the simulations described in this report, a value of 10% was used for both the fecal and feed consolidation rates as the high amount of sand in the net pen site sediments indicates that there must be relatively strong currents periodically to prevent the seafloor from becoming dominated by silt and clay.

A summary of the benthic model input parameters is provided in Table 10.

Table 10: Benthic module parameter particulars

	Parameter	Value	Source
1	Enable benthic model	yes	
1	Aerobic biomass (g/m^2/top 2 cm): min/max/initial	0, 75, 20	Grizzle et al. (in prep)
2	Anaerobic biomass (g/m^2/top 2 cm): min/max/initial	0, 5, 0.01	Estimate from Grizzle at al. (model goes to 0.0)
3	Sediment Oxygen (g/m^3): min/max/initial	0, 10, 5	Estimate & < water column
4	Sediment CO_2 (g/m^2): min/max/initial	0.0, 24 1.9	Estimate and based on Salsbury
5	Sediment sulfide (moles/m^3): min/max/initial	0.0, 1.0 0.3	Wildish et al. (2001)
6	Sediment TOC (percent): min/max/initial	0.0, 0.02, 0.0075	See discussion above
7	Suspended Oxygen (g/m^3): min/max/initial	0, 10, data	Data file
8	Suspended POC (g C/m^3): min/max/initial	0, 10, 0.47	Ward et al. 2006
9	Water POC (1/day)	0	Negligible Source
10	Fecal/FeedAmbient POC deposition (g C/m^2/day)	0.1, 0.1	See discussion
11	Fecal/Feed TOC consolidation rate (1/day)	0.1 and Varied	Cromey (2002a,b)
12	Fecal/Feed Deposition threshold (cm/s)	3.0, 4.5	Cromey (2002a,b)
13	Fecal/Feed Erosion threshold (cm/s)	6.0, 9.5	Cromey (2002a,b)
14	Fecal/Feed Erosion rate constant (g C/m^2/day)	60.4, 40	Cromey (2002a,b)

5.4. Results of the Near-Field AquaModel Simulations in the Gulf of Maine

With the extensive input data files and setting parameters, AquaModel was configured to simulate the two fish farm arrangements shown in Figure 62. Calculations were performed for a period of 15 months (from April to July of the following year). The average growth rate and biomass results of the AquaModel simulations are shown on Figure 63. The growth rate was directly related to the water temperature, but inversely related to dissolved oxygen concentration. The growth rate also decreased as the fish grew larger as normally occurs. The fish biomass results (bottom of Figure 63) show no major differences between each of the farm sizes with a final harvest mass of 5.4 and 5.2 kg for the 12- and 24-cage farms, respectively. These values

were calculated by taking the total biomass in each of the cages and dividing by the number of fish in each cage (112,500). Assuming no mortalities (conservative approach), the total biomass in each farm was just under 7,300 and 14,000 metric tons.
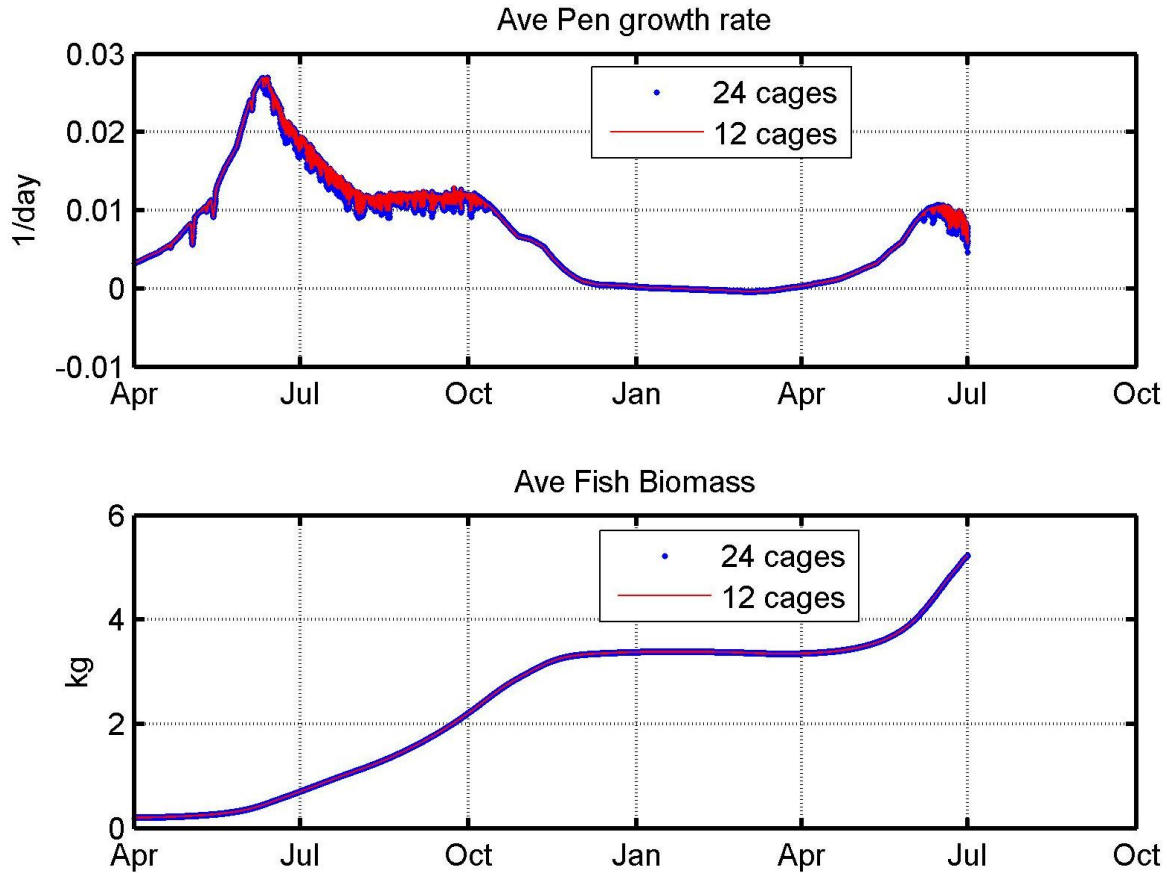
Figure 63: (Top) Comparison of the average pen growth-rate between the 24 and 12 cage farms. (Bottom) Comparison of the average fish biomass between the 24 and 12 cage farms.

The results of the average dissolved oxygen and nitrogen concentrations within the cages are shown on Figure 64. For each of the farm configurations, not once throughout the grow out cycle did the AquaModel calculations predict a dissolved oxygen concentration below 5 g/m^3 (5 mg/l). Furthermore, only a slight difference between the 12- and 24-cage configurations is evident during the summer months. The same is true for the average nitrogen levels within the cages (see bottom of Figure 64). Only a slight difference occurs during the warmer months when comparing the 12- and 24-cage configurations. In addition, comparing the average pen nitrogen levels shown on the bottom of Figure 64 with the ambient values on Figure 50, it is evident that the natural conditions dominate.
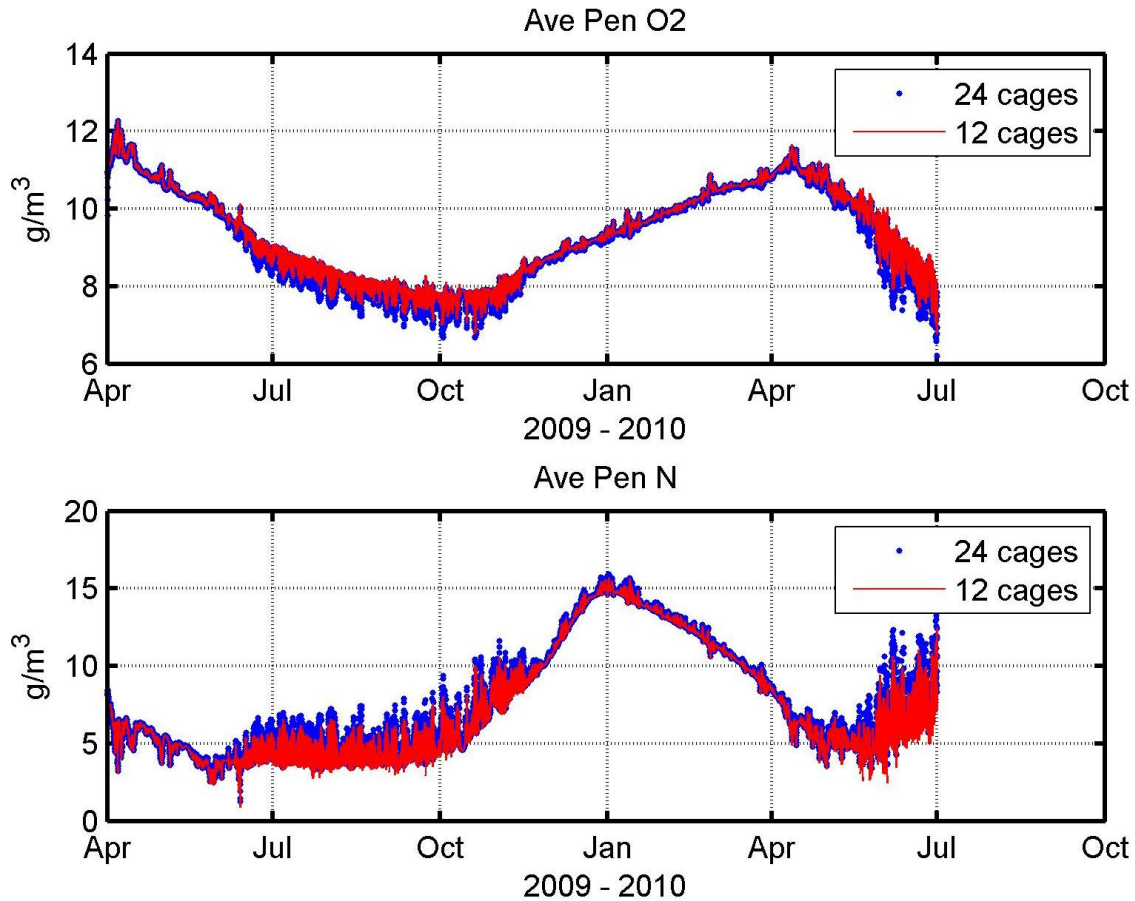
Figure 64: (Top) Comparison of the average pen dissolved oxygen between the 12- and 24-cage farms. (Bottom) Comparison of the average nitrogen between the 12- and 24-cage farms.

The next 10 plots shown in the report provide an example of the near-field capabilities of the AquaModel program and how it can be used as an assessment and monitoring tool. Even though simulations were performed for both 12- and 24-cage farms, only screen shots for the 12 cage configuration are provided. As previously mentioned, the simulations were started in April as waters in the region begin to warm (e.g. start of the grow-out cycle). The first screen-shot (Figure 65) shows the region of the Gulf of Maine with the location of the farm site just south of the Isles of Shoals (indicated by the red dot). This spot is also the location of the UNH OOA research studies. In the next screen-shot (Figure 66), the AquaModel is zoomed in to show the 12 cage locations within the farm. It also shows the position of a red colored transect line, capture cells (indicated by the grey dots) and a vertical profile point (red dot, but not clearly legible in these images). These are tools within the GIS program to acquire and view specific calculation data sets from a three-dimensional perspective.

After one month of AquaModel simulation time, Figure 67 provides information regarding the

sediment total organic carbon (TOC) deposition flux rate where the red color indicates 1% of the threshold value. The TOC concentration is shown after two months in Figure 68. The influence of the ambient conditions is evident as the increase of current velocities and directional variability affect the resulting fractional amounts. Figure 69 shows the results after 4 months of simulation time. In addition to the benthic affects, AquaModel calculates nitrogen concentrations (i.e. DIN) within the water column. Figure 70 shows the DIN plume at a depth of 10 meters on August 1st. Though a plume is evident, values are not much different than the ambient shown on Figure 50. Note that the far-field results described later in the report examine the nitrogen plume effects on a regional scale. Figure 71 provides a snapshot of the TOC deposition flux rate after 5 months. The calculations show only a modest effect with mostly aerobic organism dynamics prevailing. The TOC deposition flux rates for 6, 7, and 8 months are shown on Figures 72, 73 and 74 respectively, with nearly steady-state conditions being predicted.
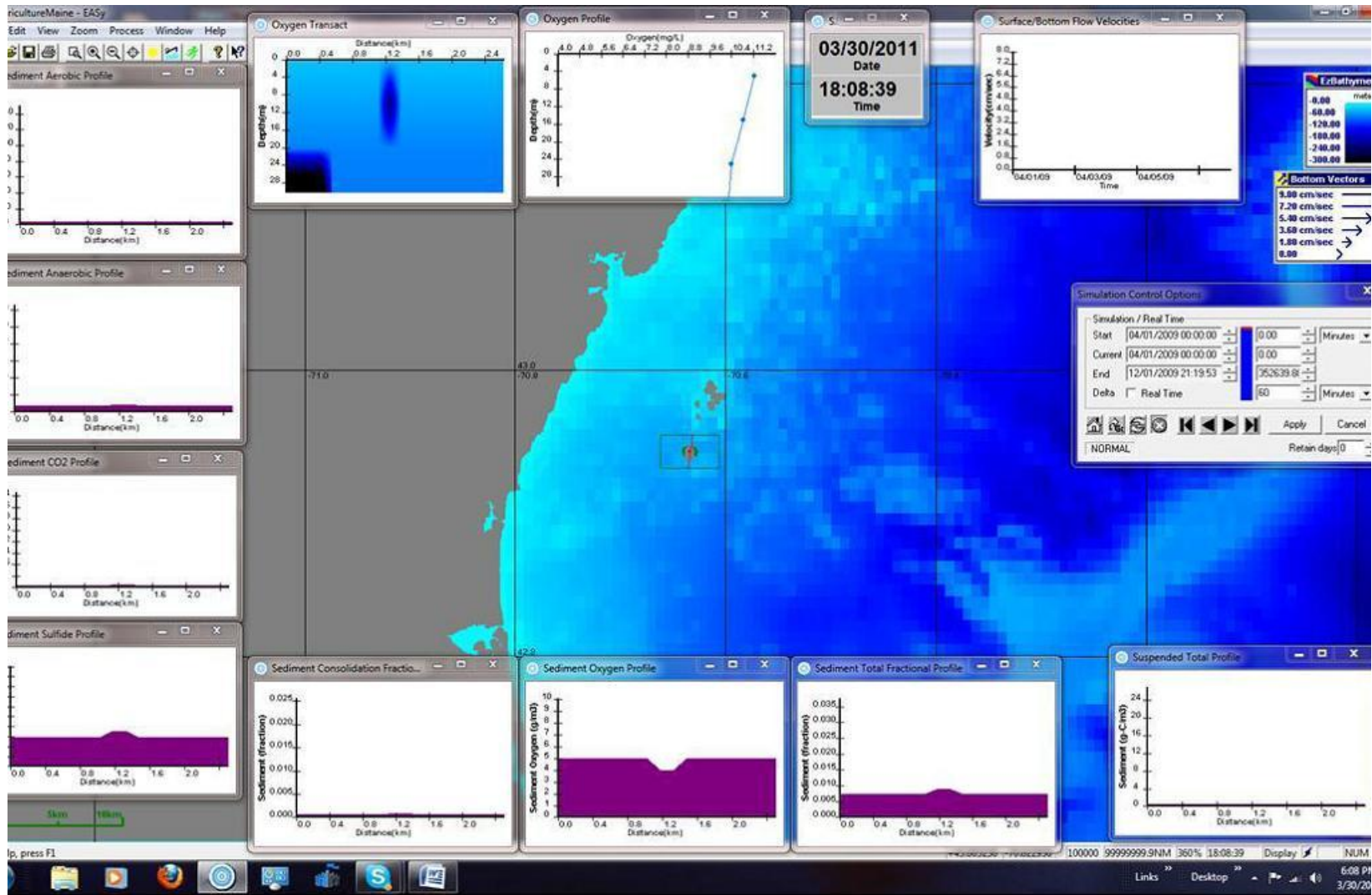
Figure 65: Gulf of Maine: Isle of Shoals 12-cage farm simulation: Showing Bathymetry in region, see scale to upper right.
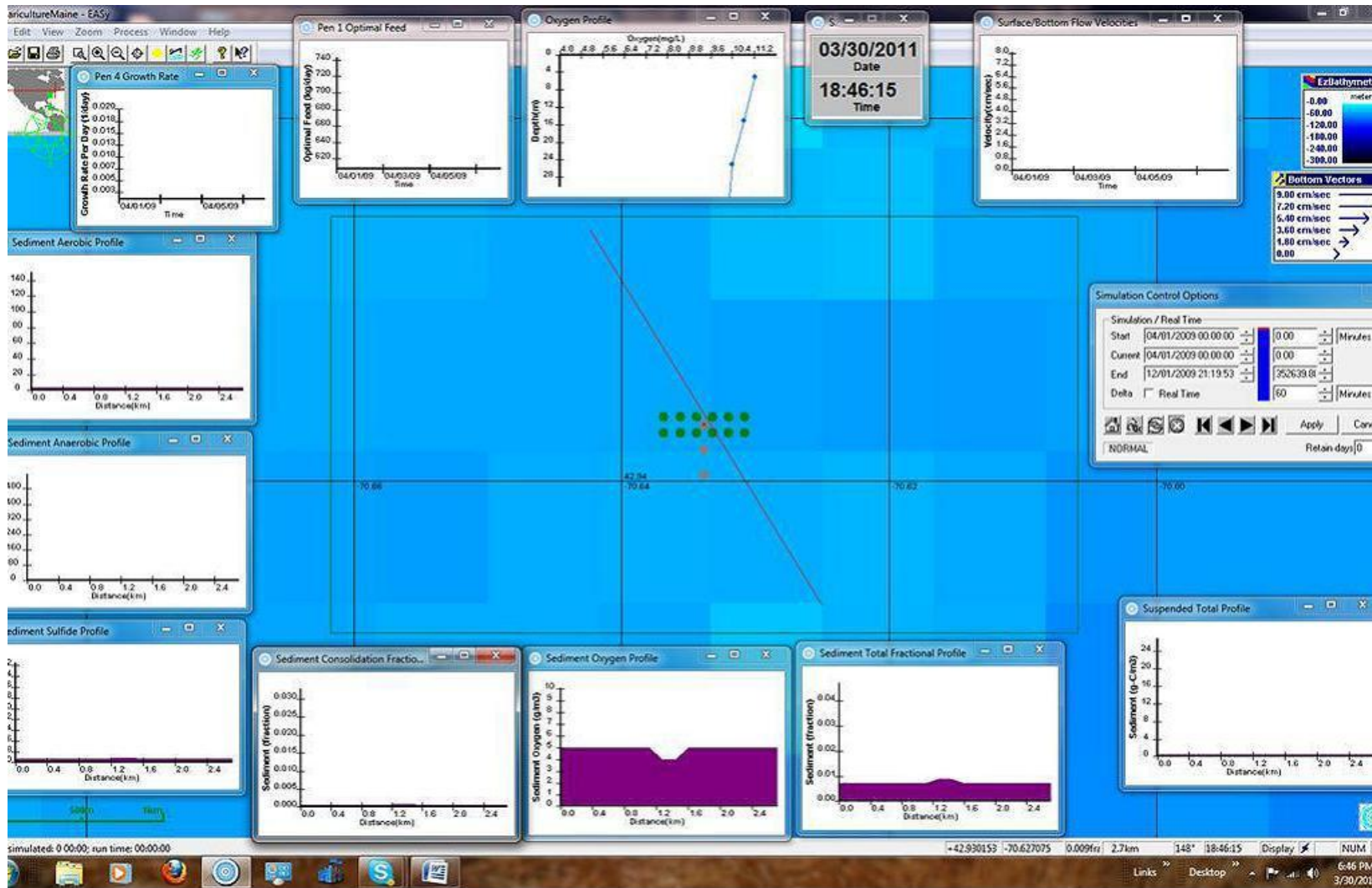
Figure 66: Bathymetry and closer up view of pen array with diagonal transect line, vertical profile location (red dot) and capture cells (grey dots).
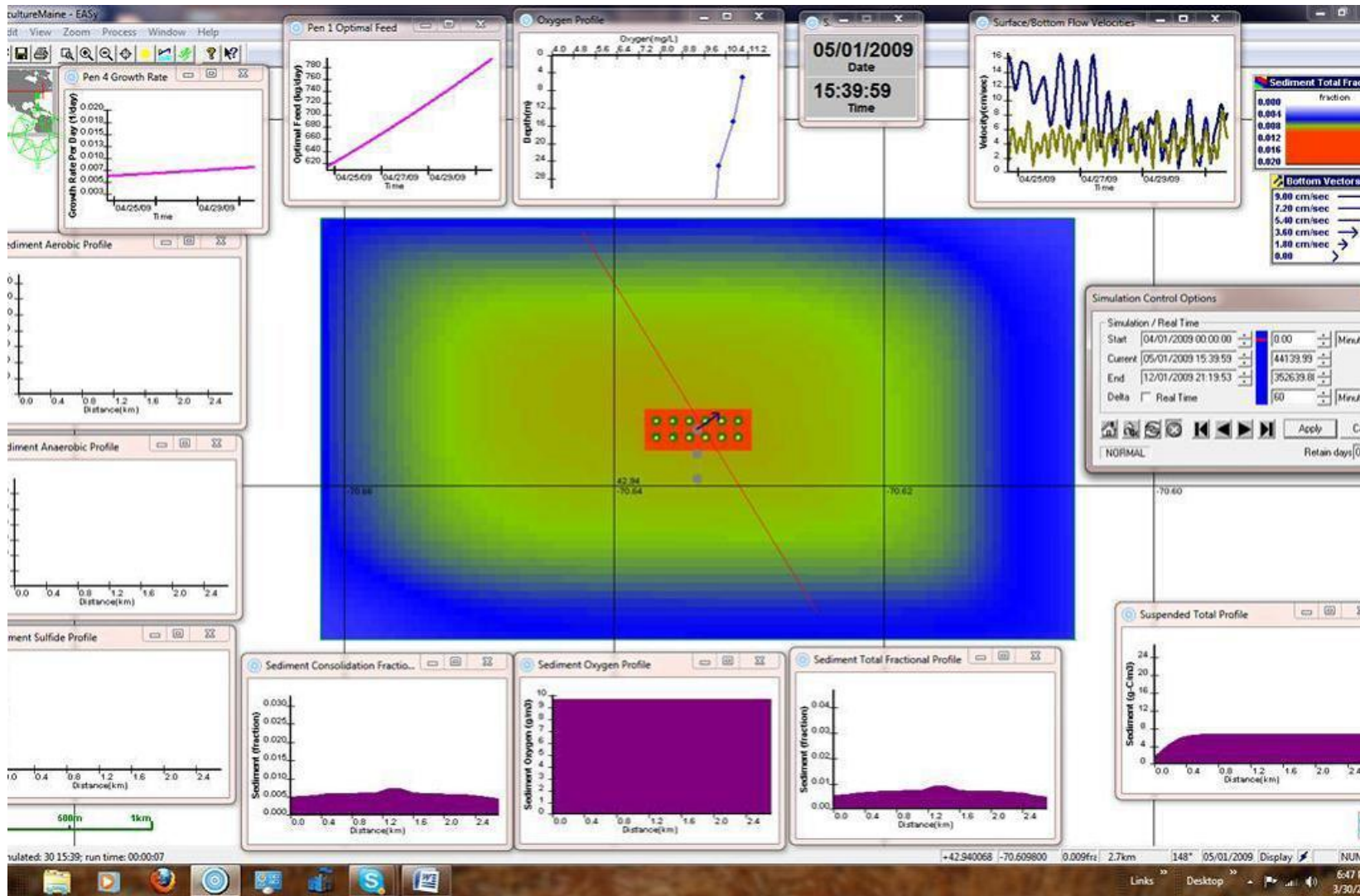
Figure 67: First snapshot in time series: Total organic carbon deposition flux state after 1 month. See scale to the upper right, red color indicates 1% and higher TOC (usually where adverse biological effects occur in sandy sediments).
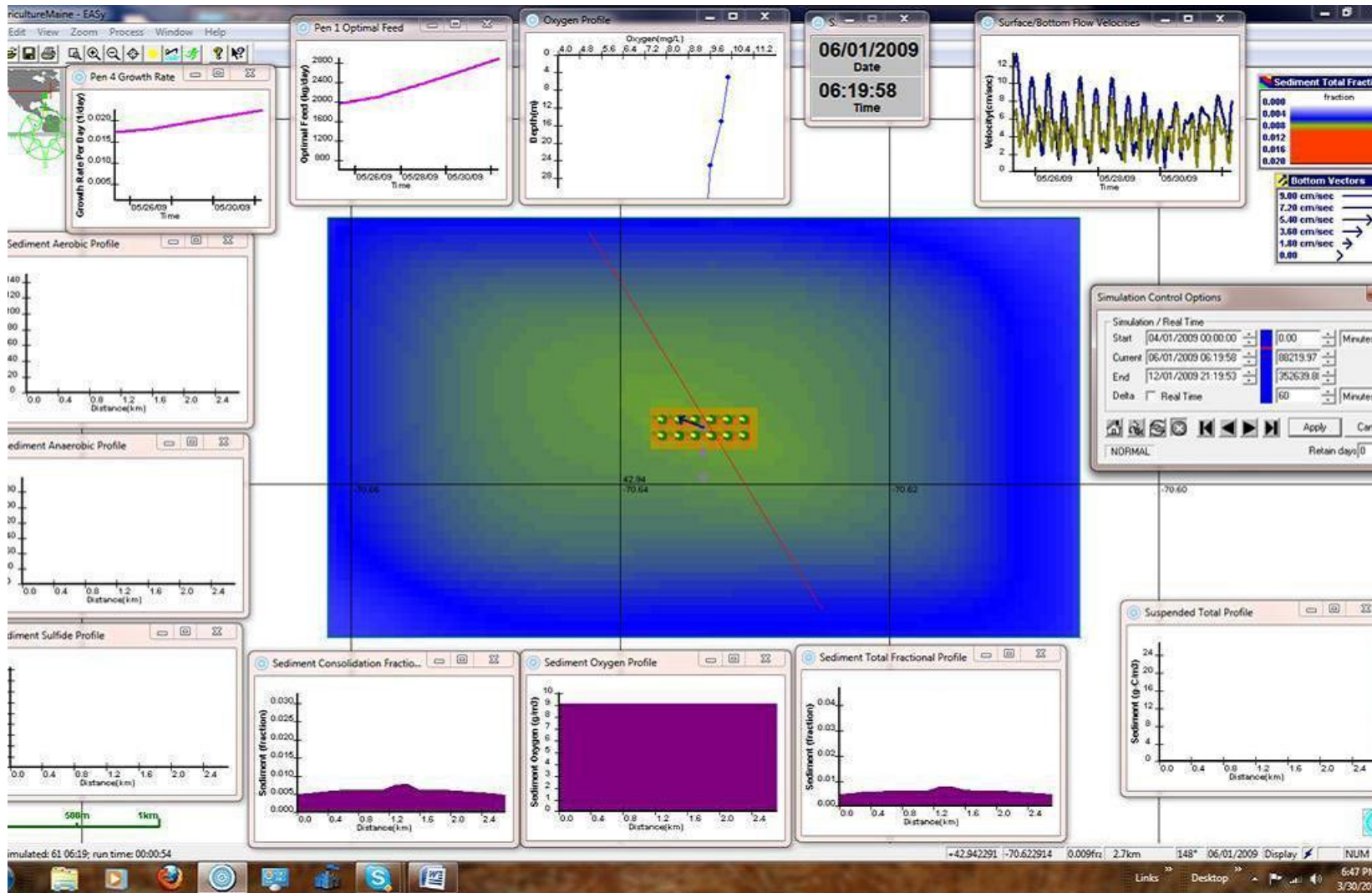
Figure 68: Total organic carbon deposition flux state after 2 months: Despite more biomass of fish, less effect due to current velocity increase and directional variability. But feed rate and growth rate rapidly increasing as the water warms and directional variability increases.
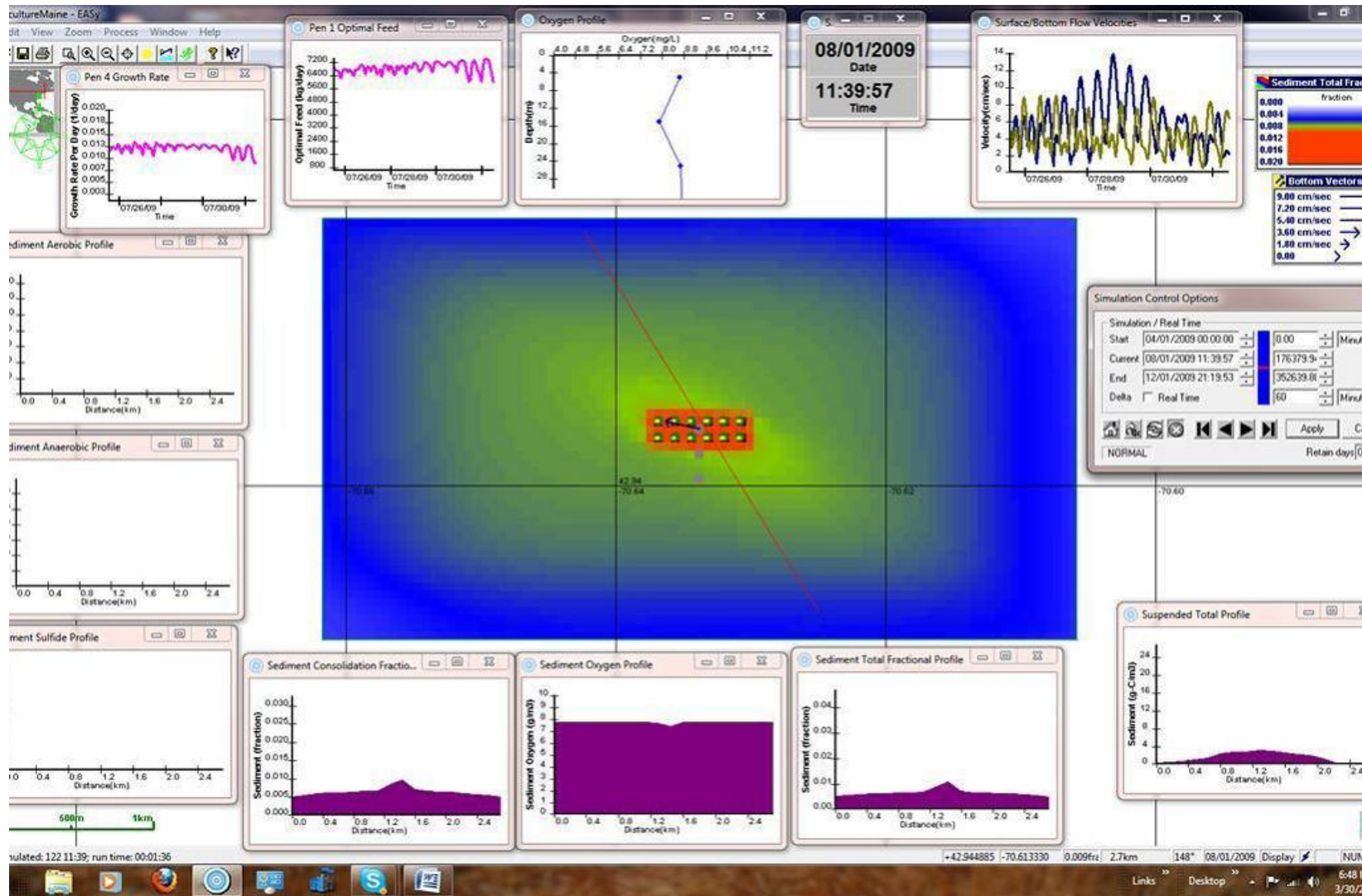
Figure 69: Total organic carbon deposition flux state after 4 months: increasing TOC under cages but just barely above 1% TOC. Growth rate dropping as fish begin to gain size.
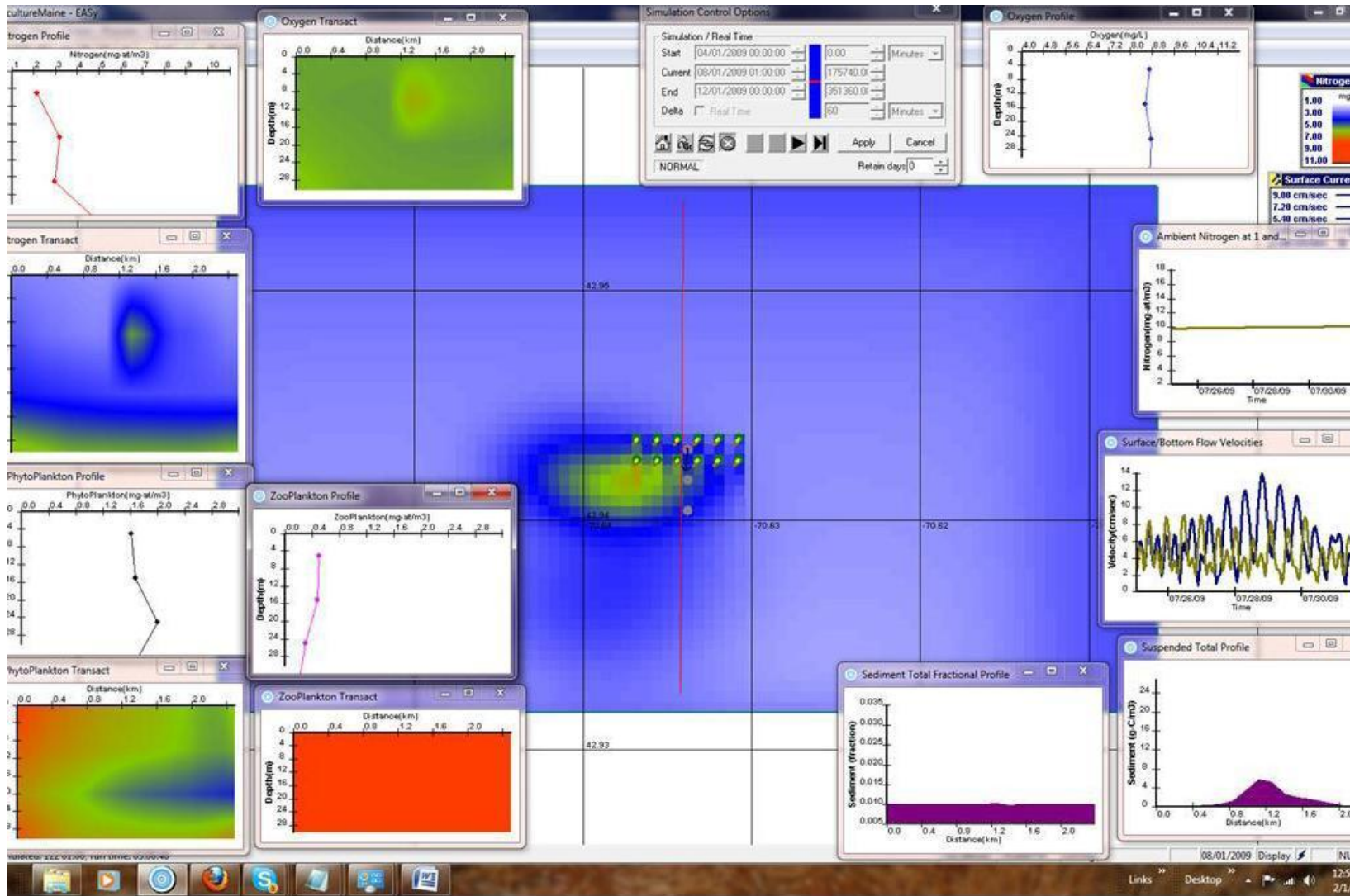
Figure 70: Model run showing time period August 1st with 10 meter depth nitrogen plume as main image and some of the 40+ X-Y plots along the red transect line. XY vertical profiles are from the middle of the pens in this snapshot but are movable, as are the capture cells (grey dots).
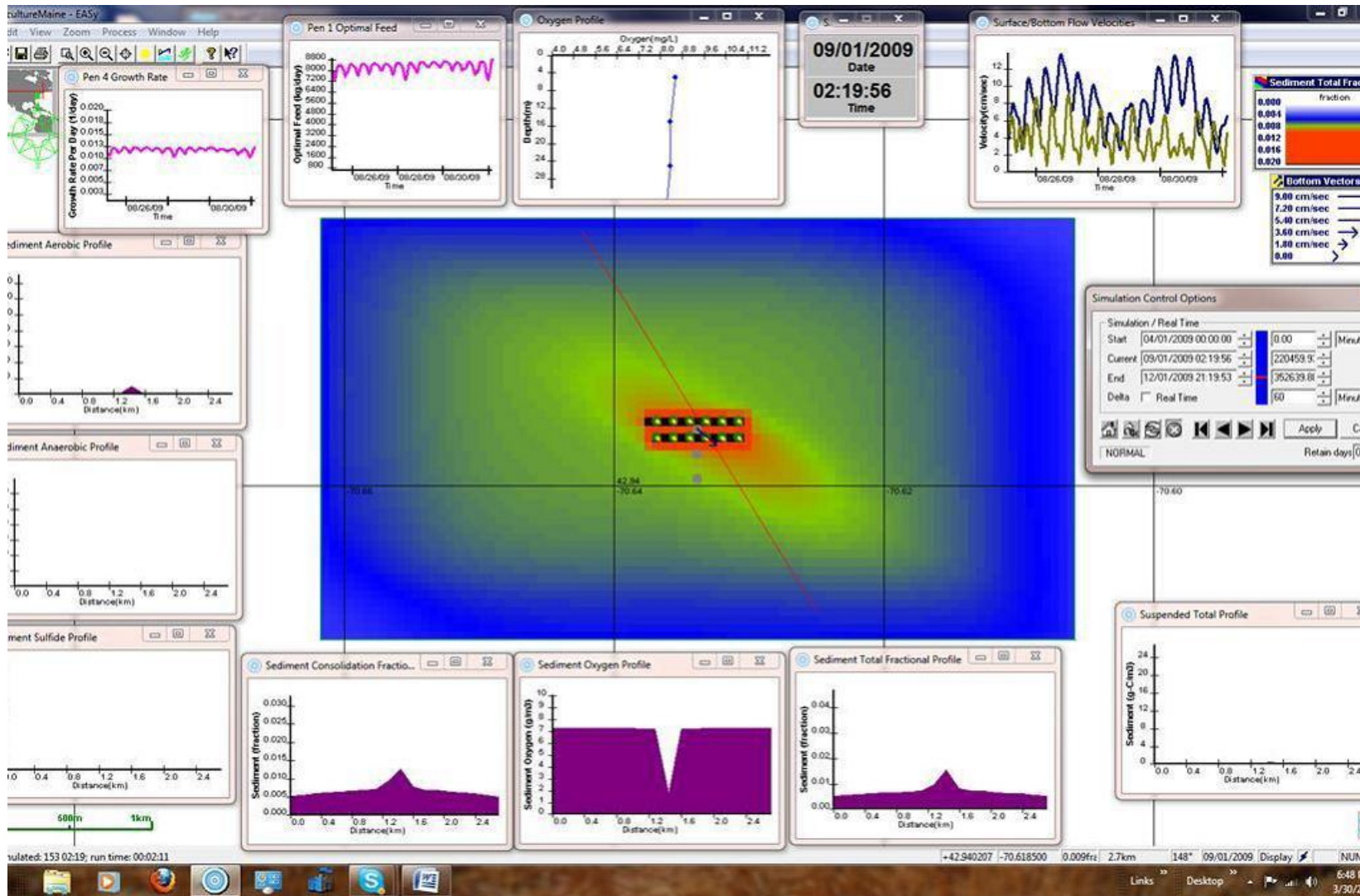
Figure 71: Total organic carbon deposition flux state after 5 months: TOC starting to exceed 1% outside of pen area but still very modest effect, mostly aerobic organisms occurring.
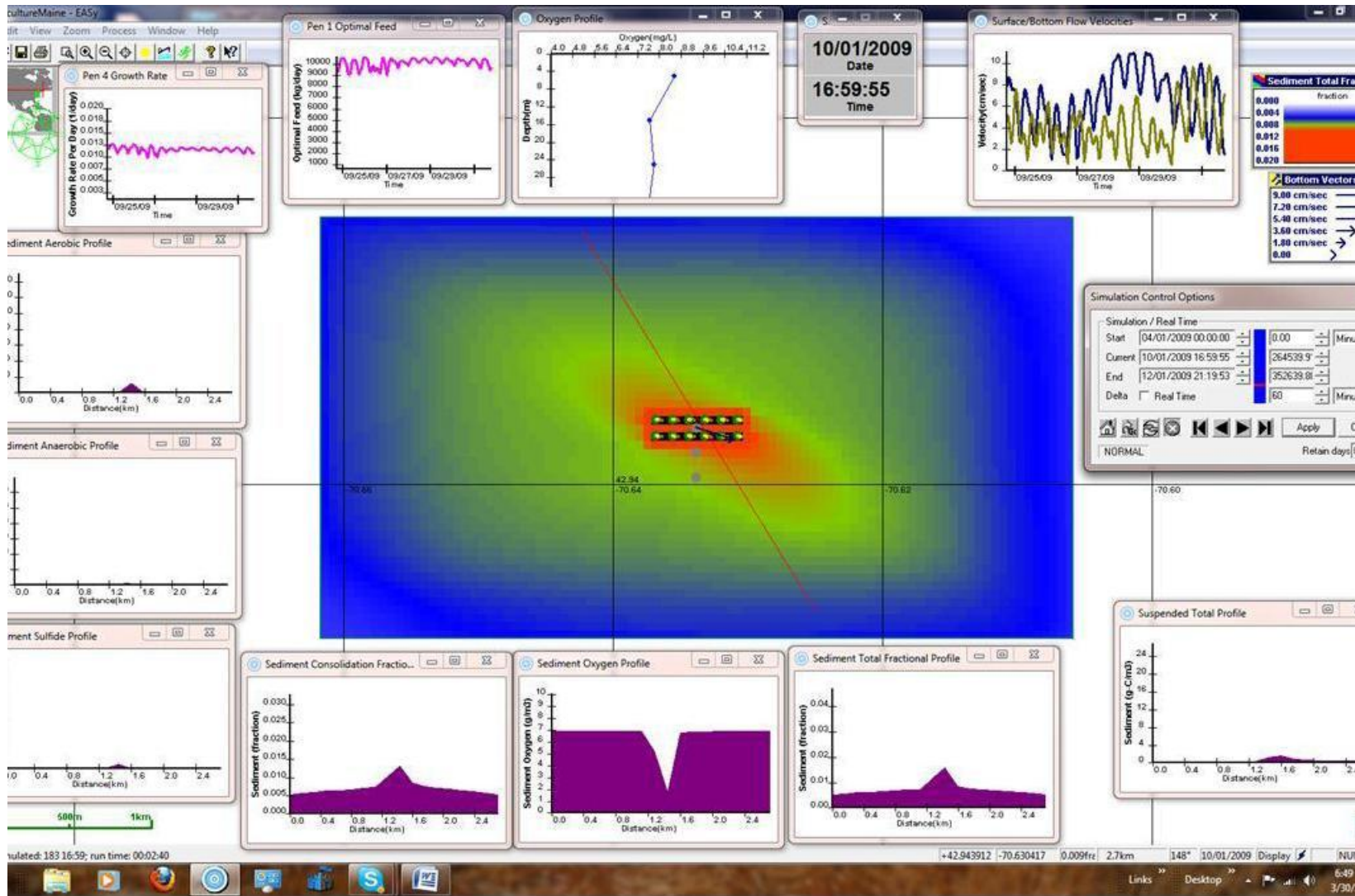
Figure 72: Total organic carbon deposition flux state after 6 months: very slight increase from the month before.
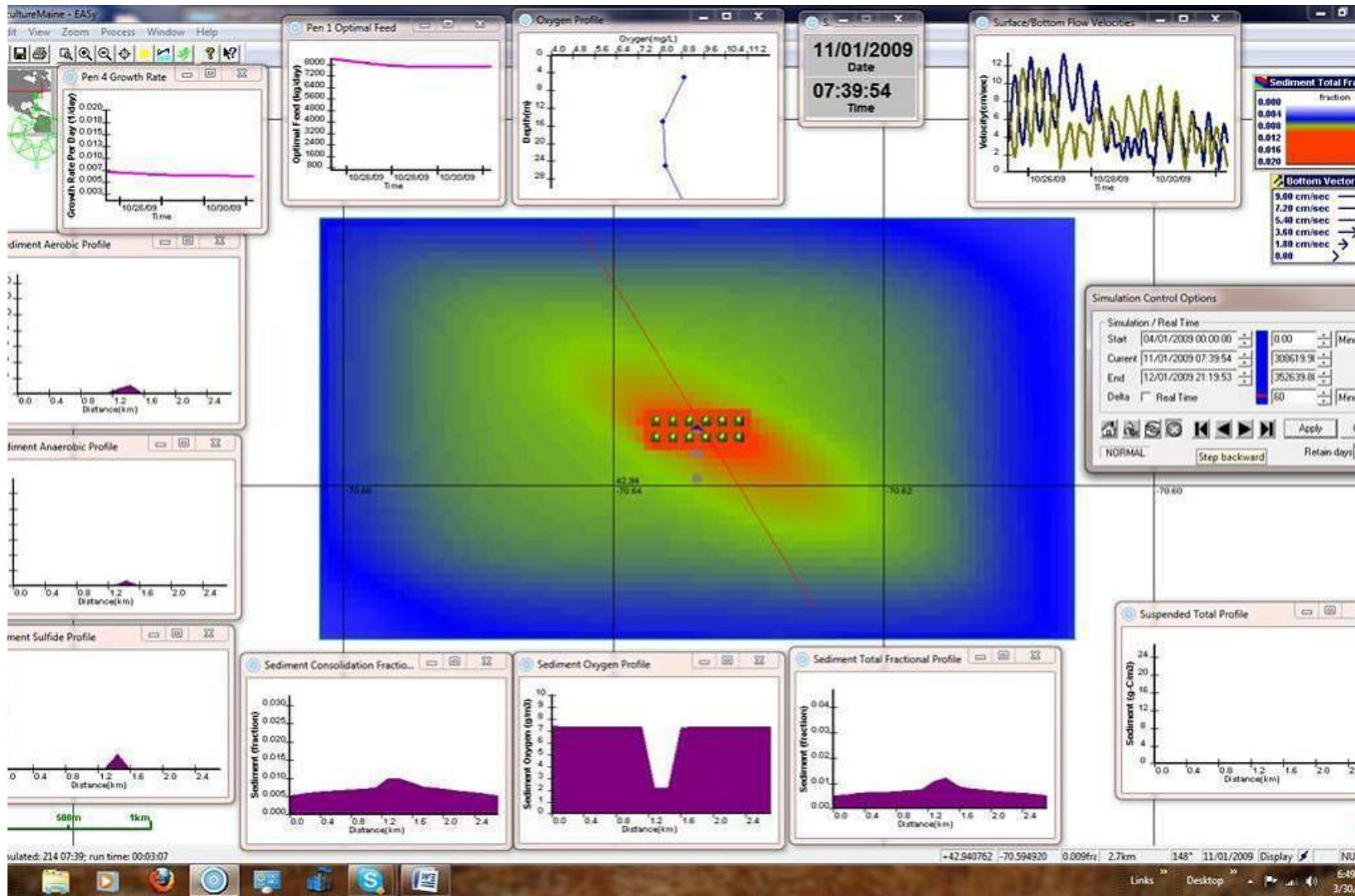
Figure 73: Total organic carbon deposition flux state after 7 months: Growth rate dropping as temperature declines. Similar effects on the sea bottom as in the previous period.
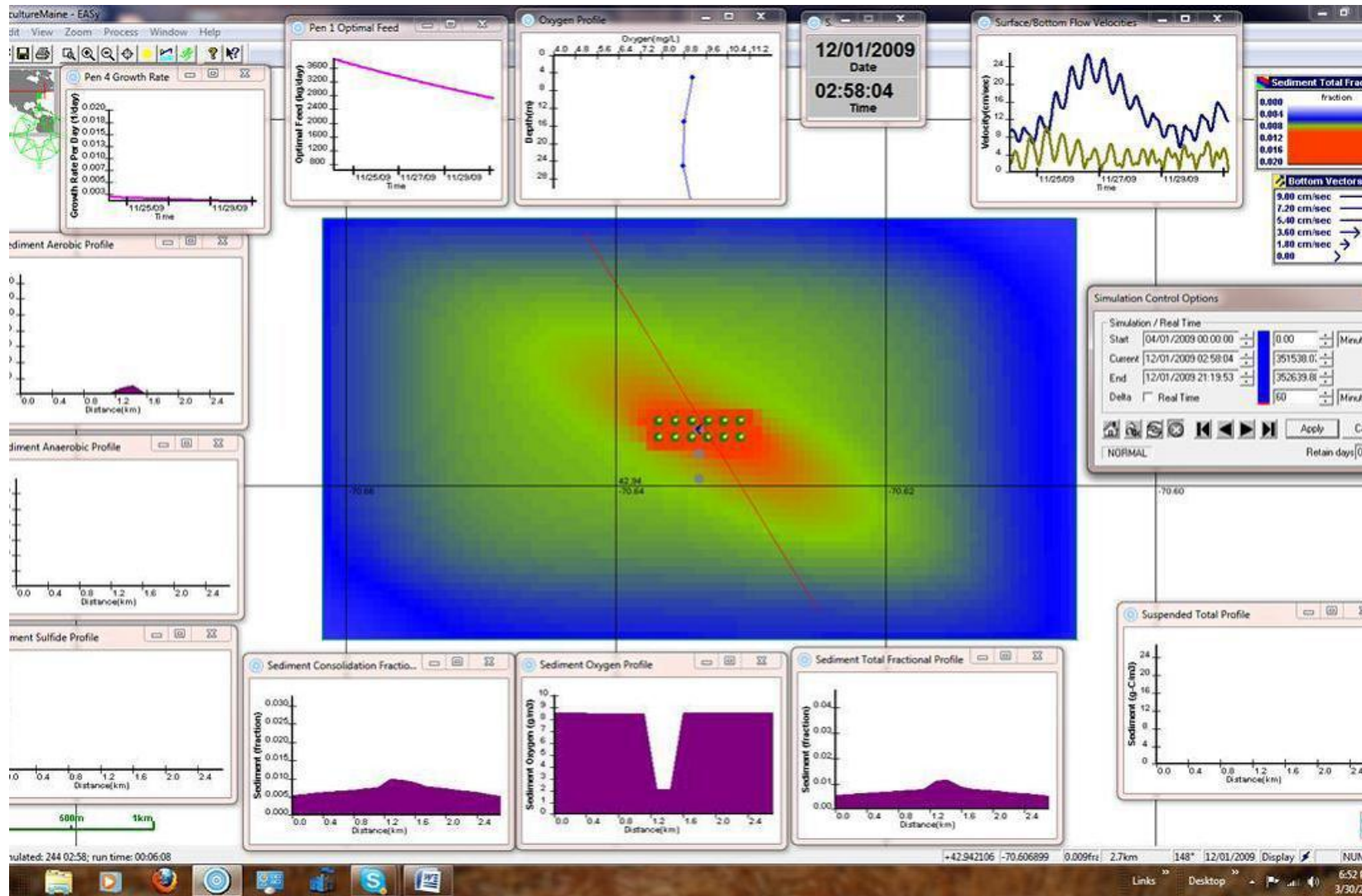
Figure 74: Total organic carbon deposition flux state after 8 months: Growth and feed rates have significantly declined in December's cold water. TOC effects are static.

5.5. Capture Cell Results

The next several plots show "capture cell" data sets. Recall that capture cell numbers numbered 1, 2 and 3 run from north to south (positions shown by the grey dots on Figures 62). The capture cells were in the same location for both the 12- and 24-cage configurations. Capture cell results can be obtained in the AquaModel program for any measured parameters but were collected in this case for the following parameters:

- Oxygen (g/m^3)
- Nitrogen (g/m^3)
- Phytoplankton (mM/m^3)
- Zooplankton (mM/m^3)
- Suspended fecal/feed material (g/m^2)
- Sediment fecal material (g/m^2)
- Sediment feed material (g/m^2)
- Sediment consolidation (g/m^2)
- Sediment Oxygen (g/m^2)
- Sediment total material (g/m^2)
- Sediment total fraction (of TOC in percent)

The next 8 plots compare the capture cell results for the 12- and 24-cage farm sizes. Reviewing the information, it is clear that the water column impact differences are negligible (Figure 75 through 78). The benthic results however, do show some differences (Figures 79 through 82). Due to the large amount of data sets acquired, an in-depth explanation of the resulting benthic dynamics would be better served in a stand alone publication and therefore not entirely presented here.
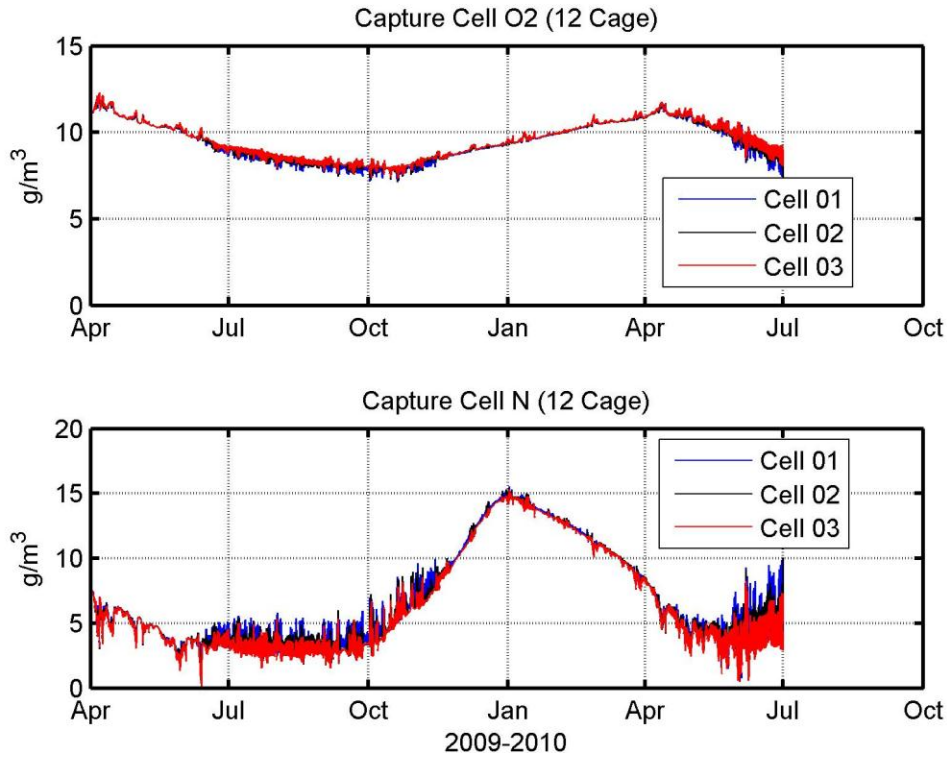
**Figure 75: Capture cell results for the 12-cage simulation showing oxygen and nitrogen concentrations.**
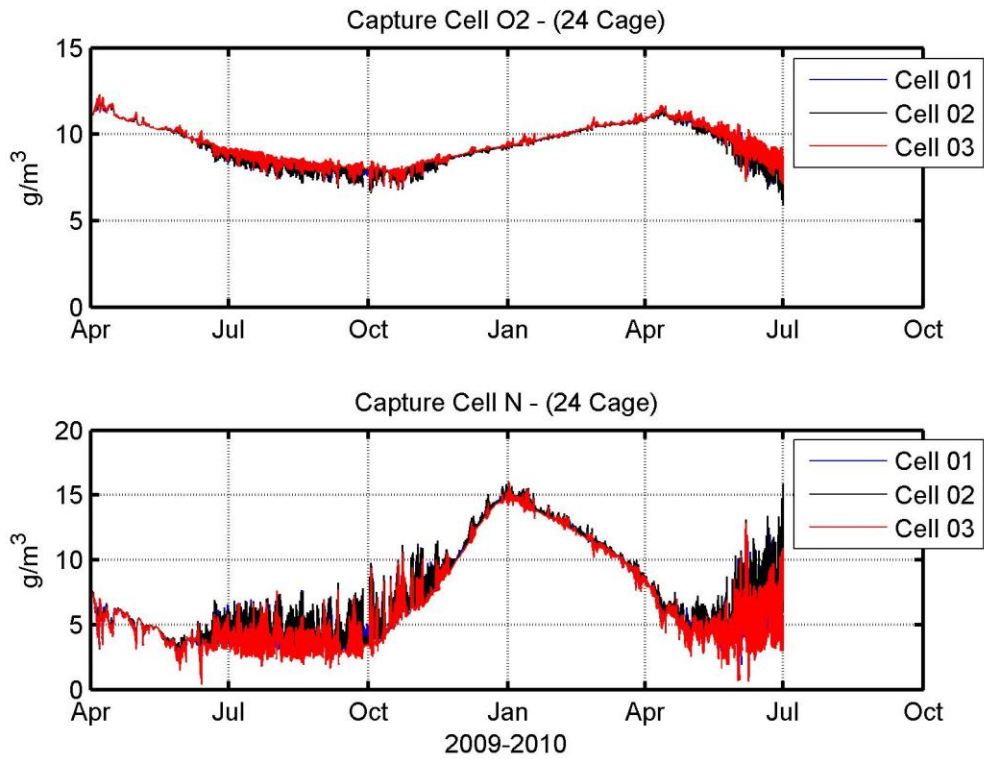
Figure 76: Capture cell results for the 24-cage simulation showing oxygen and nitrogen concentrations.
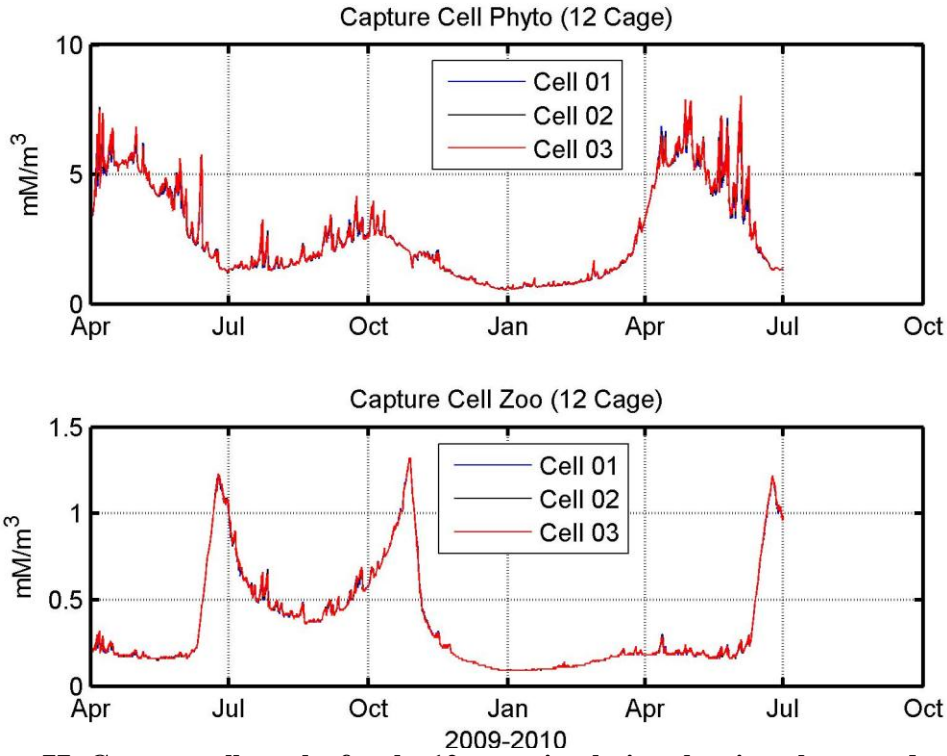
**Figure 77: Capture cell results for the 12-cage simulation showing phyto- and zooplankton concentrations.**
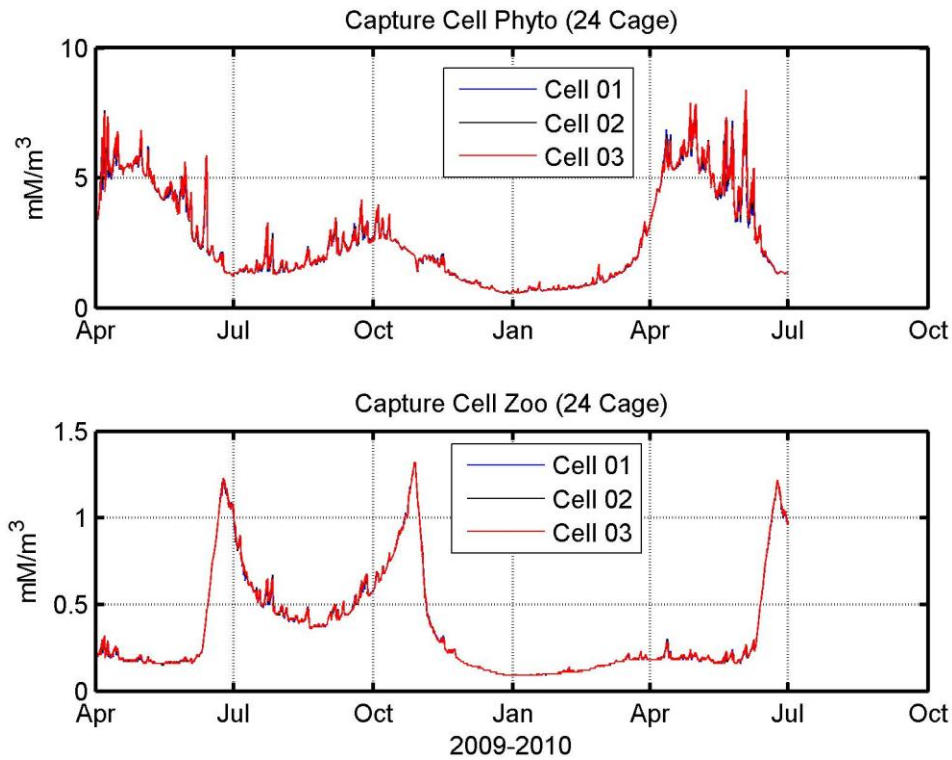
Figure 78: Capture cell results for the 24-cage simulation showing phyto- and zooplankton concentrations.
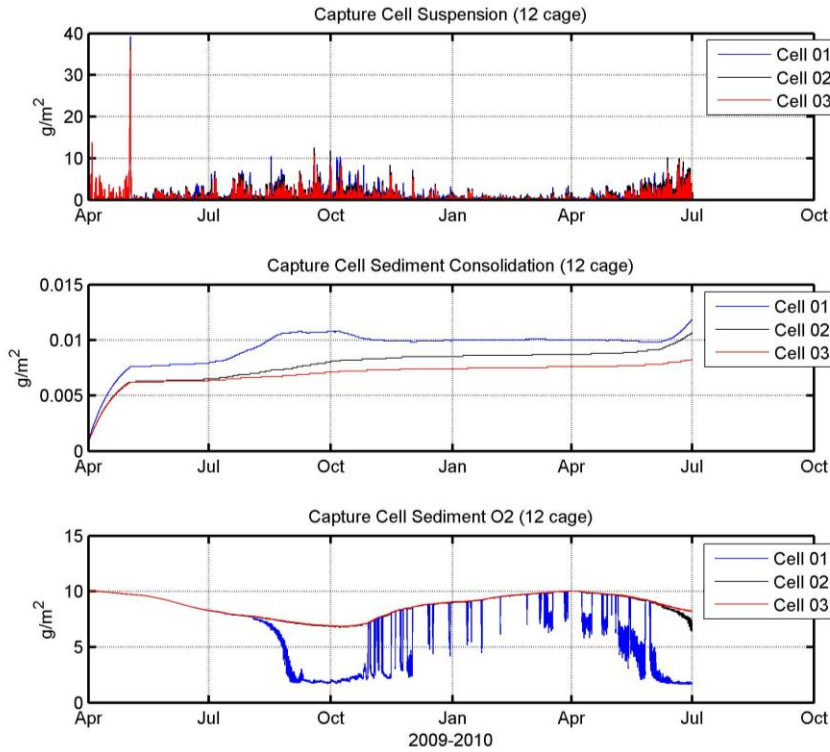
Figure 79: Capture cell results for the 12-cage simulation showing sediment suspension, consolidation, and oxygen concentrations.
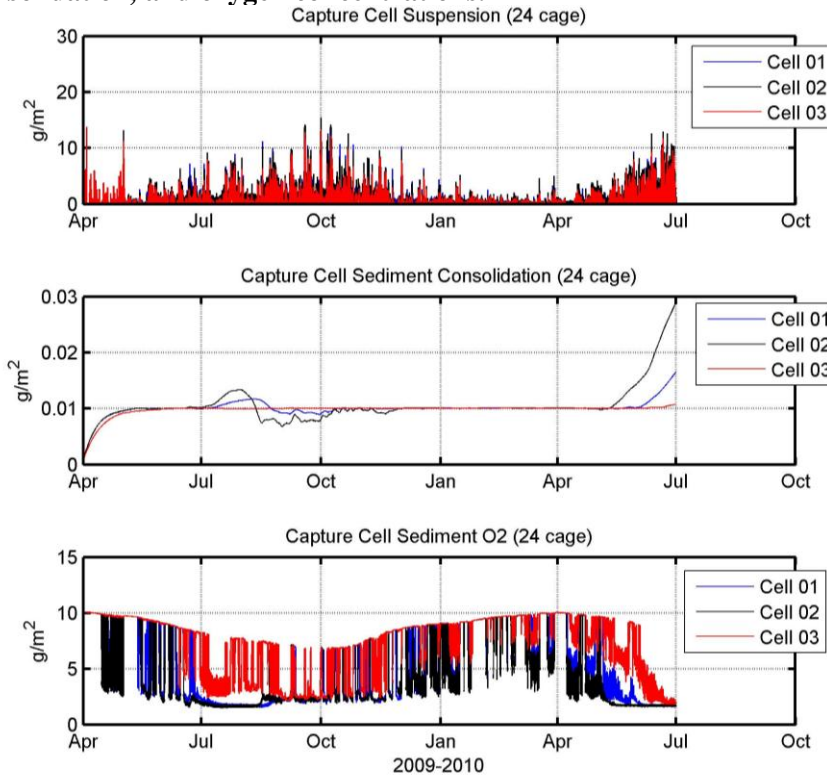

Figure 80: Capture cell results for the 24-cage simulation showing sediment suspension, consolidation, and oxygen concentrations.
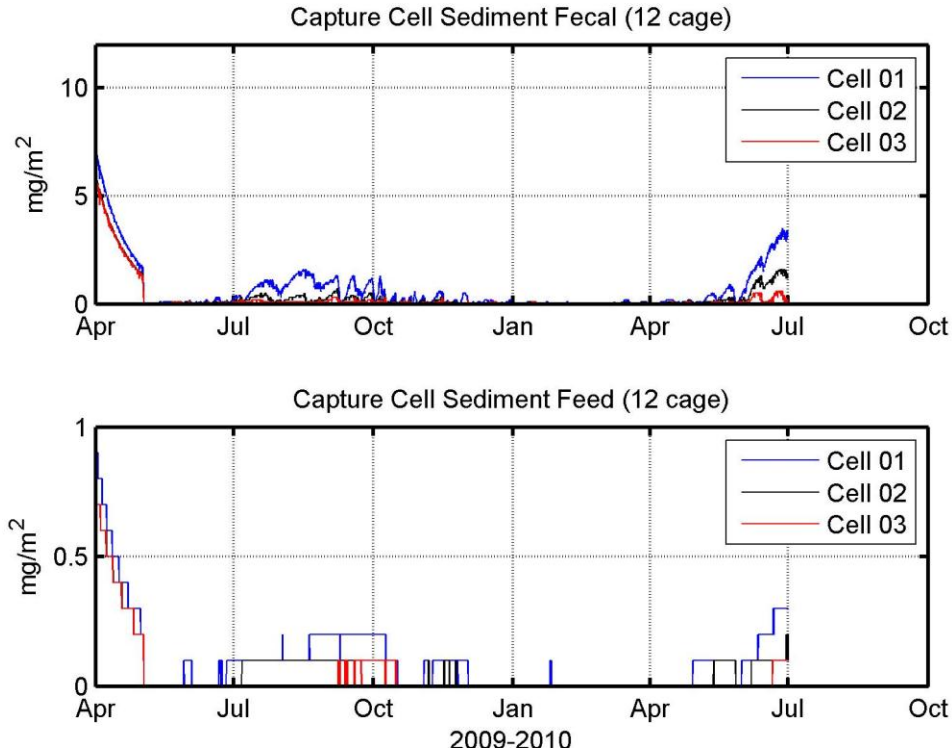
Figure 81: Capture cell results for the 12-cage simulation showing sediment fecal and feed concentrations.
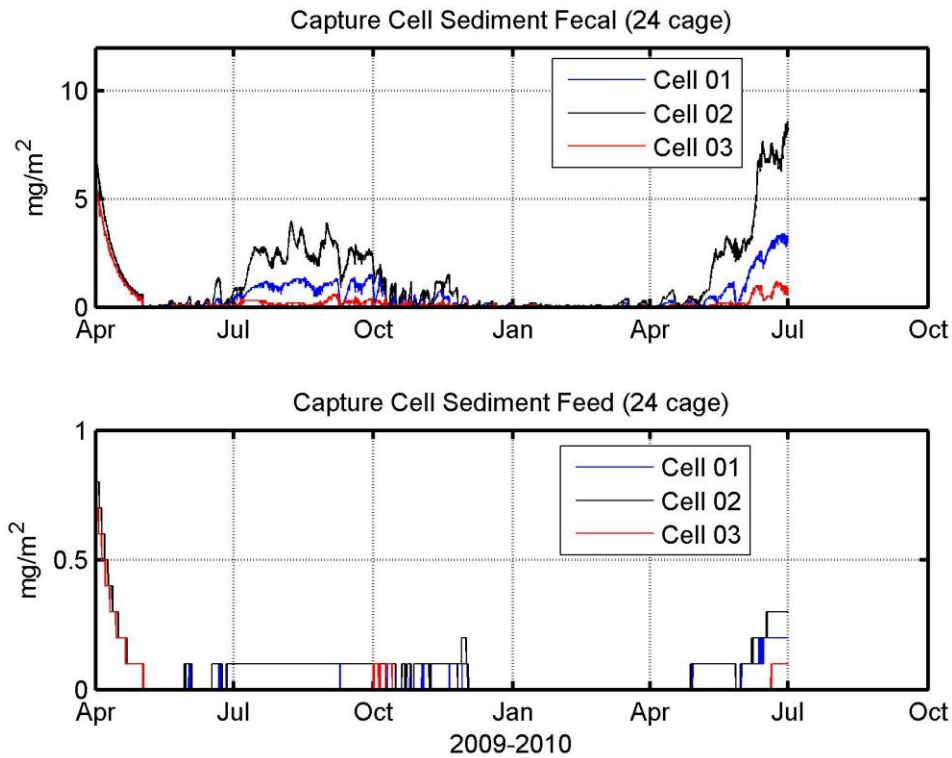

Figure 82: Capture cell results for the 24-cage simulation showing sediment suspension, consolidation, and oxygen concentrations.

5.6. Section References

Benitez-Nelson, C.R., Buesseler, K.O., and G. Crossin. (2000). Upper Ocean carbon export, horizontal transport, and vertical eddy diffusivity in the southwestern Gulf of Maine. Continental Shelf Research. Vol. 20. pp. 707-736.

Broecker, W. S. and T.H. Peng (1982). Tracers in the Sea, Lamont-Doherty Geological Observatory Press.

Cromey, C.J., Nickell, T.D. and K.D. Black. (2002a). DEPOMOD-modelling the deposition and biological effects of waste solids from marine cage farms. Aquaculture. Vol. 214. pp. 211-239.

Cromey, C.J., Nickell, T.D, Black, K.D., Provost, P.G. and C.R. Griffiths. (2002b). Validation of a fish farm waste resuspension model by use of a particulate tracer discharged from a point source in a coastal environment. Estuaries. Vol. 25, No. 5, p. 916-929.

Cromey, C., Provost, P., Black, K. (2003). Development of monitoring guidelines and modelling tools for environmental effects from Mediterranean aquaculture. Some hydrological observations at Eastern Mediterranean fish farms. MERAMED project, Newsletter 2. European Commission, Quality of Life and Mangement Resources programme. Contract Q5RS-2000-31779.

Fischer, H.B., List, E.J., Kho, R.C.Y., Imberger, J., and N.H. Brooks. (1979). Mixing in inland and coastal waters. Academic Press, NY. 483 p.

Findlay, R.H, and L. Watling. 1997. Prediction of benthic impact for salmon net-pens based on the balance of benthic oxygen supply and demand Marine Ecology Progress Series 155:147-157.

Grizzle, R., Ward, L., Irish, J.D., Fredriksson, D.W., Langan, R., Henig, C., Greene, J., Abeels, Peter, C., and A. Eberhardt (In preparation). Long-term seafloor monitoring at an open ocean aquaculture site in the western Gulf of Maine, USA: development of an adaptive protocol.

Gustafsson, O., Buesseler, K.O., Geyer, W.R., Moran, S.B., and P.M. Gschwend. (1998). An assessment of the relative importance of horizontal and vertical transport of particle-reactive chemicals in the coastal ocean. Continental Shelf Research. Vol. 18. pp. 805-829.

Harris, J.R., R.N. Gorley and C.A. Bartlett. (1993). ECos Version 2 – A User Manual. Plymouth Marine Laboratory. Plymouth, U.K.

Magni, P., Tagliapietra, D., Lardicci, C., Castelli, A., Como, S., Frangipane, G., Giordani, G., Hyland, J., Maltagliati, F., Pessa, G., Rismondo, A., Tataranni, M., Tomassetti, P., and P. Viaroli. (2009). Animal-sediment relationships: Evaluating the 'Pearson-Rosenberg paradigm' in Mediterranean coastal lagoons. Marine Pollution Bulletin. Vol. 58, pp. 478-486.

Okubo, A. (1971). Oceanic diffusion diagrams. Deep-Sea Research. Vol. 18. pp. 789-802.

Salisbury, J., D. Vandemark, A. Mahadevan, B. Jonsson, C. Hunt, W. R. McGillis. (2009). Episodic riverine influence on surface DIC in the coastal Gulf of Maine. Estuar. Coast. Shelf Science: 82 108-118.

Sanford, L.P., Panageotou, W., and J.P. Halka. (1991). Tidal resuspension of sediments in northern Chesapeake Bay. Marine Geology. Vol. 97. pp. 87-103.

Wildish, D.J., Hargrave, B.T., and G. Pohle. (2001). Cost-effective monitoring of organic enrichment resulting from salmon mariculture. ICES Journal of Marine Science. 58: 469-476.

Ward, L.G., Grizzle, R. and J.D. Irish. (2006). Environmental Monitoring Program: CINEMar/Open Ocean Aquaculture Annual Progress report for the period of 1/01/06 through 12/31/06. (http://ooa.unh.edu).

6. Circulation Modeling of the Open Ocean Aquaculture Site in the Gulf of Maine

6.1. Background

Oceanic current can be considered one of the most dominant mechanisms that affect the distribution of dissolved oxygen and nutrients within, and the transport of waste beyond a marine aquaculture facility. As part of the comprehensive modeling approach described in this study, circulation-modeling techniques were applied to the Gulf of Maine region so that far-field AquaModel simulations could be performed. The model domain area where the circulation model was applied is shown on Figure 83.
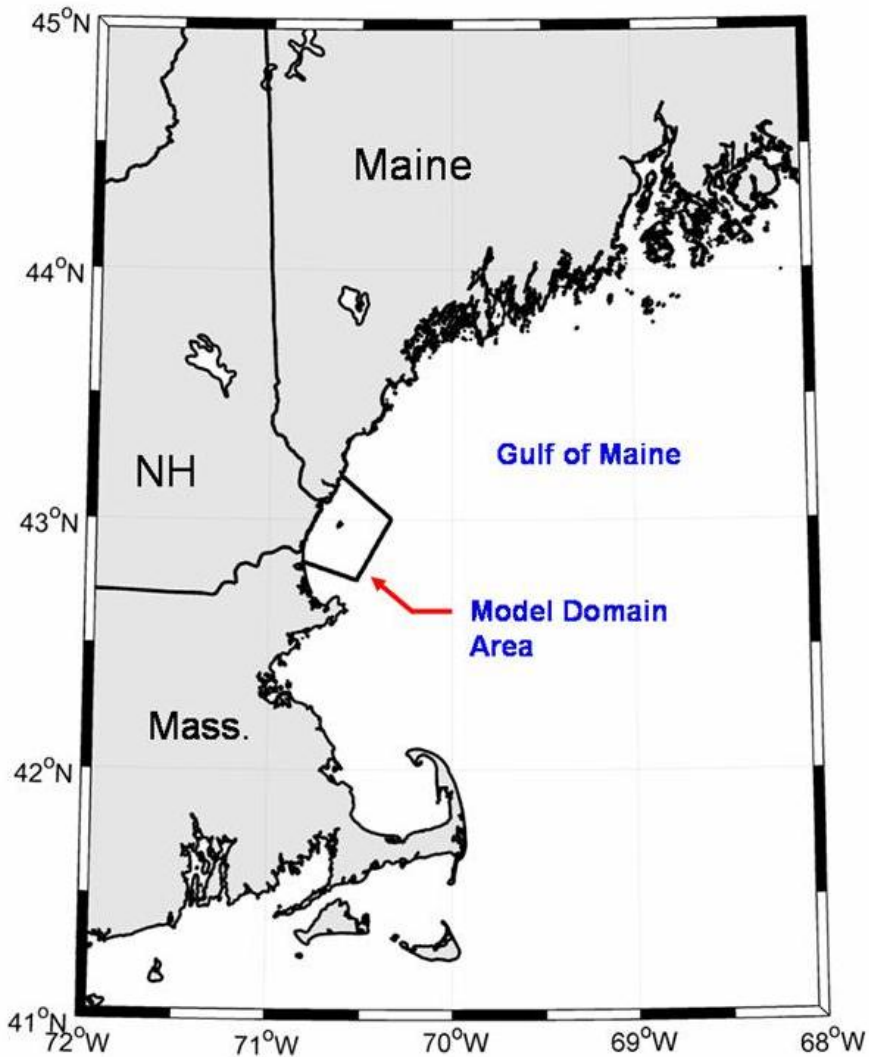

Figure 83: The area of interest is in the Gulf of Maine, off the coast of New Hampshire.

The objectives of this portion of the study are to build the domain of a numerical circulation model, describe a comprehensive set of field observations and compare model results with measurements. The regional hydrodynamic model validation process is a necessary step to produce confident AquaModel results so that concrete decisions can be made. This section of the study will provide a theoretical review of the model, along with a description of the mesh generation techniques, open boundary conditions and model control factors. Details of the field measurement data sets used for model comparisons are also included. The data sets include water column velocity and pressure measurements with tidal harmonic analyses. Results of model simulations are then compared with measured parameters and the quality of the model predictions assessed.

6.2. Modeling Procedure

6.2.1. ADCIRC Model Theoretical Review

Current velocity characteristics were obtained using the Advanced CIRCulation (ADCIRC) model in a two-dimensional, depth integrated (2DDI) configuration as describe in Luettich et al., (1992). The model utilizes the standard depth-integrated, shallow water equations obtained from the three-dimensional equations of motion, vertically averaged, and subjected to the hydrostatic assumption and Bousinesq approximation. The ADCIRC-2DDI model is based on the shallow-water equations,

$$\frac{\partial H}{\partial t} + \frac{\partial (UH)}{\partial x} + \frac{\partial (VH)}{\partial y} = 0, \tag{1}$$

$$\frac{\partial U}{\partial t} + U\frac{\partial U}{\partial x} + V\frac{\partial U}{\partial y} - fV = -g\frac{\partial \left(\zeta + \frac{P_s}{\rho_o g} - \alpha\eta\right)}{\partial x} + \frac{\tau_{sx}}{\rho_o H} - \frac{\tau_{bx}}{\rho_o H} + \frac{M_x}{H} - \frac{D_x}{H} - \frac{B_x}{H}$$

and $\tag{2}$

$$\frac{\partial V}{\partial t} + U\frac{\partial V}{\partial x} + V\frac{\partial V}{\partial y} - fU = -g\frac{\partial \left(\zeta + \frac{P_s}{\rho_o g} - \alpha\eta\right)}{\partial y} + \frac{\tau_{sy}}{\rho_o H} - \frac{\tau_{by}}{\rho_o H} + \frac{M_y}{H} - \frac{D_y}{H} - \frac{B_y}{H}.$$

In equation (1), U and V are the x and y components of the depth averaged velocity,

$$U, V \equiv \frac{1}{H} \int_{-h}^{\zeta} u, v \, dz, \tag{3}$$

and u,v are the vertically varying velocities in the x, and y directions. Also in equation (1), H= ζ +h, where ζ is the surface elevation and h is the bathymetric depth (relative to the geoid). In equations (2), the Coriolis parameter (f) is defined as

$$f = 2\Omega \sin \phi, \tag{4}$$

where $\Omega = 7.29212$ (10^{-5}) rad s^{-1} and ϕ is degrees latitude. These components are balanced by pressure gradients, stresses and dispersion. The first term on the right side of equation (2), is the surface elevation (pressure gradient) which includes the surface elevation (ζ), the atmospheric pressure at the sea surface (P_s), the reference density of water (ρ_o), the earth elasticity factor (α) and the Newtonian equilibrium tide potential (η). The imposed surface and bottom stresses are represented by τ_{sx}, τ_{sy} and τ_{bx}, τ_{by}, respectively. Also included in equations (2) are the vertically integrated lateral stress gradients (M_x and M_y), the depth-integrated horizontal momentum dispersion terms (D_x and D_y) and the baroclinic forcing (B_x and B_y).

6.2.2. Mesh Generation

The next step was to build a numerical representation of coastal New Hampshire. Coastline information was primarily obtained from electronic National Oceanic and Atmospheric Administration (NOAA) charts 13278 and 13283 with geo-referenced points. Three boundary condition types were designated within the model domain including (1) mainland, (2) island and (3) ocean boundaries (Figure 84). The boundaries were built as node strings with specific spacing characteristics. The open ocean boundary nodes were spaced at 1,500 meters. The Isles of Shoals boundary nodes were spaced at 50 meters. The mainland and Portsmouth River boundary nodes were spaced at 100 meters. An additional string of nodes, with a spacing of 50 meters, was also included in the domain surrounding the aquaculture site. This string was not used as a boundary but rather as a technique to increase the resolution of elements created at the aquaculture site.
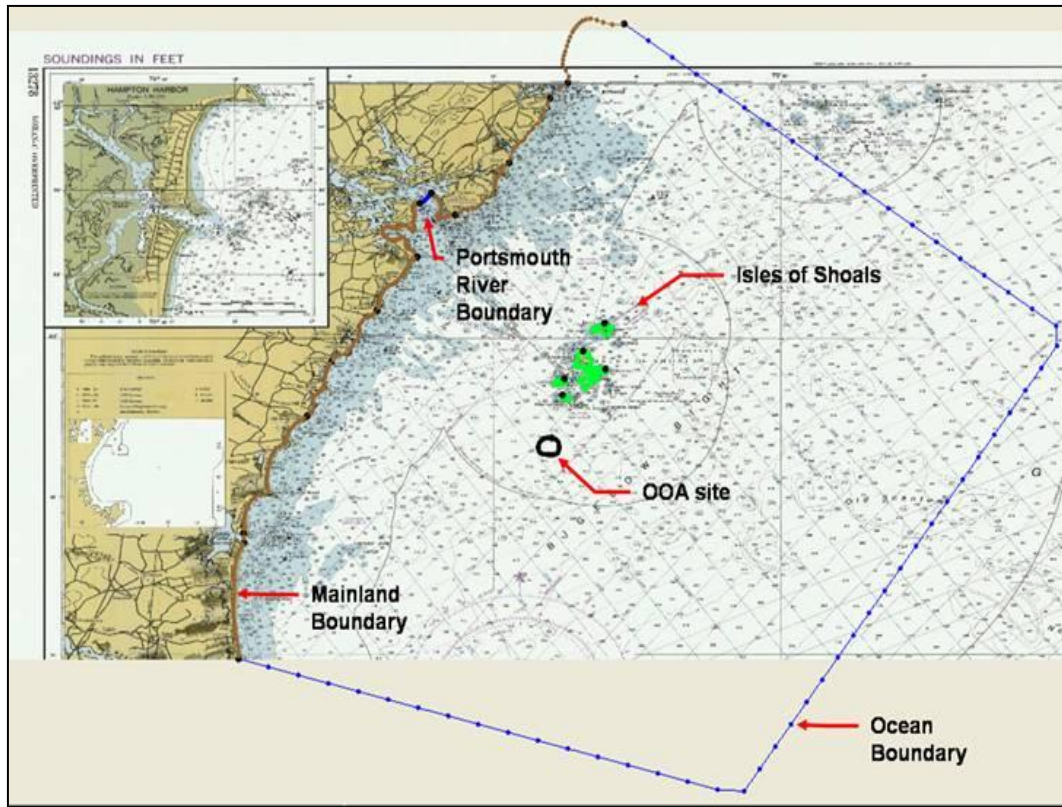
Figure 84: In the mesh generation process, island, coastline and ocean boundaries were established.

Another important component of the mesh generation process includes the use of area bathymetry. Bathymetric data sets were acquired from multiple sources. An extensive number of files were obtained from the NOAA, National Ocean Service Database (NOSDB). These data sets include information from hydrographic surveys conducted from 1930 to the present. The data sets were converted from mean low water to an estimated mean sea level (MSL) by interpolated adjustments obtained from M_2 tide numerical results of the Gulf of Maine as described Lynch and Namie (1993). The individual data sets from this website are shown on Figure 85. Also shown on the Figure is a high-resolution data set (1-meter) obtained from the Center for Coastal and Ocean Mapping (CCOM) at the University of New Hampshire, which was made as part of their hydrographic training program.

To fill in the gaps for which data did not exist, individual points were taken directly from charts 13283 and 13287. Once digitized, the values were converted from mean lower low water to MSL using a published difference value obtained at the NOAA Fort Point site located in Portsmouth, NH (the information can be found at http://tidesandcurrents.noaa.gov).
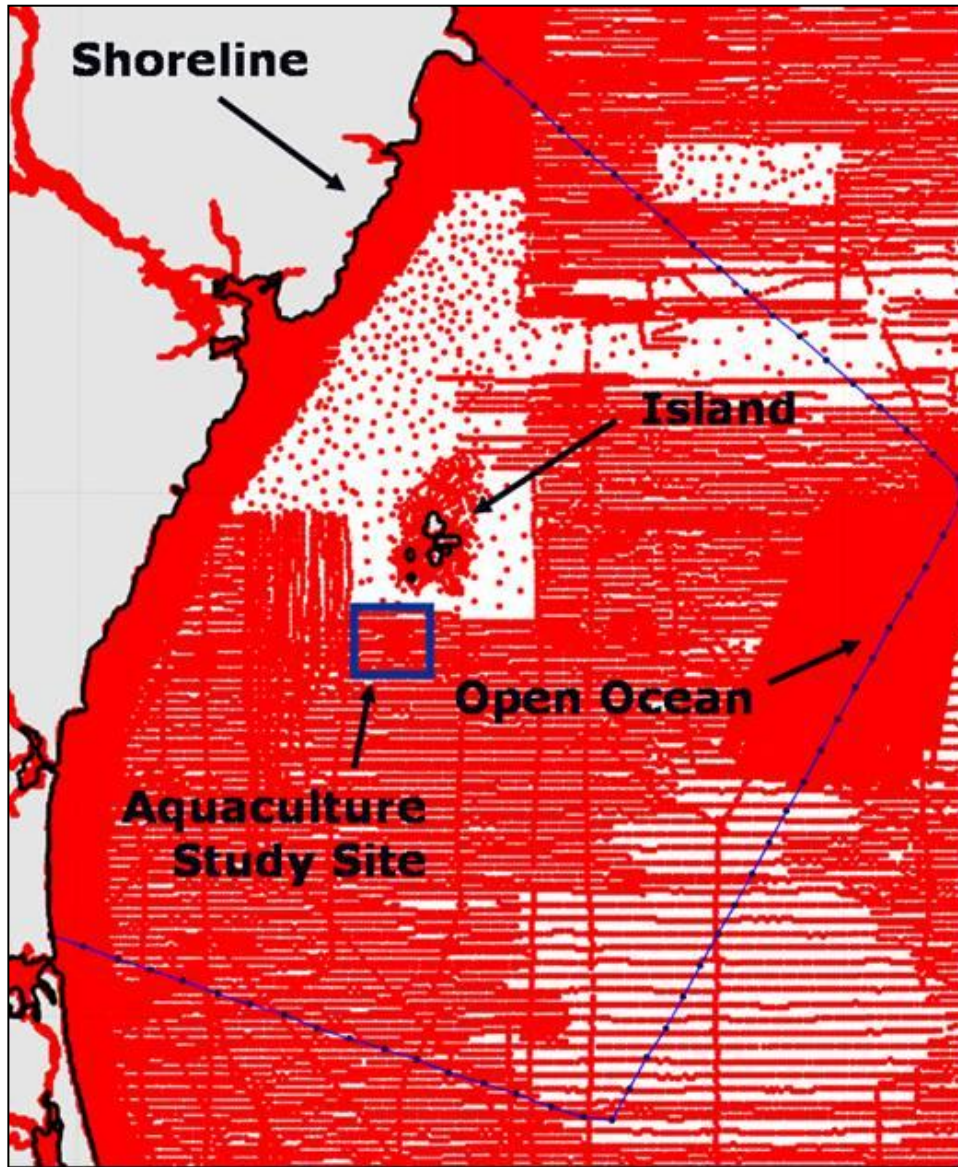
Figure 85: Bathymetric data point locations that were used in the creation of the model. A high-resolution data set was available for the OOA site.

By defining the open boundaries and having a full set of bathymetric data, an unstructured triangular mesh (e.g. having a distribution of sizes) was created. At the nodes of the triangular elements, depth values were interpolated from bathymetric data. The domain of the coastal model was created with 9,839 nodes and 19,067 triangular elements. The entire model domain is shown on Figure 86 with interpolated bathymetry shown within the EAsy GIS program used to run AquaModel.
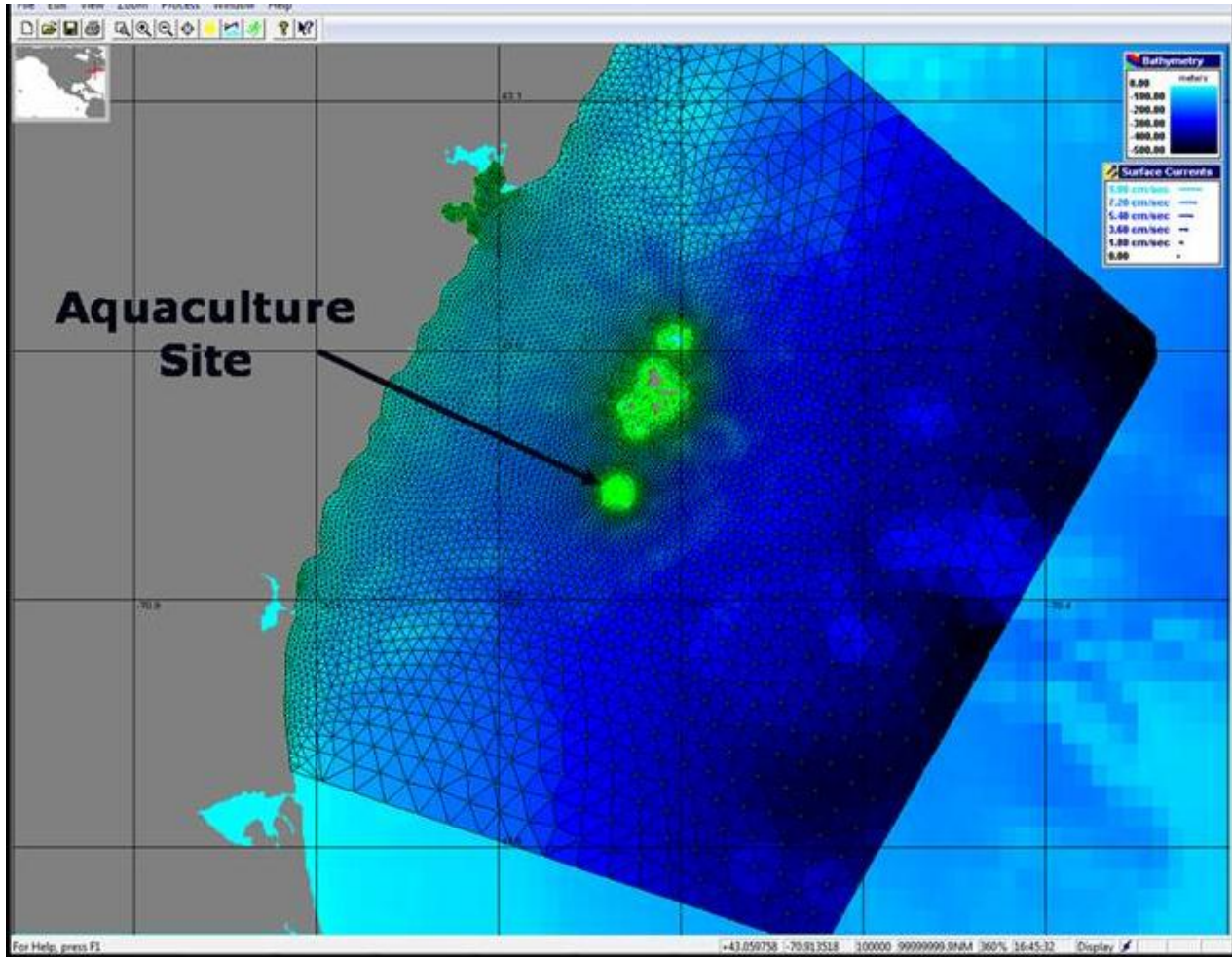
Figure 86: The coastal NH model.

6.2.3. Open Boundary Conditions

The model was forced at the open boundaries by tidal amplitudes. The initial model simulation incorporated just the M_2 (principle lunar semidiurnal constituent) component (period of 12.4206 hours). In another simulation, the model was forced with surface elevations created by two diurnal and three semi-diurnal tidal constituents – the K1, O_1, M_2, S_2, and N_2. Each node along the open boundary was given a specific set of amplitudes and phases associated with each constituent. Values were interpolated from the Eastcoast 2001, database described in Mukai et al. (2002). While the interpolated values from Mukai et al. (2002) data set, are suited for the open ocean, at the Portsmouth River open boundary, however, tidal constituents were obtained from NOAA measurements at Fort Port, NH (station ID: 8423898).

6.2.4. Model Control

To perform model simulations, the two-dimensional, depth-integrated form of ADCIRC was compiled and run from a cold start. For model control, a constant (0.0001) Corioles option and a minimum angle for tangential flow of 90° was set. In addition, finite amplitude, wetting and drying, advection and time derivative terms were applied. Wetting and drying parameters included a minimum water depth of 0.05 meters, the minimum number of dry time steps of 12, the number of re-wetting time steps of 12 and the minimum velocity for wetting of 0.02 cm/s. An iterative JCG solver type was used with an absolute convergence criterion of 10^{-5} and a maximum number of iterations per time step set at 50. Also used was a value of 0.009 for the wave continuity weighting factor and a lateral viscosity of 20.0 m^2s^{-1} (needed for model stability). In addition, a constant-hybrid bottom friction model was applied with a friction coefficient of 0.014, a break depth of 1 meter, asymptotic approach factor of 10 and friction factor increase of 1/3. Wave equation time weighting factors were set at 0.35, 0.30 and 0.35.

The model forced with the M_2 constituent was set to run for 10 days with a 5-day ramp. The model forced with five constituents was run for 25 days with a 5-day ramp. In each case, the start time was set at March 26, 2006 at 18:45:17 UTC with input nodal factors and equilibrium arguments chosen so that time series comparison of results can be made with field measurements. In addition, this time and date was chosen because, according to the field data set, the water level at the site was approximately at the mean sea level (MSL). When running ADCIRC from a cold start, it assumes water levels are at the MSL. For both simulations, the model calculations were made at a time step of 2 seconds.

6.3. Open Ocean Aquaculture Site Data

In addition to the model simulations, an extensive set of in-situ measurements were obtained at the UNH OOA site. For approximately 9 years, a moored instrumentation platform was deployed at the site. The oceanographic buoy platform was outfitted with multiple sensors collecting meteorological, wave, salinity, water temperature, tidal levels, turbidity, fluorescence, dissolved oxygen and current velocity profile data sets. A schematic of the system is shown on Figure 87. Further description of the buoy system is found in Irish et al. (2004).
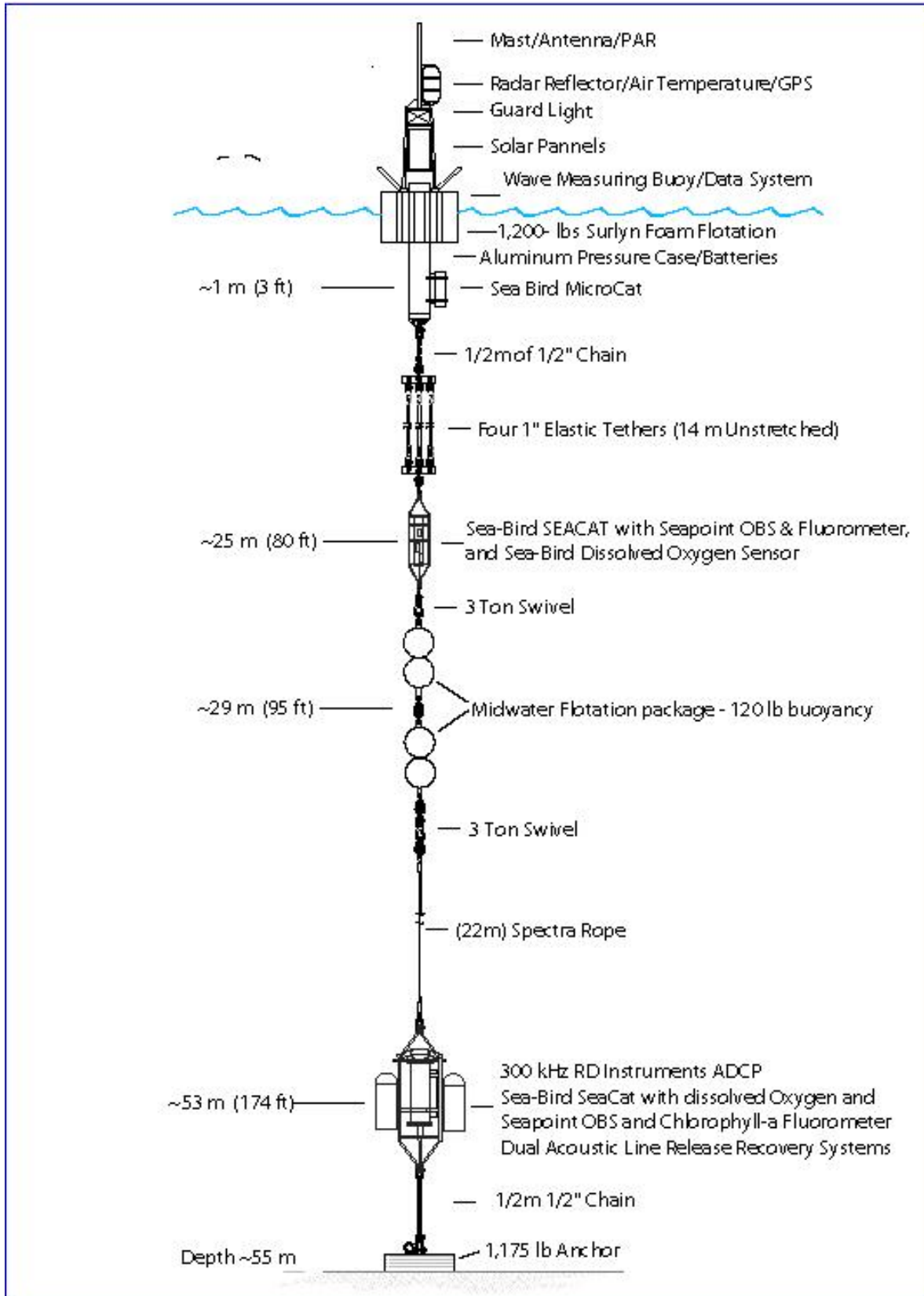
Figure 87: Schematic of the moored instrumentation system deployed at the OOA site.

Even though an extensive amount of information was obtained from the oceanographic buoy platform, only specific water elevation and current profile data sets were examined as part of the calibration of the circulation model output. Other data sets were previously discussed. One of the objectives was to find deployment data sets with minimal weather forcing components so mostly tides would be in the measurements. This was done by performing tidal harmonic analyses with the techniques described in Pawlowicz et al., (2002). With this approach, the "strength" of the most significant 35 constituents is examined with signal-to-noise (SNR) values, which allow confidence or error limits to be estimated. Low SNR values of the MSF (fortnightly) constituent indicate minimized weather effects. It was found that a data sets from March to June 2006, with a record length of 98.22 days (pressure data set), consisted mostly of tides. This data set was also one of the longest in the 9-year buoy deployment period. The water elevation data sets were obtained with a pressure sensor in a Sea-Bird Seacat mounted on the instrumentation frame near the bottom of the system (Figure 87). Current velocity data sets were collected from an upward looking Acoustic Doppler Current Profiler (ADCP) attached on the same frame. The ADCP was configured to measure 15 minute averages of velocities in the North-South (N-S), East-West (E-W) and vertical directions. Using range-gating techniques, velocities were acquired at 2-m bins from a depth of 11 to 49 meters (the moored platform was placed in 55 meters of water). The specific data sets that were analyzed for this study were acquired from March to July 2006, representing one of the longest deployments over the 9-year period.

The surface elevation data set was obtained from the pressure transducer instrument, which was started on March 28, 2006 at 23:15:17 UTC. It operated for a duration of 98.22 days collecting 9,429 observational data points at 15 minute intervals. At nearly the same time, the ADCP collected 10,650 profile data points starting on March 28, 2006 at 21:37:30 UTC, also at 15 minute intervals. In this study, the profile data set was depth-averaged. Both of these data sets were processed to obtain the K_1, O_1, M_2, S_2, and N_2 tidal constituent characteristics (amplitude and phase) using the techniques described in Pawlowicz et al. (2002). In the process, bootstrapped confidence levels were also calculated based on an uncorrelated bivariate-colored noise model (also described in Pawlowicz et al., 2002 and denoted as the "error"). The constituent amplitudes, phases and error values calculated are provided in Tables 11 and 12 for the surface elevation and ADCP data sets, respectively.

Table 11: The dominant tidal constituents obtained from elevation data set (amplitude values are in meters and phase values are in degrees). Corresponding error values are also included.

Tidal Constituent	Frequency (hr^{-1})	Amplitude (cm)	Amplitude error (cm)	Phase (deg)	Phase Error (deg)
O1	0.0387307	11.3	0.9	166.84	22.00
K1	0.0417807	14.5	1.0	193.36	3.90
N2	0.0789992	25.1	2.0	66.01	3.93
M2	0.0805114	132.3	1.8	104.58	1.03
S2	0.0833333	18.4	2.1	129.81	5.95

Table 12: Depth-Averaged tidal velocity amplitudes, phases and corresponding errors.

Constituent	Component	Amplitude $(cm\ s^{-1})$	Amplitude Error	Phase (deg)	Phase Error
O1	N-S	0.1942	0.319	253.85	115.87
	E-W	0.2609	0.410	351.00	114.22
K1	N-S	0.4420	0.399	164.50	67.72
	E-W	1.2143	0.605	338.58	29.99
N2	N-S	0.8978	0.570	331.34	33.16
	E-W	1.2039	0.479	187.51	21.45
M2	N-S	2.1650	0.484	330.62	14.0
	E-W	4.3866	0.459	216.71	5.34
S2	N-S	0.3571	0.415	21.30	72.40
	E-W	0.7063	0.448	247.77	35.46

6.4. Model Comparisons with the Measured Data

The results of the ADCIRC model simulations were then compared with data sets obtained from the ADCP at the site. The first comparison was made with just the M_2 tidal component. In the Gulf of Maine, the M_2 represents the most dominant of all constituent components (representing over 90% of the record variance), as evident in Tables 11 and 12. In the analysis, the measured M_2 tidal elevation from the OOA site was compared with the one calculated with the ADCIRC model. Time series results from the measured data sets were adjusted by using nodal factors and equilibrium arguments. Open ocean boundary input values were also adjusted with the appropriate nodal factors and equilibrium arguments. This is necessary if actual predictions are to be made with consistent temporal characteristics. The time series results are shown on Figure

88. Included on Figure 88 are the ± amplitude error values for the measured data set. As expected, the amplitude differences between the model and measured results are small. Also note on Figure 88 the 5-day ramping period applied in the model simulation and the MSL starting point for both the measured and model data sets.
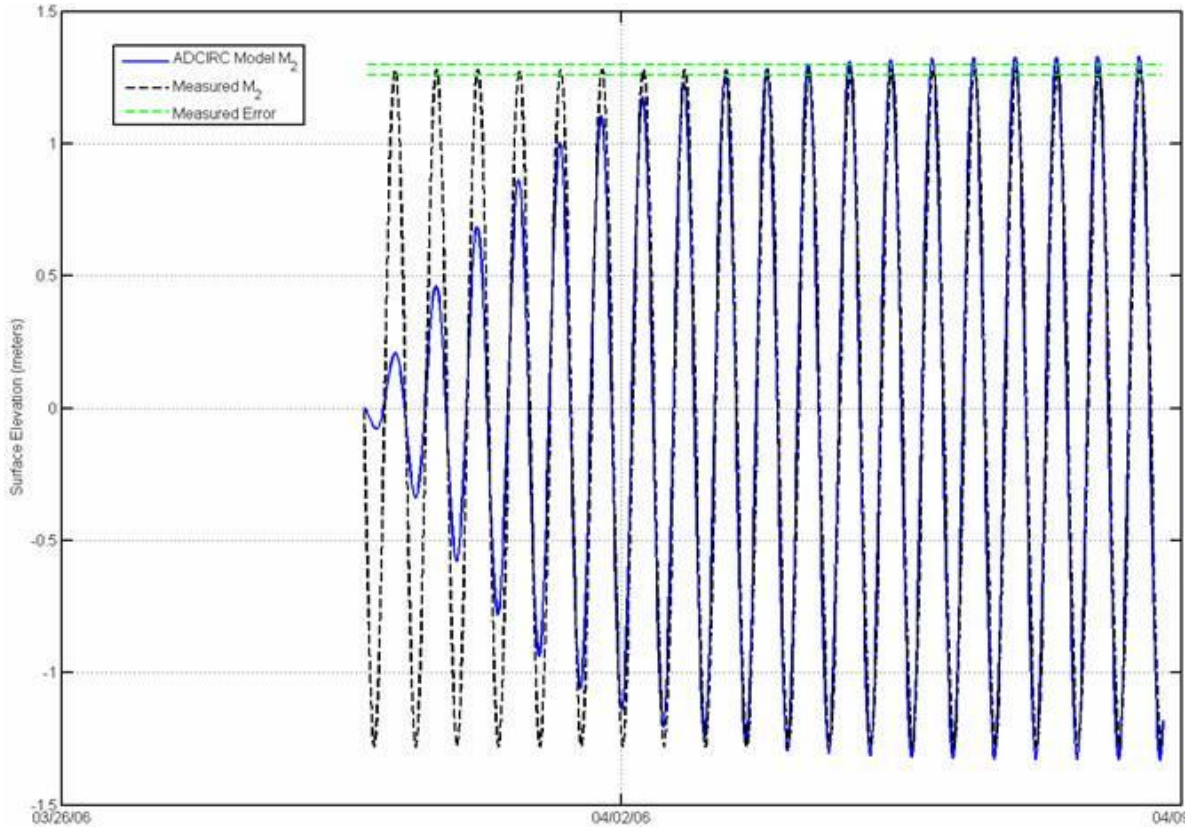

Figure 88: A comparison between the ADCIRC model M_2 surface elevation results with those measured. The dotted green line represents +/- the amplitude error value for the M_2 component as provided in Table 1.

A comparison was also made between the measured M_2 velocities. Output from the ADCIRC model yielded both X- and Y-velocity components of the M_2 tidal current. These results are shown on Figure 89. Also shown on Figure 89 are the E-W and N-S measured components from the ADCP, the +/- measured error and model 5-day ramp. Since the open ocean site elevation conditions were temporally considered, the depth averaged ADCP data also had the start date of 3/29/2006 at 18:45 UTC (from appropriate use of the nodal factors and equilibrium arguments).
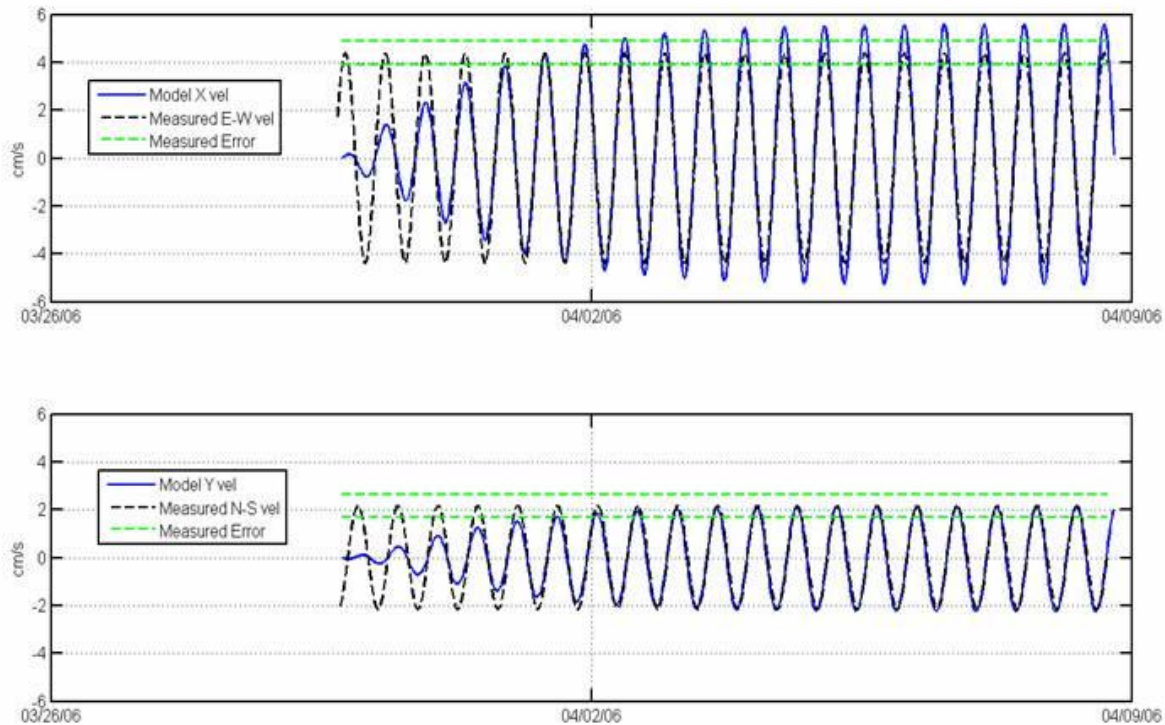
Figure 89: A comparison of model velocity results with those measured for the case of M$_2$ constituent forcing. The top panel compares the x-velocity calculated with the ADCIRC model and the measured E-W velocity component. The bottom panel compares the y-velocity calculated with the ADCIRC model with the measured N-S velocity component.

Another way to compare the relationship between the horizontal and vertical components of the tidal components is to plot them with respect to each other. For data sets from the Gulf of Maine, an M$_2$ tidal ellipse can be created and the orientation of the major and minor axes examined. The characteristics of the tidal ellipse will have implications when evaluating the dispersion of material from an aquaculture site. The direction and magnitude of the major axis will indicate the direction and magnitude of potential impact. This may also assist in the placement of nearby farms (possibly along the minor axes). However, for an M$_2$ major axis velocity of 4.4 cm s^{-1}, the horizontal displacement of the tidal ellipse is only 0.62 km.

Tidal ellipses of both the measured and model results were then created by plotting y-component vs. the x-components. Both the model and measured results are shown on Figure 90. The orientation and the minor axes are nearly identical. Only the major axis produced by the model was slightly larger. Having magnitude differences on the scale of about 1 cm s^{-1}, shows that the model has a reasonable potential for predicting tidal currents, especially since the spatial resolution of the model domain at the OOA site is approximately 50 meters.
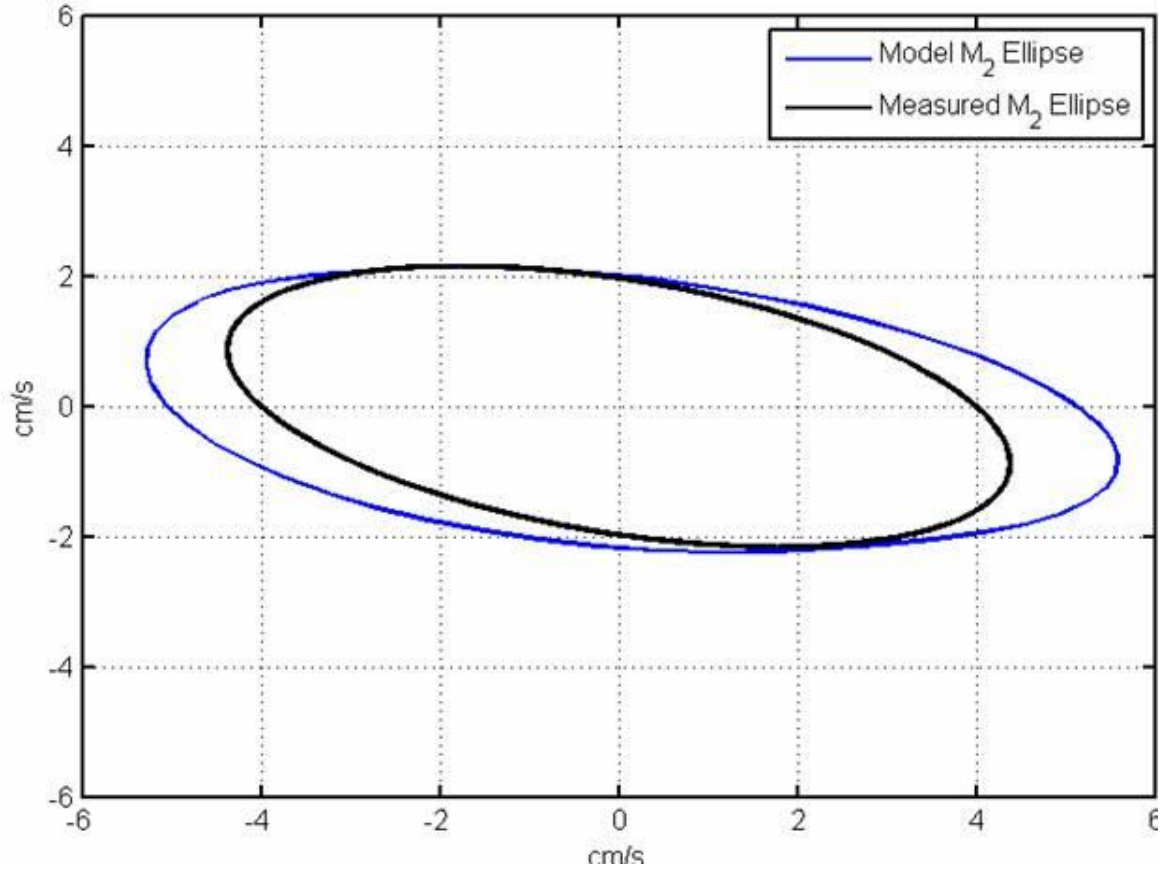
Figure 90: M$_2$ tidal ellipse comparison showing the Y and N-S velocities on the vertical axis and the X and E-W velocities on the horizontal axis.

Once the M$_2$ component of the tide (elevation and velocity) was modeled with a certain degree of confidence, the model was configured to run with the K$_1$, O$_1$, M$_2$, S$_2$, and N$_2$ tidal constituents. With the use of the appropriate nodal factors and equilibrium arguments, the surface elevation was predicted for a duration of 20 days. The model and measured results are shown on Figure 91. The variance of the model simulation and measured data sets were calculated to be 0.7911 (cm)^2 and 0.7472 (cm)^2, respectively.

The surface elevation at the OOA site was modeled reasonably well. The next step was to calculate, with the ADCIRC model, the X- and Y-velocities associated with the East- and North-going measured velocities. The time series results are shown on Figure 92. The corresponding X- and Y- model variances were 12.68 (cm s^{-1})^2 and 2.25 (cm s^{-1})^2. While the measured E-W and N-W variances were 9.27 (cm s^{-1})^2 and 2.33 (cm s^{-1})^2. With tidal harmonic analysis techniques, the amplitudes and phases for each of the 5 constituents were estimated for both measured and model results and provided in Table 13.
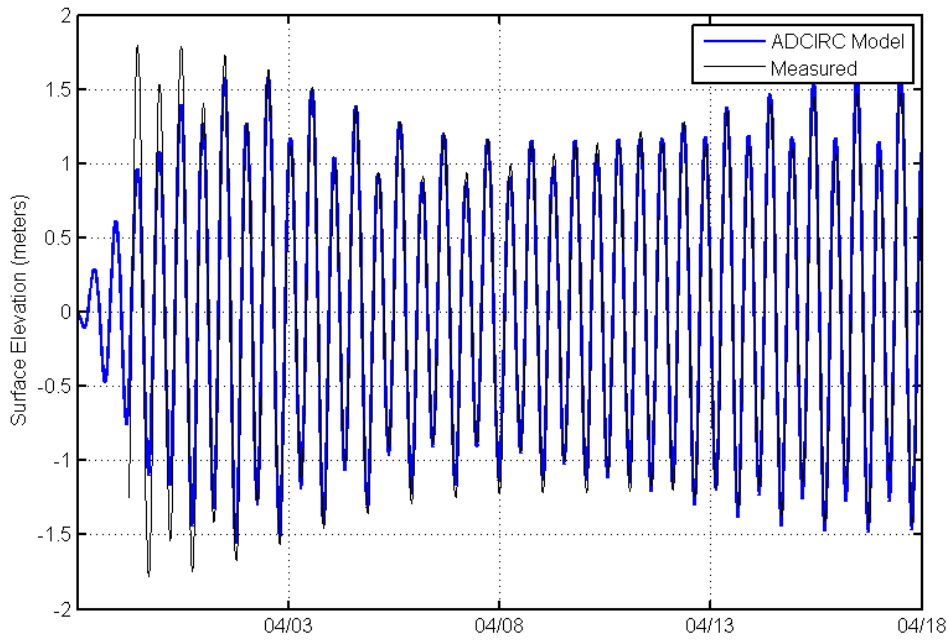
Figure 91: ADCIRC model surface elevation comparison with the measured values incorporating just the K1, O₁, M₂, S₂, and N₂ tidal constituents.
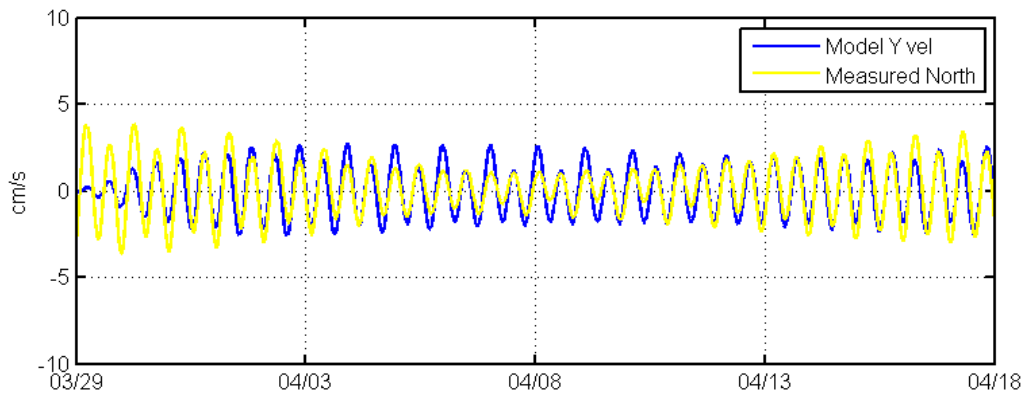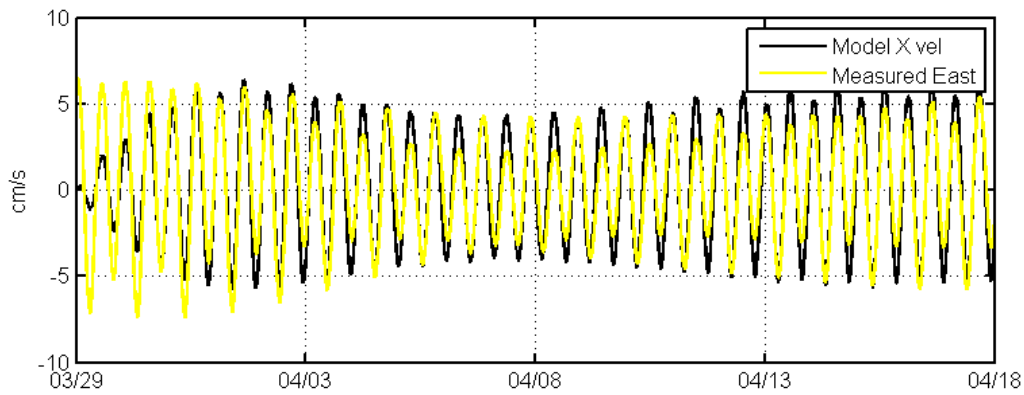

Figure 92: ADCIRC model velocity comparison with the measured values incorporating just the K1, O₁, M₂, S₂, and N₂ tidal constituents.

Table 13: Depth-averaged tidal velocity amplitudes, phases and corresponding errors.

Constituent	Component	Amplitude (cm s^{-1})	Amplitude Error	Model (cm s^{-1})	Phase (deg)	Phase Error	Model Phase (deg)
O1	N-S	0.1942	0.319	0.2268	253.85	115.87	329.62
	E-W	0.2609	0.410	0.1903	351.00	114.22	357.55
K1	N-S	0.4420	0.399	0.3554	164.50	67.72	40.88
	E-W	1.2143	0.605	0.1339	338.58	29.99	0.018
N2	N-S	0.8978	0.570	-	331.34	33.16	-
	E-W	1.2039	0.479	-	187.51	21.45	-
M2	N-S	2.1650	0.484	2.0930	330.62	14.0	321.39
	E-W	4.3866	0.459	5.2202	216.71	5.34	213.44
S2	N-S	0.3571	0.415	0.1653	21.30	72.40	329.16
	E-W	0.7063	0.448	0.8060	247.77	35.46	253.69

6.5. Summary

This section describes the circulation modeling procedure, the field data processing techniques and presents a comparison between model and measured results at the Gulf of Maine open ocean aquaculture site. Results are remarkably similar showing that the model has promise as a predictor of current that will transport aquaculture wastes from the site. The next step will be to use the hydrodynamic model output as input to the AquaModel. With the use of accurate low-flow current information and fish farm waste parameters, the suite of modeling tools will be able to quantify waste concentrations at the site and changes over time.

6.6. Section References

Fredriksson, D.W., J. DeCew, M.R. Swift, I. Tsukrov, M.D. Chambers, and B. Celikkol. (2004). The design and analysis of a four-cage grid mooring for open ocean aquaculture. Aquacult. Eng. Vol. 32, pp 95-111.

Irish, J.D., D.W. Fredriksson and Boduch, S. (2004). Environmental monitoring buoy and mooring with telemetry. Sea Tech. May 2004. pp 14-19.

Luettich, R.A., J.J. Westernink and N.W. Scheffner (1992). "ADCIRC: An advanced three-dimensional circulation model for shelves, coasts and estuaries, Report 1: Theory and Methodology of ACIRC-2DDI and ADCIRC-3DL." Technical Report DRP-92-6, U.S. Army Corps of Engineers Waterways Experimental Station, Vicksburg, MS 137 p.

Lynch, D.R., and C.E. Namie (1993). The M2 tide and its residual on the outer banks of the Gulf of Maine. J. Phys. Ocean. Vol. 23, No. 10, pp. 2222-2253.

Mukai, A.Y., Westerink, J.J., Luettich, Jr., R.A., and D. Mark (2002). Eastcoast 2001, A tidal constituent database for the Western North Atlantic, Gulf of Mexico and Carribbean Sea. U.S. Army Corps of Engineers. ERD/CHL, TR-02-24.

Pawlowicz, R, B. Beardsley, and S. Lentz. (2002). "Classical tidal harmonic analysis including error estimates in MATLAB using T_TIDE", Computers and Geosciences 28, 929-937.

7. Regional AquaModel Simulations of Aquaculture Sites in the Gulf of Maine

7.1. Overview

As described in previous sections, the intent of performing the local AquaModel simulations was to examine possible benthic impacts in response to "commercial" level fish farm operations. Calculations were made with both 12- and 24-cage fish farms. The objective of the regional simulations, on the other hand, was to investigate the influence of multiple farms upon water column parameters including dissolved oxygen and nitrogen. We address the question: could perhaps a regional effect be generated within the coastal waters with 8 large fish farms? For the two sets of regional simulations, the initial biomass conditions for each of the eight farms were set the same as the previous single farm local simulations. For instance, the 12-cage farm was setup with a containment volume having the dimensions of 50 m x 50 m x 15 m. Therefore, the total farm containment volume for the regional simulations was set at 12-times the net pen volume having the dimensions of 100 m x 300 m x 15 m. Likewise, for the 24-cage farm, the containment volume was twice that of the 12-cage farm and therefore had the dimensions of 200 m x 300 m x 15 m. For both the regional model simulations, the eight individual farms were arranged in the Southwest portion of the Gulf of Maine in a North-South orientation. The locations are shown on in the AquaModel screen-print as large blue dots on Figure 93. The Figure also shows the circulation model domain developed as described in the previous section. The UNH site is of particular interest because many of the results presented in this section are from this location.

One of the main differences between the near- and far-field simulation setup is the depth of the cage/farm (which is modeled as a point source). In the near-field simulations, the waste source (center of the cage/farm) was placed at a depth of 15 meters. This was chosen because the benthic impact of the near-field simulations was the focus of the results. The depth of the farm for the far-field simulations was set at 5 meters. This location was chosen because the fate of the dissolved wastes (e.g. nitrogen) through dispersion/diffusion and advection was the focus of the results. This could then be compared to the ambient DIN values.
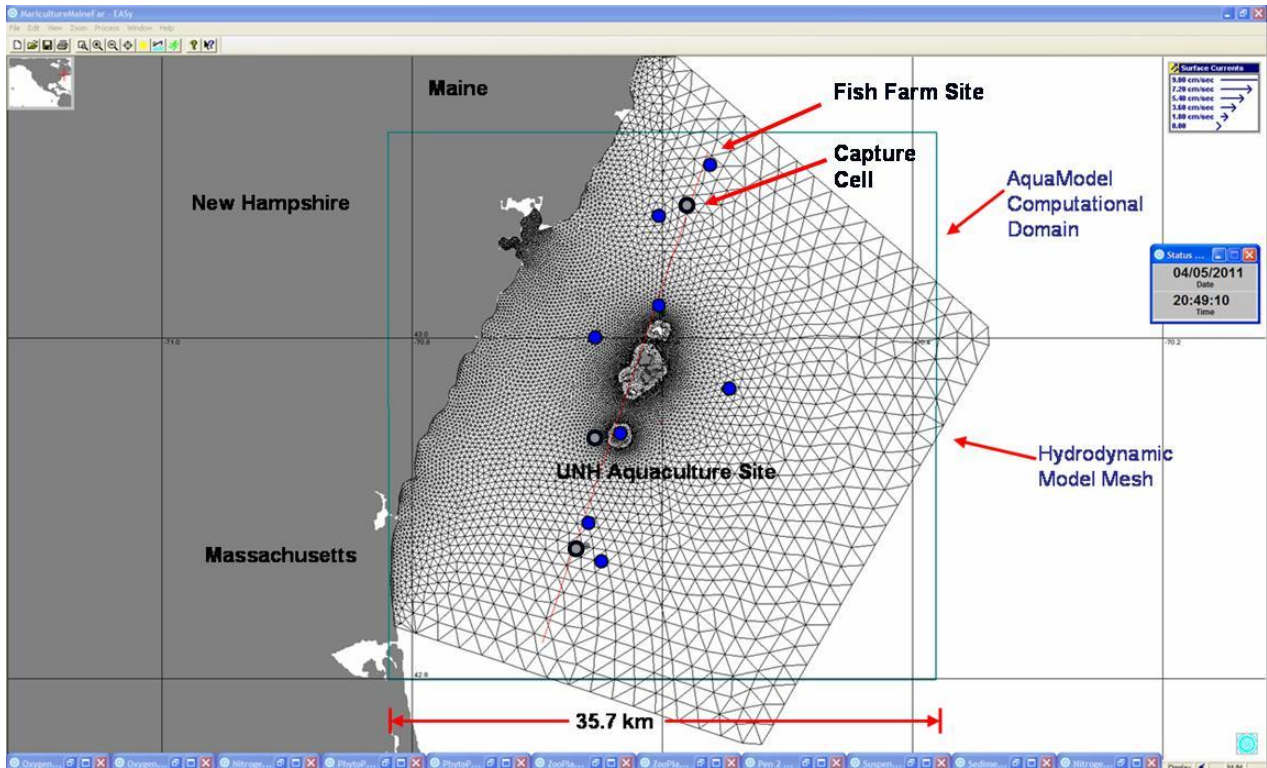
Figure 93: The locations of each farm site and capture cells configured for the regional AquaModel simulations.

7.2. Input Model Conditions

7.2.1. Domain Configuration

The far-field domain configuration in AquaModel was built to encompass the entire coastline of New Hampshire including the Isle of Shoals having the square dimensions of 35.7 km by 35.7 km. The domain incorporated a three-dimensional array of cells (51 x 51 x 4) each having the dimensions of 700 m x 700 m x 10 m. The outline of the AquaModel computational domain is also shown on Figure 93. Within the AquaModel program, the dissolved wastes are treated as a point source, which immediately becomes mixed within encompassing model cell. The user provides the latitude, longitude, and depth of the point source. In this case, the "farm" was placed near the surface so the point source was set at 5 meters. The capture cells, also shown on Figure 93, are then used to collect data from the chosen locations. In all three locations, the capture cell was set at the position closest to the surface.

7.2.2. Ambient Environmental Conditions

The same environmental conditions were used for the regional AquaModel simulations and were organized as hourly, daily and weekly data sets. The hourly data sets consisted of current velocity (cm s^{-1}) and direction (degrees) and wind speed (m s^{-1}). Note that the wind speed value is factored into the dissolved oxygen calculation. The daily data set consisted of irradiance in moles of photons/m^2/day. The weekly data sets consisted of temperature (degrees C), oxygen (g m^{-3}), nitrogen (mg m^{-3}), phytoplankton (mg of N m^{-3}), and zooplankton (mg of N m^{-3}) each at the depths of 1, 25 and 53 meters. The weekly data set also included the mixed layer depth, which determines the appropriate diffusion coefficient used during periods of the year when stratification exists. The simulations were started on April 1, 2009 and set to run until July 1, 2010, though the year is arbitrary.

7.2.3. Hydrodynamic Conditions

The only environmental condition that was different for the regional simulations were the current velocities. Since the tidal circulation patterns vary regionally throughout the domain, single point measurements were not used because they do not accurately represent the velocities at each of the farm sites. Therefore, the validated ADCIRC circulation model results were incorporated into the AquaModel program.

Within the program, the ADCIRC data is interpolated spatially and temporally for each of the model array cells. Since the ADCIRC regional velocity is depth averaged, the same velocity is applied at each depth. Depth variations at three vertical locations are represented by the residual data set processed from the ADCP records. The residual data set contains ADCP velocity vectors with the tidal component removed since it is regional represented by the ADCIRC model results. The leftover portion includes storm and density driven parts. Values at three depths including z = -11, -25 and -47 meters are incorporated in the simulation. This data set is also spatially (horizontally and vertically) and temporally interpolated to the AquaModel array cell configuration and then superimposed with the depth averaged, but regionally varying ADCIRC values. This effectively produced a 2-dimensional, 3-space, regionally velocity field for moving wastes. This approach is most likely reasonable in the deeper waters of the domain, but breaks down in shallower areas, especially near the coastline.

7.3. *AquaModel Far-field Results for the Gulf of Maine*

With the entire suite of environmental conditions and input model parameters (including the coastal circulation patterns), the regional AquaModel simulations were performed for both the 12- and 24-cage farm configurations. The growth rate, biomass and dissolved oxygen results are shown on Figures 94 and 95 and are presented for each farm configuration, but specifically for the UNH site (though the results for the other 7 farm locations are also available). Both the growth rates and DO calculated for the regional calculations were similar to those shown on Figures 63 and 64 (at the UNH site). From the far-field simulations, the fish "harvest" sizes were calculated to be 5.9 and 5.7 kg for the 12- and 24-cage configurations respectively. Recall that the previous near-field results produced values of 5.4 and 5.16 for each of the cage configurations. This increase in calculated growth is most likely due to the higher levels of dissolved oxygen near the surface, especially due to the incorporation of wind stress in the DO portion of the model. Recall that in the far-field simulations, the contained biomass was placed near the surface at a depth of 5 meters, while in the near-field simulations, the fish cages were placed at a depth of 15 meters.
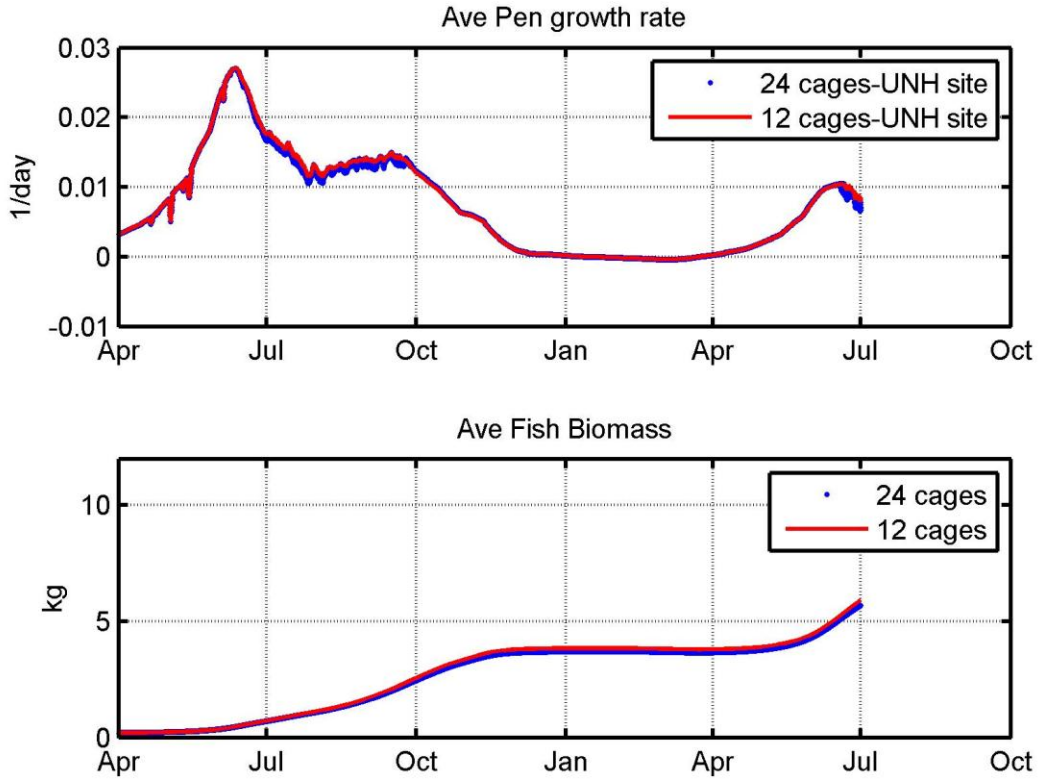
Figure 94: (Top) Comparison of the average pen growth-rate between the 24 and 12 cage farms. (Bottom) Comparison of the average fish biomass between the 24 and 12 cage farms.
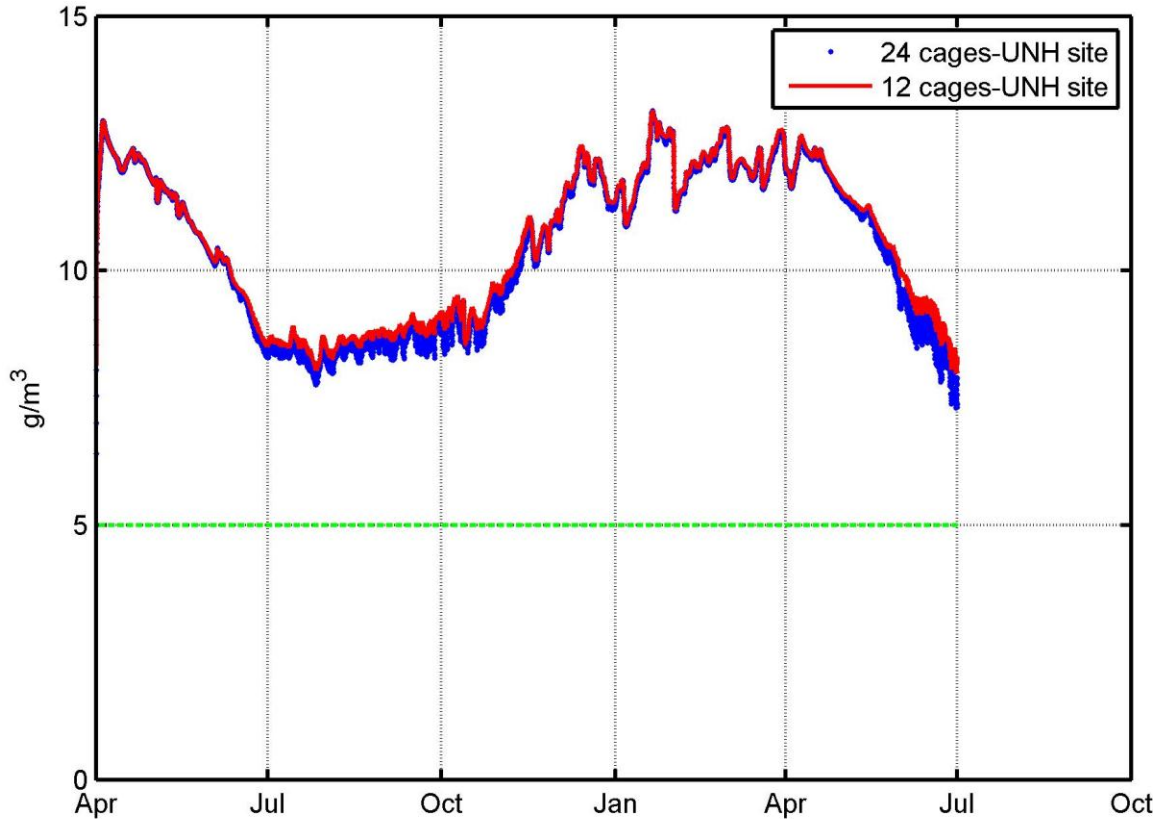
Figure 95 Comparison of the dissolved oxygen level at the UNH farm site between the 24 and 12 cage farms.

The next 5 plots show the dissolved inorganic nitrogen within the region with surface values from each at the farm sites (though data is available for other depths). The plots also provide the input DIN from the open boundaries from the ambient data sets. The surface DIN distribution results were taken during months 7 and 8 (October and November) of the far-field simulations.

The first snapshot is from 10/26/2009 (Figure 96) when the ambient DIN values were 5.25 μM, along with values north and south of the UNH site. Figure 97 shows the results 2 days later on 10/28/2009 where a clear nitrogen signal is coming from each of the farm sites. The same is shown on Figure 98 and 99 for 10/30/2009 and 11/01/2009, respectively. Over the next week, however, the ambient conditions and the dynamics of the coastal region change considerably. Higher ambient DIN concentrations move throughout the domain influencing the concentrations at the farm sites regardless of what is being produced by the biomass (Figure 100).
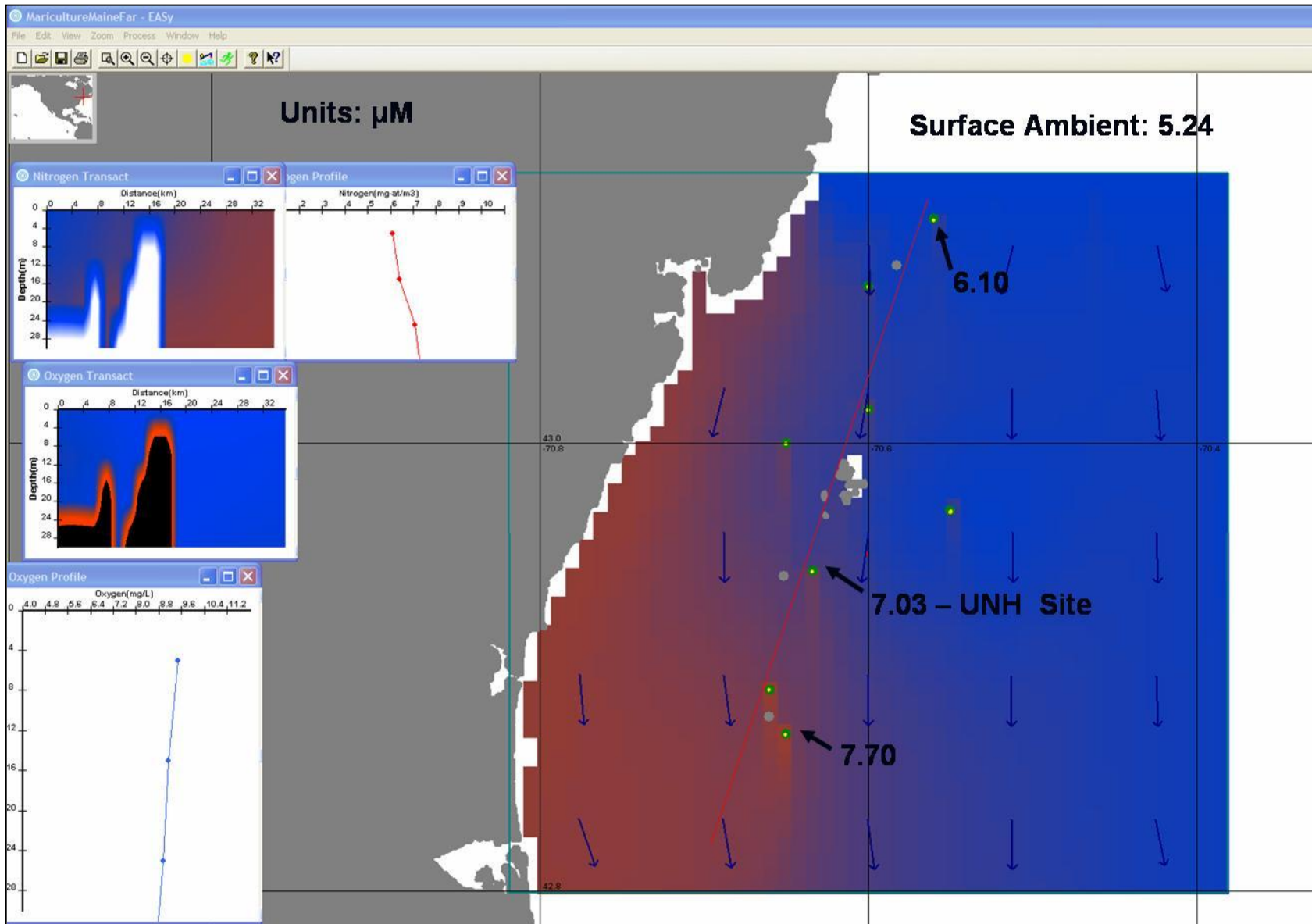
Figure 96: Surface nitrogen concentration at each of the farms sites compared with the ambient surface values (10/26).
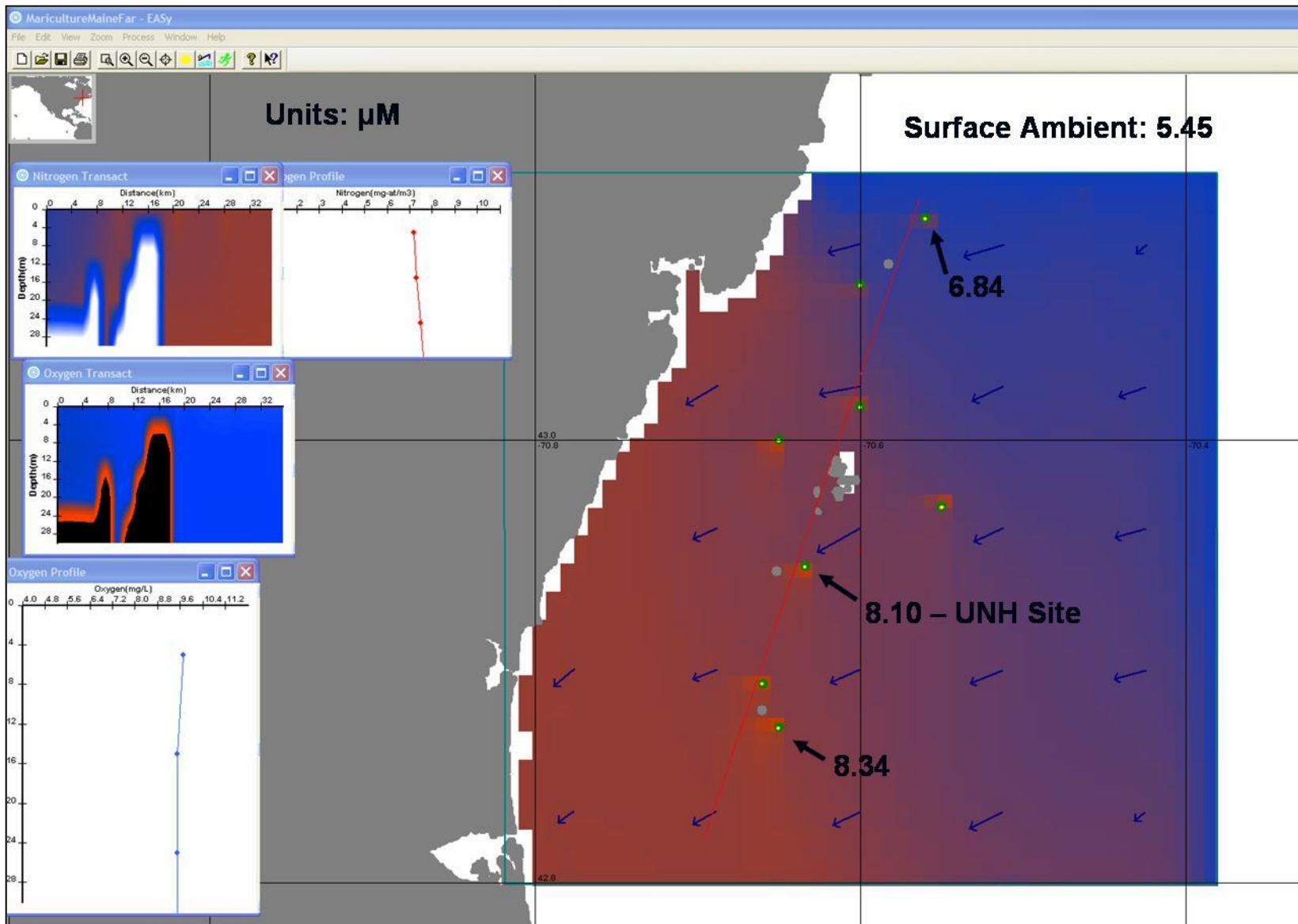
Figure 97: Surface nitrogen concentration at each of the farms sites compared with the ambient surface values (10/28).
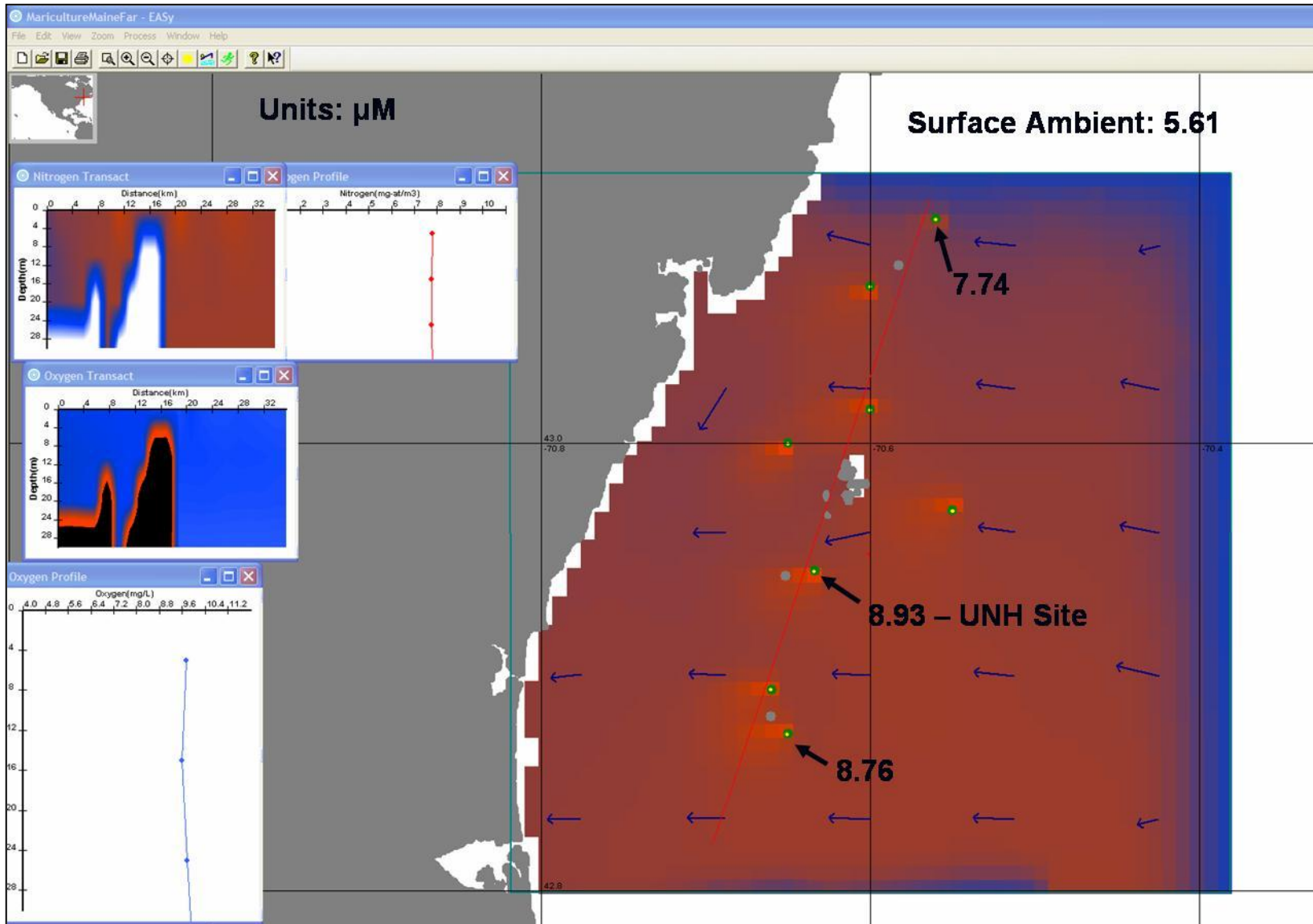
Figure 98: Surface nitrogen concentration at each of the farms sites compared with the ambient surface values (10/30).
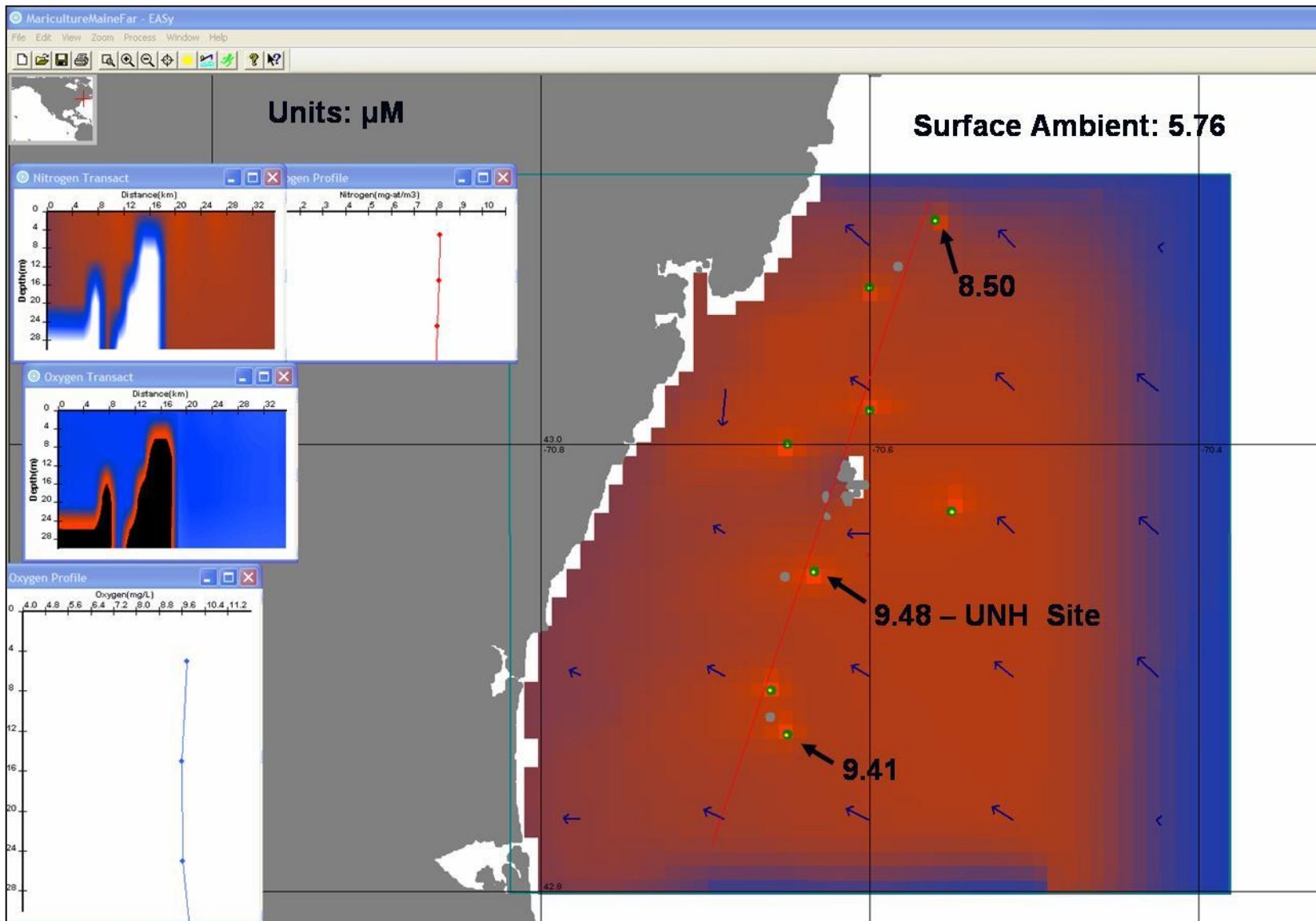
Figure 99: Surface nitrogen concentration at each of the farms sites compared with the ambient surface values (11/01).
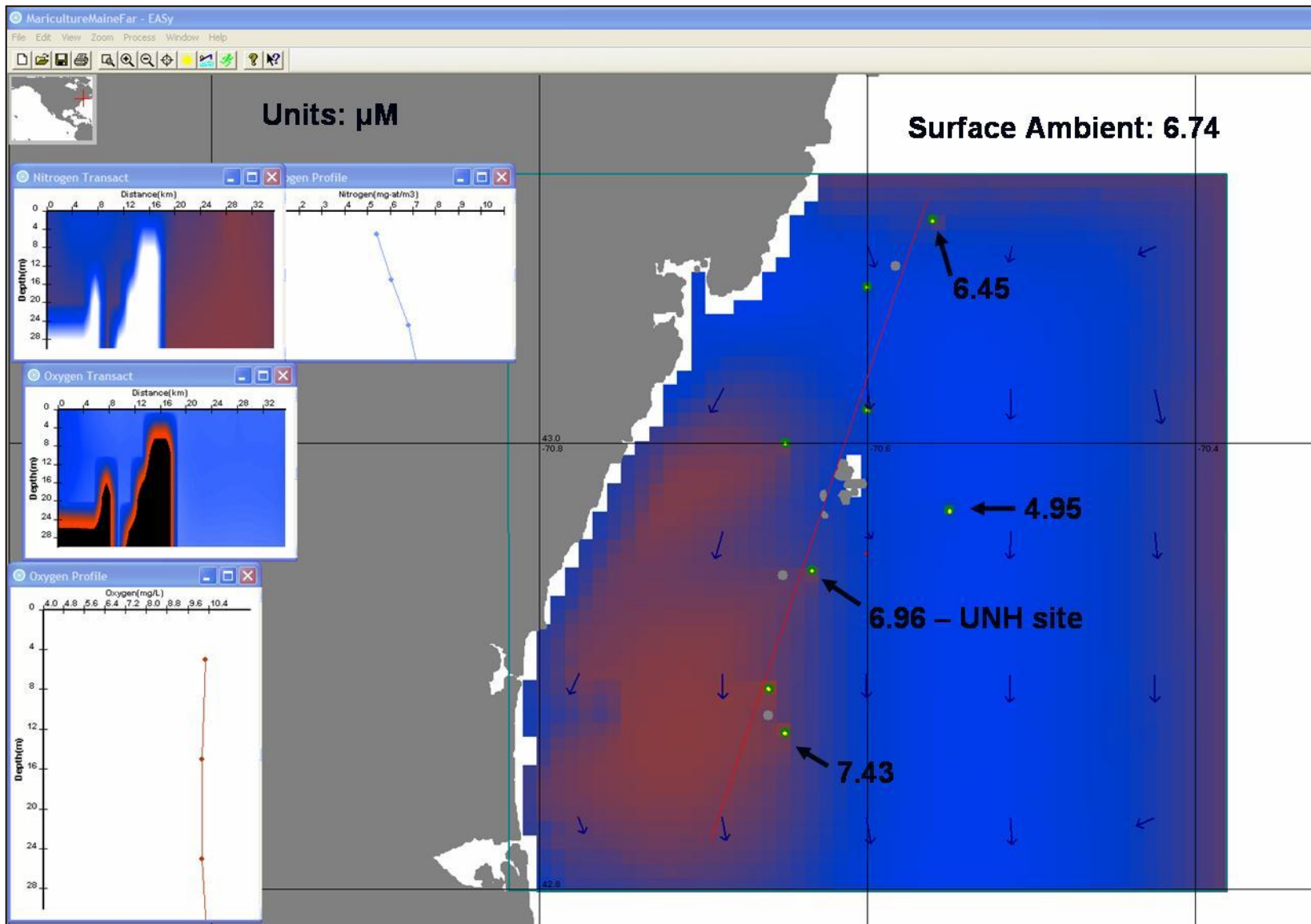
Figure 100: Surface nitrogen concentration at each of the farms sites compared with the ambient surface values (11/08).

7.4. Summary

The results of the regional AquaModel simulations, though not perfect, can provide powerful insight concerning the decision making processes of the coastal ocean where fish farming activities are proposed. Even though the nitrogen-phytoplankton-zooplankton (NPZ) results presented here need to be validated, the influence of one or more fish farms can be potentially quantified. It can be quantified with various levels of biomass and ambient conditions so that water column and benthic impacts can ACTUALLY be estimated. A tool like this is absolutely necessary to put numbers in places where most are only putting words.

8. Output of the Project and Outreach Plan

8.1. Presentations at the Spring World Aquaculture Society Meeting in San Diego, March 2010

To demonstrate to the aquaculture community the abilities of AquaModel to show the effects of an aquaculture operation on the environment, and to illustrate what has been done during the past year on modeling the UNH OOA site, presentations were made at the 2010 World Aquaculture Association meeting in San Diego. Dale Kiefer introduced AquaModel, discussed the benthic portion of the model and showed some model run results using currents and ambient conditions later discussed by Dave Fredriksson and Jim Irish. Jim Irish showed the average environmental conditions at the site collected over several years, including the temperature, oxygen and nitrate data input to AquaModel. He also discussed the observed current field. Dave Fredriksson presented the physical modeling results of the tidal currents in the region of the UNH OOA site illustrating the variations in tidal currents in the region. The AquaModel presentations received interest from the community.

- Irish, J.D., D. Fredriksson, D. Keifer, J. Rensel, F. O'Brien, 2010. Environmental Observations in support of Physical and Biological Modeling of Aquaculture Sites, Presented at the World Aquaculture Society meeting in San Diego, March.
- Fredriksson D., J. Irish, D. Keifer, J. Rensel, F. O'Brien, 2010. A Circulation Model to Investigate the Movement of Wastes from an Open Ocean Aquaculture site, Presented at the World Aquaculture Society meeting in San Diego, March.
- Modeling Offshore Fish Farms in New Hampshire and Hawaii, Kiefer et al.
- Bioenergetics of cobia and moi fish: Applications to offshore culture and modeling. Rensel et. al.

8.2. Presentations at the Aquaculture Association of Canada Annual Conference in Quebec City, May 2011.

- Rensel, J. (2011). Invited Plenary Session: Changing the adverse impacts into beneficial effects: Enrichment or west coast freshwater and marine aquaculture food webs with aquaculture wastes. Presented at the Aquaculture Association of Canada meeting in Quebec City, May.
- Fredriksson D., J. Irish, D. Keifer, J. Rensel, F. O'Brien, 2011. AquaModel software application to understand the regional effects of multiple marine fish farms in the Gulf of Maine, USA . Presented at the Aquaculture Association of Canada meeting in Quebec City, May.

8.3. Development of undergraduate course material at the U.S. Naval Academy

As part of the outreach plan to involve undergraduate students, Associate Professor David Fredriksson developed and conducted a senior level engineering course elective with a focus on Marine Aquaculture (see attached course schedule). The course was conducted at the U.S. Naval Academy during the Spring semester of 2010. As part of the course, he introduced topics related to the environmental aspects of marine aquaculture (see week 10 of the course schedule). After presenting the introductory material, he invited Professor Dale Kiefer to provide comprehensive detail on the bio-energetic characteristics of biomass within a fish farm, the corresponding waste products the possible fate of the waste products (see week 13 of the course schedule). He then presented a thorough description of the AquaModel and its components.

8.4. Dedicated internet web site

In addition to the outreach mentioned above, a dedicated web site describing the finding s of this project and details of AquaModel has been prepared and posted at www.noaa.aquamodel.net. More details on this are listed below in the Appendix to this report.

EN486D – Marine Aquaculture Engineering
Spring 2010 Outline
Updated 28 Dec 2009

Dates	Lesson #	Topic(s)
Week 1 Jan 13- 15	1 (Wed)	Introduction to Marine Aquaculture Engineering
	Lab #1 (Thurs)	**Movie: Modern Marvels, Commercial Fishing (Introduces the need for aquaculture)**
	2 (Fri)	Wave Theory Review
Week 2 Jan 19 - 22	3 (Wed)	Wave Theory Review
	Lab #2 (Thurs)	**Development of a Design Wave Condition using Excel**
	4 (Fri)	Review of Wave Parameter Calculations and Model Test Setup
Week 3 Jan 25- 29	5 (Wed)	Review of Wave and Current Forces (Morison Equation)
	Lab #3 (Thurs)	**Fish Cage Tow Test Experiment**
	6 (Fri)	Towing Test Data Processing with Excel (curve fitting)
Week 4 Feb 1 - 5	7 (Wed)	Physical Modeling of Aquaculture Systems
	Lab #4 (Thurs)	**Towing Fish Cage Models in Waves**
	8 (Fri)	Scaling Model Data for Design Purposes
Week 5 Feb 8 - 12	9 (Wed)	Heave Response Characteristics (the "Free Release Test")
	Lab #5 (Thurs)	**Performing the Free Release Test**
	10 (Fri)	Free Release Test Data Processing with Excel
Week 6 Feb 15 - 19	11 (Wed)	Exam #1 Review
	Lab #6 (Thurs)	**Exam #1**
	12 (Fri)	Mooring System Design Overview
Week 7 Feb 22 - 26	13 (Wed)	Fish Farm Mooring Buoy Hydrostatics, Catenary Equations Overview
	Lab #7 (Thurs)	**Mooring System Physical Modeling and Tests**
	14 (Fri)	Mooring System Design with Chain Catenaries
Week 8 Mar 1- 5	15 (Wed)	Oyster Aquaculture – Growth Rate Studies (Assoc. Prof. Steppe)
	Lab #8 (Thurs)	**Oyster Aquaculture – Growth Rate Studies (Assoc. Prof. Steppe)**
	16 (Fri)	Oyster Aquaculture – Growth Rate Studies (Assoc. Prof. Steppe)

Week 9 Mar 8 - 12	17 (Wed)	Oyster Measurement Study
	Lab #9 (Thurs)	**Oyster Surface Cage Construction**
	18	Oyster Surface Cage Construction
SPRING BREAK		
Week 10 Mar 22-26	19 (Wed)	Environmental Aspects of Finfish Aquaculture
	21 (Thurs)	Food and Fecal Waste Production, Soluble Wastes, Settling, Decay
	Lab #10 (Fri)	**Environmental Impact Calculations with Excel**
Week 11 Mar 29– Apr 2	22 (Wed)	Exam #2 Review
	Lab #11 (Thurs)	**Exam #2**
	23 (Fri)	Oyster Measurement Study
Week 12 Apr 5-9	24 (Wed)	Economic Aspects of Aquaculture
	Lab #12 (Thurs)	**University of MD – Horn Pt. / Choptank Oyster Co.**
	25 (Fri)	Cash Flow Analysis, Internal Rate of Return
Week 13 Apr 12-16	26 (Wed)	Bio-Energetics – Prof. Dale Kiefer (University of Southern California)
	Lab #13 (Thurs)	Bio-Energetics – Prof. Dale Kiefer (University of Southern California)
	27 (Fri)	Bio-Energetics – Prof. Dale Kiefer (University of Southern California)
Week 14 Apr 19-23	28 (Wed)	Introduction to Closed Containment Aquaculture
	Lab #14 (Thurs)	**University of MD – Baltimore City**
	29 (Fri)	Oyster Measurement Study
Week 15 Apr 26- 30	30 (Wed)	Technical Paper Presentations
	31 (Thurs)	Technical Paper Presentations
	34 (Fri)	Technical Paper Presentations
Week 16 May 3-4	35	*Final Exam Review*

APPENDIX: AquaModel Software Improvements

Overview

The development of open ocean marine aquaculture (mariculture) farms within the United States Exclusive Economic Zone (EEZ) offers the promise of profitable commercialization with low risk to the environment and wild fish stocks. With support from the *National Oceanic and Atmospheric Administration* (*NOAA*), we have helped to advance this industry by completing development of AquaModel, software that accurately predicts the environmental impacts and operations of fish farms both onshore and in the open ocean. AquaModel assists both the industry and government to predict and meet proposed rules or performance standards and to provide quick access to information needed for permitting and planning. AquaModel provides a home for data, the tools to visualize and communicate this information, and a comprehensive model to simulate operations and environmental impact of operations. Presently, there are no other comprehensive software systems to accomplish all these tasks.

The updated version of AquaModel provides mapping and modeling tools that are required by regulators and farm operators to manage sustainable mariculture development in coastal and offshore waters. During this project we have focused on three major objectives:

- To develop AquaModel' s capacity to assess regional concerns of multiple farm placement and environmental impact by developing an interface between AquaModel and commonly used 3-dimensional coastal circulation models. In this context, benthic effects are mostly or all near field, water column effects are near to far field in extent. The development of integrated GIS-modeling techniques enhances the ability of applicants to evaluate sites and the ability of government to conduct rational management.

- To demonstrate the utility of the enhanced model by running multiple simulations under differing environmental conditions and farm operations for two farms in regions where the oceanographic conditions are well known but differ greatly. These included the experimental University of New Hampshire's fish farm and at a generic location(s) in the Southern California Bight for marine finfish in coordination with HUBBS-SeaWorld Research Institute (HSWRI).

- To conduct sensitivity analyses of the multiple simulations of the two regions to determine what environmental and operational parameters are most important in determining ecologically safe and economically profitable operations. This task will AquaModel's GIS-based system that allows for a decision support system . This decision

support system was demonstrated and focused on linking our GIS to data available from the regional ocean observing systems of the Gulf of Maine (GOMOOS) and Southern California (SCOOS).

The program improvements to the AquaModel are described below.

AquaModel Software Accomplishments

During this project we distributed the integrated AquaModel software to all study participants and verified execution of the completed AquaModel projects. We enhanced AquaModel to utilize time series measurements of ocean data including: measured ocean currents, ocean temperature, mixed layer depth, irradiance, wind speed, and ambient nitrogen, oxygen, phytoplankton, and zooplankton. We coupled AquaModel with output from the JPL (Jet Propulsion Lab) 3-D Regional Ocean Modeling System (ROMS) circulation model for the Southern California Bight region. We also integrated AquaModel with the ROMS Hawaii tidal model as well as with data from the ECCO2 3-D circulation model.

We reconfigured AquaModel to utilize current data from the ADCIRC circulation model being used for the Gulf of Maine aquaculture simulation project. AquaModel reads and displays the 3-D circulation data and utilizes the current field along with imported bathymetry to simulate the distribution of dissolved materials (e.g. oxygen and nitrogen) and of particulate waste products (e.g. feed and fecal material). In the simulation mode AquaModel displays water currents at any depth along with the distribution of dissolved and waste materials as they change over time. Figure 101 shows an AquaModel display of the 3-D current data grid generated by the ADCIRC circulation model.

To evaluate the effect of tidal currents, we enhanced AquaModel to calculate and display tidal ellipses and associated data. The red ellipses in Figure 102 show subtle variations in tidal currents over the geographic area of interest. The small blue dots in an ellipse shape represent the location of current vectors over the previous 12 hour tidal period. The heavy blue dots are the center of gravity (CG) of consecutive 12 hour tidal periods. In simulation mode AquaModel allows the user to visualize temporal variations of tidal currents in this manner.
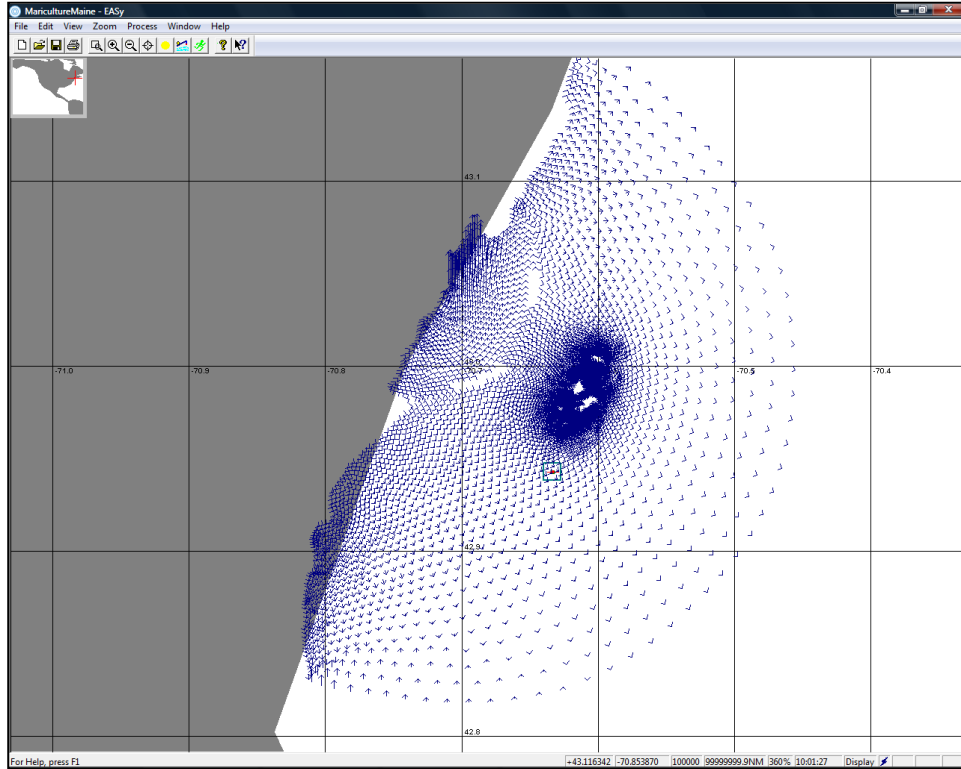
Figure 101: Current vectors created by the 3-D ADCIRC model are used to determine the distribution of dissolved and particulate wastes in the water column and along the sea bottom.
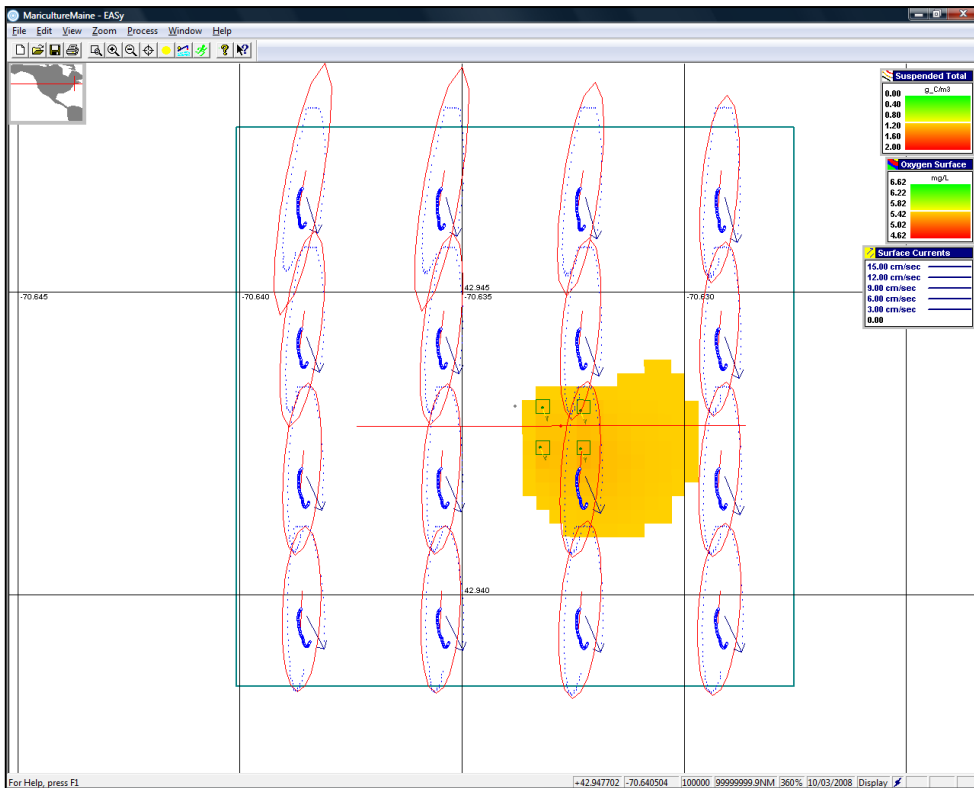

Figure 102: Tidal ellipses calculated and displayed by AquaModel show subtle variations in tidal

currents.

We created a project web site to make the results of this study available to researchers, licensing agencies, and commercial entities: www.noaa.aquamodel.net.   Figure 103 shows the web site home page. This site provides a full description of the project including internet access to the AquaModel simulation in three versions: NetViewer, GoogleMaps, and GoogleEarth. The NetViewer provides the most flexible user interface. We have recently upgraded the NetViewer to run on any of the six most popular browsers: IE, FireFox, Opera, Safari, Netscape, and Google Chrome (the previous version depended on the Java Virtual Machine which is not consistently supported by all of the popular browsers).
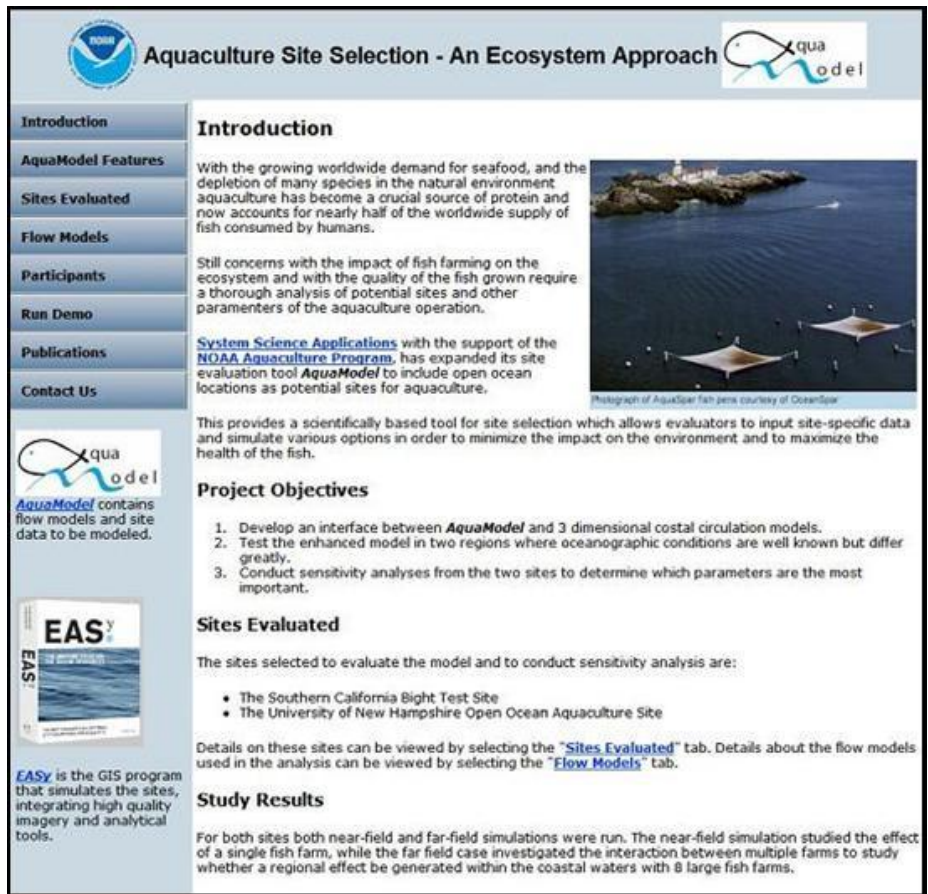
Figure 103: The project web site present project results and working AquaModel simulations.

Figure 104 shows an example of the Gulf of Maine AquaModel project displayed with our NetViewer system running in FireFox browser. The GoogleMaps version of the project also runs with the most common browsers but does not include as complete a set of functionality. The GoogleEarth version requires users to install the GoogleEarth browser from Google. This

variation provides a 3-D prospective view of the AquaModel project results.
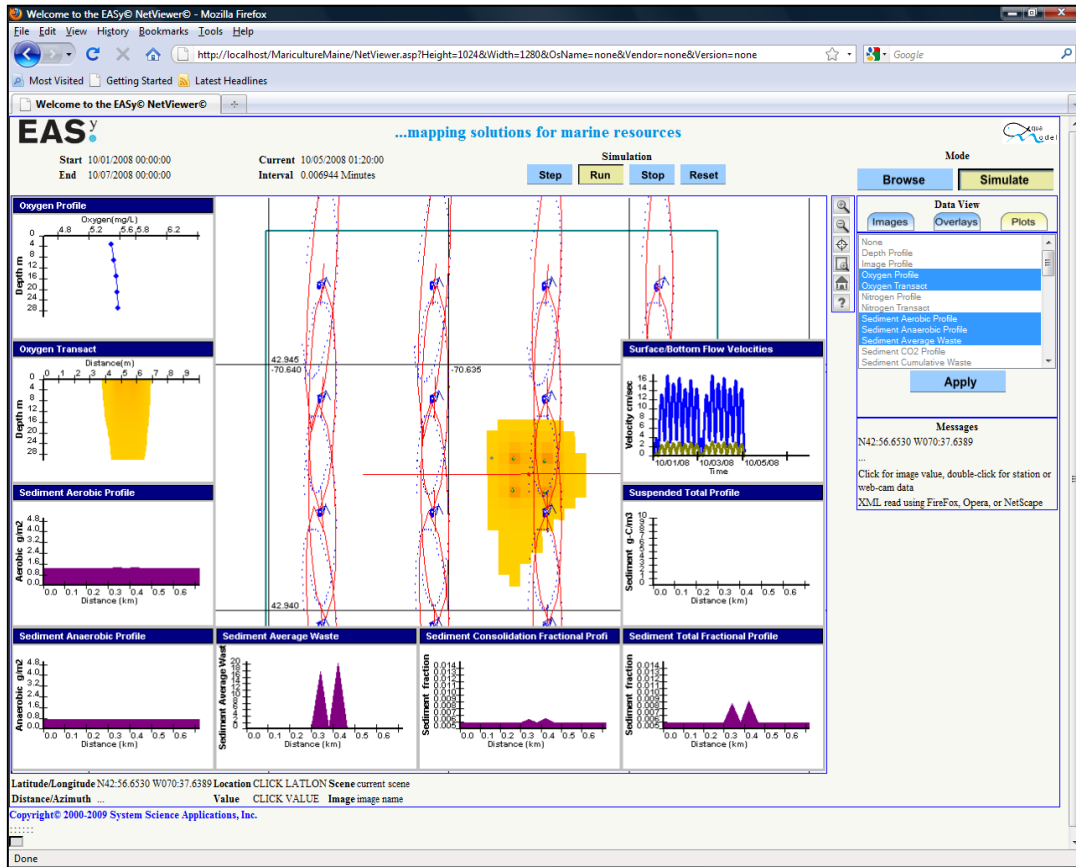
Figure 104: The NetViewer provides a sophisticated and flexible web display capability for AquaModel projects.

We created a detailed circulation model for the New Hampshire Atlantic Salmon site. The mesh of the New Hampshire coast (Previously shown in the main text as Figure X) has been built and integrated into the circulation model along with bathymetry acquired from NOAA. We also built forcing boundary conditions for use by the full 2-D and 3-D circulation models. The New Hampshire circulation model was completed and the output integrated with AquaModel so that we could compare predicted model effects with observations made at the Open Ocean Aquaculture (OOA) site.

AquaModel GIS software was modified to present hydrodynamic model output. The displayed output now includes mesh generation and interpolated bathymetry, current velocity vectors shown in Figure 105, and tidal ellipses shown in Figure 102 and 104. Another accomplishment is the optional visualization of results using the Google Earth display software.
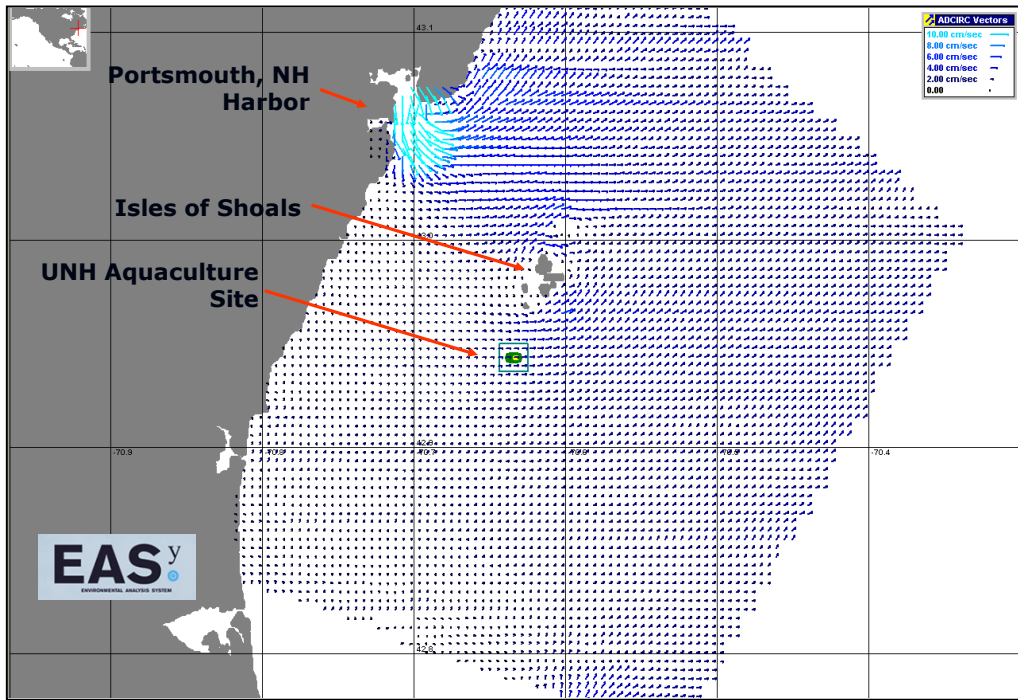
Figure 105: Hydrodynamic output from the ADCIRC model can now be presented in the EASy software. This figure shows interpolated bathymetry and the unstructured mesh used in the hydrodynamic model calculations. The UNH aquaculture site is shown at a high mesh resolution compared to the outer regions.

AquaModel Operation

To run *AquaModel* the user first identifies the sources of environmental data including bathymetry, ocean currents, and environmental conditions such as water temperature, wind speed, ambient oxygen, ambient nitrogen, ambient phytoplankton, ambient zooplankton, mixed layer depth, and average daily irradiance. *AquaModel* provides a flexibility set of options for entering each type of data. Bathymetry can be specified by an ASCII file of depth measurements, by a set of vector contours, or by a raster image. Ocean currents can be specified by a time series of current meter measurements or by a time series of 3-dimensional vectors. Environmental conditions can be specified by entering static constants into *AquaModel* or by specifying one or more Excel files that include time series data for measured values.

The user interface for specifying sources of ambient time series data, bathymetry, and ocean currents is shown in Figure 106. This interface also allows the user to scale the available ocean current vectors to evaluate a range of extreme current conditions. It also provides a capability to

merge measured ocean current data with 3-D modeled tidal current data to account for global

ocean
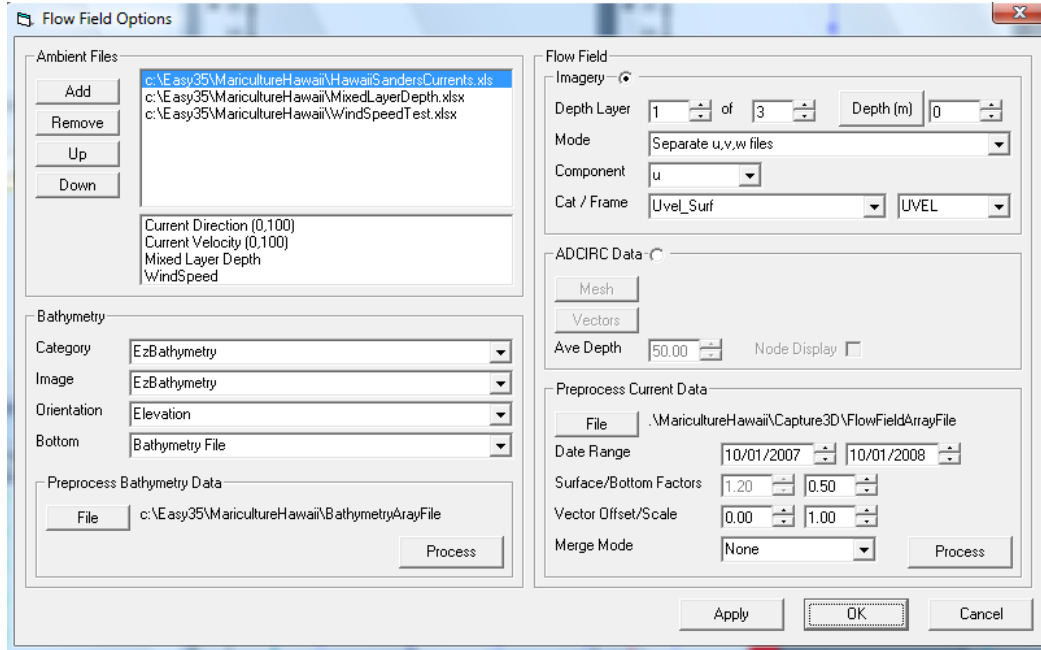
currents and/or weather conditions.

Figure 106: AquaModel provides flexible options for entering both static and time series environmental data.

Static environmental conditions are entered with in the 'Conditions' tab of the graphic user

interface shown in Figure 107. These conditions include water temperature, average daily

irradiance, mixed layer depth, and nominal wind speed for winter and summer, diffusion coefficients, tidal period and maximum tidal velocity, and ambient oxygen, nitrogen, phytoplankton, and zooplankton. It also includes parameters that are used to tune the program's plankton model to local normal ambient and plume conditions. These static parameters are superseded by measured time-series if provided by the user.

Sediment and suspended layer conditions are specified by the 'Benthic' tab of the graphic user interface shown in Figure 108. Sediment conditions include minimum, maximum, and initial values for aerobic and anaerobic biomass, sediment oxygen, CO2, sulfide, and TOC. The suspended layer is the layer of water just above the sediment. This layer is the source of ambient oxygen that is diffused into the sediment. It also transports and diffuses suspended materials along with the bottom currents. Suspended layer parameters include minimum maximum and initial values for oxygen and POC. Finally, this tab defines feed and fecal deposition, consolidation, and erosion rates and thresholds.
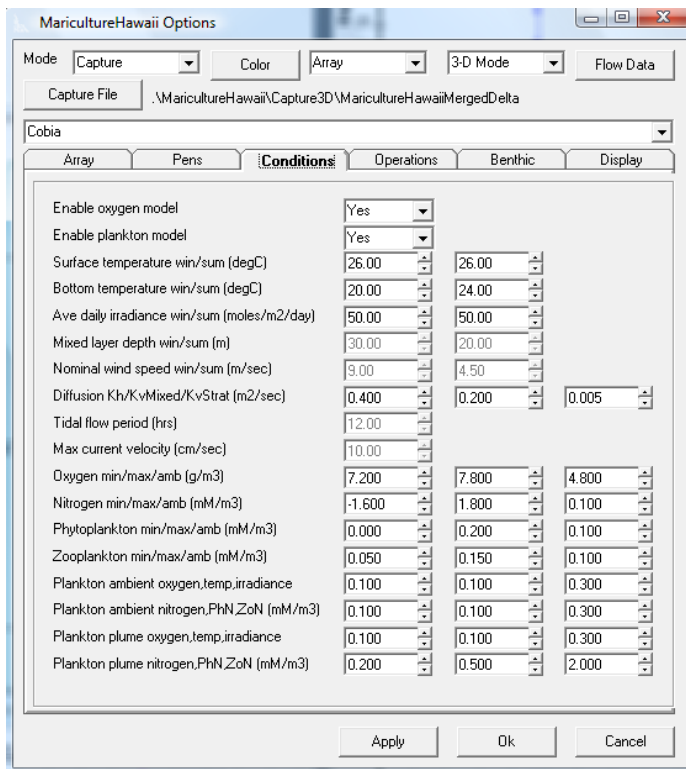
Figure 107: Static environmental conditions can be used to simulate farm operations if more detailed time series or ocean current data is unavailable.
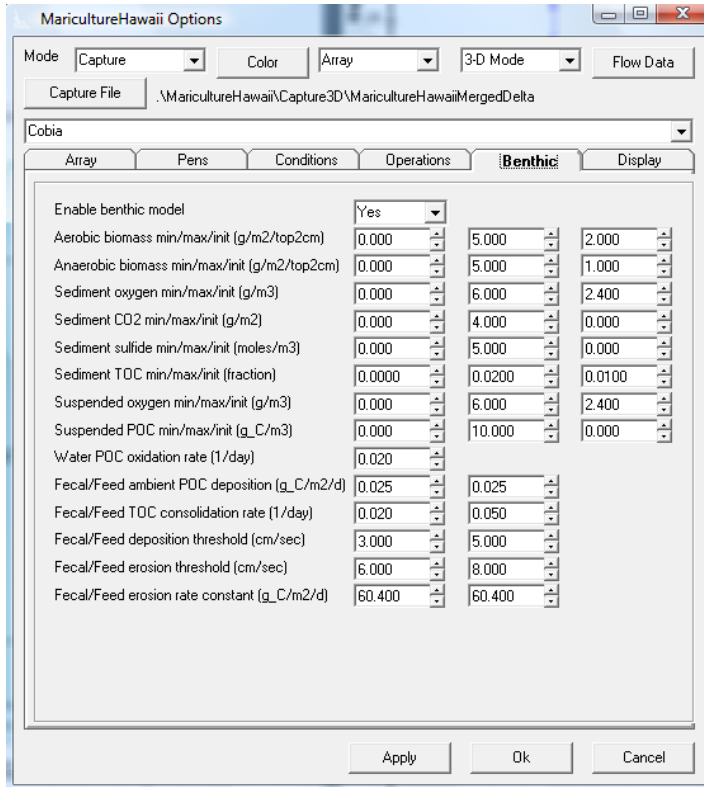
Figure 108: Sediment and suspended layer parameters define how waste materials effect the environment after they reach the ocean bottom.

The *AquaModel* analysis array is specified by the 'Array' tab of the graphical user interface shown in Figure 109. This tab defines the center and orientation of the analysis array, the array size and resolution, and the default bottom depth. The results of a simulation run are displayed as false color images, contours, and profile plots. In addition, *AquaModel* creates an Excel export file that contains a time series of calculated simulation values that can be used for post simulation offline analysis. The 'Array' tab includes three user specifiable analysis array locations. Calculated values for these capture array cells will be appended to the standard values in the Excel export file.
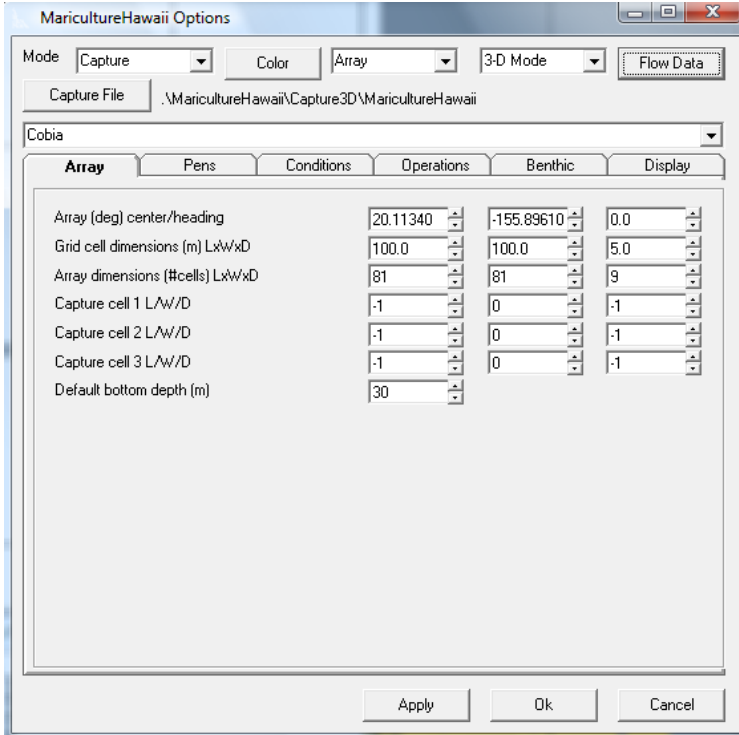
Figure 109: The analysis area of interest is specified by a geographic location, array orientation, size, and resolution.

The simulated mariculture farm pens are specified with the 'Pens' tab of the graphical user interface shown in Figure 110. The location size of each individual pen is specified along with the fish species, initial fish weight, and fish density. Pens must be located within the analysis array. While each pen must contain only one species, separate specified pens may contain different species. The user may specify as many as 99 pens although this limit could be easily increased to any practical limit. Each specified pens are simulated as a separate entity so it may represent either an individual pen for a single mariculture farm or the effect of multiple pens for a number of farms.
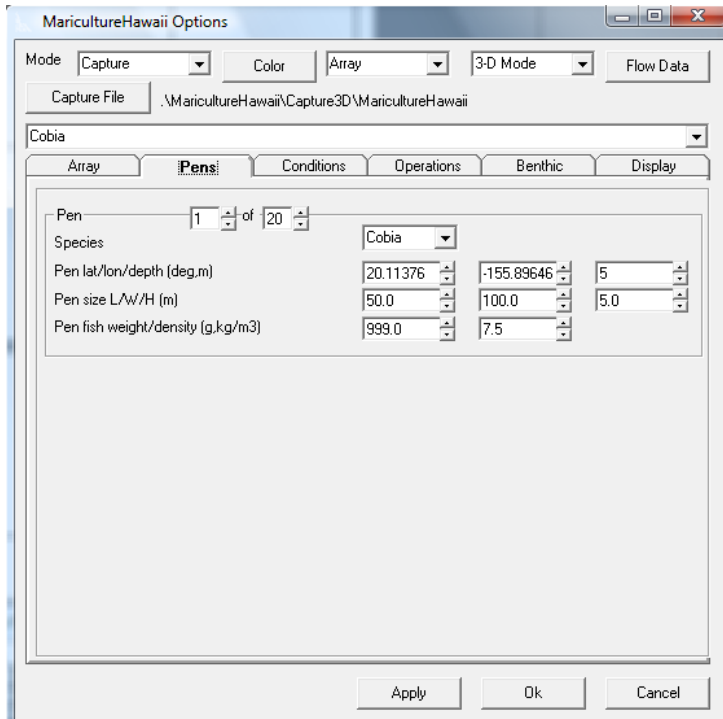
Figure 110: Fish pens are modeled as independent entries with separate geographic locations. The pens may also be of different sizes and may contain different fish densities or species.

Farm operational parameters are specified with the 'Operations' tab of the graphical user interface shown in Figure 111. The pen feed rate parameters and initial pen oxygen and nitrogen concentrations are specified along with feed and fecal settling rates. The specified minimum and maximum growth rates are used only to control the profile plot range of values.

Program operation and display parameters are located at top of the graphical user interface dialog box. These include the program mode (Display, Normal, Capture, or Replay), the ocean current vector type (2-D or 3-D), and the capture file folder. Finally, the 'Color' button allows the user to change the color of selected display items including the computational array boundary, current vectors, feed and fecal streams.
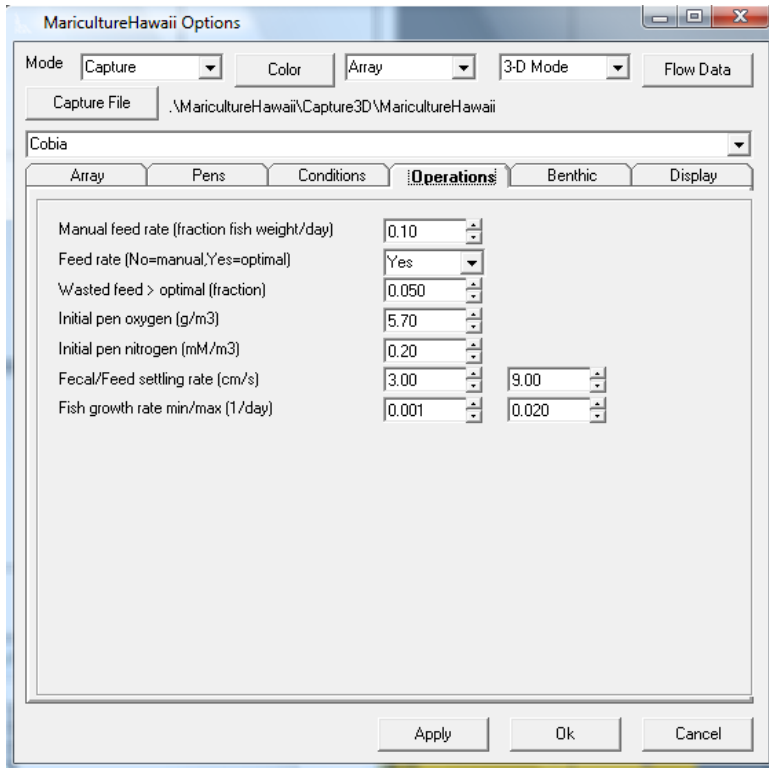
Figure 111: The operational parameters provide a capability to evaluate various farm operating scenarios including the effect of altering feed rates.

AquaModel display options are specified with the 'Display' tab of the graphical user interface shown in Figure 112. These options are used in conjunction with EASy display options to control the display of array grid cells, contours, ocean current vectors, and POC waste tracks. They also specify a mouse selection mode that determines if a left mouse double click event will display detailed pen or POC track values or will be used to identify the drill point user for profile plots.
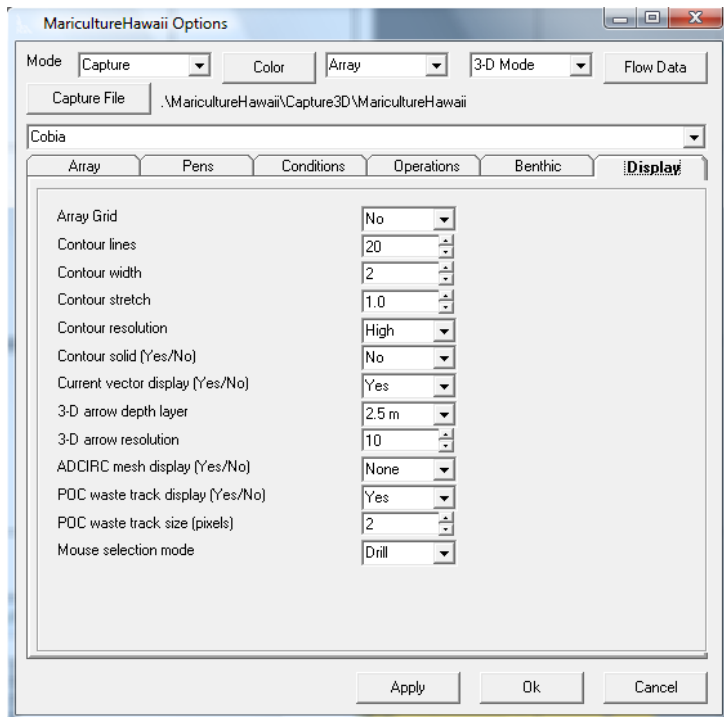
Figure 112: AquaModel and EASy display parameters allow the user to tailor false color images, contours, and profile plots to evaluate the results of a simulation run.

The EASy graphical user interface provides additional display parameters including the selection of false color images, current vectors, contours, and profile plots and associated color and size display settings. The 'Browse Images' toolbar shown in Figure 113 is used to select the false color or satellite image that is displayed in the main graphic window prior to the beginning of the simulation. During the simulation the graphic image is controlled by the 'Images' tab of the 'Data Graphics' dialog box as described below.

Figure 113: The 'Browse Images' toolbar allows the user to display selected false color or satellite images in the main graphic window.

The 'Images' tab of the 'Data Graphics' dialog box shown in Figure 114 allows the user to select a false color (or satellite) image type and/or the *AquaModel* ocean current vectors that are displayed on the EASy main graphic window during the simulation. The program animates the selected sequence of images and/or ocean current vectors to show how spatial changes occur over time. Available ocean properties that may be displayed as false color images include array

oxygen, nitrogen, phytoplankton or zooplankton at each simulated array cell depth; suspended oxygen, feed, fecal, and total waste concentration; and sediment oxygen CO_2 or hydrogen sulfide concentrations; feed, fecal, average waste, cumulative waste, and total waste concentration, total consolidation waste, and aerobic or anerobic abundance. This tab is also enables the display of calculated tidal ellipses for 3-D ocean currents.
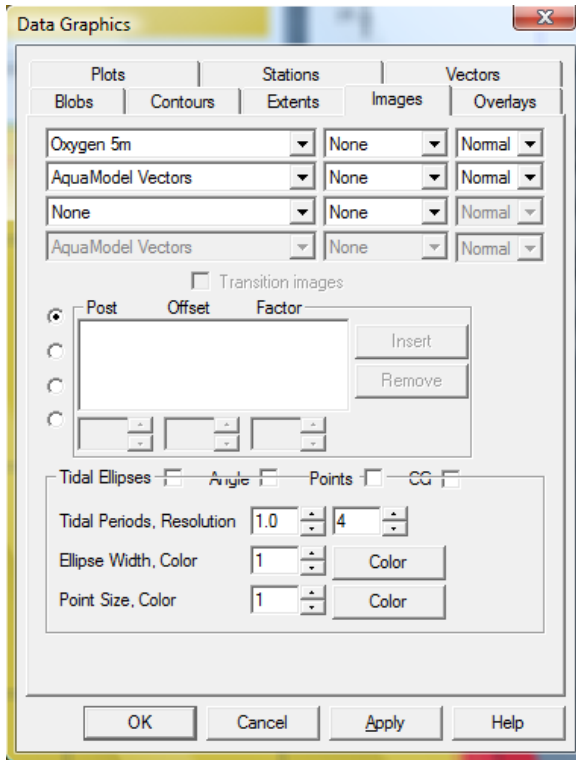

Figure 114: False color images shown in the main graphic window allow the user to visualize both spatial and temporal changes in critical ocean properties.

The 'Contours' tab of the 'Data Graphics' dialog box shown in Figure 115 allows the user to select an ocean property that will be displayed as a contour during the simulation. Ocean properties that can be displayed as false color images may also be displayed as contours. The selected contour is displayed over the selected false color (or satellite) image so that the user may determine how two parameters interact spatially. During the simulation the selected contour is animated along with the selected image to show how the two properties interact over time.
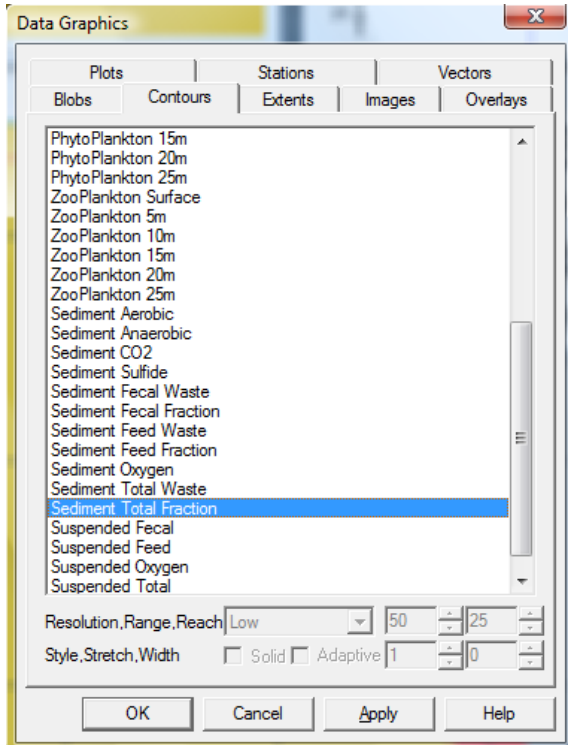
Figure 115: Contours are displayed over selected images show how two ocean parameters interact.

Profile plots are selected for display with the 'Plots' tab of the 'Data Graphics' dialog box shown in Figure 116. Four types of plots are available: depth plots (property vs. depth), time plots (property vs. time), transact plots (property vs. distance along a user defined transact line), and false color image plots (color image representing property values at array depths along a user selected transact line). Examples of the four plot types are shown below in Figure 117. The upper left figure shows a depth plot of oxygen at a user specified 'drill point', the upper right figure shows a false color image plot of oxygen along a user specified transact line, the lower left figure shows a transact plot of suspended total waste along the same transact line, and the lower right figure shows a time plot of average surface and bottom ocean current magnitude.
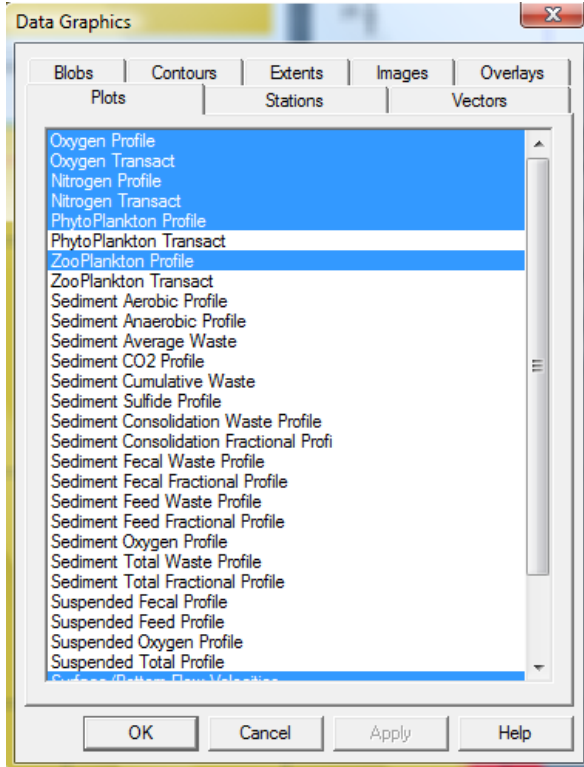
Figure 116: Plots of critical ocean properties provide for a detailed evaluation of mariculture farming effects.
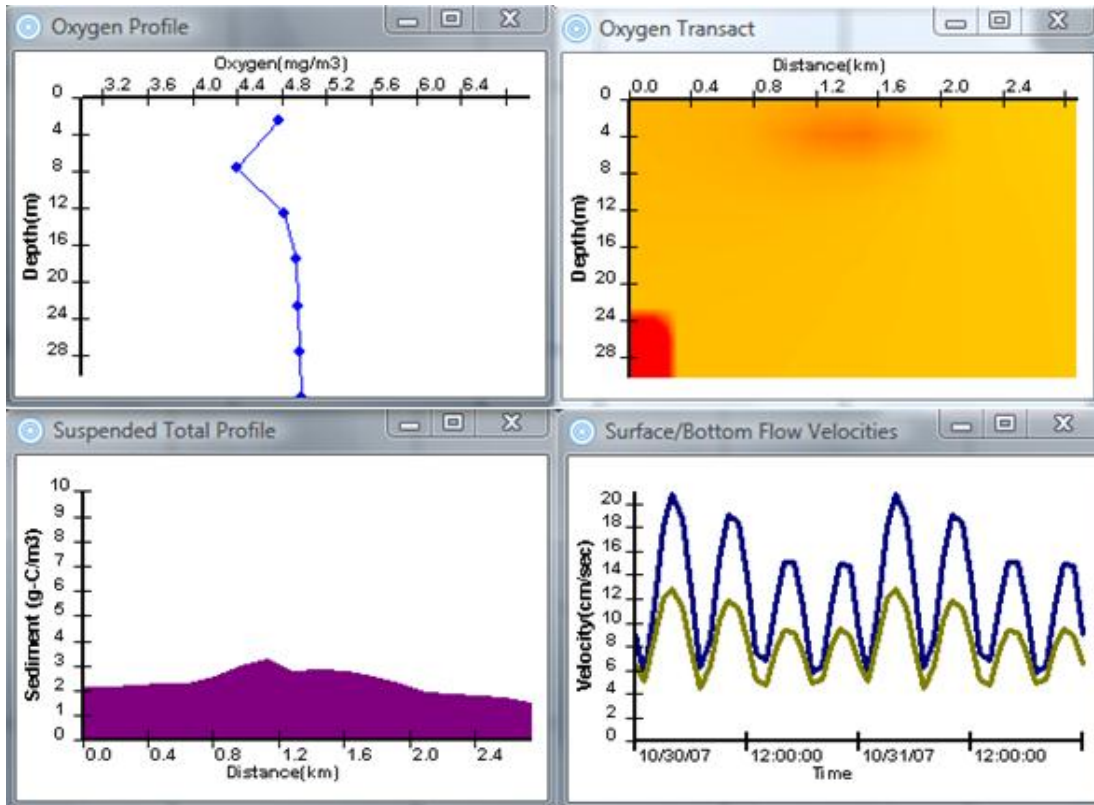

Figure 117: Four types of profile plots provide flexibility in evaluating critical ocean properties.

The 'Settings' tab of the 'Display Settings' dialog box enables general display objects and associated color, size, and resolution as shown in Figure 118. The *AquaModel* ocean current vector display is controlled by the 'Vector Arrows' panel of this tab. It defines vector length, width, and color, arrow head type and size, and vector array display resolution. Other display items that are controlled by this tab include distance units (metric or English), latitude/longitude units, legend types, display projection (Mercator, Lambert, or Arc), and geographic and profile plot background colors.
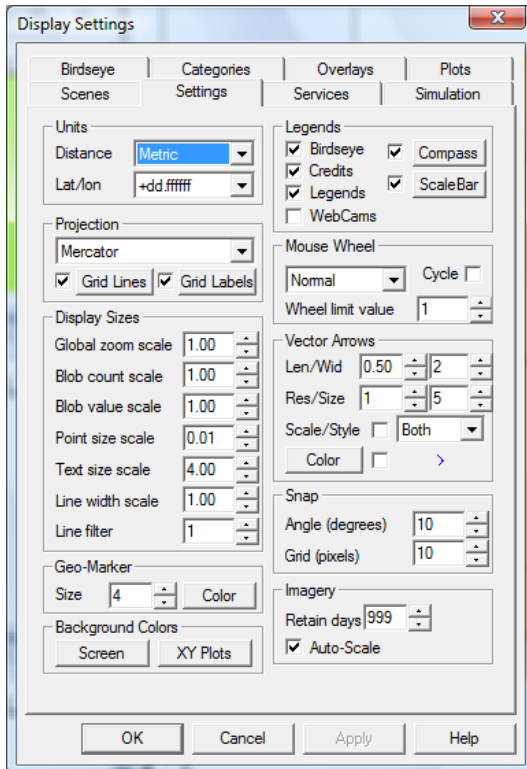
Figure 118: EASy setting controls allow the user to tailor the plan view and profile plot displays.

The 'Simulation' tab of the 'Display Settings' dialog box is used to initialize the simulation start and end dates and the display frequency as shown in Figure 119. The 'Restricted Simulation Capabilities' settings are ignored in this dialog box as they are automatically set by the AquaModel service depending on the selected operating mode (e.g. 'Normal', 'Capture', or 'Replay').
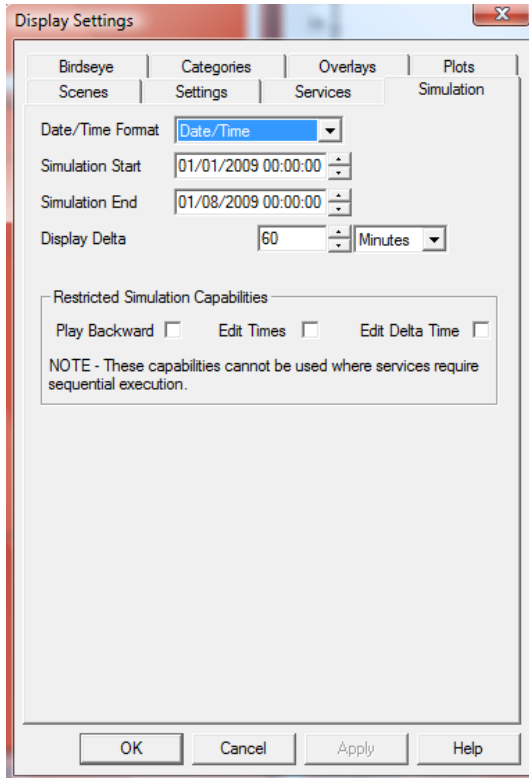
Figure 119: The simulation settings control allows the user to set the simulation start and end times as well as the display interval.

Execution of the simulation is then controlled by the 'Simulation Control Panel' shown in Figure 120. This dialog box allows the user to step, run, stop, or reset the current simulation. During the AquaModel replay mode the user may also skip to any point in the simulation or play the simulation either forward or backward.
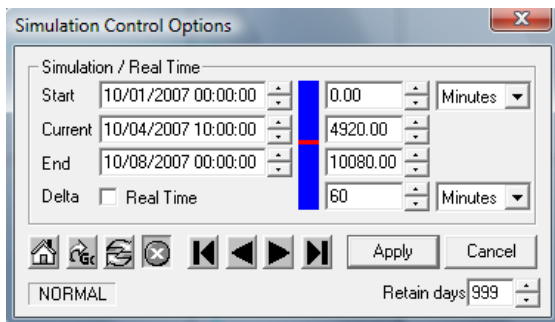

Figure 120: The new simulation control panel allows the user to skip to any point in a previously captured simulation and to play the simulation either forward or backward.

Figures 121 through 28 depict various combinations of geographic false color image, contour, and profile plots for a 24 cage farm near the big island of Hawaii. The array of dark green dots

in the center of the displays is the farm pens. A dot near the center of the array is the selected 'drill' location and the red line traversing through the array is the selected transact. Finally, the blue arrows show ocean current vectors at the displayed simulation time.

Figure 121 shows a false color image of oxygen concentration at five meters depth. The red rectangles partially obscured by land are an artifact that resulted from the bathymetry source that identified those areas to have zero depth (e.g. land). As a result *AquaModel* assumed an oxygen concentration of zero (red). The false color image is overlaid by contours that show the concentration of total waste in the near-bottom suspended layer. Profile plots include depth and false color image transact plots for oxygen, nitrogen, phytoplankton, and zooplankton; transact plots of suspended layer and sediment total wastes; and a time plot of average surface and bottom ocean currents.

Figure 122 shows a false color image of nitrogen concentration at five meters depth overlaid by contours of sediment total waste.

Figure 123 shows a false color image of phytoplankton concentration at five meters depth overlaid by contours of nitrogen concentration at five meters depth.

Figure 124 shows a false color image of zooplankton concentration at five meters depth overlaid by contours of phytoplankton concentration at five meters depth.
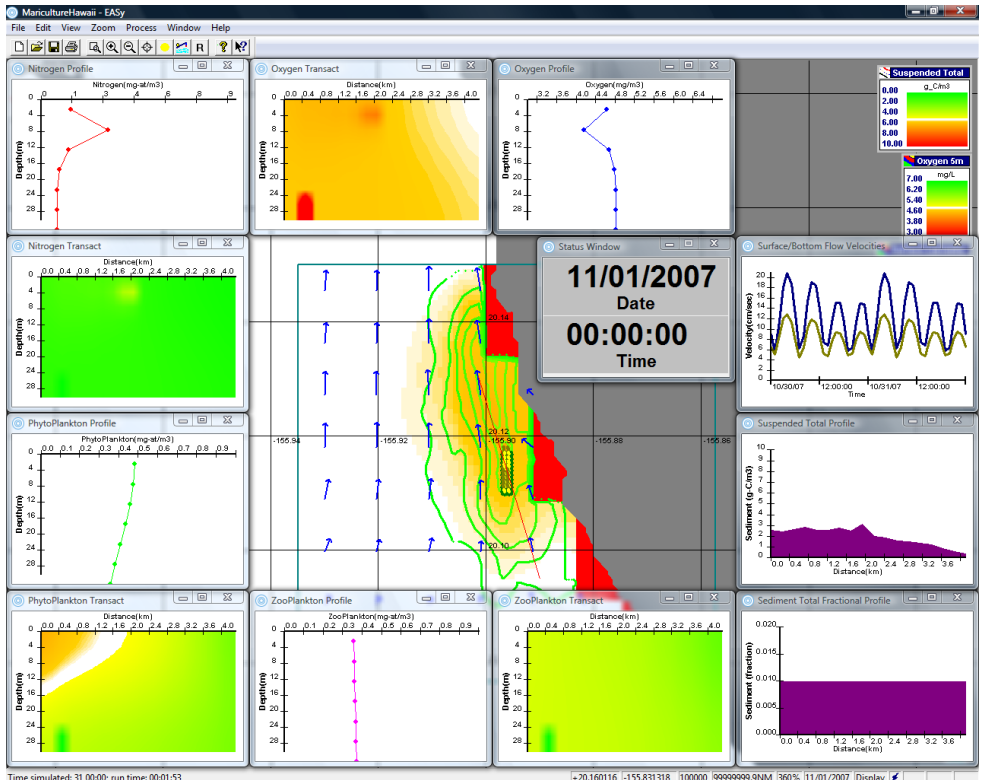
Figure 121: The combined display of a false color image (oxygen), contours (suspended total waste), current vectors, and profile plots provides users with a comprehensive tool for the analysis of critical ocean conditions.
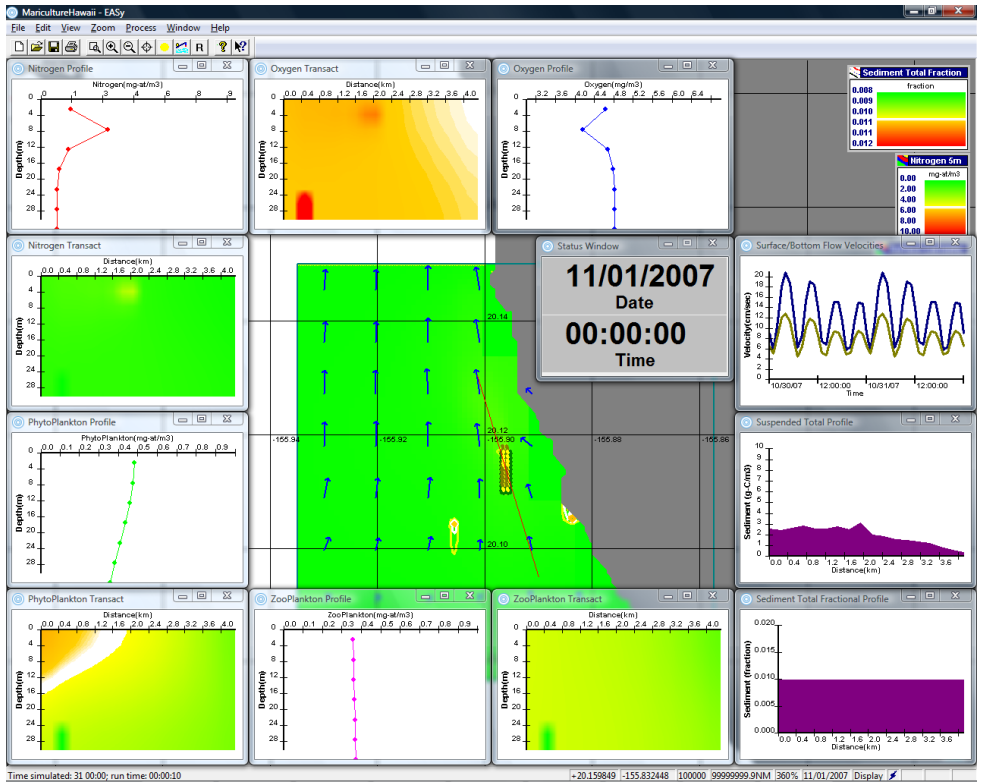

Figure 122: The lack of a nitrogen plume shows that excess nitrogen is being consumed by the available phytoplankton. The contours show only tiny areas where waste is being accumulated.
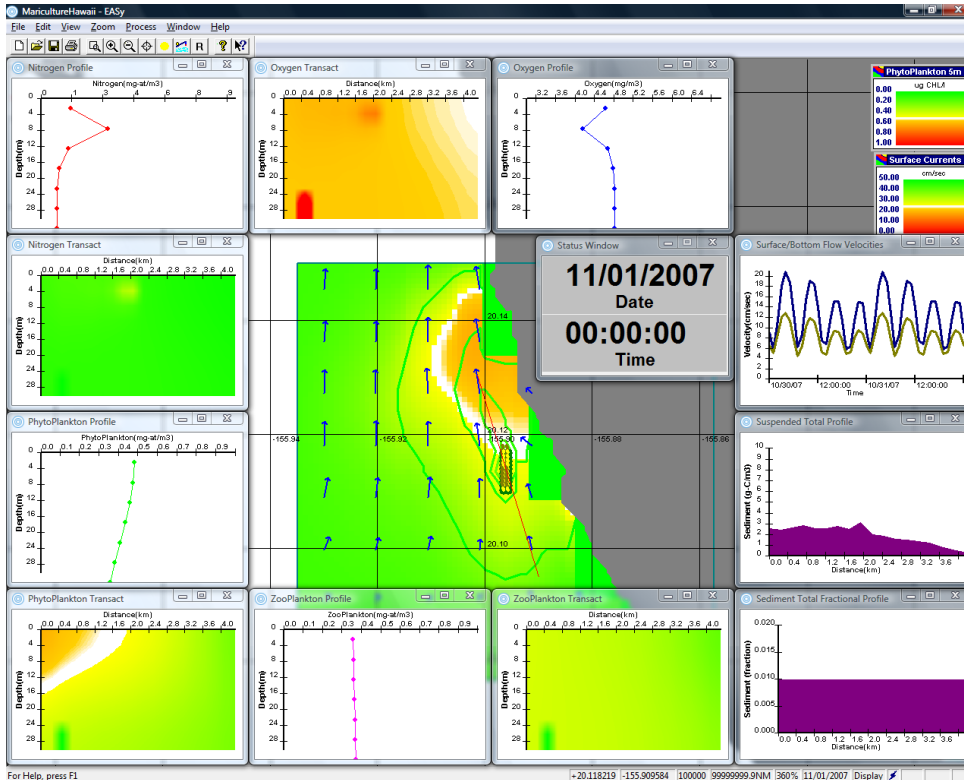
Figure 123: Phytoplankton is abundance (false color image) near the farm eliminates excess dissolved nitrogen (contours).
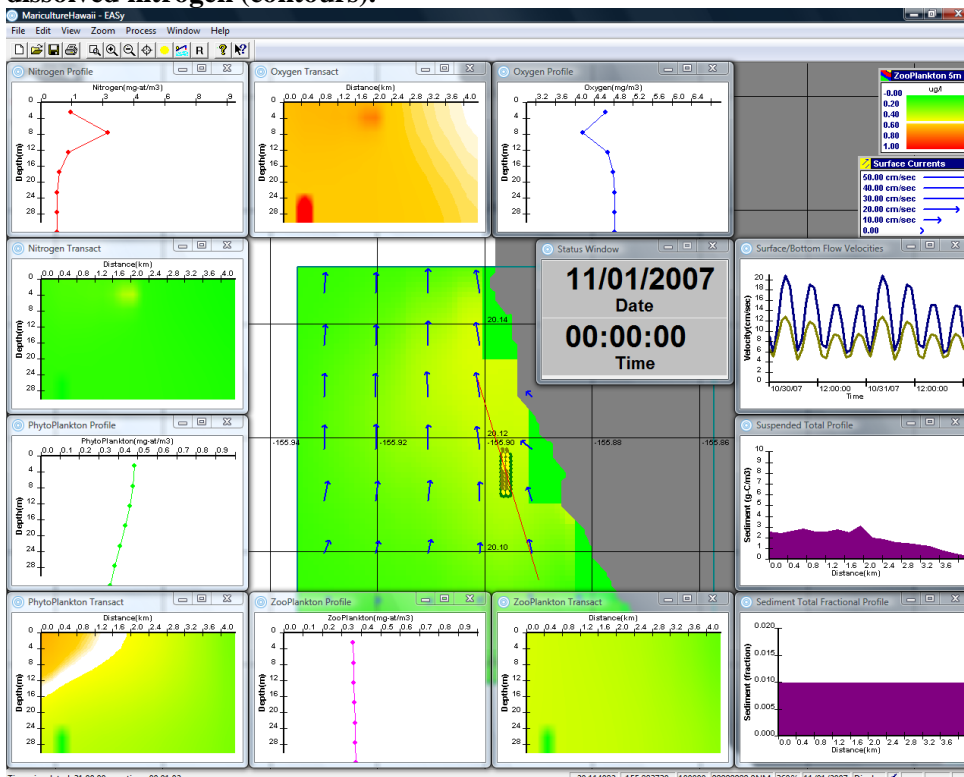

Figure 124: Zooplankton abundance (false color image) near the farm controls excess phytoplankton growth (contours).

AquaModel Features:

A complete list of the current AquaModel software features is presented below.

Displays:

- Coast line data from many sources including World Data Bank (WDB-II), World Vector Shoreline (WVS) and ArcShape files
- Detailed bathymetry
- Satellite imagery (over 50 formats)
- Navigation charts
- Multimedia
- User defined GIS points, lines, and shapes
- Profile plots (single or multiple trace, histograms, pie-charts, false color charts)
- Blob (bubble) plots
- Contours
- Current vectors
- Tidal ellipses
- Metadata
- Google Maps
- Google Earth

Modeling Capabilities

- Ocean currents: 2-D, 3-D, or merged
- Constant or dynamically changing ambient conditions data
- Modeled dissolved materials: oxygen, nitrogen, phytoplankton, zooplankton
- Modeled fish farm waste materials: feed, fecal
- Modeled benthic materials: Suspended layer of feed waste, fecal waste and oxygen, Sediment layer of feed waste, fecal waste, oxygen, hydrogen sulfide and carbon dioxide, aerobic and anaerobic biomass, Multispecies capability, Default characteristics of several commercially important species included: cod, cobia, Atlantic salmon, and striped bass.
- Animated plan and profile displays: Dissolved, suspended, and sediment materials, Surface and bottom flow velocities, Fecal and feed waste streams, Fish pen and waste stream properties

Analysis tools:

- Statistical analysis of imagery and
- 3-D perspective view
- Query measurement, bathymetry, and imagery
- Computed water volume within a user specified region (e.g. bays)
- Built in Analysis of Variance (ANOVA)
- Levenberg-Marquardt multi-dimensional surface search routine
- Kernel method 3-dimensional density function calculation
- USGS 3-D earth magnetic model (intensity, declination, and magnitude)
- 3-D current drift model

- Fast Fourier transforms
- Standard statistical functions

Simulation:

- User defined simulation times (start, end, direction, and step)
- Simulation capture and replay capability
- Animate imported satellite images and ArcShape files
- Animate blob plots, false color images, and profile plots of measurement data
- Play/step forward or backward or skip to specified simulation times (where compatible with simulation model)

Import Tools:

- Database wizard imports ASCII, Excel, or database measurement data
- ASCII wizard imports ASCII geographic measurement data to false color raster images
- Batch importing of satellite imagery and aerial photographs

Export and Conversion Tools:

- Export modeled properties to Excel for offline analysis
- Convert animated project data (graphic plan view and profile plots) to GoogleMaps or GoogleEarth animated displays to NetCDF image format files
- Export graphic displays to BMP, GIF, JPEG, PNG, or TIFF files
- Subset and convert imagery files in any supported format to NetCDF image format
- Convert ArcShape data to Excel
- Integrated with 'R' and 'S' statistical packages for interactive or off-line analysis of image or profile plot data